UNIVERSITY OF SOUTHAMPTON

FACULTY OF ENGINEERING, SCIENCE & MATHEMATICS

School of Ocean & Earth Science

Hydrothermal Plumes and Processes in the Indian Ocean

By

Carla Marie Sands

Thesis for the degree of Doctor of Philosophy

June 2006

UNIVERSITY OF SOUTHAMPTON

ABSTRACT

FACULTY OF ENGINEERING, SCIENCE AND MATHEMATICS

SCHOOL OF OCEAN AND EARTH SCIENCES

Doctor of Philosophy

HYDROTHERMAL PLUMES AND PROCESSES IN THE INDIAN OCEAN

by Carla Marie Sands

The predicted cycling of the whole ocean through hydrothermal plumes is comparable to the mixing time of the oceans (few thousand years). Hence, understanding hydrothermal plume processes is crucial if their impact on the global geochemical cycles of elements is to be assessed. One of the most important processes that has been demonstrated to modify the gross chemical flux from venting to the oceans is the oxidative precipitation of dissolved Fe (II). It has been hypothesised that this might vary significantly from one ocean basin to another along the path of thermohaline circulation. To test that hypothesis, hydrothermal plume samples were collected from the first confirmed hydrothermal vent fields in the Indian Ocean, at Kairei and Edmond, close to the Rodriguez Triple Junction, during the RRS Charles Darwin cruise CD128 in 2001. The samples were analysed to determine the concentrations of dissolved iron and manganese and particulate Fe, Mn, Al, Ca, Mg, Cu, Zn, P, V, As, Y and the rare earth elements. For a subset of the samples, the concentrations of Fe, Mn, Cu and P in different size fractions of the particulate phase were also measured.

Dissolved Fe and Mn concentrations are high in the Kairei and Edmond hydrothermal plumes compared to Atlantic and Pacific hydrothermal plumes previously studied. Particulate Fe concentrations are also high while particulate Mn concentrations remain low throughout the plume. Of the total (i.e. particulate plus dissolved) Fe which emerges from the vents, approximately 20-30% is lost from the plume via the removal of Fe-sulfide phases formed early in the buoyant plume. Further loss of Fe due to the oxidation and formation of particulate Fe-oxide phases results in a total Fe loss of 50-70%. For the very young non-buoyant plume samples, there is very little *in situ* particulate Fe present.

The behaviour of the chalcophile elements (Cu, Zn, Cd and Pb), elements which exist as oxyanions in seawater (P, V and As), as well as the rare earth elements and Y are consistent with previous studies of elemental behaviours in hydrothermal plumes in the Atlantic and Pacific Oceans. The observed behaviours of these elements with respect to particulate Fe suggests that the differing Fe (II) oxidation rates between ocean basins do not impact the processes taking place within hydrothermal plumes. In addition, fractionation of Fe, Mn, Cu and P in the Edmond hydrothermal plume between the dissolved, colloidal and fine and coarse particulate phases shows consistency with previous conclusions based on only one of these phases.

The P/Fe and V/Fe ratios of the hydrothermal particulate samples are intermediate to those of particulate samples from the Atlantic and Pacific Oceans suggesting that as previously hypothesised, these ratios are dependent on dissolved ambient phosphate concentrations. Hence, there remains the potential to use these ratios from sediment cores as paleo-proxies for dissolved phosphate concentrations.

Graduate School of the
National Oceanography Centre, Southampton

This PhD dissertation by

Carla Marie Sands

has been produced under the supervision of the following persons

Supervisor/s: Professor Chris German
Dr Peter Statham

Chair of Advisory Panel: Professor Martin Palmer

Member/s of Advisory Panel: Not applicable

Contents

List of Figures

List of Tables

DECLARATION OF AUTHORSHIP

I, **CARLA MARIE SANDS**

declare that the thesis entitled

Hydrothermal Plumes and Processes in the Indian Ocean

and the work presented in it are my own. I confirm that:

- this work was done wholly or mainly while in candidature for a research degree at this University;
- where any part of this thesis has previously been submitted for a degree or any other qualification at this University or any other institution, this has been clearly stated;
- where I have consulted the published work of others, this is always clearly attributed;
- where I have quoted from the work of others, the source is always given. With the exception of such quotations, this thesis is entirely my own work;
- I have acknowledged all main sources of help;
- where the thesis is based on work done by myself jointly with others, I have made clear exactly what was done by others and what I have contributed myself;
- none of this work has been published before submission

Signed: …….
.
Date:……

Acknowledgements

Firstly I would like to thank both my supervisors Prof. Chris German and Dr. Peter Statham for all their time, support and advice, I wouldn't have got this far without either of them. I consider it a privilege to have worked with Chris, one of the biggest names in hydrothermal research, he has always been an inspiration, particularly in my (as he would put it) 'darkest Yorkshire moments'! I never failed to leave his office feeling re-motivated and enthused about my work. Thanks especially to Peter for never failing to make the time to sit down and discuss my work with me and for being so prompt with advice and feedback.

Many, many thanks to Dr Doug Connelly, not only for maintaining my sanity (and expanding my general knowledge) during the numerous hours spent in the clean room seemingly producing iron out of thin air but particularly for always being there both as a friend and colleague to share his knowledge, bounce ideas off, 'borrow' equipment from, and provide a decent meal and glass of wine (or two) at a time when it was greatly needed. Thanks also to Darryl Green for assistance with analyses and providing me with someone to insult on a regular basis, Andy Milton also for assistance with analyses and Brian Dickie for having the foresight to install a radio in the aforementioned clean room.

Finally, this thesis is dedicated to my late granddad. He was fascinated by what was to be found beneath the ocean surface and would have been amazed by some of the things I have seen during the course of my research – I only wish I could have shared some of them with him. Many, many thanks of course go to my much loved Mum and Dad (who mistakenly thought they'd fulfilled their financial duties to me when I left university the first time!). I'm especially grateful to them for their support during the final stages of writing up as well as their complete faith in me that I would get to the end of this.

Support for this study was provided by NERC grant NER/A/S/1999/00090

1 Chapter 1 Introduction

1.1 Background

The existence of hydrothermal vents was suspected some time before the first observations of the phenomena in the late 1970s (Corliss et al., 1979; Spiess et al., 1980). Prior to their discovery, metal-rich sediments had been found along many parts of the mid-ocean ridge system (see Fig. 1) including the East Pacific Rise (Bostrom & Peterson, 1969), the mid-Atlantic Ridge (Scott et al., 1974) and the Indian Ridge (e.g. Bonatti, 1975). Metal-rich sediments were also discovered in the Red Sea (Degens & Ross, 1969) which is a young ocean. In addition, many cores taken at sites in the Atlantic, Pacific and Indian Oceans by the Deep Sea Drilling Project were found to have metalliferous sediments at the base of the sediment column, just above the basaltic basement. This suggests that the metal-rich sediments were originally formed close to the ridge axis. The sediments were also similar in composition to those found at the mid-ocean ridges (e.g. Dymond et al., 1973). Some authors suggested that the origin of these sediments were hydrothermal solutions formed from the interaction of seawater with newly formed basalt (e g. Corliss, 1971; Dymond et al., 1973; Piper, 1973). Other explanations such as authigenic metal-rich phases (formed by slow precipitation of metals from seawater) being undiluted by terrigenous or biogenic sediments (e.g. Bender et al., 1971; Bonatti, 1975) or simply the deposition of fine terrigenous sediment with high transition metal to aluminium ratios (Turekian & Imbrie, 1966) were also put forward. However, further evidence of hydrothermal activity was provided through the detection of excess ^{3}He in the deep oceans, both in the Pacific Ocean, in the south and above the East Pacific Rise (Clarke et al., 1969; Craig et al., 1975; Lupton & Craig, 1975) and in the Atlantic Ocean, above the mid-Atlantic Ridge (Jenkins et al., 1972; Jenkins & Clarke, 1976) as well as in Red Sea brines (Lupton et al., 1977). The only source of ^{3}He in the deep ocean is degassing from the earth's mantle (^{3}He from tritium decay is generally not significant at mid-ocean ridge depths; Lupton, 2001), hence some form of hydrothermal circulation was most likely to be responsible.

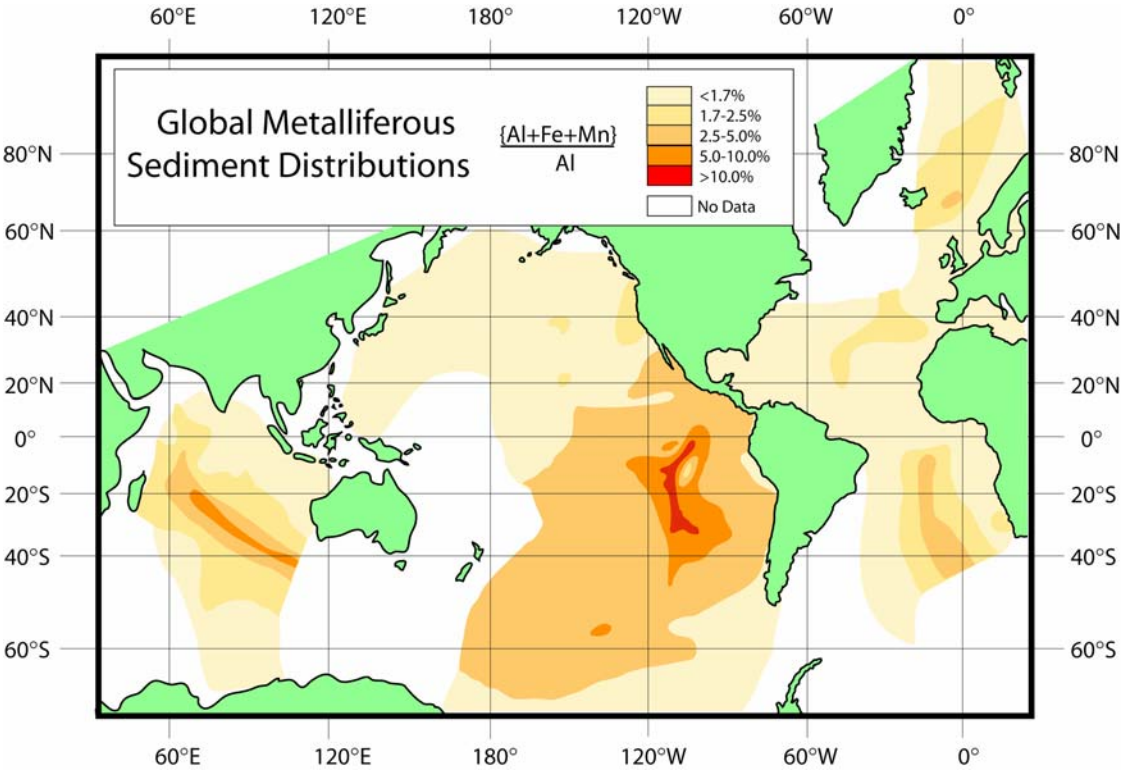

Figure 1 Map showing distribution of metal-rich sediments in the oceans. Higher (Al +Fe +Mn)/Al ratios represent the most metal-rich sediments and are focused along the mid-ocean ridges (after Bostrom et al., 1969)

The first sites of hydrothermal venting were actually discovered in the East Pacific Ocean (Corliss et al., 1979; Edmond et al., 1979, 1982; Spiess et al., 1980) and it was initially suggested that the phenomenon was only associated with fast spreading mid-ocean ridges. Since then, sites of hydrothermal venting have been discovered throughout the worlds oceans along ridges of all spreading rates. It has been hypothesised that the incidence of hydrothermal activity has a linear relationship with spreading rate (i.e. magmatic supply), hydrothermal plume incidence increasing with increased spreading rate/magmatic supply (Baker & Hammond, 1992; Baker et al., 1996). However German & Parson (1998) found evidence that tectonic segmentation can also be a controlling factor, particularly along slow spreading ridges. A recent study based on the most up to date information on hydrothermal activity (both actual vent locations and hydrothermal plumes where the vent has not yet been located) found that for 50% of the mid-ocean ridge system which has been surveyed for hydrothermal activity (in total ~20% of the global ridge system), where the spreading rate is 10-150mm/yr there is a loose linear

correlation between the magmatic budget and hydrothermal activity (Baker & German, 2004).

The most widely studied vents are those in the Pacific (particularly those on the East Pacific Rise) and North Atlantic representing the two extremes of global thermohaline circulation. Comparatively little research has taken place in the Indian Ocean and confirmation of the suspected existence of hydrothermal vents on the Central Indian Ridge occurred only relatively recently (Gamo et al., 2001; Gallant & Von Damm, 2006).

Hydrothermal vents are the result of the penetration of seawater downwards through the permeable ocean crust where it is heated and then reacts with the underlying substrate. In the majority of cases this substrate is basalt but in some instances the hydrothermal system may be hosted in ultramafic rocks. This is the case at the Rainbow and Logatchev hydrothermal vent sites in the Atlantic Ocean (Bogdanov et al., 1996; Douville et al., 2002). With increasing heat and pressure the fluids become buoyant, rise up and are injected back into the ocean. These fluids are hot (up to 405°C), acidic (pH = 2.5 – 5.9, Von Damm, 1995), reducing and have a composition greatly altered compared to seawater. They are completely depleted in Mg due to its fixation in basalts, depleted in sulfate due to precipitation as anhydrite and reduction to hydrogen sulfide (Von Damm, 1995) and highly enriched in Li, K, Rb and Cs due to leaching from basalts. Fe and Mn are enriched to millimolar levels (Von Damm, 1995) compared to their nanomolar levels in seawater (Bruland, 1983). Silicon is also enriched to millimolar levels compared to micromolar levels in seawater and a number of dissolved gases are present in high concentrations within the fluids including hydrogen sulfide, carbon dioxide, methane, helium-3 and hydrogen.

On emerging from the vents the hot, acidic, reducing fluids rapidly mix with the surrounding seawater which is cold, mildly alkaline and well oxygenated; a dilution of 1000:1 is reached in around 5 minutes (McDuff, 1995). Many chemical reactions occur; initially metal sulfides are formed followed by iron oxide precipitation. The buoyant fluids rise as a turbulent plume continuing to entrain and mix with the ambient seawater. The incorporation of colder, denser seawater into the plume increases the density of the

plume as it rises until typically between 150 and 400m above the vent (Cowen & German, 2001) at a dilution of 10^4:1 (Lupton, 1995) and after approximately an hour (Speer & Rona, 1989) neutral buoyancy is reached. At this stage the non-buoyant plume is dispersed laterally. The exact pattern of dispersal depends on ocean currents (Edmond et al., 1982) and local topography (German et al., 1998b). Using numerical simulations of ocean circulation, Speer et al. (2002) have shown that in all oceans, dispersion may be constrained by, and follow the ridges for great distances. In the Atlantic, the deep rift valley of the Mid Atlantic Ridge constrains the plume dispersion as the height of the non-buoyant plume is usually less than that of the valley walls (Baker et al., 1995), whereas in the Pacific there are no such constraints and plumes have been observed thousands of kilometres from their origin (Lupton & Craig, 1981; Edmond et al., 1982). Consequently hydrothermal plumes have a major role in influencing global ocean chemistry.

The chemical and physical anomalies present in hydrothermal plumes and the spatial extent of plumes allow detection of hydrothermal activity without knowing the precise seafloor location of vent sites. The physical properties used to locate hydrothermal plumes are temperature and light transmission anomalies (either light attenuation or light scattering). The temperature anomaly can be positive or negative depending on the ambient deepwater salinity gradient. In the deep Pacific where salinity increases with depth, the non-buoyant plume is warmer and more saline than ambient seawater, whereas in the deep Atlantic the salinity decreases with depth and the non-buoyant plume is cooler and fresher than ambient seawater (Speer & Rona, 1989). Light transmission anomalies arise from the precipitation of particles within the plumes and it has been shown, for example, that there is a strong relationship between nephelometer values and one of the commonly used chemical tracers of hydrothermal activity which is total dissolvable manganese (Nelsen et al., 1986). As well as manganese, other chemical anomalies that are most often used to trace plumes are methane and ^{3}He which are all enriched ~10^6-fold in hydrothermal fluids (Von Damm, 1990). Mn and CH_4 have been used because they can be measured precisely while at sea (Baker et al., 1995), however discrete samples only provide coarse resolution of a dynamic feature. The development of in situ continuous chemical analysers (e.g. Chin et al., 1994) for Fe and Mn has led to higher resolution data which can be directly correlated with temperature and light transmission data. Detection limits were initially quite high (>20nmol/l) and although

this does not prevent their use in hydrothermal plumes due to the high concentrations of dissolved Fe and Mn which are present, newer analysers are reducing detection limits considerably to less than 2nmol/l (Connelly et al., 2005; Prien et al., in prep.), thus allowing tracking of plumes over greater distances.

1.2 Hydrothermal influence on global geochemical cycles

A fundamental concept in the study of ocean chemistry is that of 'mass balance'. Assuming an element is at 'steady state', then the sources of any element (e.g. river run off or atmospheric deposition) to the ocean must be matched by the sinks for that element (e.g. burial in sediments). Hydrothermal activity can act as a source or a sink for various elements and for some elements it is a significant fraction of the overall geochemical balance. Magnesium, for example, is completely removed from seawater during hydrothermal circulation (Von Damm, 1990). Prior to the discovery of hydrothermal venting the known sinks for Mg could only account for ~50% of the river flux of dissolved Mg (Drever, 1974). Edmond et al. (1979) made some of the first flux estimates based on data from the Galapagos hot springs, concluding that such sites are a major sink for Mg and SO_4 and a source for Li and Rb.

The influence of hydrothermal activity on global geochemical cycles is not confined to the circulation of water through the ocean crust. In fact the time taken for the entire ocean volume to circulate through the ocean crust is on a timescale of millions of years (Mottl, 1983). This is much greater than the residence time of water with respect to riverine input in the ocean of ~4 x 10^4 years (Broecker & Peng, 1982). Hence, only the geochemical cycles of those elements that are highly enriched or depleted in vent fluids will be impacted by hydrothermal circulation. However, the hydrothermal plumes resulting from this circulation also have an influence due to their scavenging behaviour and potential long-range dispersal. The predicted cycling of the entire ocean through hydrothermal plumes via entrainment of ambient seawater has been estimated at ~2 x 10^5 years by Kadko (1993) from measurements of ^{210}Pb scavenging and ^{3}He fluxes. An alternative estimate can be made from the global high temperature axial water flux estimated by Schultz & Elderfield (1997) of 2.4-3.5 x 10^{13}kg/yr and the assumption that

entrainment of seawater into the non-buoyant plume occurs at a factor of 10^4 (Lupton, 1995). The high temperature axial water flux consists of focused and diffuse flow, therefore an estimate of the proportion of this flux which occurs as focused flow must be made. Recent measurements of heat flux at 9°50'N on East Pacific Rise suggest that focused venting is an order of magnitude less than diffuse venting (Ramondenc et al., 2006) which would give a cycling time through hydrothermal plumes of ~4-6 x 10^4 years (assuming 10% focused flow and 90% diffuse flow as an approximation). However, this estimate of diffuse versus focused flow was obtained using discrete measurements, i.e. at several individual sites, in a similar manner to earlier estimates from other authors who came to the same broad conclusions (Rona & Trivett, 1992; Schultz et al., 1992). In contrast, Viers et al. (2006) used a more innovative technique where they intercepted and surveyed entire plumes from both focused and diffuse sources at the Endeavour hydrothermal site. From their measurements of heat flux they concluded that the high temperature axial water flux is divided equally between focused and diffuse flow, which would reduce the estimate to ~8-11 x 10^3 years. The key point is that any element which is scavenged and has an oceanic residence time of this order or less will have its geochemical cycle affected by this process. For example, the rare earth elements (REEs) which are enriched in hydrothermal vent fluids are scavenged in sufficient quantities from seawater by Fe-oxyhydroxide particles for this hydrothermal activity to act as a net sink of these elements (German et al., 1990), in many cases balancing the riverine input of individual REEs (Rudnicki & Elderfield, 1993).

Quantification of global hydrothermal fluxes is not a straightforward task. Vent fluid composition is highly variable (Von Damm, 1990; 1995) and an estimate of the total flux of hydrothermal fluids to the oceans is required. Various methods have been employed by different authors, Edmond et al. (1979) estimated a hydrothermal Si flux to the oceans of 3.1 x 10^{12} mol yr^{-1} based on a global ridge axis heat flux estimate derived from the ^{3}He flux from the ocean, the heat to ^{3}He ratio of vent fluids (Jenkins et al., 1978) and the temperature/concentration relationship of Si in the vent fluids. A similar estimate is obtained using the Palmer & Edmond (1989) estimate of global hydrothermal flux from the Sr isotope budget of the oceans (Treguer et al., 1995). In contrast, Mortlock et al., (1993) estimated a Si flux of 0.1–0.4 x 10^{12} mol yr^{-1} from Ge/Si ratios which is only 10% of the earlier estimates, but is in agreement with the estimate of 0.2-0.4 x 10^{12} mol yr^{-1}

which is obtained if using the hydrothermal water flux from Li isotope data estimated by Elderfield and Schultz (1996). Presently we can only estimate fluxes of elements from hydrothermal vents to ~one order of magnitude.

The estimates of global hydrothermal fluxes like that for Si detailed above, are only gross fluxes, providing no insights into the fate of the elements once they have entered the oceans. Flux estimates of elements to the ocean associated with hydrothermal plume processes can also be made in a number of ways and have proved equally variable. Early estimates of the removal of phosphorus via adsorption onto Fe particles were based on the P content of metalliferous sediments on the East Pacific Rise and gave values of 4 to 5 x 10^9 mol yr^{-1} (Froelich et al., 1977). Rudnicki & Elderfield (1993) used scavenging rates from modelling and an estimate of the Fe flux based on vent fluid concentration and hydrothermal water flux to give a figure of 1.1 x 10^{10} mol yr^{-1}. Wheat et al. (1996) based their estimate on an average P/Fe ratio for hydrothermal Fe-oxyhydroxide particles and an Fe flux calculated from heat loss estimates to give 7.7 x 10^9 mol yr^{-1}. Each author uses a different river flux estimate for comparison to show the percentage impact of this flux but taking an Fe river flux estimate of 3.3 x 10^{10} mol yr^{-1} (Elderfield & Schultz, 1996), the hydrothermal phosphorus sink associated with plume scavenging varies between 12 and 33% which is a significant fraction of the overall sink. An estimate by Kadko et al. (1993) which compares the P oceanic residence time with scavenging residence times also falls within this range at 20%.

The examples of silicon and phosphorus demonstrate the uncertainties associated with hydrothermal flux estimates and highlight that there is still much to be learnt.

1.3 Processes in hydrothermal plumes

1.3.1 Dissolved constituents as tracers

As previously described, a number of dissolved constituents within hydrothermal plumes are employed as tracers of hydrothermal plume activity, most commonly manganese, methane and helium-3. Mn is enriched ~10^6 fold in vent fluids compared to seawater and is usually the most abundant transition metal after iron (Bruland, 1983; Von Damm,

1995). Although it has been shown that Mn (II) may behave conservatively in hydrothermal plumes near to the vent source (Cowen et al., 1990; Mottl & McConachy, 1990; Chin et al., 1994), its overall behaviour within plumes is non conservative (Lilley et al., 1995). Whereas iron is rapidly oxidised (see '1.3.2 Particle formation'), Mn remains in solution. Although Mn (II) is thermodynamically unstable with respect to oxidation in oxygenated seawater, the kinetics of the reaction are much slower than that of Fe (II). The oxidation of Mn and its removal onto particles is a microbially catalysed process (Cowen et al., 1986) occurring in the non-buoyant plume. The residence time of Mn within a plume varies from weeks (e.g. Kadko et al., 1990) to several years (Lavelle et al., 1992). Dissolved Mn measurements have been used to provide an estimate of the mixing ratio between the hydrothermal fluids and ambient seawater (James & Elderfield, 1996). Also, the percentage of total Mn in particulate form can be used as an indicator of plume age (Klinkhammer et al., 1985).

Methane is enriched by a factor of ~10^5 over ambient deep ocean levels (Welhan & Craig, 1983) and also behaves non-conservatively within hydrothermal plumes. Like manganese, it is removed by microbial activity in the non-buoyant plume (Lilley et al., 1995). A number of processes are responsible for the presence of CH_4 within vent fluids including outgassing from the mantle, direct leaching from basalt and microbial production (Welhan & Craig, 1983; Welhan, 1988).

Primordial helium from the earth's mantle has a distinct isotopic ratio which enables its use as a tracer in the deep ocean (Lupton & Craig, 1981). Due to its chemical inertness (and therefore conservative behaviour) helium-3 can be used to measure plume dilution more accurately than manganese. Additionally, measurements of ^{222}Rn which is also enriched in vent fluids can be combined with those of ^{3}He to estimate plume age (Kadko et al., 1990). Like ^{3}He, ^{222}Rn is chemically inert. However, it is also radioactive with a half-life of 3.83 days. This means that any variation in the ^{222}Rn/^{3}He ratio within a hydrothermal plume is purely a function of ^{222}Rn decay and therefore the age of the plume can be derived from measurements of this ratio. Radon-222 measurements have also been combined with those of Mn (Rudnicki & Elderfield, 1992; Gendron et al., 1994) to provide plume age measurements, again employing the conservative nature of

Mn. Rudnicki & Elderfield found similar ages for hydrothermal plume samples using either $^{222}Rn/^{3}He$ or $^{222}Rn/Mn$ ratios.

The value of Mn, CH_4 and ^{3}He measurements becomes more powerful when they are combined. CH_4 anomalies alone may not be indicative of hydrothermal activity but the presence of ^{3}He and Mn can help to confirm it. CH_4/Mn ratios within plumes can be used to provide information regarding the underlying nature of the associated hydrothermal system. Lupton et al. (1993) used these ratios to infer whether plumes along the East Pacific Rise were derived from young evolving hydrothermal systems or older, more stable systems. This is based on the premise that the relative concentration of volatiles such as CH_4 decreases as the system reaches a more stable state.

Although H_2S and H_2 are enriched in vent fluids, they have not generally been employed as tracers. This is because although elevated concentrations of both have been measured in hydrothermal plumes (Kadko et al., 1990; McLaughlin-West et al., 1999; Radford-Knoery et al., 2001), they tend to decrease relatively rapidly due to microbial oxidation (H_2) and precipitation/oxidation (H_2S); Kadko et al. (1990) calculated a residence time of ~10hrs for H_2 in the Endeavour plume in the Pacific while Radford-Knoery et al. (2001) calculated H_2S would decrease below detection limits within 4-5hrs of release from the vent at the Rainbow hydrothermal plume in the Atlantic.

1.3.2 Particle formation

In the first few seconds after the hydrothermal fluids emerge from the vents, metal sulfides rapidly precipitate. Up to 50% of the iron (II) which is present at millimolar concentrations precipitates in this manner (Mottl & McConachy, 1990; Rudnicki & Elderfield, 1993). The proportion of Fe (II) which precipitates as sulfides is dependent on the H_2S/Fe ratio of the vent fluid (Field & Sherrell, 2000); a higher ratio resulting in greater sulfide formation. Within the buoyant plume this is followed by precipitation of the Fe (II) as iron oxyhydroxides and the co-precipitation of elements that exist as oxyanions in seawater; V, P, As and Cr (German et al., 1991a; Feely et al., 1992). Once the Fe-oxyhydroxide particles reach the non-buoyant plume co-precipitation of the oxyanions ceases (German et al., 1991; Feely et al., 1992). Scavenging of elements such

as yttrium, thorium, beryllium and the rare earth elements which began in the buoyant plume continues in the non-buoyant plume and is the dominant process (German et al., 1991a; 1991b).

It has been suggested that this change in co-precipitation/scavenging behaviour may be due to the increase in pH as the plume is diluted by seawater (Ludford et al., 1996). The surface charge of FeOOH particles is affected by pH (Stumm & Morgan, 1996). At a pH of <6.7 the particles have a positive surface charge whereas at pH >6.7 they have a negative surface charge. Hence, the FeOOH particles should initially scavenge anions but once the vent fluids become sufficiently diluted they should start to scavenge cations.

The extent to which each reaction occurs is controlled by the rate at which dissolved Fe (II) is oxidised hence iron plays a major role in the chemical evolution of hydrothermal plumes. In fact iron (II) oxidation is one of the main controls on the chemical processes within plumes.

Redox behaviour of iron in hydrothermal plumes

The rate of oxidation of Fe (II) exerts a major control on the formation of the Fe-oxyhydroxide particles and therefore the rates of other reactions within hydrothermal plumes. Several authors have calculated Fe (II) oxidation half times based on the pseudo first order rate law (Millero et al., 1987);

$$-\frac{d[Fe(II)]}{dt} = k_1[Fe(II)]$$

where $k_1 = k[OH^-]^2\,[O_2]$ and $t_{½} = ln2 / k_1$.

The half time can be calculated either from measured Fe data or from measurements of O_2 and pH (temperature and salinity measurements are also required for this calculation).

In the Atlantic the half-life is rapid with a timescale of minutes. Rudnicki and Elderfield (1993) calculated a half time of 2.1mins based on particulate Fe data (from nephelometry correlations) obtained at the TAG site combined with modelling of time and plume

heights. In contrast half time estimates for the Pacific vary from 12 hours based on pH and O_2 data (Massoth et al., 1998) to 42 hours based on experimental Fe observations (Massoth et al., 1994; 1998). Taking into account the path of global thermohaline circulation, the half time for the Indian Ocean was expected to be intermediate to that of the Atlantic and Pacific. Field and Sherrell (2000) used pH and O_2 data for ambient seawater to calculate expected half times for Fe (II) oxidation in the Atlantic, Pacific and Indian oceans, giving values of 17-27 mins for the Atlantic, 1.3 hrs for the Indian and 3.3-6.4 hrs for the Pacific.

The time scale for a buoyant plume to reach neutral buoyancy (τ) is of the order of one hour (Lupton, 1995; Speer & Helfrich, 1995). This is given by the equation:

$$\tau = \pi N^{-1}$$

where N = the background buoyancy frequency. In other words, this timescale is a function of the surrounding ocean, not the nature of the individual plume. Given that the buoyancy frequency will not vary widely between oceans (since N is a function of density and density gradient), the time to reach neutral buoyancy will be reasonably constant, whereas the Fe (II) oxidation half times vary by an order of magnitude between the Atlantic and Pacific oceans. This means that the proportion of dissolved Fe (II) emitted from a vent that is delivered to the non-buoyant plume will vary systematically along the path of the global thermohaline circulation. Rudnicki & Elderfield (1993) estimated that all of the Fe (II) remaining after sulfide precipitation would be removed from solution ~150m above Atlantic vents which is well before neutral buoyancy will be reached. However, based on their calculated longer half times for the Atlantic, Field & Sherrell (2000) suggest that up to half of the total Fe present at the top of the buoyant plume will still be Fe (II). In the Pacific, slower oxidation rates mean that most of the oxidation probably takes place in the non-buoyant plume (Field & Sherrell, 2000). For the Indian Ocean, if the half time for Fe (II) oxidation is 1.3hrs, then, assuming 100% oxidation after 5 half times (6.5hrs) and current speeds of 2cm/s, dissolved Fe (II) would be completely precipitated and dispersed no further than 1km from the vent site.

Field & Sherrell (2000) adjusted the parameters within their model to assess the sensitivity of Fe oxidation to different conditions. They found that Fe (II) oxidation rates were most sensitive to ambient pH and to a lesser extent, ambient O_2 concentrations.

This is to be expected as the rate constant k_1 has a second order dependence on $[OH^-]$ but only first order dependence on $[O_2]$. Variability in vent fluid chemistry exerted only a minor influence.

Although vent fluid chemistry may not greatly affect the Fe (II) oxidation rates, it does affect the amount of iron that reaches the non-buoyant plume. Hence, vent fluid composition plays a role in the resulting fluxes because it is the iron oxyhydroxide particles that are involved in the scavenging and co-precipitation of other elements from the surrounding seawater. The quantity of Fe reaching the non-buoyant plume depends on the initial losses due to sulfide formation and fallout (Field & Sherrell, 2000) which is dependent on the Fe/H_2S ratio of the vent fluid. Ratios vary from <0.1 at, for example, 17.5°S on the East Pacific Rise in the Pacific Ocean (Charlou et al., 1996) where elemental sulfur has been observed in plume particle samples (Feely et al., 1996), to 24 at the Rainbow hydrothermal site in the Atlantic (Douville et al., 2002). Low Fe/H_2S ratios favour sulfide formation which will minimise the proportion of total Fe delivered to the non-buoyant plume whereas high Fe/ H_2S ratios will result in less sulfide formation and a greater proportion of the initial Fe being delivered to the non-buoyant plume. Hence the global budgets of elements that are co-precipitated or scavenged by Fe are affected not just by ambient conditions at hydrothermal vent sites but also the vent fluid composition.

1.3.3 Metals

The behaviour of many metals within the hydrothermal plume are intimately linked to that of iron. The chalcophile elements (e.g. Cu, Cd, Ag) present in the vent fluids are precipitated as sulfides along with iron in the initial buoyant plume (Mottl & McConachy, 1990). Once the non-buoyant plume is reached these elements show a decreasing ratio with Fe in the particulate phase suggesting that they have either undergone oxidative dissolution or settled out of the plume (Lilley et al., 1995).

Co-precipitation of the oxyanions including P, V and As with the Fe-oxyhydroxide particles takes place within the buoyant plume and ceases once neutral buoyancy is reached. This is apparent from the constant oxyanion/Fe ratio of particles in the non-buoyant plume. German et al. (1991a) found constant ratios up to 1200m from the

source of the TAG hydrothermal plume while Metz & Trefry (1993) have shown that V/Fe ratios remain constant in plume particles for at least 80 days. These particles eventually settle out, forming metal rich sediments.

From observations of Pacific and Atlantic Ocean hydrothermal plumes Feely et al. (1991) found a direct correlation between the P/Fe ratios in hydrothermal plume particles and the ambient dissolved P concentration. Hence in the Pacific where the dissolved P concentration is higher than in the Atlantic, the P/Fe ratio is also higher. For As which has similar dissolved concentrations in both oceans they found that the As/Fe ratio was also similar in both oceans. However V, which also has similar dissolved concentrations throughout the oceans (Middelburg et al., 1988) has a higher V/Fe ratio in the Atlantic than in the Pacific (Metz & Trefry, 1993; Feely et al., 1994a). Feely et al. (1998) further investigated the V/Fe ratios at several sites in the Atlantic and Pacific and demonstrated that there is an inverse correlation between the V/Fe ratio in hydrothermal plumes and ambient dissolved phosphate levels. A suggested reason for this relationship is that P competes more effectively for the sites on the Fe-oxyhydroxide particles and therefore where dissolved P concentrations are high, V/Fe ratios will be low and vice versa (Metz & Trefry, 1993; Feely et al., 1994a). Dissolved P concentrations in the Indian Ocean are intermediate to that of the Atlantic and Pacific Oceans (CLIVAR). Based on the above observations both the V/Fe and P/Fe ratios should also be intermediate to those measured in the Atlantic and Pacific.

Once the non-buoyant plume has been reached, uptake of oxyanions evidently ceases whereas scavenging of a number of other particle reactive species (e.g. REEs, Th and Be) onto the Fe-oxyhydroxide particles continues. Particles in the non-buoyant plume at the TAG hydrothermal site (Atlantic) show an increasing REE/Fe ratio with decreasing iron content, suggesting that scavenging continues as the plume is further diluted and the particles settle out (German et al., 1990). The REE distribution patterns show that their origin is both from the hydrothermal vent fluids and seawater. Sherrell et al. (1999) examined REE data from the East Pacific Rise. Here the picture is complicated by the slower Fe (II) oxidation rates in the Pacific which mean that particulate Fe initially increases with distance from the vent site in the non-buoyant plume despite increasing dilution with ambient seawater. The REE/Fe ratio however, still increases with

decreasing Fe content. Sherrell et al. interpret this to be the result of simple mixing between fresh FeOOH particles and background material re-suspended from the sediments. They suggest that the trends seen in the TAG data result from the drawdown of dissolved REE at high particulate Fe concentrations, however the data of Sherrell et al. does not extend beyond the initial particulate Fe maximum in the non-buoyant plume, therefore it is impossible to discount the possibility that continued adsorption of REEs takes place in this Pacific plume in the same manner as at TAG in the Atlantic. The fact that, in the Pacific, the REE/Fe ratio continues to increase once the particles reach the underlying sediments and that the REE/Fe ratio in the sediments increases with distance off axis from the ridge crest (Owen & Olivarez, 1988; Olivarez & Owen, 1989) also suggests continued adsorption would occur within the plume.

Although hydrothermal vent fluids are enriched in the REEs, this scavenging and subsequent settling of the Fe-oxyhydroxide particles to form metalliferous sediments means that hydrothermal systems are in fact a net sink for the rare earth elements (German et al., 1990).

1.4 This study

The vast majority of studies of hydrothermal activity have been concentrated in the Atlantic and Pacific Oceans which lie at the two extremes of global thermohaline circulation; in effect much of the mid-ocean ridge system remains unexplored. Figure 2 shows the location of known vent sites and sites where the detection of plumes indicate hydrothermal activity but the existence of vents is yet to be confirmed. Further sites have been discovered since the publication of this map; two new vent fields on the southern Mid-Atlantic Ridge (German et al., 2005) and four new vent fields in the Lau Basin in the Pacific (Tivey et al., 2005). The Indian Ocean is an important link between the Atlantic and Pacific ridge systems, both in terms of understanding the evolution of vent fauna throughout the oceans (Tyler et al., 2002; Van Dover et al., 2002) and the impact of variability in hydrothermal chemistry. The effect of the ambient seawater conditions on hydrothermal plume particle formation, especially through iron oxidation, and scavenging is a key component to a better quantification of global hydrothermal chemical fluxes.

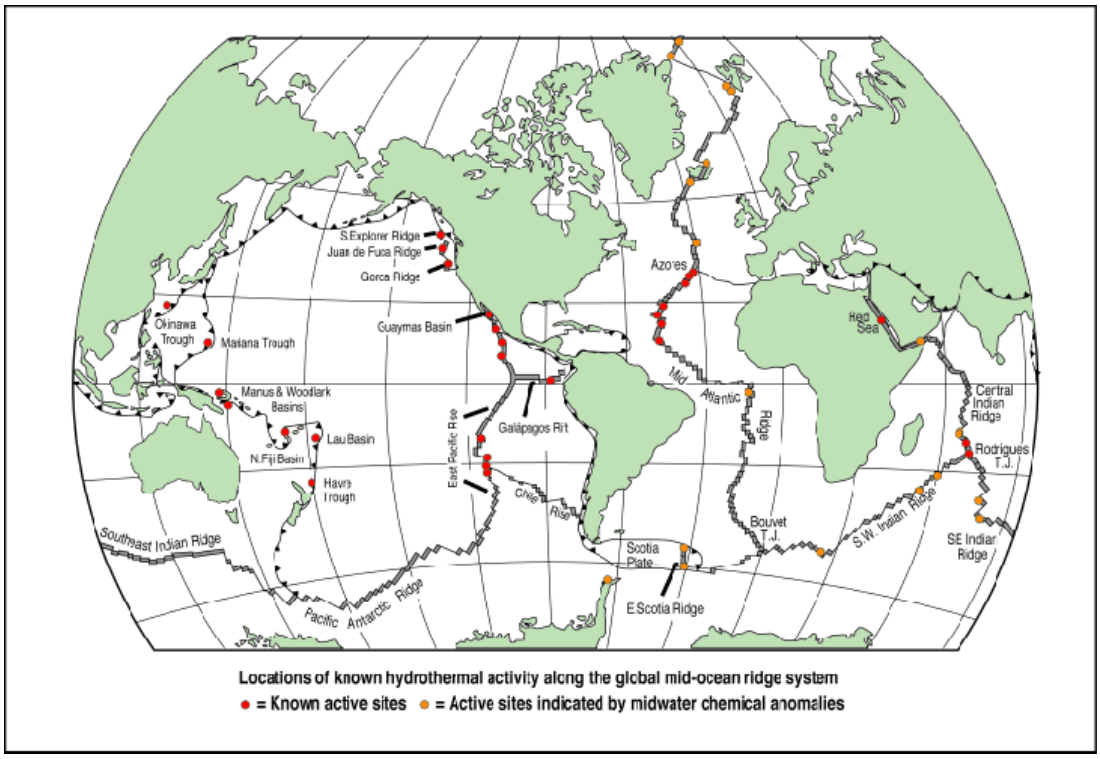

Figure 2 Known sites of hydrothermal venting confirmed from actual observations (red) of the vent site, or inferred from water column anomalies (orange), for example ^{3}He or dissolved Mn (from German & Von Damm, 2004). As indicated in the text, this status is constantly evolving as new sites are discovered.

This study focuses on the Kairei and Edmond vent sites located at 25°19'S, 70°02'E and 23°53'S, 69°36'E respectively, on the Central Indian Ridge, north of the Rodriguez Triple Junction (Fig. 3). The Rodriguez Triple Junction is the convergence point of the three Indian Ocean spreading ridges that separate the Indian, African and Antarctic plates. The Central Indian Ridge (CIR) lies to the North of the triple junction, separates the African and Indian plates and has a full spreading rate of ~50 mm yr^{-1}. The Southeast Indian Ridge (SEIR) separates the Indian and Antarctic plates and has a spreading rate of ~60 mm yr^{-1} while the Southwest Indian Ridge (SWIR) which separates the Antarctic and African plates has a much slower spreading rate of ~16 mm yr^{-1} (Tapscott et al., 1980; Munschy & Schlich, 1989; DeMets et al., 1990; Sempere & Klein, 1995).

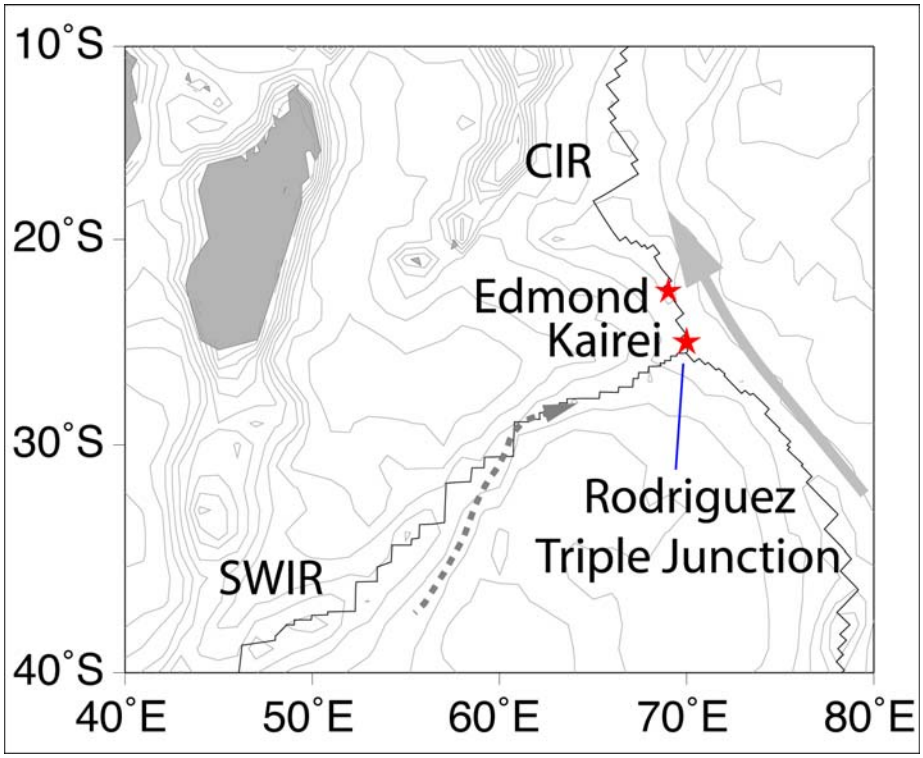

Figure 3 The location of the Kairei and Edmond hydrothermal vent sites near the Rodriguez Triple Junction in the Indian Ocean. Also shown are the paths of the Circumpolar Deep Water (dashed arrow) and the boundary current (solid arrow) mentioned below. (SWIR = South West Indian Ridge, CIR = Central Indian Ridge)

Deepwater circulation near the two vent sites is dominated by the transport of Circumpolar Deep Water (CDW) which is formed predominantly from North Atlantic Deep Water (e.g. van Aken et al., 2004). The majority of the CDW flow is transported east along the southern boundary of the Ocean. Fractures in the SEIR allow this water to flow through to the Eastern Indian Ocean where they form a "reverse flow" western boundary current that passes north-west along the eastern flank of the SEIR and then north along the eastern flank of the CIR (Toole & Warren, 1993). Some of this CDW flows northwards along the eastern flank of the SWIR where fractures allow the water to enter the CIR rift valley (Pollard & Read, 2001).

Hydrothermal plumes were first detected on the Central Indian Ridge in the late 1980's (Pluger et al., 1990; Jean-Baptiste et al., 1992) and in the region of the Rodriguez Triple Junction in 1993 (Gamo et al., 1996) but actual observation of a hydrothermal vent field

did not occur until 2000 at the Kairei site (Gamo et al., 2001). The Edmond vent field was discovered a year later in 2001 (Van Dover et al., 2001). In addition to the Kairei and Edmond vent fields, five more plumes were detected on the Central Indian Ridge between 17°and 20°S in 2001 (German et al., 2001). Hydrothermal plumes have also been detected on the Southeast Indian Ridge (Scheirer et al., 1998) and the Southwest Indian Ridge (German et al., 1998a; Bach et al., 2002).

Results of this study, which is primarily concerned with the hydrothermal plumes at the Kairei and Edmond sites, complement the vent fluid studies of Gamo et al. (2001) at Kairei and those of Gallant & Von Damm (2006) at both Kairei and Edmond. The vent fluids from the Kairei hydrothermal vent were found to have similar physical characteristics and composition to fluids from other basaltic hosted hydrothermal vents along mid-ocean ridges in the Pacific and Atlantic. The main vent fluid characteristics at Kaire and Edmond are detailed in Table 12. The vent fluid temperatures are as high as 365°C at Kairei and 380°C at Edmond, which are at the upper end of the global range of temperatures observed in vent fluids (up to 405°C, see e.g. German & Von Damm, 2004).

The pH of the vent fluids are 3.5 and 3.1 at Kairei and Edmond which are within the range usually observed in fluids from basaltic hosted hydrothermal systems. The alkalinities are also within this range being -0.46 and -0.5 meq/kg respectively (German & Von Damm, 2004; Gallant & Von Damm, 2006). The chlorinities are 640mmol/kg at Kairei and 930mmol/kg at Edmond which are both higher than seawater and at the higher end of the globally observed range (Butterfield et al., 2003). A chlorinity higher than seawater shows that the vent fluids are dominated by the liquid phase from the phase-separated seawater (the temperatures and pressures encountered by the circulating hydrothermal fluids are sufficient to enable phase separation to occur). Consistent with this, are the relatively low H_2S concentrations of 4.0 (Kairei) and 4.7mmol/kg (Edmond) because dissolved gases tend to be concentrated in the vapour phase rather than the liquid phase. Concentrations of H_2S in vent fluids can reach up to 110mmol/kg as at one vent at 9-10°N on the East Pacific Rise (Von Damm, 1995).

At Kairei the Fe and Mn concentrations of 5.4mmol/kg and 840µmol/kg respectively (Gamo et al., 2001) are within the ranges observed for similar hydrothermal vent sites: <0.1 to 18mmol/kg for Fe and 20 to 4500µmol/kg for Mn (Von Damm, 1995; Butterfield et al., 2003). The Fe/H_2S ratio of 1.4 is at the lower end of the overall range of <0.1 to 24 observed in various vent fluids in these environments (Von Damm, 1995; Butterfield et al., 2003), however it is similar to many vent systems such as TAG and MARK in the Atlantic and those on the East Pacific Rise. The Edmond vent fluids have Fe and Mn concentrations higher than those at Kairei; 12.8mmol/kg and 1430µmol/kg respectively (Gallant & Von Damm, 2006). These are also within the range of those previously recorded at other hydrothermal sites with the Fe concentration being at the higher end of the observed range. The Fe/ H_2S ratio of 3.2 is higher than Kairei but is still within the globally observed range. Copper concentrations are high at both vent sites, in fact at Kairei the concentration of 210µmol/kg exceeds the range of 0-162µmol/kg observed to date for all known types of vent and the concentration at Edmond (160µmol/kg) is at the top of this range (German & Von Damm, 2004). Zinc concentrations however are within the range observed (0-740µmol/kg) for basaltic hosted hydrothermal systems. These values are consistent with our existing knowledge of vent fluids: temperature is known to affect the Cu concentrations in vent fluids, generally significant quantities are only observed where the exit temperature of the fluids are ≥ 350°C whereas Zn is less sensitive to temperature (Von Damm, 1990; Von Damm, 1995).

As already discussed the Fe (II) oxidation rates are reported to differ significantly between the Pacific and the Atlantic (Rudnicki & Elderfield, 1993; Massoth et al., 1994; Field & Sherrell, 2000), being much shorter in the Atlantic (half time of 2 to 27 minutes) than the Pacific (half time of 4 to 42 hours). In the Indian Ocean which lies midway on the path of the global thermohaline circulation, redox conditions indicated, prior to this study that the Fe (II) oxidation rate should be intermediate to that of the Atlantic and Pacific Oceans, with a predicted half time of 1.3 hrs (Field & Sherrell, 2000).

1.4.1 Specific objectives

The main issues to be addressed by this study are:

1) **Ascertain whether the different Fe (II) oxidation rate in the Indian Ocean fundamentally affects the processes taking place within the hydrothermal plume, or if we see the same patterns of behaviour previously observed in Atlantic and Pacific Ocean hydrothermal plumes.** This is done by measuring the concentration of particulate elements in hydrothermal plume samples. As discussed in '1.3.3. Metals', three broad patterns of behaviour with respect to Fe have been observed for elements in the particulate phase in Atlantic and Pacific hydrothermal plumes. Briefly, the chalcophile elements (e.g. Cu, Zn, Cd, Pb) show a decreasing ratio with Fe as the plume is diluted suggesting these elements are lost from the plume relative to Fe and that the elements reside in a different phase to Fe (i.e. sulfides), the oxyanions (P, V, As, Cr) exhibit a fixed ratio with Fe throughout plume dilution which implies there is no loss or gain of these elements relative to Fe, while particle reactive elements (REEs, Y, Th, Be) show an increasing ratio with Fe as the plume is diluted suggesting they are scavenged from the surrounding seawater.

2) **Elucidate further the processes taking place in the plume from information on complementary particulate, colloidal and dissolved fractions**. Previous studies of hydrothermal plume processes have mainly focussed on one phase within the plume, either the dissolved phase or the particulate phase. The exceptions to this are James & Elderfield (1996) who measured both particulate and dissolved Fe, Mn, Cu and Cd at the TAG and Snakepit hydrothermal sites in the Atlantic, James et al. (1995) who measured dissolved and particulate Fe and Mn along with a number of other elements in the particulate phase at the Broken Spur site in the Atlantic and Massoth et al. (1994) who measured dissolved and particulate Fe and Mn only, at the Cleft Segment on the Juan de Fuca Ridge in the Pacific Ocean. More specifically this study will:

    a) Measure particulate and dissolved Fe, to allow the calculation of total Fe in the plume samples. In conjunction with the vent fluid concentrations and the dilution factor of the samples, the amount of Fe which has been lost from the plume can

be estimated and compared with the predictions of previous authors (Mottl & McConachy, 1990; Rudnicki & Elderfield, 1993).

b) Measure particulate and dissolved Cu, P and Mn. Although inferences about the behaviour of elements within hydrothermal plumes can be made from the study of just one phase, in some cases, study of the complementary phase is required to confirm the suggested behaviour. For example, it is known that Cu, which precipitates as sulfides soon after emerging from the vent, is lost from the hydrothermal plume as it is diluted. This has been attributed to either the preferential settling of sulfides and/or their oxidative dissolution (German et al., 1991a). If oxidative dissolution is occurring then some enrichment of Cu in the dissolved phase might be expected. As this cannot be determined from the particulate data alone, complementary dissolved phase data are also required.

c) Study the colloidal phase for Fe, Mn and Cu to assess if there are separate processes taking place in this phase. Where the particulate phase has been investigated, either the >1.0μm or >0.4μm fraction has been studied, and for the dissolved phase, it has been the >0.4μm fraction. No attempt has yet been made to study the colloidal phase. As Fe (II) forms Fe (III) colloids (e.g. Honeyman & Santschi, 1989; Wu & Luther III, 1994) when it is initially oxidised, if we are to fully understand the processes taking place within hydrothermal plumes then it is crucial that the colloidal phase is also studied. For this study, 'particulate' samples in the >1.0μm, >0.4μm and >0.1μm size fractions were collected along with complementary 'dissolved' samples in the <0.4μm and <0.1μm size fractions. The purpose of the 0.1μm samples was to enable the first study of the colloidal phase within hydrothermal plumes.

3) **Test the hypothesis that there is a linear relationship between P/Fe or V/Fe in hydrothermal plume particles and ambient dissolved phosphate in the oceans, by measuring these ratios in the Indian Ocean hydrothermal plume samples**. Existing data from Atlantic and Pacific hydrothermal plumes suggests that there is a linear relationship. If this relationship holds true for the Indian Ocean, do these

ratios therefore still have potential as paleo-proxies for past seawater phosphate concentrations?

1.4.2 Thesis structure

In this opening chapter an overview of hydrothermal venting and the current state of research in this field has been presented. The processes known to occur within hydrothermal plumes have been discussed, as well as the background to this study and the issues to be addressed. The contents of the remainder of the thesis are outlined below.

Chapter 2 explains the sampling methods and shows the sampling locations as well as providing details of the analytical methods used.

Chapter 3 focuses on Fe and Mn data only. The depth profiles of light scattering data in conjunction with the dissolved (<0.4μm) and particulate (>0.4μm fraction only) Fe and Mn data as well as other data from the cruise where the samples were collected are used to characterise the hydrothermal plumes at Kairei and Edmond. Losses of Fe from the plume due to sulfide precipitation are estimated using the complementary dissolved and particulate data. Fe (II) oxidation is discussed, again in conjunction with other data arising from the cruise which also allows plume age and *in situ* particulate Fe estimates.

Chapter 4 discusses the >1.0μm particulate samples which were collected via *in situ* filtration. The results are compared with earlier studies of similar hydrothermal plume samples in order to determine whether Fe (II) oxidation appears to be affecting the processes within the plume.

In Chapter 5 the main theme is the >0.4μm particulate samples which were filtered once the hydrothermal plume water samples were back on board the ship. These are also compared to earlier studies of hydrothermal plume samples of the same size fraction. Also discussed in this chapter are the findings arising from the different size fractions

which were sampled, as well as the relationship of the P/Fe and V/Fe ratios with ambient dissolved phosphate in the Indian Ocean.

Chapter 6 synthesizes the conclusions of this study and gives recommendations for future work to advance research in this field.

2 Chapter 2 Sampling and Methods

2.1 Sampling

Sampling took place during the RRS Charles Darwin cruise CD128 to the Indian Ocean in May/June 2001. Samples were collected from hydrothermal plumes overlying both the Kairei and Edmond vent sites in the region of the Rodriguez Triple Junction (Fig. 4), with particular focus on the Kairei site. At Kairei, samples were taken at locations ranging from 100m to 4km away from the actual vent site and at Edmond, between 20 and 500m from the vent field location. Background profile samples were also taken from the ridge flanks and the rift valley. Details of each sampling station are shown in Table 1 and the locations of the main CTD stations are illustrated in Figs. 6 and 7.

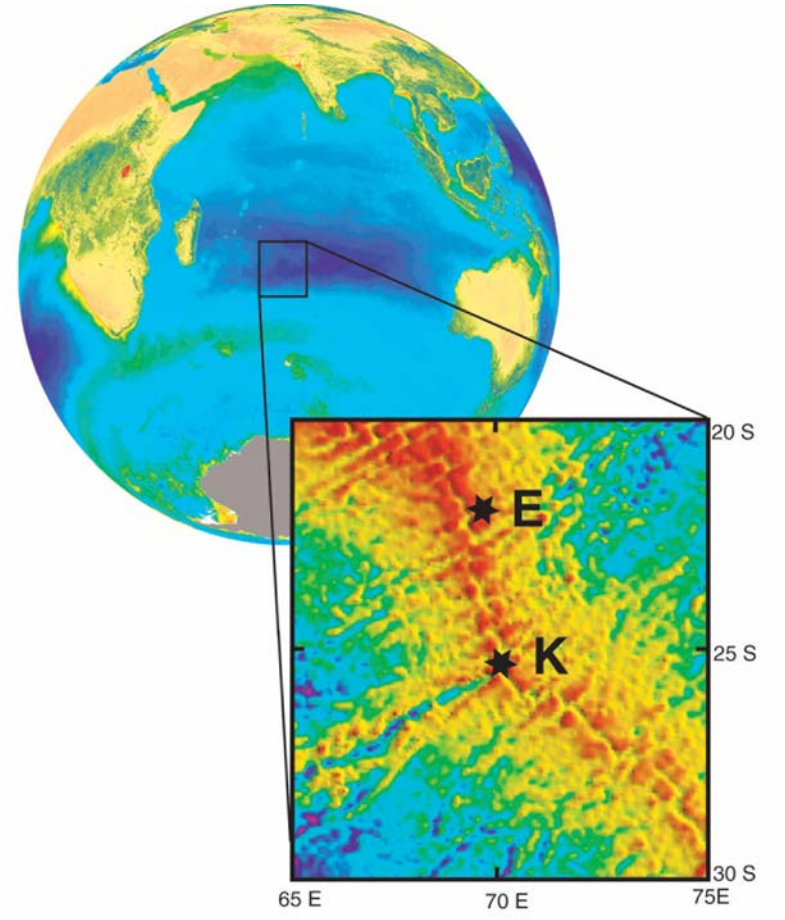

Figure 4 The location of the Kairei (K) and Edmond (E) hydrothermal vent sites at depths of ~2450m and 3300m respectively, near the Rodriguez Triple Junction in the Indian Ocean. The inset diagram shows the topography of the region where red is the shallowest and blue is the deepest topography.

Station	Latitude (S)	Longitude (E)	Approximate distance from vent site (km)	SAPs samples (>1.0µm) if applicable	
				Depth (m)	Additional sample identifier
Kairei	**25°19.17'**	**70°02.40'**			
CTD 02	25°19.63'	70°02.80'	1.09	2248	
CTD 04	25°18.59'	70°01.92'	1.34	n/a	
CTD 05	25°19.28'	10°02.56'	0.34	n/a	
CTD 06	25°18.43'	70°01.82'	1.68	n/a	
CTD 07	25°19.33'	70°02.50'	0.34	2354	
CTD 10	25°17.77'	70°00.69'	3.87	n/a	
CTD 11	25°17.82'	70°00.32'	4.29	2400	
CTD 17	25°19.30'	70°02.59'	0.40	2293	
CTD 18	25°19.10'	70°02.10'	0.52	2342	
CTD 19	25°18.77'	70°01.89'	1.13	2323	
CTD 20	25°19.29'	70°02.46'	0.24	2273	
CTD 21	25°19.20'	70°02.45'	0.10	2298	
Edmond	**23°52.69'**	**69°35.83'**			
CTD 01	23°52.63'	69°36.11'	0.49	2900	
CTD 23	23°52.72'	69°35.86'	0.08	2799	
SAP01	23°52.70'	69°35.86'	0.02	2600	s/n001
				2800	s/n002
				2850	cosap02
				2900	s/n003
				2950	cosap04
SAP02	23°52.63'	69°35.79'	0.13	2800	s/n001
				2900	s/n002
				3000	cosap02
				3100	s/n003
				3200	cosap04
Background					
CTD 16	24°41.40'	71°07.89'	Ridge flank background profile		
CTD 22	25°25.97'	70°03.03'	Rift valley background profile		

Table 1. CTD stations where samples were collected. Locations including distance from vent sites are shown. Where stand alone pumps (SAPs) were deployed their depths are shown, 'n/a' are CTDs where the SAPs were not deployed.

Seawater samples were collected in 10 litre Niskin bottles; sample depths were chosen based on real time light scattering anomalies recorded by the Seatech Light Scattering Sensor mounted on the CTD rosette. One litre of seawater from each Niskin bottle sample was filtered under nitrogen pressure of about 0.8 atmospheres, through an in-line mounted 47mm Whatman Cyclopore 0.4µm filter. At sampling stations CTD 7 and CTD

23, another 1 litre of seawater from each Niskin bottle was also filtered through a 47mm Whatman Cyclopore 0.1µm filter. The seawater samples were acidified with 1ml of 14M sub-boiled distilled HNO_3 while the filters were placed in sealable plastic petri dishes in re-sealable plastic bags and frozen.

Figure 5 CTD rosette showing deployment of 3 stand alone pumps (SAPs) mounted at the top of the frame.

Additionally, at some CTD stations, stand alone pumps (SAPs) were deployed on the CTD rosette to collect large volume particulate samples by in-situ filtration through 293mm Nucleopore polycarbonate 1.0µm filters (see Fig. 5 above). Deployment on the CTD rosette allowed optimum sampling within the plume using the real time CTD data. Stand alone pumps were also used at two locations close to the Edmond site without the CTD; at these locations five pumps were deployed simultaneously from the stern of the ship on a plastic coated wire to collect large volume particulate samples through the plume.

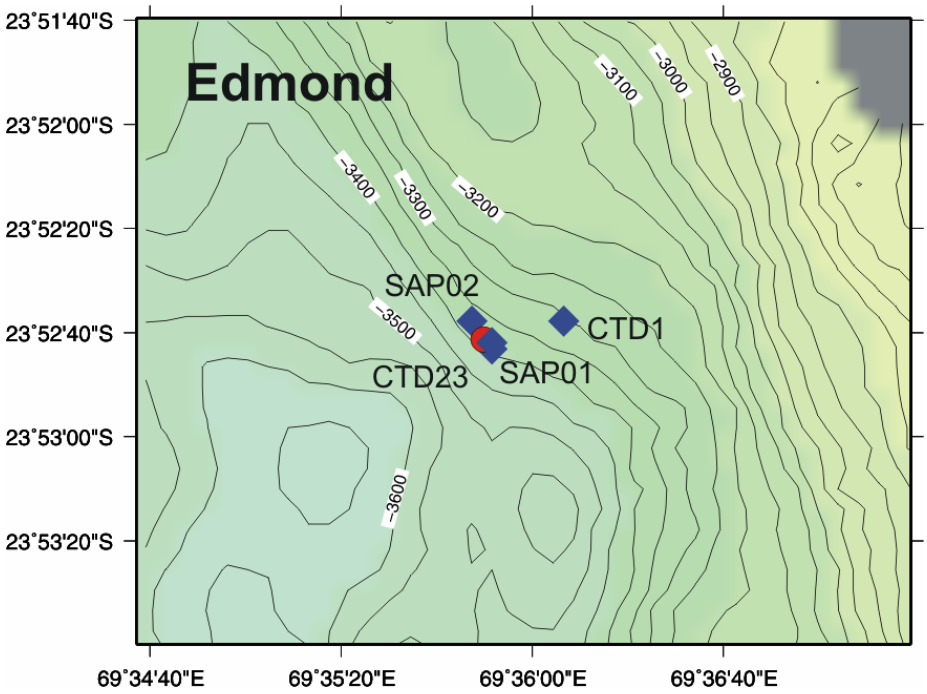

Figure 6 Contour map of the Edmond hydrothermal vent site area showing the locations of the vent (red circle) and the CTD stations and stand alone pump (SAP) deployments (blue diamonds).

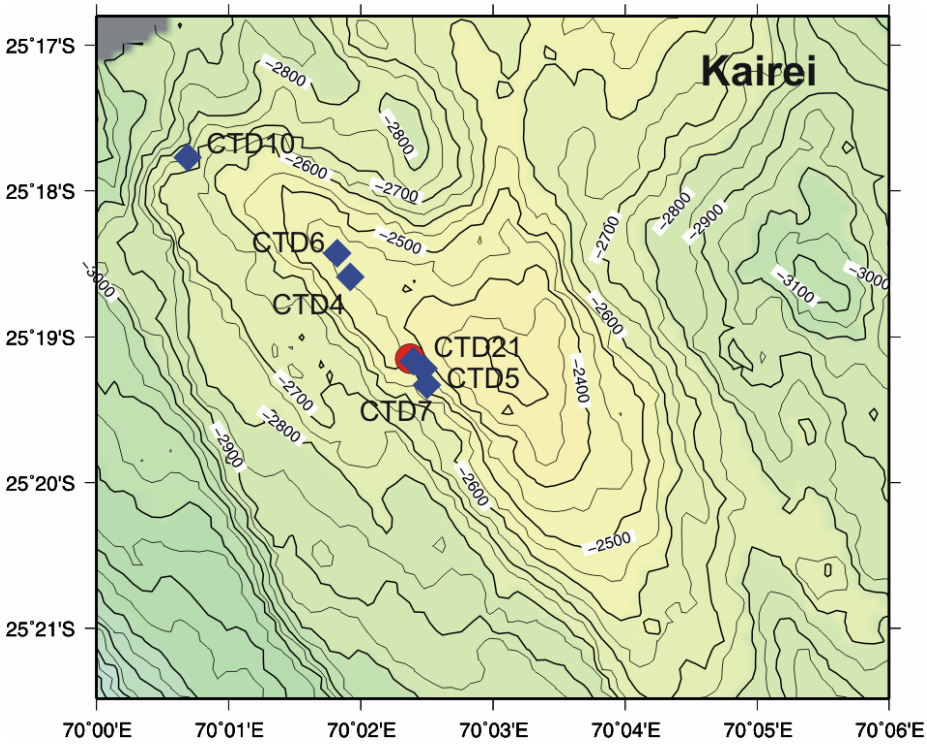

Figure 7 Contour map of the Kairei hydrothermal vent site area showing the location of the vent (red circle) and the locations of the main CTD stations (blue diamonds).

2.2 Determination of dissolved Fe, Mn and Cu in filtered hydrothermal plume samples

A number of methods have been used to determine the concentration of dissolved iron, manganese and copper in seawater for both shipboard and laboratory analysis. Due to the low concentrations (nanomolar) of these elements in seawater, most methods involve a pre-concentration step followed by analysis; there are also methods for the direct analysis of trace metals in seawater. The main pre-concentration methods involve either complexation with a chelating agent, followed by solvent extraction (Danielsson et al., 1978; Bruland et al., 1979; Statham, 1985) or the use of a chelating ion exchange resin such as Chelex-100 (Kingston et al., 1978; Bruland et al., 1979) or 8-hydroxyquinoline (Obata et al., 1993).

The method used here was complexation with ammonium pyrrolidine dithiocarbamate (APDC) and diethylammonium diethyl dithiocarbamate (DDDC) followed by solvent extraction with chloroform after Bruland et al. (1979) and Statham (1985). This method is well established at Southampton, having been used successfully for many years. The efficiency of recovery for each element is dependent on the pH at which the extraction is performed (Kinrade & Van Loon, 1974; Danielsson et al., 1978; Statham, 1985). Iron and manganese can be successfully co-extracted by adjusting to a pH of 6.5-7.5 (D. P. Connelly, pers. comm.), however copper must be extracted at a lower pH of 4.5–5.0.

2.2.1 Cleaning Procedures

Teflon separatory funnels

The funnels were initially acid cleaned by immersing in 50% (v/v) HCl for one week, rinsing in Milli-Q water, then immersing for a further week in 50% (v/v) HNO_3 before rinsing in sub boiled distilled (SBD) water.

Prior to each batch of extractions, the funnels were further cleaned by adding 3ml each of complexant and chloroform, shaking for 30mins and discarding the complexant and

chloroform. A 10% HNO_3 solution was placed in the funnels during storage between processing batches of samples.

Teflon screw cap vials

The vials (Savillex, 15ml capacity) were initially cleaned by washing with micro detergent, rinsing in Milli-Q water and soaking for one week at room temperature in a 50% HCl solution. They were then rinsed in SBD water, soaked for a further week at room temperature in a 50% HNO_3 solution, rinsed in SBD water and dried in a Class 100 laminar flow cabinet (after Kremling et al., 1999).

Plastic ware

Pipette tips, sample storage vials and sample cups (for atomic absorption spectroscopy analysis) were cleaned by soaking in a 25% HNO_3 solution for one week at room temperature, rinsed in SBD water and dried in a Class 100 laminar flow cabinet.

Teflon bottles used for reagent storage were soaked for one week at room temperature in a 50% HCl solution, rinsed in Milli-Q water, soaked for a further week at room temperature in a 50% HNO_3 solution, rinsed in SBD water and dried in a Class 100 laminar flow cabinet (Moody & Lindstrom, 1977).

2.2.2 Preparation of reagents

Sub boiling distilled water

Milli-Q water was further purified by sub boiling distillation in a quartz still. In this method, the water is radiatively heated without boiling. The vapour condenses on a quartz finger cooled by circulating water and is collected via a tube into a clean Teflon bottle. Radiative heating prevents aerosol formation that can lead to unpurified water being carried over in conventional distillation.

Ammonia solution

Purified ammonia solution was prepared by isothermal distillation. A Teflon bottle containing SBD water was placed in an airtight container containing analytical reagent grade ammonia solution. The ammonia equilibrates between the two solutions leading to an ultra pure ammonia solution.

Chloroform

Primar trace metal analysis grade chloroform (Fisher Scientific) was certifiably pure enough (Fe concentration <0.05ppm, Mn <0.005ppm and Cu <0.01ppm) to be used without further purification. Analytical blanks confirmed these low metal concentrations in the chloroform.

Complexant

The complexant was prepared using 2% (w/v) ammonium pyrrolidine dithiocarbamate and 2% (w/v) diethylammonium diethyl dithiocarbamate in SBD water. The solution was filtered through a Whatman No1 filter, placed in a Teflon separatory funnel and purified of metals by extraction with Primar chloroform. The extraction was done using 3ml of chloroform, shaking for 6 minutes and then discarding the chloroform. This procedure was repeated 10 times. The complexant solution was stored in a Teflon bottle in the refrigerator and used within 48 hours, after this time the complexant solution becomes unstable and extraction efficiency is unpredictable (Kremling et al., 1999).

Sub boiling distilled nitric acid

Analytical reagent grade concentrated nitric acid was further purified by sub boiling distillation in a quartz still as previously described for sub boiling distilled water.

2.2.3 Pre-concentration and extraction of trace metals from seawater

All procedures were carried out in a clean wet station within a class 100 clean room. The Teflon separatory funnels were cleaned using the procedure described in '2.2.1 Cleaning Procedures'. Samples were extracted in batches of ~30. At the start and end of each batch of samples, four blanks were run using ~100ml of SBDW, 3ml of complexant and 3ml of chloroform (ammonia solution blanks were determined separately). It was only necessary to make up one batch of complexant for each set of samples since the samples could be processed within the 48hrs in which it is necessary to use the complexant.

For each seawater sample, 100ml was placed in a separatory funnel. The appropriate amount of ammonia solution required to bring the acidified samples back into the required pH range (~6.5-7.5 for Fe and Mn, 4.5-5.0 for Cu) for trace metal extraction was added (this was determined by taking a 20ml sub-sample and adding NH_3 solution until the required pH was reached and calculating the amount required for 100ml) and the samples then shaken. Chloroform (3ml) and complexant solution (3ml) were added and the samples mixed on a rotating device for 6 minutes. The $CHCl_3$ and seawater phases were allowed to separate and the $CHCl_3$ layer drained into a 15ml Teflon screw cap pot. Next, 2ml each of chloroform and complexant was added to the aqueous fraction and the samples mixed for another 6 minutes before allowing separation and draining of the new chloroform layer, combining it with the first. This last step was repeated once more. The funnels were then taken through a cleaning step using 2ml each of complexant and $CHCl_3$, shaking for 6mins, then discarding the complexant and $CHCl_3$.

The extracted samples were acidified with 100µl of SBD conc. HNO_3 and dried down on a hotplate at ~75°C, a further 50µl of SBD conc. HNO_3 was added to re-dissolve the sample and again dried down. This step oxidises any organic residue and breaks down the dithiocarbamates (Bruland et al., 1979). The sample was then re-dissolved in 100µl of SBD conc. HNO_3 and diluted to a total volume of 1ml with 900µl of SBD H_2O and transferred to a sample vial. Sample vials were placed in racks, in re-sealable polythene bags and stored in a refrigerator to reduce evaporative losses. The whole process provides a concentration factor of 100 times.

2.2.4 Determination of iron, manganese and copper in pre-concentrated samples using Graphite Furnace Atomic Absorption Spectroscopy

All samples were measured on a Varian SpectrAA 300 Zeeman Atomic Absorption Spectrometer with Varian Zeeman Graphite Furnace Atomiser and all analyses were carried out using pyrolytically coated partitioned graphite tubes. The manufacturer's recommended furnace operating conditions were followed for copper but for iron and manganese, the cleaning step and atomisation stage were adjusted slightly from the manufacturers recommended settings. Varian recommend a 2 second step at 2300°C for Fe and 2400°C for Mn, which is the same temperature as the atomisation stage for each element. However, this did not clean the tube successfully as carry over effects were observed. A 2 second step at a higher temperature of 2600°C for both Fe and Mn resolved the problem. For the atomisation stage, Varian recommend that the gas flow is turned off. However, the absorbances recorded for Fe and Mn over the chosen calibration range (up to 100µg/l for Fe and 50µg/l for Mn) without gas flow were too high, i.e. they exceeded the absorbance at which the concentration versus absorbance relationship remains linear, hence some gas flow was introduced at the atomisation stage to bring the absorbance back into a linear range. The resulting absorbances were still found to be consistent.

A mixed Fe, Mn and Cu 1000µg/l stock standard solution was prepared from commercially available standards (Z-tek) and working standards were freshly prepared from this stock solution for each batch of measurements. Four replicate measurements were made for each sample; where the relative standard deviation of the mean of the measurements exceeded 5% and there was no obvious outlier, the measurement was repeated.

As previously mentioned, blanks were determined by extraction of SBD water. For Fe, the blanks varied from 0.2 to 0.5nmol/l between batches while the detection limits (3σ of the blank) were 0.2 to 1.1nmol/l. For Mn, blanks were from <0.01nmol/l to 0.04nmol/l, detection limits were 0.15nmol/l or less. Cu blanks varied from 0.04nmol/l to 0.35nmol/l while the detection limit varied from 0.08nmol/l to 0.7nmol/l. These figures are

summarised in Table 2 along with the precision of the analyses and the extraction efficiencies which are discussed below.

Precision was determined by replicate extractions of a laboratory low metal seawater (LMSW) standard. For each batch of ~30 samples, between 4 and 6 LMSW extractions were carried out. The Fe, Mn and Cu concentrations of the LMSW were 81.1 ± 3.7nmol/l, 4.3 ± 1.1nmol/l and 1.4 ± 0.3nmol/l respectively. For Fe, the precision varied from 4.1% to 13.4% between batches. For Mn, precision varied between 3 and 5.5% except for one batch, which was 13.7%. The precision for the Cu LMSW measurements varied between 9 and 25%.

Extraction efficiency was determined by extraction of NASS 5 certified seawater reference material for trace metals (National Research Council Canada); for Fe it was 106 ± 12%, for Mn, 119 ± 12% and for Cu, 104 ± 12% when all data except outliers are considered. Although the Mn extraction efficiency could be cause for concern, results for some samples which had previously being extracted in batches where the NASS 5 extraction efficiency was 100 ± 5% for Mn were compared to results from batches where the efficiency was higher than 100% and were found to be consistent. A number of contributory factors could account for the higher than expected Mn recoveries, e.g. the prolonged use of Teflon separatory funnels with dithiocarbamates can lead to degradation of the funnel walls which leads to carry over of trace metals from one extraction to the next (Muller et al., 1991). This may also explain the poor precision of the Cu measurements which were the final extractions to be carried out after the funnels had been used for many other extractions.

Element	Blanks (nmol/l)	Detection Limit (3σ)	Precision (%)	Extraction efficiency (%)
Fe	0.2 – 0.5	0.2 – 1.1	4.1 – 13.4	106 ± 12
Mn	<0.01 – 0.04	≤ 0.15	3 – 5.5 (13.7)	119 ± 12
Cu	0.04 – 0.35	0.08 – 0.7	8 - 25	104 ± 12

Table 2 Analytical performance of method for trace metals in filtered hydrothermal plume samples. Precision is the relative standard deviation of the replicate LMSW measurements where n = 4 to 6 (n = number of samples)

2.3 Stand Alone Pump (SAP) >1.0µm Particulate Samples

The SAP particulate samples were collected and digested by Hedy Edmonds (University of Texas Marine Science Institute) who then provided a 5ml aliquot of the digested filters for further analysis at Southampton. The 293mm Nucleopore filters were digested by placing them in 30ml acid cleaned Savillex Teflon vials and refluxing for 72 hrs with 20ml of hot concentrated Seastar grade nitric acid.

2.3.1 Major element analysis by ICP/AES

The following elements were determined by Inductively Coupled Plasma Atomic Emission Spectroscopy (ICP/AES): Fe, Mn, Al, Mg, Ca, P, V, As, Cu, Zn, Y and Na. La, Ce and Pb were also attempted but although the concentration of the elements within the samples was well above detection limits, the calibrations were unsuccessful (data were very scattered). These elements were later measured using ICP/MS (Inductively Coupled Plasma Mass Spectrometry).

Sample preparation

The expected concentrations of the minor elements (Y, La, Ce, Pb) meant that the digested samples needed to be measured without dilution. However, the ICP/AES procedure requires samples to be in dilute acid (0.6M HCl or 0.8M HNO_3) whereas the digested samples were still in concentrated nitric acid. Therefore, a 2ml sub-sample of each sample digest was taken using a hand pipette and placed in a 15ml Savillex Teflon screw cap vial (the Savillex Teflon vials had previously been acid cleaned by immersing in 50% nitric acid at a temperature of 50-60°C for ~48hrs, rinsing in SBD water and allowing to dry in a Class 100 laminar flow cabinet). The vials containing the sub-samples were placed on a hotplate at moderate temperature and allowed to gently evaporate to dryness. The resulting residue was re-dissolved in 200µl 8M HNO_3, made up to a total volume of 2ml with 1.8ml H_20 and transferred to an acid cleaned sample vial (see '2.2.1 Cleaning Procedures' under 'Plastic ware').

Several blanks were processed and measured. At one CTD station during sample collection, the stand alone pumps were deployed on the CTD rosette but not switched on, these filters serve as complete sample processing blanks (referred to as 'dip blanks'). When the sample filters were digested, new filters straight from the box were also processed. Finally, when the 2ml sub-samples were dried down and re-dissolved, blanks of 2ml conc. HNO_3 were processed (referred to as 'procedural blanks').

Analysis of samples by ICP/AES

The samples were measured on a Perkin Elmer Optima 4300DV Optical Emission Spectrometer with a dedicated AS 93plus Autosampler. A glass concentric nebuliser (manufactured by Glass Expansion pty) was used, the sample uptake rate was set to 0.95ml/min and the carrier gas (Argon) flow rate to 0.85l/min. A glass cyclonic spray chamber was used as these have high solution transport rates, good stability and good matrix effect characteristics (Green et al., 2003). Five multi-element standards were prepared from commercially available standards (Fisher Scientific and VWR Aristar), the proportions of the major elements within each standard were varied to enable identification of any interference issues. The majority of the elements were measured using axial plasma view with the exception of Ca, Mg, Mn and Fe which were viewed radially. Axial orientation generally has a higher sensitivity than the radial orientation but this does vary as a function of wavelength. Results are the mean of three replicate measurements.

External precision for the ICP/AES analysis was calculated from 10 replicate measurements of one of the standard solutions and found to be better than 1.5% for all elements except As which was 9.7%. Unfortunately the nature of the sampling means that there are no replicate samples and therefore it is not possible to calculate precision for the whole analysis. Limits of detection (calculated as 3 times the standard deviation of 10 replicate blanks) were less than 1.3µg/l for Al, Mn, Mg, V and Y. For Cu and Fe, they were less than 2.7µg/l, while for Ca, P, Zn and As they varied from 8.3 to 14.3µg/l. Although some of these limits of detections (those for Al, Mn, Mg, Cu, Fe and Zn) are higher than typically observed for this technique and the instrument used (D. Green, pers. comm.) the concentrations recorded in the samples were well above these limits (see Appendix 1 for full details of limits of detection and precision).

2.3.2 Rare earth and minor element analysis by ICP/MS

The rare earth elements (La, Ce, Nd, Dy, Pr, Sm, Gd, Er, Yb, Eu, Tb, Ho, Tm, Lu) and Pb and Cd were measured using Inductively Coupled Plasma Mass Spectrometry (ICP/MS).

Sample preparation

A 1ml sub-sample of each sample digest was taken using a hand pipette, placed in a 15ml Savillex Teflon screw cap vial (which had been acid cleaned using the same procedure described under 'Sample preparation' in '2.3.1 Major element analysis by ICP/AES') and placed on a hotplate at moderate temperature to slowly evaporate to dryness. The resulting residue was then re-dissolved in 2ml of 2% HNO_3 which had been spiked with 10µg/l In, Re, Ga and Bi to act as an internal drift monitor for the ICP/MS measurements. In some cases the sample residue proved resistant to dissolution and it was necessary to place the sample vials in an ultrasonic bath to aid their dissolution. Blanks were also processed in this manner.

Analysis of samples by ICP/MS

The samples were measured on a VG PlasmaQuad PQ2+ ICP/MS by external calibration using rock standards BIR-1 and BRR-1 (US Geological Society) and JB-3 and JB-1 (Geological Survey of Japan standards) which were spiked with 10ppb of In, Re, Ga and Bi to act as an internal drift monitor. Four multi-element standards were also prepared from commercially available standards (Fisher Scientific and VWR Aristar) to be used as an independent check, these were also spiked with 10µg/l of In, Re, Ga and Bi. Before the sample run the ICP/MS was tuned for optimum sensitivity and stability using a multi-element tuning solution containing Co, Y, In, La, Re, Bi, and U. Once tuned, the instrument was then left for a further 30 minutes to fully stabilise. During this time a random order sampling procedure for the samples, standards and various blanks (with a drift monitor solution run every 6 samples) was entered in to the ICP/MS software. Data was then acquired in peak-jumping mode, for a total of 2 minutes per sample/standard/blank analysis (4 x 30 second repeats). After each analysis, a wash

solution containing 2% HNO_3 was run until background levels were achieved (3 minutes). The data quality was monitored throughout the run by examination of the statistics produced after each analysis. Any anomalous results were noted and re-run at the end of the procedure. Following completion of the run, the raw integrated count per second data was exported from the ICP/MS processing software by spreadsheet. The data processing procedure applies a blank, interference, drift and internal (matrix) correction to the raw data and then performs a multi-standard calibration based on the recommended values (Govindaraju, 1994) of the rock standards that were also run during the procedure.

Internal precision of the 4 x 30 second repeat measurements was better than 4.1% for all elements except Cd which was 12.1%. External precision, which was calculated from repeated measurements of the same standards over several runs, varied from 2.9 to 8.5% and accuracy (i.e. comparison of the reference values of the rock standards to the measured value) varied from 1.4 to 7.8%. Limits of detection were 2-5ng/l for La through to Sm, except for Ce which was 9ng/l and ≤1ng/l for Eu through to Lu, for Pb it was 0.5µg/l and for Cd it was 10ng/l. Concentrations for all samples for all elements were above the limits of detection (see Appendix 1 for full details of limits of detection, precision and accuracy).

2.4 Niskin >0.4µm Particulate Samples

2.4.1 Filter Digest Method

The following procedure was carried out in a laminar flow hood in a Class 1000 clean room. The method for leaching the particulate matter from the filters follows that of German et al. (1991a) which is suitable for the digestion of hydrothermal sulfide and oxide phases. Each 47mm filter was placed in 20ml of concentrated sub-boiling distilled (SBD) nitric acid in a 30ml Savillex Teflon screw cap vial (which had been acid cleaned using the same procedure described under 'Sample preparation' in '2.3.1 Major element analysis by ICP/AES'). The vials were then heated to reflux on a Teflon hotplate for between 36 and 48 hours at which point the filters were brittle and just beginning to disintegrate.

To analyse the samples using ICP/AES they were required to be in a 0.8M HNO_3 solution. The predicted concentrations of the elements of interest were too low to allow a straightforward dilution of an aliquot of the conc. HNO_3 digest, hence, the resulting solutions were carefully pipetted into 15ml Savillex Teflon screw cap vials (acid clean as described previously) and placed on a Teflon hotplate to evaporate. Each filter was also washed by adding two separate aliquots of 20ml of SBD water to the 30ml vials. The water from each wash was added to the leach solution (again by carefully pipetting from the 30ml vials) as it evaporated. Eventually the whole solution was evaporated to dryness. The resulting residue was re-dissolved in 1ml of 8M HNO_3, made up to 10ml using 9ml of SBD water to give a 0.8M HNO_3 solution and transferred to an acid cleaned sample vial.

2.4.2 Major Element Analysis by ICP/AES

Concentrations of the following elements within the leach solutions from the 47mm filters were determined by Inductively Coupled Plasma Atomic Emission Spectroscopy (ICP/AES): Fe, Mn, Al, Mg, Ca, P, Cu, Zn and Na.

The samples were measured on a Perkin Elmer Optima 4300DV Optical Emission Spectrometer with a dedicated AS 93plus Autosampler. Five multi-element standards were prepared from commercially available standards (Fisher Scientific and VWR Aristar), the proportions of the major elements within each standard were varied to enable identification of any interference issues. Results are the mean of three replicate measurements.

External precision for the ICP/AES analysis was calculated from 10 replicate measurements of one of the standard solutions and found to better than 1.0% for all elements except Al (4.0%). Precision for the whole analysis cannot be calculated as the nature of the sampling means there are no replicate samples. The limits of detection were less than 0.5µg/l for all elements except P, which was 1.8µg/l; this is still well below the concentrations measured in the samples (see Appendix 1 for full details of limits of detection and precision).

3 Chapter 3 Iron and manganese CTD profiles and iron oxidation

3.1 Introduction

Because of their elevated concentrations in hydrothermal vent fluids, iron (Fe) and manganese (Mn) serve as important tracers of hydrothermal plume extent and nature. In this chapter, dissolved (<0.4μm) Fe and Mn data for a number of CTD profiles from the Edmond and Kairei hydrothermal plumes are presented, together with complementary particulate (>0.4μm) Fe and Mn data for selected CTD profiles. All such data are presented in combination with light scattering sensor data (which is also an important tool in hydrothermal plume characterisation) in order provide the context and setting of these hydrothermal plumes.

The availability of both dissolved and particulate data allows the total Fe within the plume to be calculated, which, in conjunction with the dissolved Mn data, allows estimates of Fe loss from the plume to be obtained. In combination with Fe (II) oxidation data for the Kairei and Edmond hydrothermal plumes, as determined by Statham et al. (2005), *in situ* particulate Fe is also estimated, together with the plume ages of particular samples.

Hydrothermal plume samples were collected in Niskin bottles mounted on a CTD rosette. Upon recovery aboard ship these samples were filtered through 0.4μm filters in a trace metal free environment. A full description of sampling and analytical methods was given in Chapter 2.

3.2 Results

3.2.1 CTD profiles and dissolved (<0.4μm) Fe and Mn

Dissolved (<0.4μm) iron and manganese data from the filtered hydrothermal plume samples collected at the Kairei and Edmond sites are shown in Table 3. CTD locations at Edmond and Kairei are shown in Figures 6 and 7 (Chapter 2) and the location of the

dissolved samples relative to the vent and plume for the Kairei site are shown in Figure 8 below. Concentrations for Fe range from 3.9nmol/l to a maximum of 370nmol/l for the Kairei samples and from 7.3nmol/l to 350nmol/l at Edmond. For Mn, the concentrations range from 1.0nmol/l to a maximum of 120nmol/l near Kairei and from 2.9nmol/l to 130nmol/l for the Edmond samples. These values are high compared to Mid-Atlantic Ridge hydrothermal plumes; both the Fe and Mn values at Kairei and Edmond are higher than the maximum concentrations of 100nmol/l and 40nmol/l respectively, reported from the TAG hydrothermal plume (James & Elderfield, 1996). Other hydrothermal plumes in the Atlantic have even lower reported maximum dissolved Fe and Mn concentrations, e.g. at Snakepit the values are 85nmol/l and 32nmol/l respectively (James & Elderfield, 1996), at Broken Spur they are lower still, 32nmol/l and 14nmol/l respectively (James et al., 1995). The Kairei and Edmond concentrations are also higher than those observed at the Cleft segment on the Juan de Fuca Ridge in the Pacific Ocean (130nmol/l and 110nmol/l respectively (Massoth et al., 1994)) and also on the Gorda Ridge (70nmol/l and 40nmol/l respectively (Massoth et al., 1998)) but are comparable to values observed on the East Pacific Rise where the maximum [Fe] was 320nmol/l and the maximum [Mn] was 190nmol/l (Field & Sherrell, 2000).

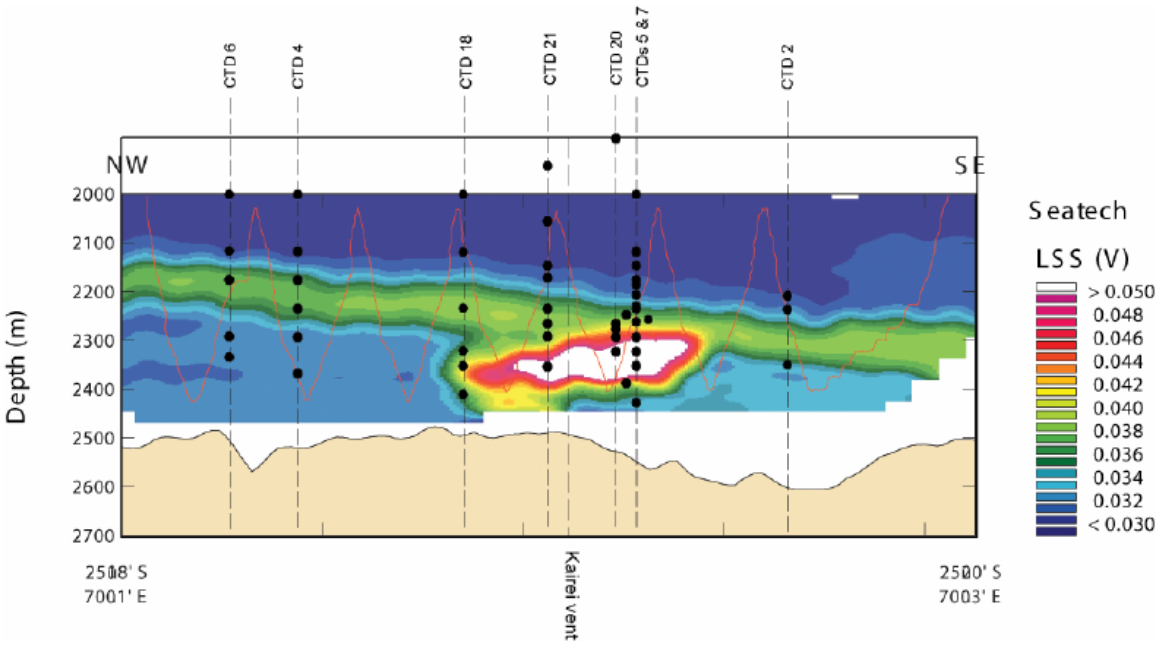

Figure 8 Contoured NW-SE cross-section of optical backscatter signals obtained by CTD tow-yo through the Kairei hydrothermal plume (red trace). Hottest colours indicate location of buoyant plume interception. Vertical black lines and circles show locations of 8 further vertical CTD casts with Niskin bottle sampling depths projected onto this tow-yo section for context.

CTD #	Depth (m)	Dissolved (<0.4µm) Fe (nmol/l)	Dissolved (<0.4µm) Mn (nmol/l)
		Kairei	
CTD 4	2076	18.4	1.4
	2175	31.2	10.0
	2224	27.8	9.3
	2273	36.3	9.3
	2322	26.1	8.0
	2383	27.5	8.4
CTD 5	2076	7.5	2.7
	2150	110	32.1
	2175	332	123
	2199	290	77.5
	2224	368	107
	2248	302	94.6
	2273	254	94.3
	2295	58.8	17.9
	2322	54.6	18.0
	2347	19.5	6.3
	2373	21.3	6.1
	2435	16.1	6.5
CTD 6	2076	3.9	1.4
	2174	7.1	2.5
	2224	15.1	4.1
	2273	18.6	4.6
	2321	41.9	11.7
	2357	37.5	8.1
CTD 7	2176	41.8	80.7
	2232	21.4	7.2
	2268	75.4	24.1
	2273	43.0	11.5
	2320	26.2	6.7
	2322	50.9	15.2
	2347	11.9	5.0
	2371	191	63.7
CTD 10	1978	8.9	0.7
	2175	23.1	9.5
	2224	19.9	2.2
	2273	28.9	7.0
	2297	29.9	8.3
	2322	26.3	7.8
	2347	26.2	7.2
	2371	13.1	4.1
CTD 18	2076	6.3	1.2
	2272	15.4	3.5
	2322	18.4	5.2
	2345	20.4	6.9
	2371	9.6	2.6
	2420	7.2	2.2
CTD 20	1980	31.3	1.0
	2273	12.2	2.2
	2298	77.4	21.9
	2307	51.3	12.9
	2322	33.1	8.1
	2347	20.6	7.9
	2371	14.9	5.3
CTD 21	2026	26.4	1.2
	2120	310	99.7
	2199	316	76.6
	2220	275	94.0
	2273	291	84.3
	2298	300	104
	2320	89.7	23.6
	2372	52.8	13.8
		Edmond	
CTD 23	2469	8.5	2.9
	2781	321	132
	2819	350	55.4
	2960	7.3	2.9
	3008	131	56.4
	3019	130	63.5
	3057	174	37.1
	3107	161	50.6
	3156	50.6	11.3
		Background	
CTD 16	1978	15.1	0.6
	2076	16.0	2.7
	2174	2.7	1.4
	2273	14.5	1.7
	2371	7.4	2.6
	2469	3.5	2.6
CTD 22	1978	18.0	1.4
	2076	5.0	1.4
	2175	13.9	1.7
	2273	7.3	2.2
	2371		2.5
	2469	4.7	1.7

Table 3. Concentrations of dissolved (<0.4µm) Fe and Mn in filtered hydrothermal plume samples from the Kairei and Edmond sites (for standard deviations associated with the measurements, please see Appendix 2)

Profiles of dissolved Mn and Fe together with the light scattering sensor (LSS) output for eight CTD stations from Kairei are shown in Figs. 9 to 12 (note changes of scale for Fe, Mn and LSS between CTDs 5, 7, 21 and the remaining CTD profiles). The equivalent set of profiles for CTD station 23 at the Edmond hydrothermal field are shown in Fig. 6 (same scales as for CTDs 5, 7, and 21 at Kairei). CTDs 5, 7 and 21 (Figs. 9 and 10) were occupied closest to the Kairei vent (100-300m from USBL (ultra short baseline) navigation), CTDs 4 and 6 (Fig. 11) were approximately 1.5 km from the vent and CTD 10 (Fig. 12) was the furthest away at a distance of ~4 km. CTD station 23 (Fig. 13) was occupied close (<100m) to the Edmond vent site while CTD 16 and CTD 22 (Fig. 14) represent background profiles from the eastern ridge-flank and within the rift-valley respectively. Both were occupied ~180km from the Edmond vent site with CTD 16 lying ~130km due East of Kairei and CTD 22 situated within the rift-valley, ca.12km "upstream" away from the Kairei plume. Increases in dissolved Fe and Mn concentrations are generally coincident with increases in the LSS signal. Of the Kairei profiles, the maximum LSS anomalies were recorded at CTD casts 5, 7 and 21.

The maximum LSS anomaly for CTD 5 of 0.08-0.12 volts (Fig. 9) occurs over a depth range of ~150m from 2130 to 2280m. There is also a smaller anomaly of ~0.02 volts from 2280m to 2320m. The LSS anomalies coincide with increases in the dissolved Fe and Mn concentrations. Dissolved Fe reaches the maximum measured for the Kairei samples of 370nmol/l while dissolved Mn reaches a maximum concentration of 120nmol/l. CTD 21 has a similar maximum LSS anomaly of 0.08-0.15 volts over a similar depth range to CTD 5. Maximum dissolved Fe and Mn concentrations are also similar, being 320nmol/l and 105nmol/l respectively.

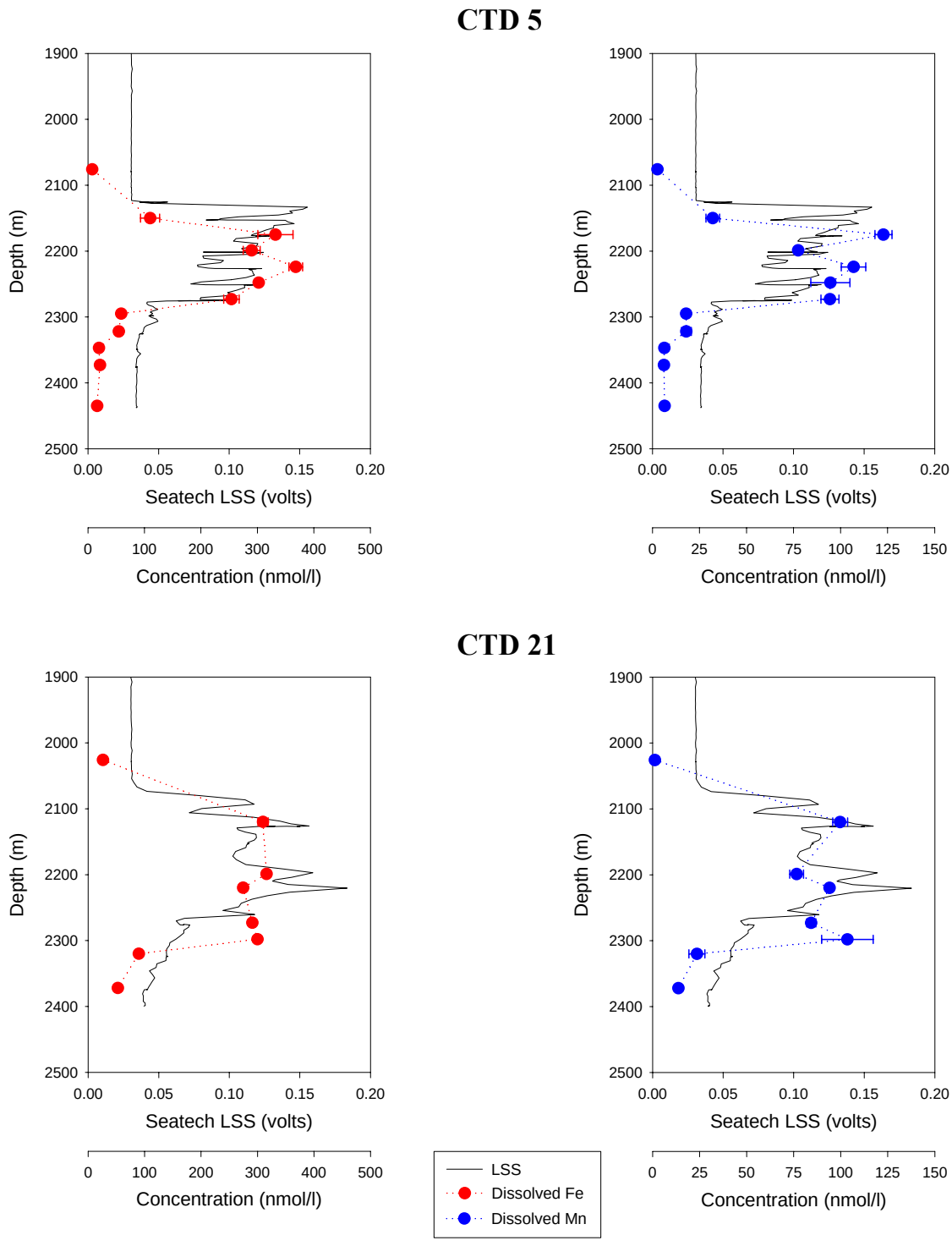

Figure 9 'Near field' Kairei CTD stations 5 and 21: profiles of optical backscattering (Seatech LSS) and dissolved (<0.4µm) Fe and Mn concentrations.

CTD 7 also has maximum LSS anomalies of 0.08-0.12 volts (Fig. 10). However, both the dissolved Fe and Mn concentrations are generally an order of magnitude lower than those of CTDs 5 and 21. The reason for this is apparent when the LSS profiles for CTDs 5 and 21 are compared with that of CTD 7. Whereas CTDs 5 and 21 have high LSS anomalies which persist throughout the plume depth, CTD 7 consists of multiple discrete layers where the LSS signal is elevated, interspersed with background seawater (where the LSS signal returns to the levels measured above the plume). Sampling these layers to ensure that the hydrothermal plume is intercepted is a challenge and it appears that the majority of samples, although enriched in dissolved Fe and Mn, still represent significant dilution compared to the plume signals in CTDs 5 and 21.

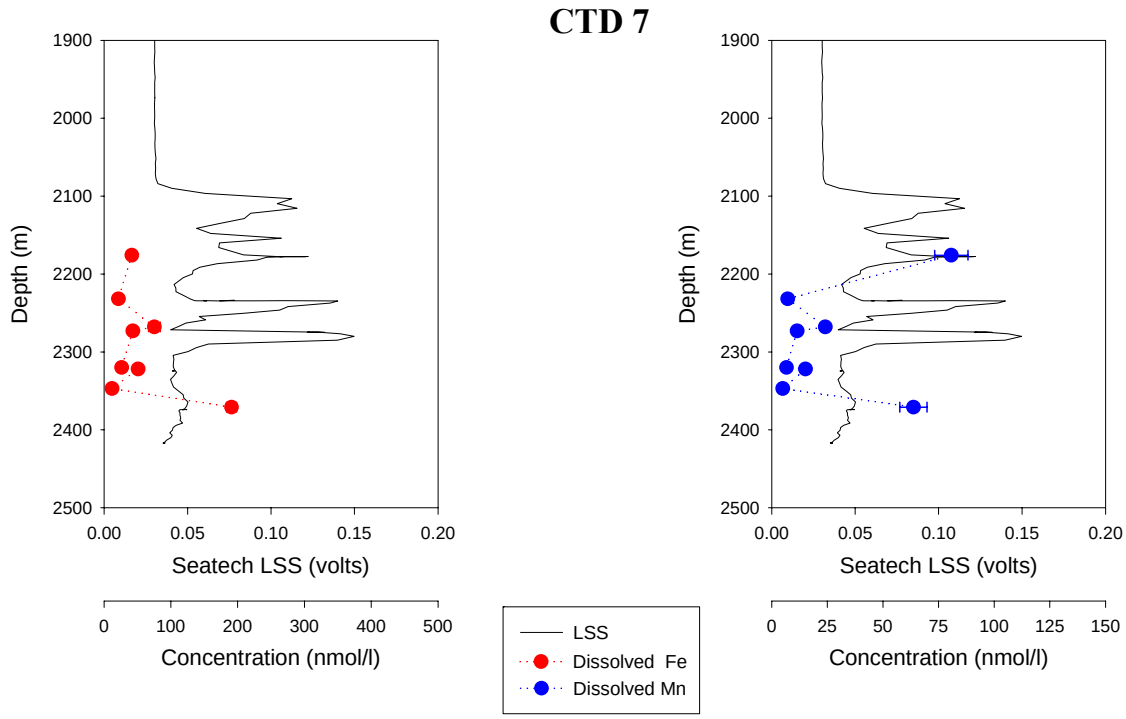

Figure 10 'Near field' Kairei CTD station 7: profiles of optical backscattering (Seatech LSS) and dissolved (<0.4µm) Fe and Mn concentrations.

CTDs 5, 7 and 21 all have common features which are the sharp gradients in the LSS signal, unlike the remaining CTDs which have smoother gradients. This is a feature which is characteristic of near field plumes (Chin et al., 1998) consistent with all these CTDs being less than 400m from the vent source.

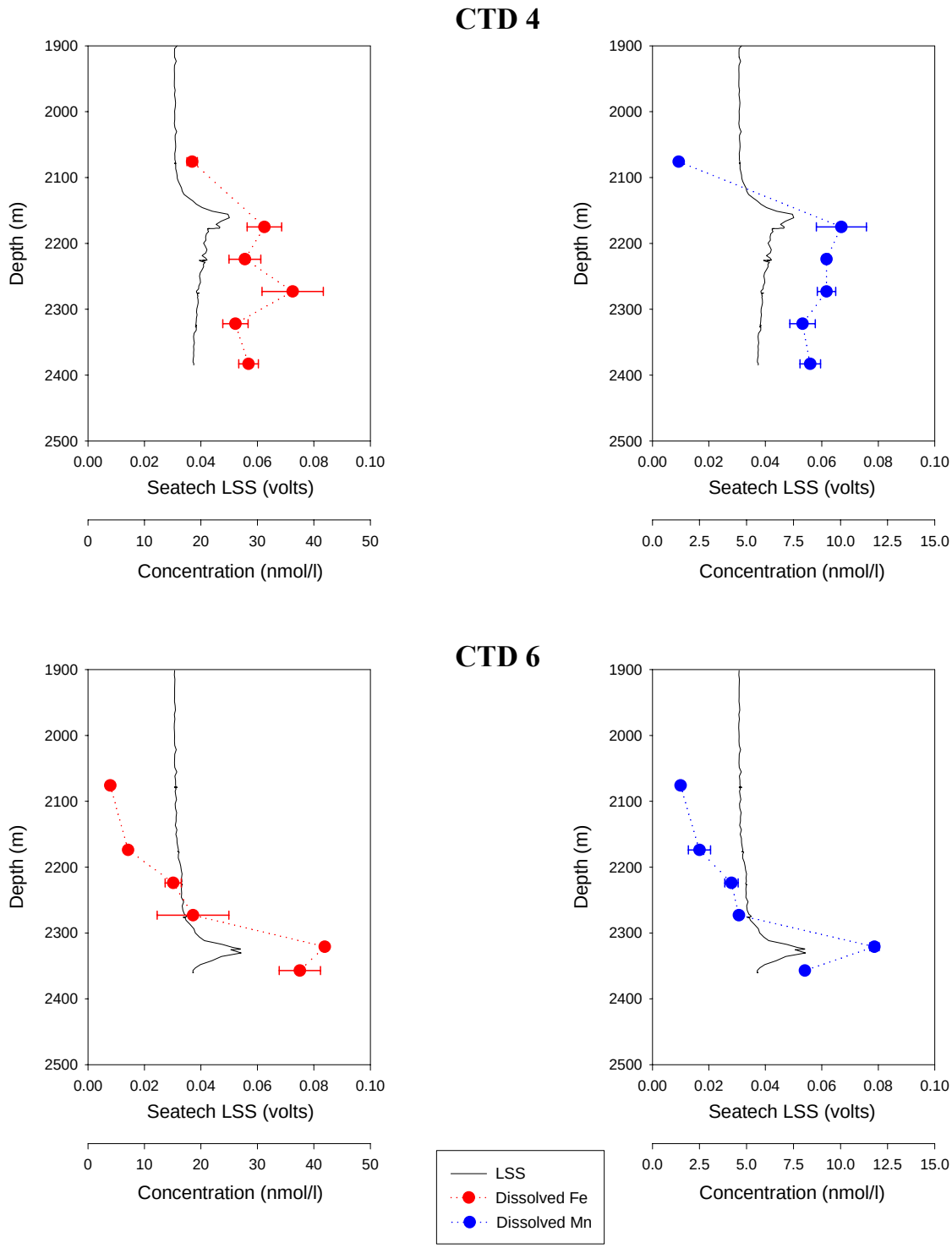

Figure 11 'Mid field' Kairei CTD stations 4 and 6: profiles of optical backscattering (Seatech LSS) and dissolved (<0.4µm) Fe and Mn concentrations.

CTDs 4 and 6 (mid field stations, Fig. 11) have maximum LSS anomalies of 0.02 volts which are almost an order of magnitude smaller than CTDs 5 and 21. The depth range of the elevated LSS signal is much narrower than observed for CTDs 5 and 21; this can also be seen in Fig. 9 where the plume is much thicker at CTD stations 5 and 21 compared to CTDs 4 and 6. Unlike e.g. CTD 5 where the LSS signal returns to background levels below the plume, at CTD 4 the LSS signal never returns to the level recorded above the plume. The maximum LSS signal for CTD 4 is much shallower than for CTD 6. Maximum dissolved Fe concentrations are 42nmol/l and 31nmol/l and maximum dissolved Mn concentrations are 12nmol/l and 10nmol/l. These are also an order of magnitude smaller than at the near field sites, CTD 5 and 21.

For CTD 10 (far field station, Fig. 7), the maximum LSS anomaly is 0.01 volts over a depth range of ~130m. Maximum dissolved Fe and Mn concentrations are 30nmol/l and 8nmol/l, which are similar to, but lower than those at CTDs 4 and 6.

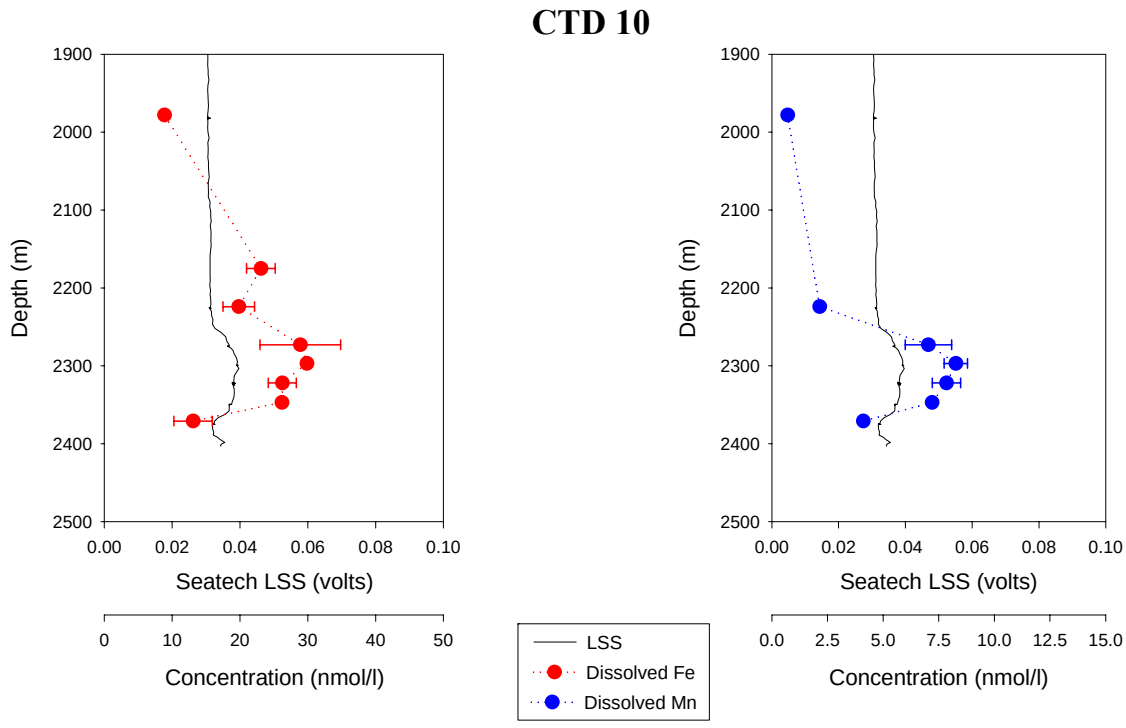

Figure 12 'Far field' Kairei CTD station 10: profiles of optical backscattering (Seatech LSS) and dissolved (<0.4µm) Fe and Mn concentrations.

The Edmond profile, CTD 23, has two distinct LSS anomalies (Fig. 13). The first, between 2760m and 2890m, has a maximum LSS anomaly of ~0.1 volts and the second from 2980m to 3160m, has a maximum LSS anomaly of 0.05 volts. Maximum dissolved Fe and Mn concentrations are 350nmol/l and 130nmol/l. Like the near field Kairei profiles, the gradients of the LSS signal are very sharp, consistent with the close proximity of this CTD station to the vent (<100m). Although it is not unusual to see more than one distinct LSS anomaly in a profile (compare, for example, CTD 5 from the Kairei hydrothermal plume) the two anomalies here are separated by a depth of 90m where, not only the LSS signal returns to background levels but the dissolved Fe and Mn concentrations also return to background levels. This suggests that there could be two distinct vent sources contributing towards the overall profile but it is not conclusive evidence. Rudnicki et al. (1994) recorded a similar feature in a profile from the TAG hydrothermal field for a common source.

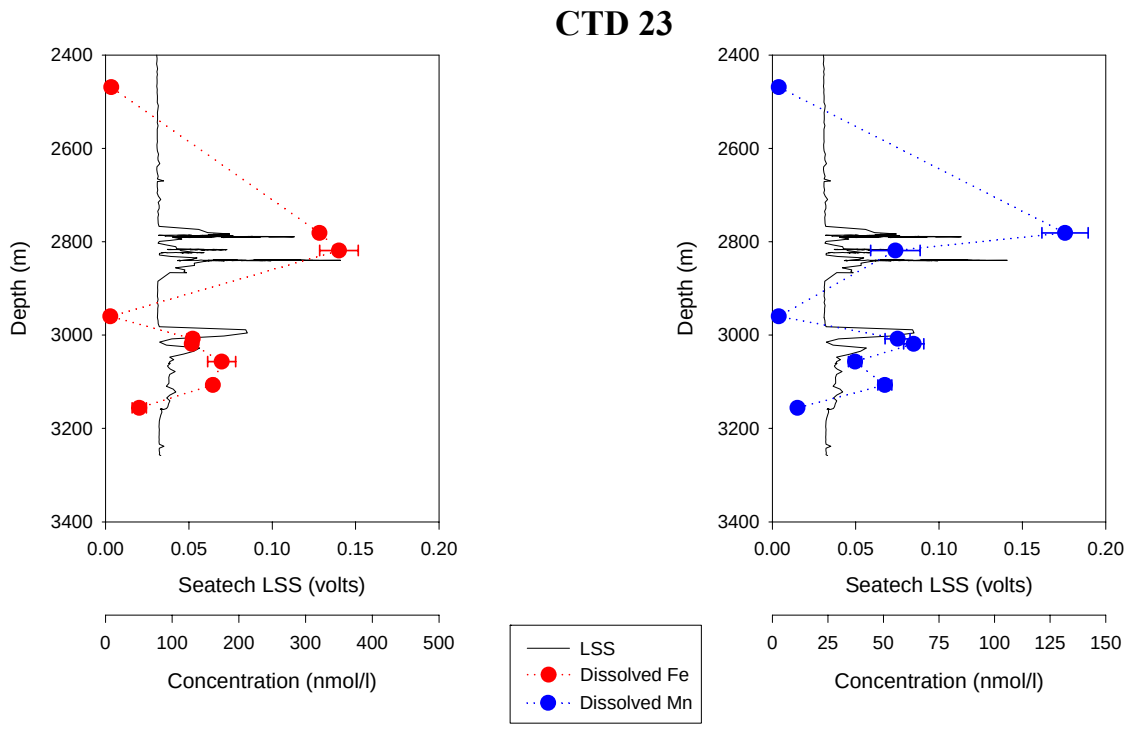

Figure 13 Edmond CTD station 23: profiles of optical backscattering (Seatech LSS) and dissolved (<0.4µm) Fe and Mn concentrations (note that although it is not necessarily valid to connect the dissolved Fe and Mn data points, it has been done for clarity in this and previous figures).

For both of the background profiles, CTD 16 and CTD 22, the LSS signal of ~0.03 volts remains constant, as would be expected (Fig. 14). Dissolved Fe varies from 3nmol/l to 16nmol/l while dissolved Mn varies between 1.4nmol/l and 2.7nmol/l. These concentrations are higher than the background levels in the deep Indian ocean of ~1.0nmol/l for Fe (Saager et al., 1989) and 0.14nmol/l for Mn (Morley et al., 1993). For CTD 22 which was inside the rift valley, this could be due to a general elevation of Mn and Fe levels as a consequence of multiple hydrothermal inputs, similar to that found by Aballea et al. (1998) throughout the axial valley of the Mid Atlantic Ridge in the region of the Azores Triple Junction. However this would not explain the concentrations recorded for CTD 16 which was ~130km off-axis. The most likely explanation, therefore, is that this is due to the limitations of sampling using a steel framed CTD rosette and standard cabling as opposed to a titanium framed CTD rosette and Kevlar coated CTD. There may also have been some contamination of the Niskin bottles which had already been used earlier in the cruise to sample in the hydrothermal plumes. Despite this, the key point is that when the 'background' concentrations are compared to those measured for CTD 5 and CTD 4, it is apparent that they are still 1-2 orders of magnitude lower than the elevated levels seen in the plume.

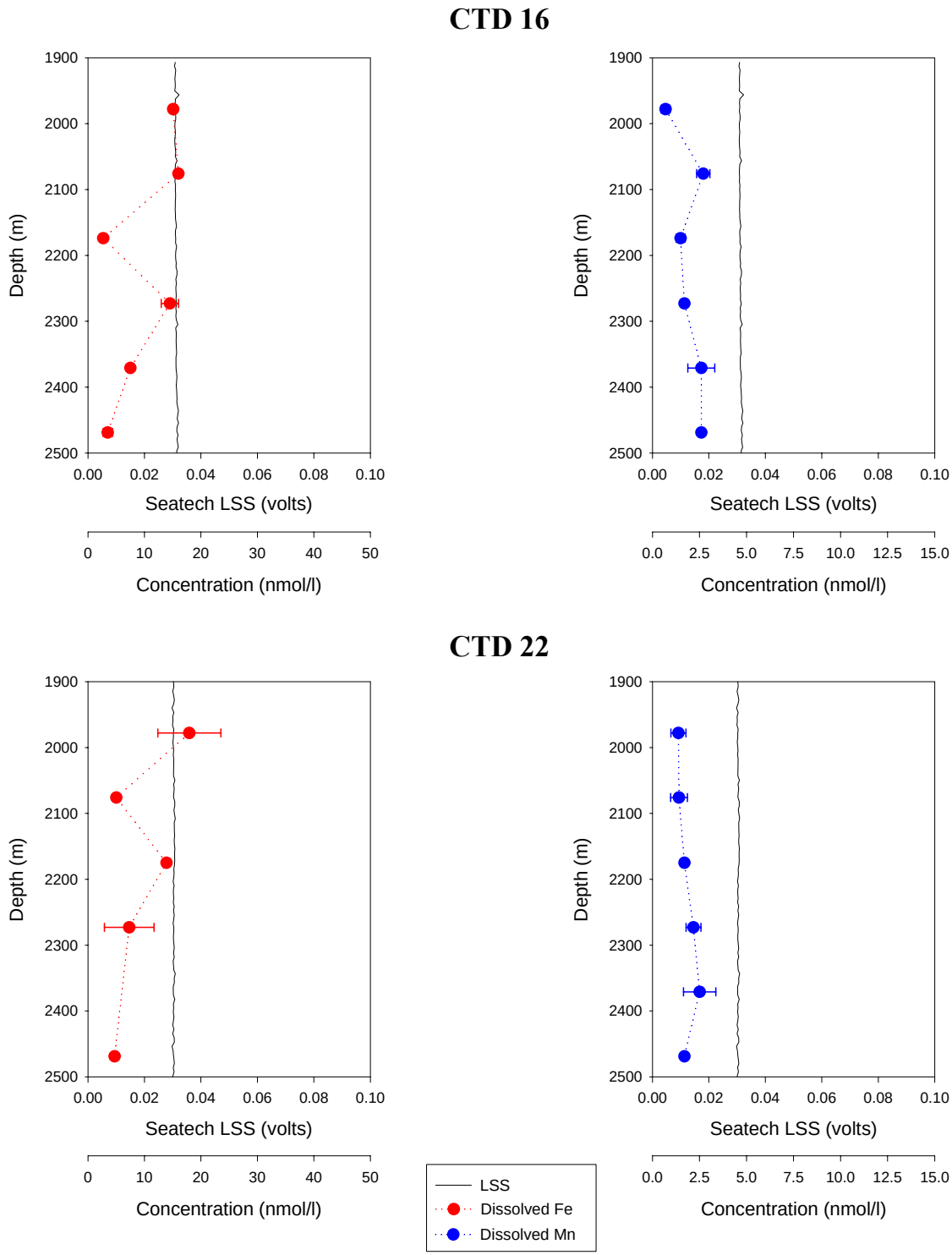

Figure 14 'Background' CTD stations 16 (ridge flank) and 22 (ridge axis): profiles of optical backscattering (Seatech LSS) and dissolved (<0.4µm) Fe and Mn concentrations.

3.3 CTD Profiles and particulate (>0.4µm) Fe and Mn

Particulate (>0.4µm) Fe and Mn data from CTD Niskin bottle samples are shown in Table 17/Appendix 6 and are also summarised below in Table 4. Concentrations of particulate Fe range from 8nmol/l up to 350nmol/l for the Kairei samples, with the exception of the CTD 7 sample at 2176m, which will be discussed further below. For the Edmond samples they range from 10nmol/l up to 440nmol/l. The maximum concentrations observed are comparable to those measured in particulate samples from both the Pacific (e.g. Feely et al., 1996) and the Atlantic (Edmonds & German, 2004). Particulate manganese concentrations vary from 0.1nmol/l to 3.1nmol/l at Kairei but all fall between 0.2nmol/l and 0.3nmol/l in the Edmond hydrothermal plume. These values are also comparable to those reported for Atlantic and Pacific hydrothermal plume particles (Feely et al., 1996; Edmonds & German, 2004) and fall below 10% of the total Mn concentration for all samples, except those where dissolved Mn is low (<3nmol/l).

For CTD 7, separate aliquots from the Niskin samples were also filtered through 0.1µm filters, as well as 0.4µm (i.e. non-sequentially). The particulate Fe concentrations from the 0.1µm filter should either be similar or higher than for the 0.4µm filter of the same sample. For the CTD 7 2176m sample the particulate [Fe] for the >0.1µm sample is only 220nmol/l compared to 1040nmol/l for the >0.4µm sample (see Table 17 for data). In conjunction with the LSS profile which does not exhibit any unusual features at this depth, it suggests that there may have been a problem with the collection or processing of this particular >0.4µm sample. For the purposes of further discussion, this sample will be excluded. The deepest sample for CTD 7 at 2371m is anomalous when compared to the remaining samples, however this is most probably due to the incorporation of re-suspended sediment as the CTD rosette frame did in fact make contact with the sea floor on this cast (Tyler & CD128 Science Party, 2001). Particulate Fe is enriched in this sample whereas particulate Mn is similar to other samples, this would be consistent with incorporation of re-suspended metalliferous sediments, which are rich in Fe and poor in Mn, close to the vent source. There is also evidence for re-suspended sediment in the LSS profile for CTD 7 where there is an increased signal below 2350m, which is not seen in the other LSS profiles at Kairei. This sample will also be excluded from any further discussion.

CTD #	Depth (m)	Particulate (>0.4µm) Fe (nmol/l)	Particulate (>0.4µm) Mn (nmol/l)
	Kairei		
CTD 5	2076	8.2	1.8
	2150	51.6	1.1
	2175	183	0.2
	2199	280	3.1
	2224	254	1.4
	2273	344	1.8
	2295	31.9	0.6
	2347	18.4	1.4
	2373	7.8	0.5
	2435	9.9	0.2
CTD 7	2176	1040	0.4
	2232	41.5	0.7
	2268	34.6	0.3
	2273	21.8	0.3
	2320	13.8	0.2
	2347	10.5	0.2
	2371	170	0.6
CTD 21	2026	17.5	0.7
	2120	220	0.2
	2199	98.1	0.1
	2220	96.3	0.1
	2273	118	0.1
	2298	288	0.2
	2320	54.6	0.2
	2372	21.5	0.2
	Edmond		
CTD 23	2469	12.9	0.3
	2781	440	0.2
	2819	103	0.2
	2960	10.3	0.3
	3008	177	0.2
	3019	264	0.3
	3057	57.4	0.3
	3107	117	0.3

Table 4. Concentrations of particulate (>0.4µm) Fe and Mn in hydrothermal plume samples from the Kairei and Edmond sites. (complementary dissolved data were presented in Table 3 and particulate data for other elements is presented in Table 17)

Depth profiles of the particulate data and associated light scattering sensor data are shown in Figs. 15 and 16. CTDs 5, 21 (Kairei) and 23 (Edmond) all show elevated concentrations of particulate Fe co-incident with increased light scattering sensor signals, compared to the 'background' concentrations seen above and below the plume where the LSS signal is at background levels. The particulate Fe profile for CTD 7 shows that these samples generally have lower Fe concentrations than samples from CTDs 5 and 21 with equivalent LSS signals. Particulate Mn concentrations vary very little for either the Kairei or Edmond samples (less than 1.0nmol/l except for CTD 5) and any variation which is present does not show a strong correlation with the LSS signal.

The most noticeable feature of the profiles is that, although the maximum LSS anomalies for CTD 7 are similar to those for CTD 5 and 21, the LSS trace for CTDs 5 and 21 stays high throughout the ~200m plume depth whereas CTD 7 has narrow (~10s of metres thick) layers of high LSS signal with almost completely clear background water in between. This may explain the much lower particulate Fe concentrations recorded at CTD 7 compared to CTDs 5 and 21 despite the similar maximum LSS signal; the 'flushing length' for a Niskin bottle is ~8-10m, hence it is possible that when the bottle was fired based on the LSS signal, the water within the Niskin could have been relatively 'clean' water from a layer just below the high LSS signal layer.

It is worth noting that the light scattering signal does not depend solely on the concentration of particles present, the size and composition of the particles are also relevant (Baker et al., 2001). Larger particles can in fact result in a lower light scattering signal, so for example if part of the hydrothermal plume is dominated by larger sulfides the LSS signal may be lower, even if the concentration is similar to other parts of the plume which are dominated by finer grained sulfides and/or Fe-oxyhydroxide particles.

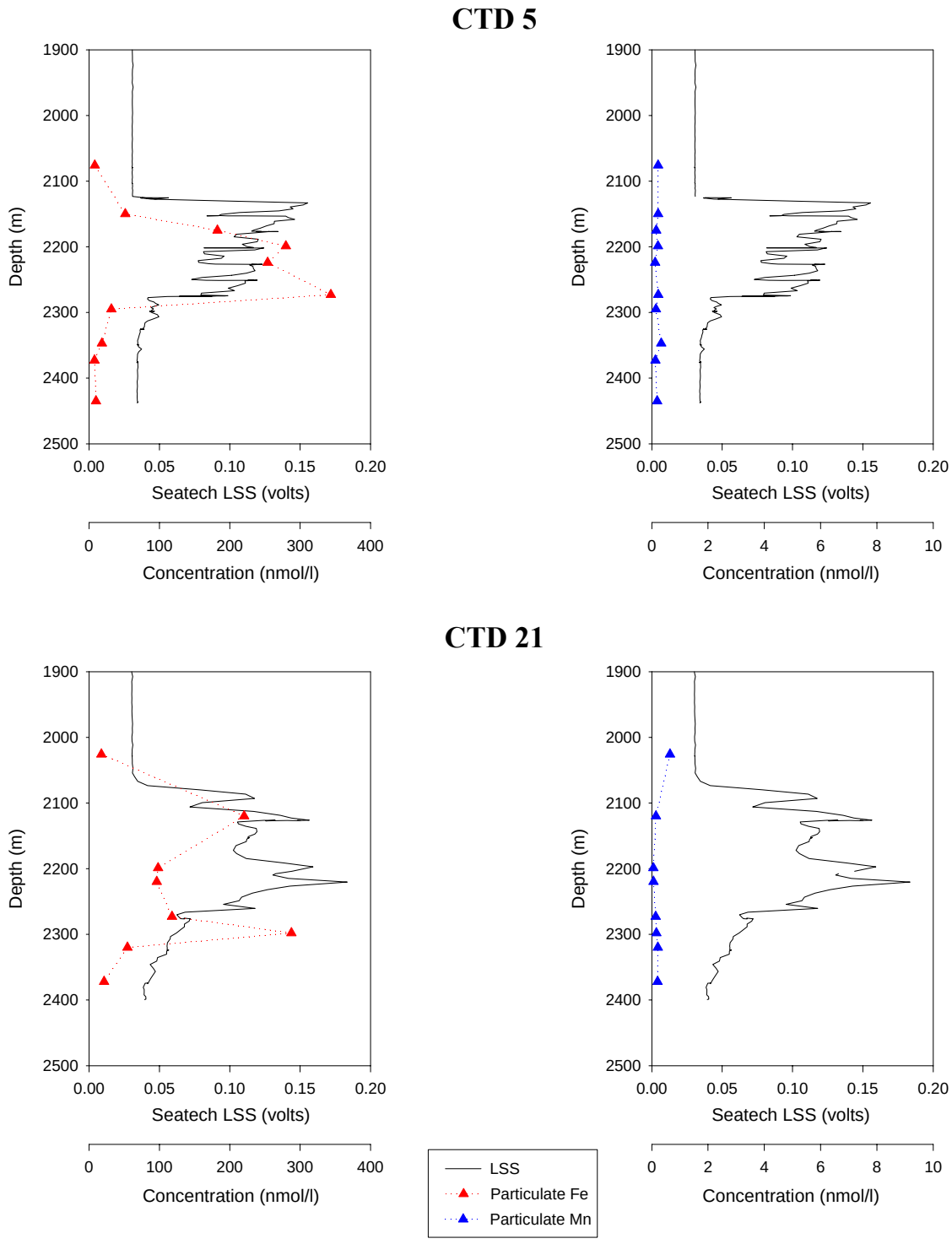

Figure 15 'Near field' Kairei CTD stations 5 and 21: profiles of optical backscattering (Seatech LSS) and particulate (>0.4µm) Fe and Mn concentrations.

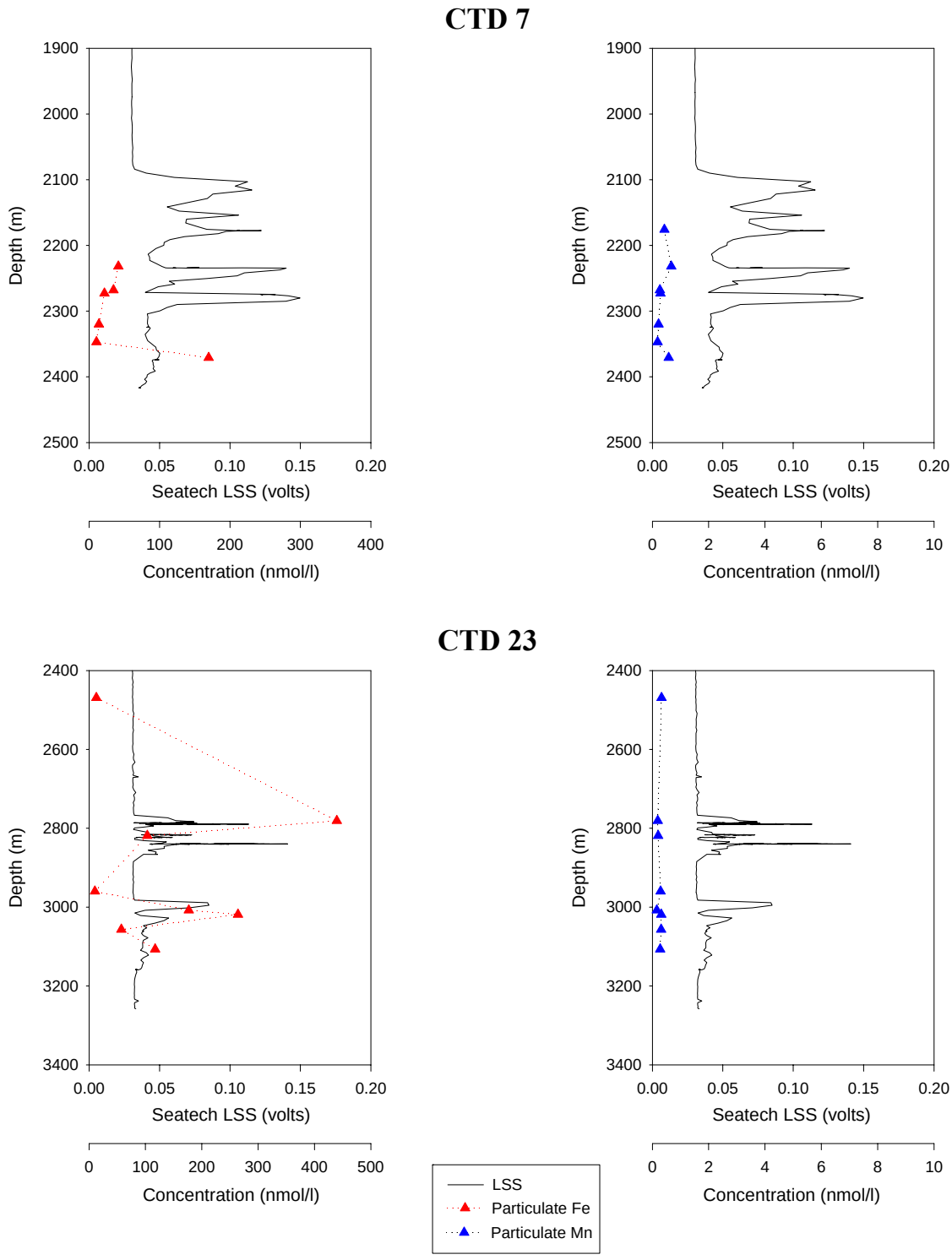

Figure 16 'Near field' Kairei CTD station 7 and Edmond CTD station 23: profiles of optical backscattering (Seatech LSS) and particulate (>0.4µm) Fe and Mn concentrations.

3.4 Discussion

3.4.1 CTD Profiles

CTDs 5 and 21 were the closest in proximity to the Kairei vent site; the stations were occupied 13 days apart. Although the fine detail in the two profiles illustrates the inherent variability due to currents and tidal variation that would be expected in the open ocean, the overall trend is very similar, i.e. the depth and height of the plume and the concentrations of dissolved Fe and Mn are all comparable. This consistency in the properties of the hydrothermal plume is an important factor if plume data are to be used to assess their impact on the geochemical cycles of certain elements.

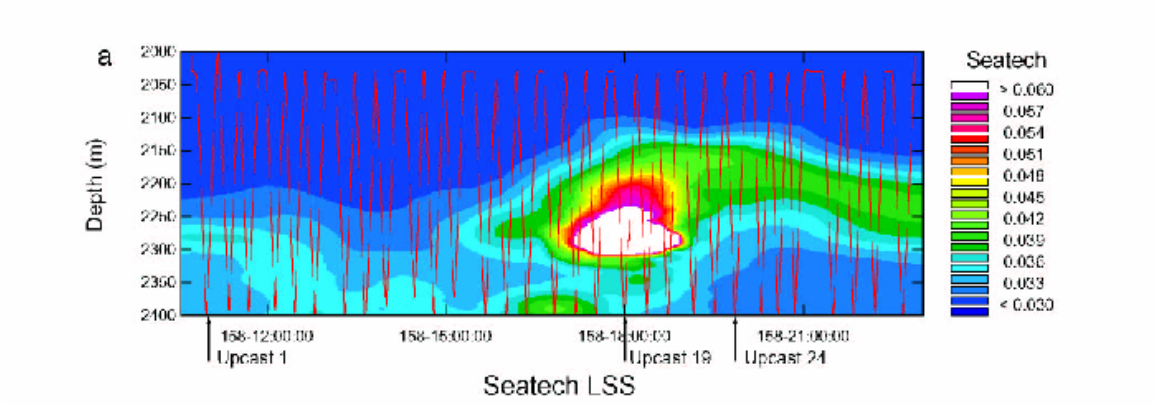

Figure 17 Variation of the Kairei hydrothermal plume height over time as shown by optical backscatter (Seatech LSS) data. (Red lines show the continuous CTD profiling through the plume, figure from Rudnicki & German, 2002).

CTDs 4 and 6 were recorded ~32 hours apart, both at a similar distance (~1.5km) from the Kairei vent site. The lower concentrations of dissolved Fe and Mn and the lower LSS anomaly compared to CTDs 5 and 21 demonstrate that the plume is being diluted as it moves further away from its source. The shape and magnitude of the two profiles are very similar except that the LSS maxima, which vary from 2175m to 2360m are offset by 200m. This is consistent with the findings of Rudnicki & German (2002) where a 12.5 hour monitoring profile of the Kairei non-buoyant plume found that the plume particle maximum varied between 2150m to >2350m. This variability is demonstrated in the time profile of LSS versus depth in Fig. 17.

3.4.2 Mixing Ratios

Dissolved Mn can be used to estimate the mixing ratio of vent fluid to seawater in a hydrothermal plume (James & Elderfield, 1996). This assumes that no dissolved Mn is lost from the plume via oxidation. We know that dissolved Mn does undergo oxidation, however it occurs on much longer timescales than iron and therefore mainly in the far field plume; the residence time of Mn within a plume varies from weeks (Kadko et al., 1990) to several years (Lavelle et al., 1992). Close to the vent, Mn has been shown to behave conservatively (e.g. Cowen et al., 1990; Kadko et al., 1990). The mixing ratio (MR) can be calculated from:

$$MR = \frac{[Mn]_{vf} - [Mn]_{sw}}{[Mn]_{hp} - [Mn]_{sw}}$$

where: $[Mn]_{vf}$ = the concentration of dissolved Mn in the vent fluid = 840µM at Kairei (Gamo et al., 2001) and 1430µM at Edmond (Gallant & Von Damm, 2006); $[Mn]_{sw}$ = the concentration of dissolved Mn in the surrounding seawater = 0.14nM (Morley et al., 1993); $[Mn]_{hp}$ = the concentration of dissolved Mn in the hydrothermal plume sample.

Mixing ratios for samples from CTDs 5 and 21 near the Kairei vent field are shown in Table 5. The least dilute samples have a mixing ratio of 7 to 9 x 10^3. Lupton et al. (1995) predicted that a hydrothermal plume is diluted by a factor of ~10^4 by the time it reaches neutral buoyancy. If this is the case then it is possible that the least dilute samples collected at Kairei intercepted the buoyant plume. However the distances of CTDs 5 and 21 from the vent source (~340m and ~100m respectively, see Chapter 2) would also have to be consistent with this possibility. Knowing that the depth of the plume is 2100-2300m, from the light scattering profiles presented earlier in the chapter and the depth of the vent source is 2450m (Gamo et al., 2001), we know that the height of rise of the plume is 150-350m. If we assume an inverted cone with a vertical angle of 30° for the buoyant plume (Turner, 1973) then the radius of the buoyant plume at the level of neutral buoyancy will be from 90-200m. This means samples from CTD 21 could feasibly be within the buoyant plume area.

If the buoyant plume was intercepted then potential temperature and potential density anomalies should be evident in the CTD profiles. The mixing ratios for samples from CTD 23 at Edmond show that despite being a similar distance from the vent as CTDs 5 and 21 are from the Kairei vent, these samples are an order of magnitude more dilute.

Sample	Measured dissolved Mn (nmol/l)	Mixing ratio
Kairei		
CTD 5 2175m	123	6800
CTD 5 2199m	78	11000
CTD 5 2224m	107	7900
CTD 5 2248m	95	8900
CTD 5 2273m	94	8900
CTD 21 2120m	100	8400
CTD 21 2199m	77	11000
CTD 21 2220m	94	8900
CTD 21 2273m	84	10000
CTD 21 2298m	104	8100
Edmond		
CTD 23 2781	132	10900
CTD 23 2819	50	29000
CTD 23 2960	3	520000
CTD 23 3008	56	25000
CTD 23 3019	64	23000
CTD 23 3057	37	39000

Table 5. Mixing ratios for samples from CTDs 5, 21 and 23 calculated from dissolved Mn concentrations for the vent fluids and the samples (see text for vent fluid figures)**.**

Inspection of the potential temperature and sigma-2 (potential density normalised to 2000 decibars pressure) for CTD 5 in relation to the light scattering sensor data (Fig. 18) reveals that there are small increases in temperature (<0.02°C) and decreases in density (<0.005kg/m^3) co-incident with increases in the LSS signal in the depth range of the least dilute samples. Resolution of the CTD instrument deployed (Seabird 911plus) is ~0.0002°C for temperature and better than 0.0001kg/m^3 for density hence the anomalies

are true observations rather than signal noise. For CTD 21, the relationship between increased temperature, decreased density and an increased LSS signal is less clear (Fig. 18), although comparison with the temperature and density profiles of the ridge axis background profile, CTD 22, in Fig. 18 shows that the background water column profile is smoother with none of the stepwise changes in temperature and density which are seen in CTDs 5 and 21.

Rudnicki & German (2002) presented CTD casts from a time-series profile of the Kairei hydrothermal plume and found temperature anomalies of approximately +0.1°C for the buoyant portion of the plume and light scattering sensor anomalies of >300mV. The LSS anomalies seen in CTDs 5 and 21 and the associated temperature changes are more in line with data for the non-buoyant portion of the plume where they recorded temperature anomalies of +0.02°C and LSS anomalies of 70-80mV.

Direct comparison of CTDs 5 and 21 with that of the background profile CTD 22 are also inconclusive. The plot of CTD21 and 22 (Fig. 19) shows there is a positive temperature deviation from that of the background water column between 2210m and 2340m of ~0.02 to 0.03°C (shown by the shaded area in the plot in Fig. 19). However comparison of CTD 5 with CTD 22 (also Fig. 19) shows very different profiles, this is most likely a consequence of the two profiles being conducted 12 days apart. Tidal variations observed at the site of the Kairei hydrothermal plume result in the height of the plume varying by ~200m (Rudnicki & German, 2002) so the tidal state may have been very different during the two CTD casts. This is consistent with both the strong boundary current that flows along the ridge axis of the Central Indian Ridge (Toole & Warren, 1993) and findings that vertical mixing is stronger above rougher topography such as mid-ocean ridges (Polzin et al., 1997).

From the available data it is only really possible to conclude that the least dilute samples from CTDs 5 and 21 may be from the very dilute portion of the buoyant plume but it is more likely that they represent very young “zero age” non-buoyant plume samples.

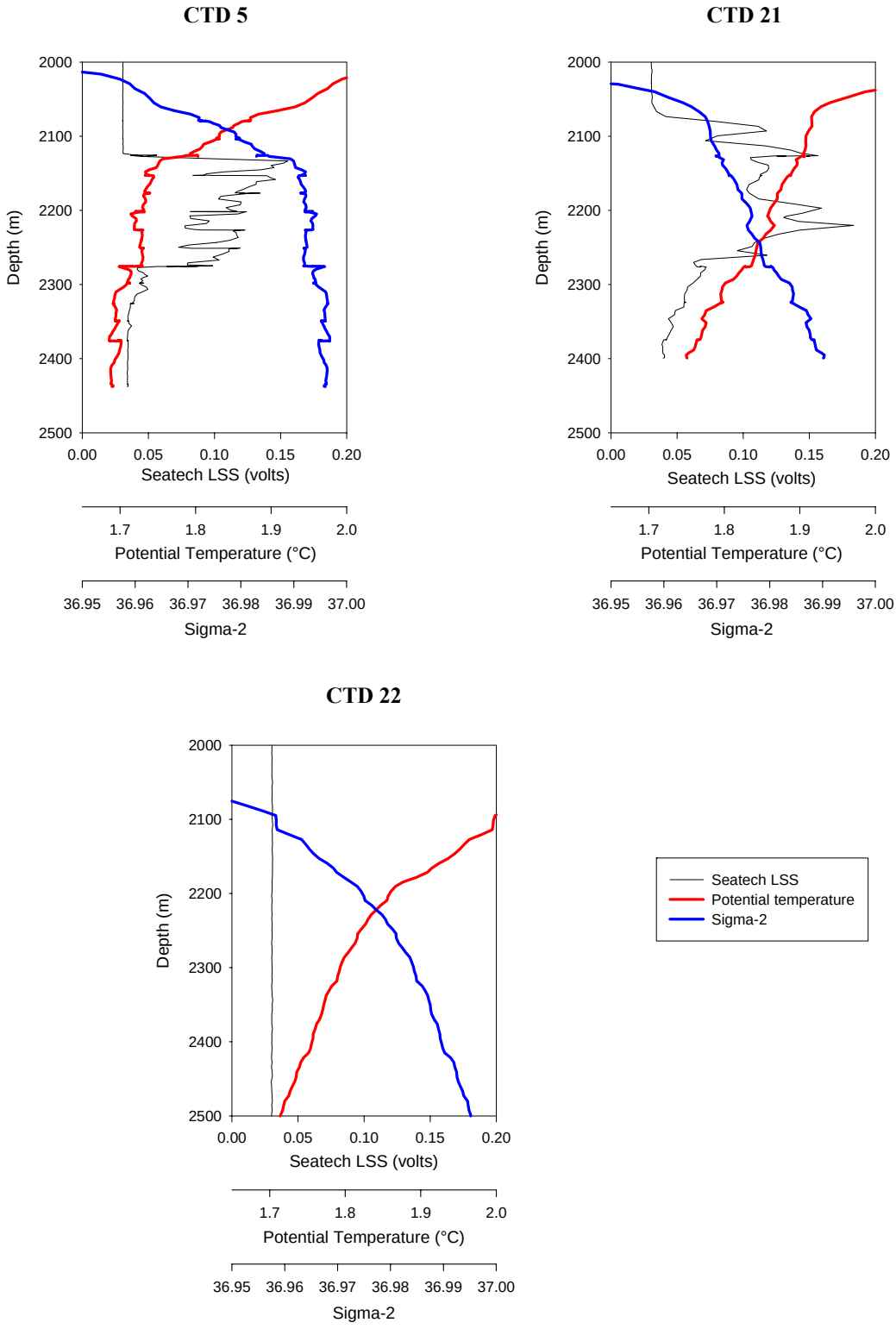

Figure 18 Potential temperature and density profiles of Kairei 'near field' CTD stations 5 and 21 and 'background' station CTD 22 (rift-valley). Sigma-2 is the potential density normalised to 2000 decibars pressure.

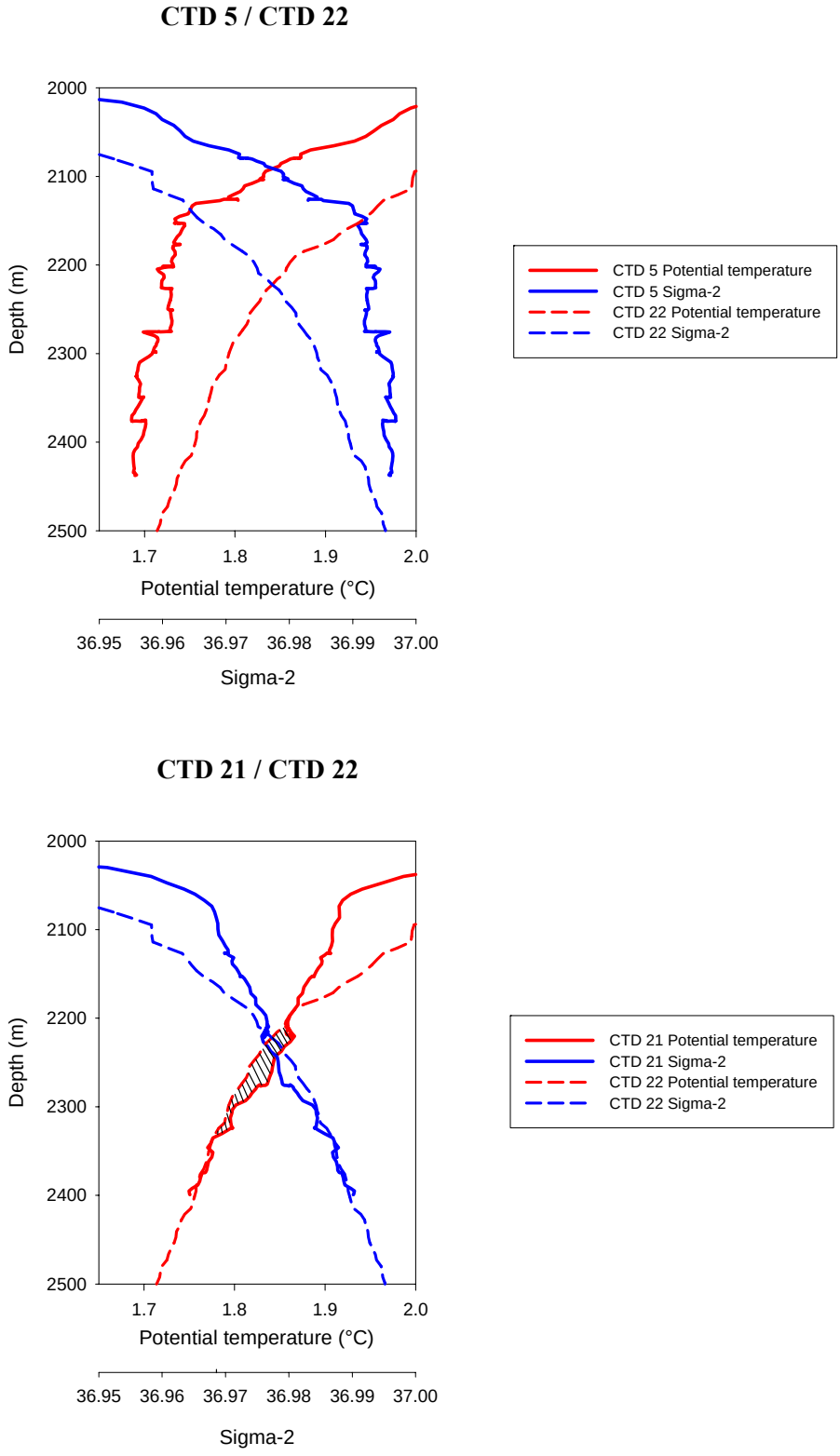

Figure 19 Comparison of potential temperature and density profiles for Kairei 'near field' CTD stations 5 and 'background' station CTD 22 (rift-valley) and also for Kairei 'near field' CTD stations 21 and 'background' station CTD 22 (The shaded area shows the small positive temperature anomaly of CTD 21 compared to the background water column represented by CTD 22)

3.4.3 Total Fe calculations

The measured particulate Fe and dissolved Fe concentrations of the hydrothermal plume samples can be combined to give us the total Fe concentration in the samples. Combining the mixing ratio calculations of vent fluid to seawater in the hydrothermal plume samples (Table 5) with the vent fluid Fe concentration allows us to estimate the maximum Fe concentration we could expect to find in the samples if we assume a simple dilution model (i.e. conservative behaviour). Table 6 shows the measured total Fe in those samples for which both particulate and dissolved data are available, as well as the theoretical maximum Fe possible based on the mixing ratios calculated from the dissolved Mn data.

All the samples except one from Edmond and one from Kairei have a measured total Fe concentration which is lower than the maximum theoretical Fe concentration. If the only process occurring within the plume is straightforward dilution with ambient seawater then the measured and theoretical total Fe concentrations should be the same. However we already know that Fe is lost from the plume as the large grained sulfides which form in the early buoyant plume settle out (e.g. Mottl & McConachy, 1990). Therefore it is to be expected that the measured total [Fe] would be less than the theoretical total [Fe] and this is indeed the case. The fraction of Fe in the particulate phase compared to the dissolved phase varies between 23% and 67% of the total, but there does not appear to be any correlation with, for example, total Fe.

For the Edmond sample (CTD 23 2819m) where the measured total Fe exceeds the theoretical maximum total Fe, the difference is less than 3% which is within error limits (see Appendices 1 and 2). For the Kairei sample (CTD 5 2199m), the measured total Fe concentration exceeds the theoretical maximum total Fe by 15% which exceeds the error limits. The combined error for the total Fe measurement is 570±15nmol/l although this is a conservative estimate as the particulate measurements are based on one sample only. However it is possible that close to the vent site, settling particles can be recycled back into the plume as reported at the TAG hydrothermal plume in the Atlantic (German & Sparks, 1993) which may lead to an ‘excess’ of particulate material.

Sample	Dissolved Fe 0.4µm (nmol/l)	Particulate Fe 0.4µm (nmol/l)	Mixing ratio[1]	Total Fe (Dissolved + Particulate)[2] (nmol/l)	Theoretical maximum total Fe (nmol/l)[3]	Total Fe as a % of theoretical maximum
Kairei						
CTD 5 2150m	110	51.6	26000	162	205	79
CTD 5 2175m	332	183	6900	515	789	65
CTD 5 2199m	290	280	11000	570	497	115
CTD 5 2224m	368	254	7900	622	686	91
CTD 5 2273m	254	344	8900	598	605	99
CTD 5 2295m	58.8	31.9	47000	90.7	114	79
CTD 7 2268m	75.4	34.6	35000	110	154	71
CTD 7 2273m	43.0	21.8	74000	64.8	73	88
CTD21 2120m	310	220	8400	530	640	83
CTD21 2199m	316	98.1	11000	414	491	84
CTD21 2220m	275	96.3	8900	371	603	61
CTD21 2273m	291	118	10000	409	541	76
CTD21 2298m	300	288	8100	588	665	88
CTD21 2320m	89.7	54.6	36000	144	151	96
CTD21 2372m	52.8	21.5	62000	74.3	88	85
Edmond						
CTD 23 2781m	321	440	11000	761	1178	65
CTD 23 2819m	350	103	29000	453	442	103
CTD 23 3008m	131	177	25000	308	504	61
CTD 23 3019m	130	264	23000	394	568	69
CTD 23 3057m	174	57.4	39000	231	332	70
CTD 23 3107m	161	117	28000	278	452	62

Table 6. Actual and theoretical total Fe measurements for Kairei (CTDs 5, 7 and 21) and Edmond (CTD 23) samples.

[1]The mixing ratio is based on the dissolved Mn concentrations and vent fluid concentrations of 840µmol/l for Kairei (Gamo et al., 2001) and 1430µmol/l for Edmond (Gallant & Von Damm, 2006).
[2]This is the measured total Fe from summing the measured dissolved and particulate 0.4µm fractions.
[3]Assuming that dissolved Mn behaves conservatively (see text) and vent fluid [Fe] is 5400µmol/l for Kairei (Gamo et al., 2001) and 12800µmol/l for Edmond (Gallant & Von Damm, 2006).

Estimates of Fe loss

A plot of total Fe (measured dissolved [<0.4μm] Fe plus measured particulate [>0.4μm] Fe) versus dissolved Mn for the Kairei samples is shown in Fig. 20. Total Fe and dissolved Mn are positively correlated; as the dissolved Mn concentration decreases (i.e. as the plume is progressively diluted by mixing with ambient seawater), the total Fe concentration also decreases. The vent fluid ratio at Kairei (Gamo et al., 2001) is also shown on the plot. If there were no loss of Fe from the plume as it is progressively diluted then the data points should coincide with the vent fluid line. However the data points predominantly lie beneath the vent fluid ratio suggesting that some Fe has been lost from the plume. Comparison of the vent fluid ratio with the linear regression through the total Fe content of the samples allows an estimate of the quantity of Fe which has been lost from the plume: approximately 20% of the original vent fluid Fe is missing. We already know that in the first few seconds after hydrothermal fluids emerge from a vent, Fe sulfides (as well as other metal sulfides) rapidly precipitate. Previously, estimates have suggested that up to 50% of the total Fe (II) in vent fluids is precipitated in this manner (Mottl & McConachy, 1990; Rudnicki & Elderfield, 1993) and that many of these heavy sulfides settle out of the buoyant plume. Later estimates by James & Elderfield (1996) for the TAG and Snakepit hydrothermal plumes which were also based on complementary dissolved and particulate data, as in this study, suggested up to ~26% of vent fluid Fe was lost as sulfides. This is in good agreement with the data from Kairei.

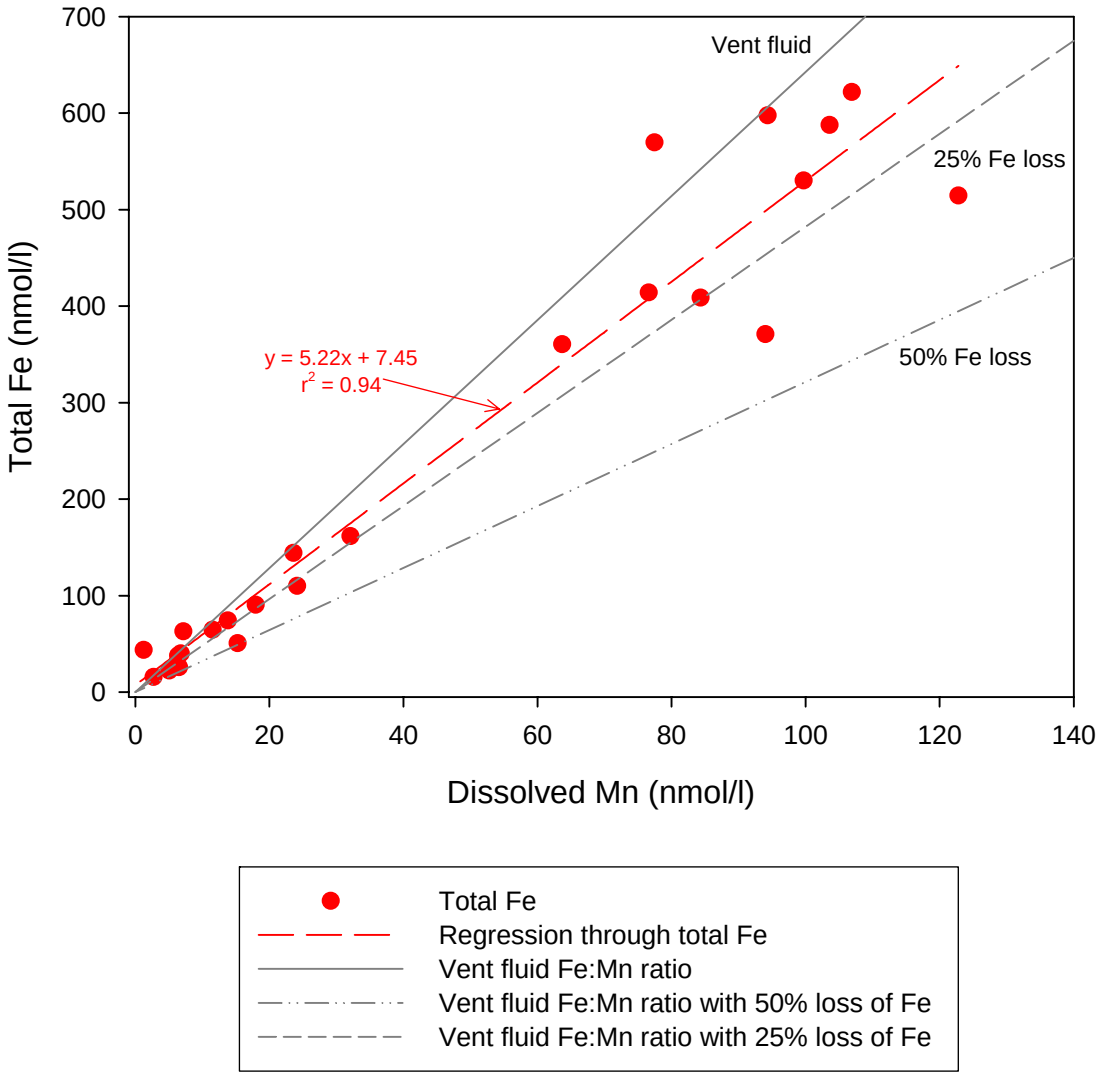

Figure 20 Total Fe (measured dissolved [<0.4µm] Fe plus measured particulate [>0.4µm] Fe) versus dissolved (<0.4µm) Mn for Kairei hydrothermal plume samples. Regression is through all data. Vent fluid ratio and vent fluid ratios with possible Fe losses are shown for comparison.

A similar plot of total Fe versus dissolved Mn is shown for the Edmond samples in Fig. 21. Again, total Fe and dissolved Mn are positively correlated with the total Fe concentration decreasing as the dissolved Mn concentration decreases. The vent fluid ratio at Edmond (Gallant & Von Damm, 2006) is also illustrated and as for Kairei, the total Fe data points lie predominantly below the vent fluid ratio suggesting that Fe has been lost from the plume. Comparison with the linear regression through the total Fe data suggests that ~30% of the original vent fluid Fe has been lost. As for Kairei, this is in good agreement with the estimate of James & Elderfield (1996) and suggests that a

loss of 20-30% for vent fluid Fe due to sulfide precipitation and settling is a more accurate estimate than the earlier ~50% estimates which were based on particulate data alone (Mottl & McConachy, 1990; Rudnicki & Elderfield, 1993).

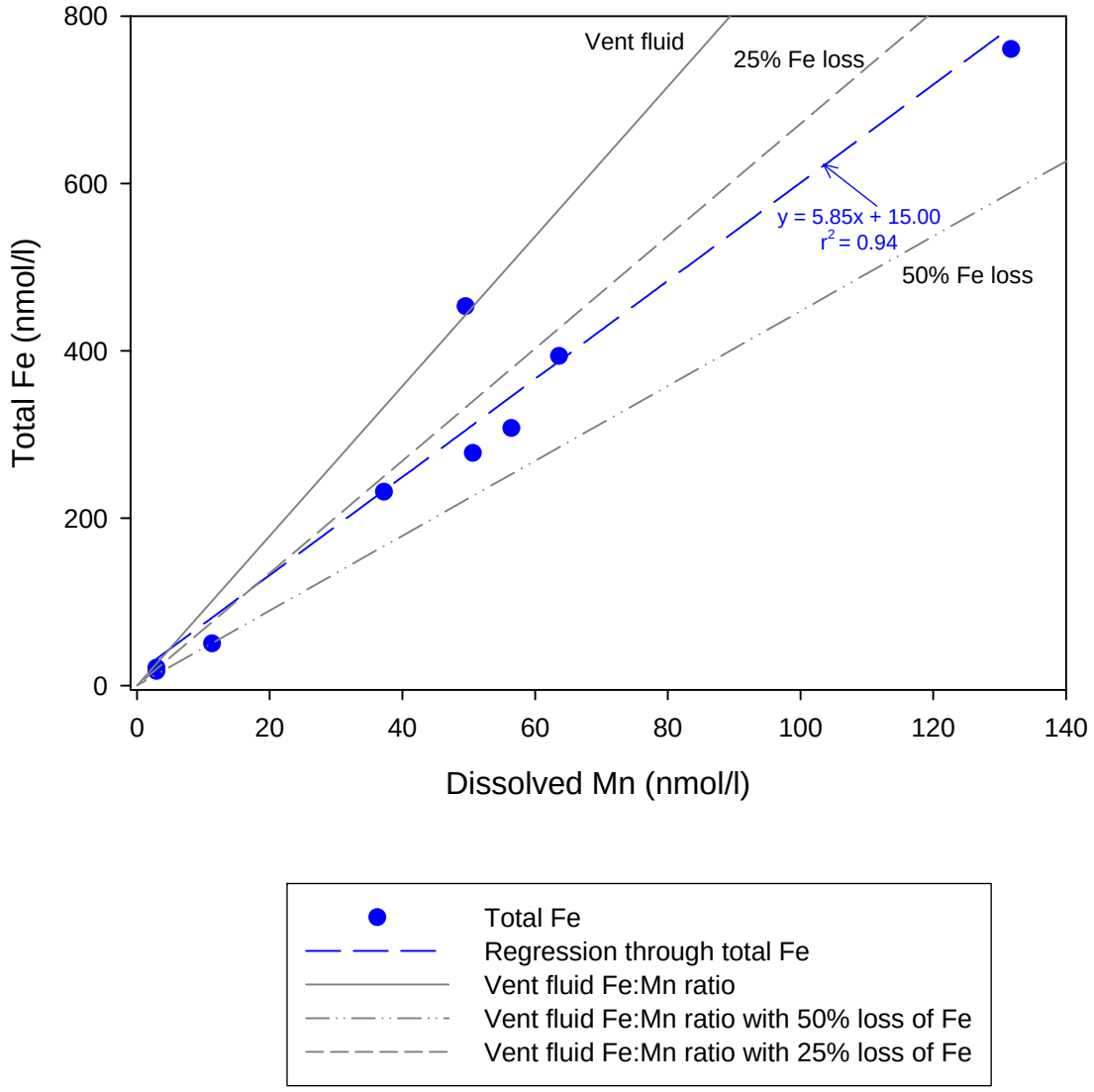

Figure 21 Total Fe (measured dissolved [<0.4µm] Fe plus measured particulate [>0.4µm] Fe) versus dissolved (<0.4µm) Mn for Edmond hydrothermal plume samples. Regression is through all data. Vent fluid ratio and vent fluid ratios with possible Fe losses are shown for comparison.

As vent fluid concentrations of Fe, Cu, Zn and H_2S are available for the Kairei and Edmond sites, we can check whether the 20% and 30% losses of Fe suggested above are feasible. The primary sulfide minerals formed in the early buoyant plume are pyrite (FeS_2), pyrrhotite ($Fe_{(1-x)}S$ where x=0.2 to 1.0), chalcopyrite ($CuFeS_2$) and sphalerite

(ZnS, can also be ZnFeS), the exact stoichiometry of the sulfides can vary and the proportions of each sulfide phase varies between sites (Feely et al., 1987; Mottl & McConachy, 1990). For the purposes of this estimate, it is assumed that the sulfides are of a simple composition, that all vent fluid Cu is removed as $CuFeS_2$, all vent fluid Zn is removed as ZnS and any 'excess' Fe is removed as FeS.

	Kairei[a]	**Edmond[a]**	**Snakepit[b]**
Vent fluid [Fe] (mmol/kg)	5.4	12.8	2.6
Vent fluid [H_2S] (mmol/kg)	4	4	6
Vent fluid [Cu] (µmol/kg)	210	220	20
Vent fluid [Zn] (µmol/kg)	80	130	50
Estimated loss of Fe (%)	20	30	25
Estimated loss of Fe (mmol/kg)	1.1	3.8	1.3
H_2S required for Cu and Zn removal as $CuFeS_2$ and ZnS (mmol/kg)	0.5	0.5	0.1
H_2S required for removal of estimated Fe loss as FeS (in addition to Fe removed as $CuFeS_2$)	0.8	3.6	1.3
Total H_2S required	1.3	4.1	1.4

Table 7. Calculations showing feasibility of estimated Fe loss due to sulfide formation

[a] Kairei and Edmond vent fluid data are from Gamo et al., 2001 and Gallant & Von Damm, 2006.

[b] Snakepit vent fluid data from Edmond et al., 1995 and estimate of Fe loss from James & Elderfield, 1996

Table 7 above shows the concentrations of Fe, Cu , Zn and H_2S in the vent fluids and the figures demonstrating that the suggested losses of Fe from the Kairei and Edmond sites appear to be feasible based on this simple estimate. The figures above also suggest that only one third of the vent fluid H_2S is removed as sulfides at Kairei whereas at Edmond all the H_2S is taken up as sulfides. The estimate for Snakepit is shown for comparison to show that this simple calculation works for data from another hydrothermal site.

Figure 22 shows a plot of just the dissolved (<0.4µm) Fe versus dissolved (<0.4µm) Mn for the Kairei samples. The linear regression through the dissolved Fe data when compared with the vent fluid ratio suggests that ~50% of Fe has been lost from the dissolved phase. We would expect to see loss of Fe from the dissolved phase because as already discussed, Fe sulfides rapidly precipitate as the hydrothermal fluids emerge from

the vents. This is followed by further oxidation and precipitation of dissolved Fe (II) as Fe (III) oxyhydroxides (Mottl & McConachy, 1990; Rudnicki & Elderfield, 1993). From the total Fe versus dissolved Mn plot for the Kairei samples (Fig. 20) it is already apparent that ~20% of the vent fluid Fe has been completely lost from the plume. In conjunction with the dissolved Fe plot in Fig. 22, this suggests that a further 30% of the original vent fluid dissolved Fe (II) has either precipitated in the plume as fine grained sulfides (which have not subsequently settled out of the plume) or been oxidised to form particulate Fe (III) oxyhydroxides. Initially colloidal Fe (III) is formed which then aggregates to form particulate Fe, however the colloidal Fe (III) would be measured in the <0.4μm fraction so it can be assumed that the loss is due to particulate Fe formation.

As dissolved Mn essentially behaves conservatively close to its vent source (e.g. Cowen et al., 1990; Kadko et al., 1990) the dissolved Mn concentration should be a function of dilution of the plume, but, some evidence of dissolved Fe loss relative to dissolved Mn (i.e. negative departure from linearity in Fig. 22) would be expected, rather than the essentially linear relationship exhibited. However, as the dissolved Fe and Mn concentrations in the vent fluids are 5400μM and 840μM respectively (Gamo et al., 2001) whereas the maximum concentrations in these samples are 370nM and 120nM respectively, the resulting plot is in fact only the very lowest portion (<<1% of the whole) of a much larger curve and therefore will appear linear. A linear relationship for dissolved Fe and Mn at these lower concentrations has also been observed at the TAG, Snake Pit and Broken Spur hydrothermal sites in the Atlantic Ocean (James et al., 1995; James & Elderfield, 1996)

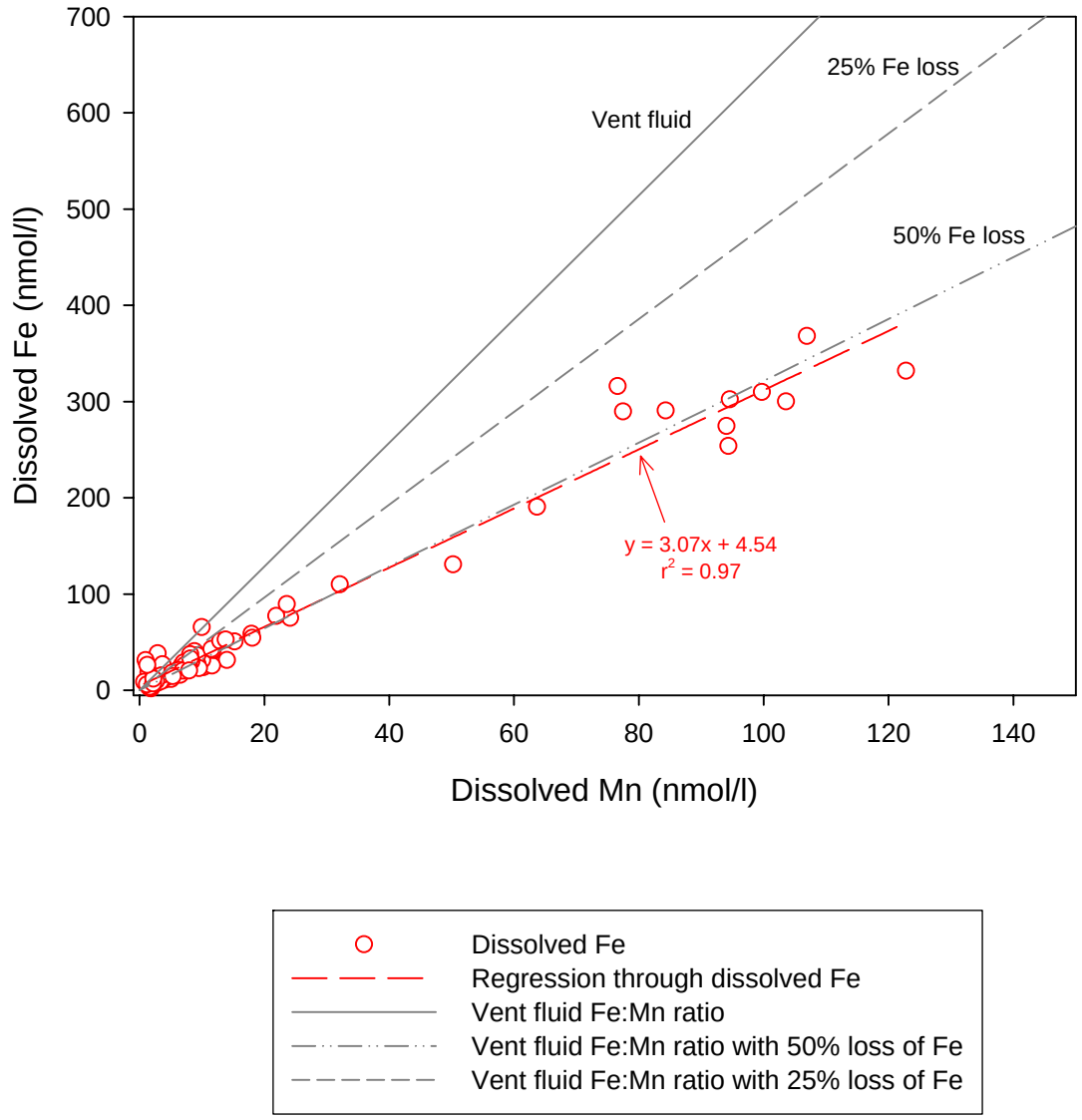

Figure 22 Dissolved (<0.4µm) Fe versus dissolved (<0.4µm) Mn for Kairei hydrothermal plume samples. Regression is through all data. Vent fluid ratio and vent fluid ratios with possible Fe losses are shown for comparison.

A plot of the dissolved (<0.4µm) Fe and Mn data for the Edmond samples is shown in Fig. 23. The linear regression through the data has a lower correlation coefficient than the Kairei data, which is mainly due to the smaller number of samples collected at Edmond. Only one sample has [Mn] >70nmol/l which means the high-endmember is poorly constrained compared to Kairei. The vent fluid concentrations of Fe and Mn are higher than at Kairei, being 12800µmol/l and 1430µmol/l respectively (Gallant & Von Damm, 2006), therefore as at Kairei, we are observing a very small proportion of the overall trend. Although the linear regression for the dissolved Fe data is not as robust as

that for Kairei, comparison with the vent fluid ratio suggests that ~70% of the dissolved Fe (II) present in the vent fluids is missing. From the total Fe plot (Fig. 21) it was estimated that ~30% of Fe has been completely lost from the plume leaving ~40% in the particulate phase either as fine grained sulfides or oxyhydroxides. Although the proportion of dissolved Fe (II) either lost completely from the plume or transformed to the particulate phase appears to be higher at Edmond than at Kairei, the scatter in the Edmond data should be noted. However the figures here serve as a first estimate of Fe losses from the plume.

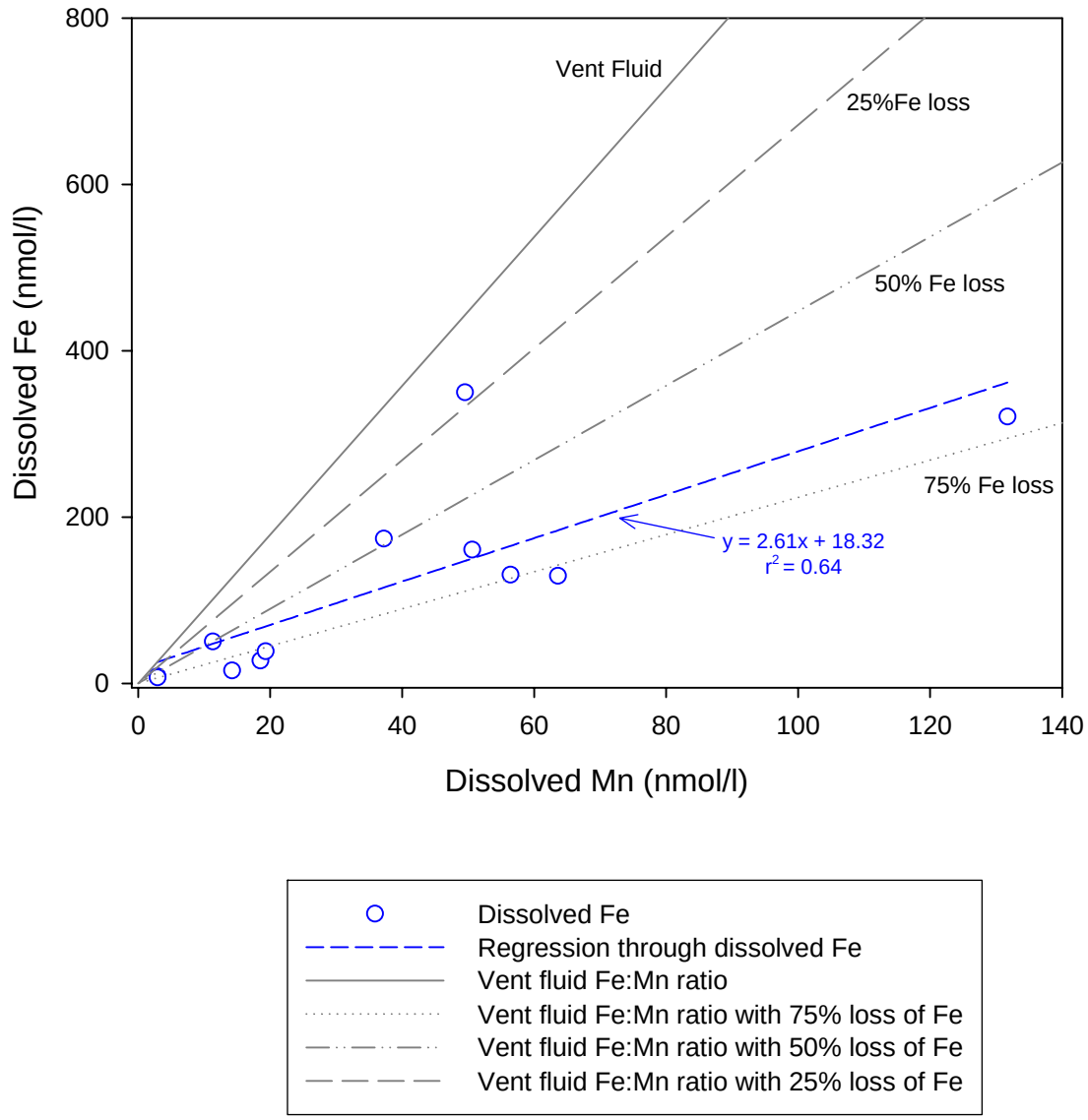

Figure 23 Dissolved (<0.4µm) Fe versus dissolved (<0.4µm) Mn for Edmond hydrothermal plume samples. Regression is through all data. Vent fluid ratio and vent fluid ratios with possible Fe losses are shown for comparison.

Overall, the data from the Kairei and Edmond hydrothermal plume samples suggest that 70-80% of the total dissolved Fe (II) emerging from the vents is still present in the plume at the time of sample collection, either as dissolved or particulate Fe. The 20-30% that has been lost is consistent with rapid precipitation of sulfides in the early stages of plume formation followed by deposition to the seafloor. Of the total Fe remaining in the plume, approximately 50% is present in the dissolved (<0.4μm) phase in the 'youngest' least dilute samples which, dissolved Mn concentrations suggest are very young non-buoyant plume samples. As the time taken for the non-buoyant plume to be reached is ~1 hour (Speer & Rona, 1989) and $t_{½}$ for Fe (II) oxidation at these stations of 2.3hrs (Statham et al., 2005) this makes sense, there should be at least 50% of any Fe (II) not precipitated as sulfides, still in solution. This contrasts with the North Atlantic where $t_{½}$ for Fe (II) oxidation is ~20mins so there is no dissolved Fe found in non-buoyant plume samples and the Pacific where $t_{½}$ is up to ~6.4hrs (Field & Sherrell, 2000) so little particulate Fe is precipitated prior to reaching the non-buoyant plume. If we assume that the dissolved Fe (II) remaining in the Indian Ocean plumes will be quantitatively oxidised and precipitated within 5 half times, i.e. ~12 hours and assume a deep ocean current of 2cm/s then there should be no dissolved Fe remaining further than ~1km from the vent site. Clearly the results from CTDs 4 and 6 which are 1.3km and 1.7km from the vent respectively, show that there are significant concentrations of dissolved Fe (up to 40nmol/l, see Table 3) which may suggest higher current speeds in this area. The dissolved Fe concentrations at CTDs 4 and 6 represent ~50% of the original vent fluid Fe, i.e. effectively only one half-life (2.3hrs) has elapsed. For a distance of 1.5km this suggests a current speed of 18cm/s. Current speeds as high as this have been recorded at e.g. the Rainbow hydrothermal site in the non-buoyant plume (Khripounoff et al., 2001).

3.4.4 *In situ* particulate Fe calculations

Although we have data on the total Fe in the samples, the particulate Fe will not be representative of the *in situ* particulate Fe in the plume at the time of sample collection because the time taken to get the sample back on board ship and processed is longer (2-5 hours) than the oxidation half time for dissolved Fe at this location, i.e. this delay will have allowed further Fe (II) oxidation and particulate Fe to form, after the Niskin bottles

were closed and the samples taken. By recording the time of the CTD rosette sampling and the time of subsequent sample processing on board ship, however, then - knowing the Fe (II) oxidation rate, the *in situ* Fe (II) data was calculated (Statham et al., 2005) for some of the most Fe-rich samples from CTD stations 23 at Edmond and 21 at Kairei. The difference in total Fe and *in situ* Fe (II) can then tell us how much particulate Fe there was in the sample in the non-buoyant plume at the time of collection. Table 8 shows the data.

Sample	Total Fe (nmol/l)	*In situ* Fe II (nmol/l)	*In situ* particulate Fe	% *In situ* particulate to total Fe
Kairei				
CTD 21 2120m	530	465	65	12
CTD 21 2220m	371	397		
CTD 21 2273m	409	151	258	63
CTD 21 2320m	144	72	72	50
CTD 21 2372m	74.3	44.1	30	41
Edmond				
CTD 23 2960m	17.6	41.3		
CTD 23 3008m	308	339		
CTD 23 3019m	394	366	28	7
CTD 23 3057m	232	228	4	2
CTD 23 3107m	278	281		

Table 8. *In situ* particulate Fe for Kairei and Edmond samples calculated from total Fe (dissolved [<0.4µm] Fe plus particulate [>0.4µm] Fe) and *in situ* Fe II data (Statham et al., 2005)

The data suggests that for the samples collected at Edmond, there was very little or no particulate Fe present in the non-buoyant plume at the time of collection. This correlates with the relatively low maximum concentrations of Fe (~50nmo/l) collected by *in situ* filtration of these samples, as retained on SAP filters (see Chapter 4 for full details) compared to previous studies at the TAG and Rainbow hydrothermal sites (~200nmol/l at TAG, ~400nmol/l at Rainbow (German et al., 1991a; Edmonds & German, 2004)). For the Kairei samples, the data suggests that there was a significant fraction of particulate Fe present in the plume, unlike the Edmond samples. This initially seems odd as CTDs 21 and 23 are both very close to their respective vents (~0.1km), however comparison with the LSS profiles shown earlier for each CTD (Figs. 9 and 13) reveals that the samples

shown in Table 8 for CTD 23 generally have much lower LSS signals than the samples for CTD 21. This is consistent with a lower *in situ* particulate loading for the CTD 23 samples.

These calculations give us some information on the processes occurring within hydrothermal plumes. However the uncertainties in the calculations (for example, the fact that four of the ten samples have an *in situ* Fe (II) concentration which exceeds the total Fe) serve to highlight the importance of future hydrothermal plume studies focussing on *in situ* measurements, as well as collecting samples which are processed on board ship and analysed later in the laboratory.

3.4.5 Plume Age Calculations

Assuming Fe (II) follows first order kinetics then:

$$[Fe] = [Fe]_{t=0}\, e^{-k_1 t}$$

This means that if we know the Fe (II) concentration at the time of sample collection (*in situ* Fe (II) in Table 8 above) and plume dilution (estimated from dissolved Mn data, figures are in Table 6), the initial Fe concentration and the rate constant k_1 for Fe (II) oxidation ($0.303 hr^{-1}$ (Statham et al., 2005)) we can calculate the age of the plume from:

$$t = -\frac{1}{k_1} \ln \frac{[Fe]}{[Fe]_{t=0}}$$

The initial concentration of Fe (II) is the vent fluid concentration, however some of the vent fluid Fe (II) will have precipitated as sulfides. This must be estimated to give an initial Fe (II) concentration before any dilution of the plume. For this calculation, we will use the percentage Fe loss estimated earlier in the section 'Estimates of Fe Loss' (20% for Kairei and 30% for Edmond) which gives an initial 'available' Fe (II) concentration (after sulfide precipitation) of 4.3mmol/l at Kairei and 9.0mmol/l at Edmond.

Results of the plume age calculations are shown in Table 9 below. Using the plume dilution factor from the dissolved Mn data, the original Fe (II) concentration that the samples would have had before dilution can be estimated. From this, the plume age can be calculated.

Sample	*In situ* Fe II (nmol/l)	Dilution factor (based on Mn data)	Original Fe II conc^{n} (mmol/l)	Plume age (hrs)
Kairei				
CTD 21 2120m	465	8400	3.9	0.3
CTD 21 2220m	397	8900	3.5	0.7
CTD 21 2273m	151	10000	1.5	3.4
CTD 21 2320m	71.5	36000	2.6	1.7
CTD 21 2372m	44.1	61000	2.7	1.5
Edmond				
CTD 23 2960m	41.3	520000	22	*
CTD 23 3008m	339	25000	8.5	0.2
CTD 23 3019m	366	23000	8.4	0.2
CTD 23 3057m	228	39000	8.9	0.1
CTD 23 3107m	281	28000	7.9	0.4

Table 9. Plume age calculations for Kairei and Edmond samples where *in situ* Fe (II) data are available.
* not valid as concentration exceeds the initial calculated Fe conc^{n} after taking account of sulfide formation

The plume ages for the Edmond samples are very low when considering that it takes ~1 hr to reach the non-buoyant plume (Lupton, 1995). This suggests that either the estimate of Fe loss to sulfides is too high or the dilution factor calculated from the dissolved Mn data is too high. If the dilution factor were too high this could suggest that Mn is not behaving conservatively and there has been loss of Mn from the plume resulting in a higher estimated dilution. However there is no evidence from the relationship of total Fe and dissolved Mn for Edmond in Fig. 21 which is essentially linear (if Mn were being lost from the plume then some negative curvature may be expected) and the particulate Mn throughout all plume samples is uniformly low compared to all the dissolved Mn data. It is more likely that the Fe loss estimate is high; a plume age for the youngest samples of ~1hr requires only a 10% loss due to sulfide formation (giving an initial 'available' Fe (II) concentration of 11.5mmol/l).

For Kairei, the plume ages appear more realistic (although the two shallowest samples have ages <1hr). CTD 21 was located ~0.1km from the vent; assuming a current of ~2cm/s it would take ~1.5hrs to travel 0.1km. Taking into account the elapsed time for the initial vent fluids to reach the non-buoyant plume, the ages of 1.5 to 3.4 hrs seem reasonable. Comparison with literature data is difficult because other estimates of plume age have been for samples much further away from the vent (e.g. Rudnicki & Elderfield, 1992; Chin et al., 1994). However plume age estimates using Fe (II) measurements and the Fe (II) oxidation half time by Chin et al. (1994) showed good agreement with estimates for the same samples made using ^{222}Rn and Mn measurements by Gendron et al. (1994).

3.4.6 Calculation of rate constant k_1 for Fe (II) oxidation

The first prediction of Fe (II) oxidation rates in the Indian Ocean was by Field & Sherrell (2000) which gave a value of 1.3hrs based on WOCE data from a station at ~29°S 55°E. This is lower than the experimental value calculated by Statham et al. (2005) of 2.3hrs, in the Kairei and Edmond hydrothermal plumes. As we have data from the Kairei and Edmond areas, we can calculate the rate constant k_1 to see how this compares to both the Statham et al. and Field and Sherrell values.

The equation for the rate of oxidation of Fe (II) is given by (Millero et al., 1987):

$$-\frac{d[Fe(II)]}{dt} = k_1[Fe(II)]$$

where: $k_1 = k[OH^-]^2\,[O_2]$ and $t_{½} = ln2 / k_1$.

$$\log k = 21.56 - \frac{1546}{T} - 3.29I^{½} + 1.52I$$

$$I = 0.0199S$$

and T = temperature, I = ionic strength, S = salinity

Temperature, salinity and dissolved oxygen concentrations were measured at each CTD station, the ridge flank profile at CTD 16 at a depth of 2298m was chosen for this calculation. [OH] can be calculated from pH which was not measured and is also not available in the WOCE dataset. However pH can be calculated using the CO2SYS program (Lewis & Wallace, 1998), this requires total carbon and total alkalinity data as well as phosphate and Si concentrations. These data are available from the WOCE datasets, Station 514 on the IO3 transect at 20°00'S 70°45'E was chosen as it is the closest available station to CTD 16. Data from a depth of 2294m was selected. Data used for the calculation of k_1 and the results are shown in Table 10 below.

	Position	**Depth (m)**				
			Temperature (°C)	**Salinity**	**Dissolved O_2[a] (µmol/kg)**	
CTD 16	24°41'S 71°08'E	2298	1.872	34.713	184.3	
			Alkalinity (µmol/kg)	**Total Carbon (µmol/kg)**	**PO_4^{3-} (µmol/kg)**	**Si (µmol/kg)**
IO3 Stn 514	20°00'S 70°45'E	2294	2376	2271	2.28	106.11
			pH_{sws}	**pK_w**	**pOH[b]**	
Data from CO2SYS			7.857	14.133	6.276	
			Rate Constant k_1	**Half time $t_{½}$ (mins)**	**Half time $t_{½}$ (hrs)**	
Calculated values			0.00936	74.04	1.23	

Table 10. Half time for Fe (II) oxidation calculated from background data in the vicinity of the Kairei and Edmond hydrothermal sites.
[a] Mean of four measurements taken at plume depths
[b] $pOH = pK_w - pH_{sws}$

The half time for Fe oxidation calculated from Kairei and Edmond data of 1.2hrs is much lower than the experimental value of Statham et al. of 2.3hrs. However the calculated value is based on the temperature, salinity, pH and $[O_2]$ of the ambient water at Kairei and Edmond; conditions right in the plume where oxidation is taking place will be slightly different but are they sufficient to account for the difference in calculated and experimental half times? For example there may be a small increase in temperature and a coincident decrease in salinity (see e.g. Fig. 18 for CTDs 5 and 21). A 0.1°C increase in

temperature however (which although possible in a buoyant plume (e.g. Rudnicki & German, 2002) is unlikely in a non-buoyant plume, CTDs 5 and 21 show temperature anomalies of ~0.02°C in the plume) would lower the half time by only 2 minutes. Likewise, a 0.1 increase in salinity (again unlikely in the non-buoyant plume as the buoyant plume at Kairei only shows an increase of 0.0005 (Rudnicki & German, 2002)) would only increase the half time by ~1 minute.

Dissolved O_2 concentrations from the Kairei hydrothermal plume samples are lower than those of the background ridge flank samples, 179.3±2.3µmol/kg compared to 184.3±0.6µmol/kg. A lower dissolved O_2 concentration will increase the half time, but a 5.0µmol/kg reduction will only increase it by ~3mins. Although total alkalinity and total carbon have not been measured in hydrothermal plumes, they have been measured in vent fluids (Von Damm, 1990; 1995). Total alkalinity is generally zero while total carbon ranges from 4 to 290mmol/kg, i.e. it is elevated above that of seawater (~2300µmol/kg). If we assume therefore that alkalinity may be slightly lower in the plume while total carbon may be elevated, we can estimate the affect that this may have on the half life: for example either a reduction in alkalinity of 20µmol/kg or an increase in total carbon of 20µmol/kg would increase $t_{½}$ to 1.6hrs.

None of the above parameters are able to account for the whole difference between the calculated and experimental half times; the remaining parameter which affects the half time is pH. Is there sufficient change in pH within a hydrothermal plume to account for the increased experimental half time? The pH required to give a half time of 2.3hrs can be calculated, it is 7.721, i.e. a decrease in pH of 0.14 would be necessary. There is little data on the pH variations within hydrothermal plumes, however pH measurements of a buoyant hydrothermal plume in the Lau Basin showed a maximum decrease in pH of 0.05 (Edmonds, Pers. Comm.) so it is unlikely that a change of 0.14 would be seen in a non-buoyant plume.

The experimental results of Statham et al. (2005) suggested Fe (II) oxidation does not strictly follow first order kinetics and that there may be other processes at play. These may include interactions of Fe (II) with dissolved organic matter/organic binding ligands (e.g. Johnson et al., 1997; Santana-Casiano et al., 2000), the oxidation of sulfides

producing Fe (II) in solution (Rimstidt & Vaughan, 2003) or the reduction of Fe (III) back to Fe (II) by the superoxide radical O_2^- which is produced during Fe (II) oxidation (King et al., 1995). The above calculations seem to corroborate that there are some additional factors, as adjusting the parameters to the conditions that may be found in a non-buoyant plume does not alter the half time sufficiently. To assess the affect that other processes may be having on the Fe (II) oxidation rate, it would be necessary to measure all the required parameters within the non-buoyant plume and calculate the half time, then compare this to the experimental value. Massoth et al. (1998) did exactly that for plumes on the Gorda Ridge in the Pacific Ocean and calculated a half time of ~12hrs based on conditions in the plume. This is longer than that of 6.4hrs predicted by Field & Sherrell (2000) for the Gorda Ridge using ambient seawater data from a WOCE station, which indicates that conditions within the plume seem to extend the Fe (II) oxidation half time. The experimental half time measured by Massoth et al. was 42hrs which like the experimental value for the Indian Ocean is higher than the calculated value. This again suggests that other processes may be at play. Massoth et al. did also fit their results to second order kinetics; although this reduced the experimental half time to 39hrs, it still does not account for the whole difference between the experimental and theoretical values. Table 11 summarises the different Fe (II) oxidation half times, discussed above, which have been calculated and reported for the Indian Ocean and Gorda Ridge in the Pacific Ocean.

These calculations of the rate constant for Fe (II) oxidation show, that while such exercises are useful and have their place, experimental data are crucial to properly determine what is going on in natural systems.

Method used to obtain Fe (II) Oxidation Half Time	Fe (II) Oxidation Half Time (Hrs)
Indian Ocean	
Calculated from ambient data from WOCE Transect IO7C Station 682[1]	1.3
Calculated from ambient data close to Kairei and Edmond (pH calculated from data at WOCE Transect IO3 Station 514)	1.2
Experimental observation[2] - assuming 1st order kinetics	2.3
Pacific Ocean – Gorda Ridge	
Calculated from ambient data from WOCE Transect P17N Station 45[1]	6.4
Calculated from 'in-plume' data[3]	12
Experimental observation[3] - assuming 1st order kinetics	42
- assuming 2nd order kinetics	39

Table 11. Fe (II) Oxidation half times from published literature and this study for the Indian Ocean and Gorda Ridge in the Pacific Ocean. Values for Gorda Ridge are shown to illustrate the difference between various methods used to derive the Fe (II) oxidation half time. While calculations from ambient data provide an estimate of the Fe (II) oxidation rate in the surrounding ocean, they cannot account for the conditions in the plume which will be slightly different. The 'in-plume' result uses data measured within the plume which should be more accurate. Experimental observation (where samples are taken from the plume and oxidation rate determined from measuring Fe back on board ship) replicates plume conditions including any additional influencing factors such as e.g. microbial interaction, although it does not reflect *in situ* pressure which may affect the oxidation rate. For further details, see main text.

[1] Field & Sherrell (2000)
[2] Statham et al. (2005)
[3] Massoth et al. (1998)

3.4.7 Summary

Dissolved and particulate Fe and dissolved Mn are all high in the Kairei and Edmond hydrothermal plumes but particulate Mn is always low, consistent with the slow oxidation of Mn which behaves pseudo-conservatively over the distances away from a vent which are discussed here. The maximum dissolved concentrations in the Indian Ocean, measured in this study are high compared to Atlantic and most Pacific hydrothermal plumes reported previously. Comparison with the vent-fluid Mn data reveals why this is, the strongest plume signals represent $<10^4$ fold dilution, i.e. these are very young, concentrated plume signals indicative of fluids recently emplaced at plume-

height at the top of the buoyant plume. This is consistent with USBL navigation records from the CTD which show that samples were taken within 100m of the vents, which is within the area of buoyant plume lateral spread as calculated from the height of rise of the plume

The total Fe versus dissolved Mn data enables us to see how much Fe has been removed (20-30%) even in the youngest samples which have recently reached non-buoyant plume height. This is consistent with the removal of that Fe, along with all available Cu and Zn in the vent fluids via the formation of poly-metallic sulfides with the available H_2S in those vent fluids. The dissolved Fe versus dissolved Mn data suggests that there is further dissolved Fe loss via *in situ* oxidation and removal into the particulate phase. This is consistent with oxidation times which are not significantly longer than plume emplacement times.

From the measured total Fe we can subtract the calculated *in situ* Fe(II) to obtain the proportion of Fe that was in the particulate phase at time of plume sampling, these are generally small numbers confirming that the samples were 'fresh'. Using the known Fe oxidation rate, and assuming that we accurately know how much Fe has been removed as sulfides, we can calculate the age of the samples from when they initially emerged from the vents. Those calculations yield unreasonably young ages for the Edmond samples, which suggests the estimates of the proportion of Fe removed as sulfides should be revised downwards to ~10%. This remains consistent with available Cu, Zn and H_2S vent fluid concentrations.

A limitation to the work to date (Statham et al, 2005) is that the calculation of oxidation rates requires a linear fix, however it is probably more complex than that. To progress that, however, requires a more comprehensive data-set of additional parameters as well as a better understanding of the processes related to Fe (II) oxidation. Any future study of Fe cycling in hydrothermal plumes should at least measure concentrations of organic matter, *in situ* pH, *in situ* dissolved [O_2], *in situ* temperature and *in situ* salinity.

4 Chapter 4 Particulate (>1.0µm) samples: Inter-comparison with earlier studies.

4.1 Introduction

Previous studies of hydrothermal plumes in the Atlantic and Pacific Oceans have found that although there are similarities in the reactions taking place within plumes, the rate of iron (II) oxidation varies significantly (Field & Sherrell, 2000; Statham et al., 2005). This is important because it is iron oxidation and the precipitation of iron oxyhydroxide particles, which serves to modify the gross fluxes of dissolved metals to the oceans at all vent sites (e.g. German et al., 1991a). The aim of this chapter is to determine whether the plume processes identified previously in the Atlantic and Pacific Oceans are also broadly applicable to the Indian Ocean.

As described in Chapter 2, stand alone pump samples (SAPs) were deployed on a CTD rosette to collect large volume particulate samples by in-situ filtration through 293mm Nucleopore 1.0µm filters. This chapter will focus solely on these >1.0µm SAP samples, enabling a direct comparison with the data of German et al. (1991a) from the TAG hydrothermal site in the Atlantic, and the data of Edmonds & German (2004) from the Rainbow hydrothermal site in the Atlantic, which were also obtained using SAPs and 1.0µm filters.

For reference, vent fluid characteristics from the Kairei and Edmond sites which were the subject of this study as well as those of the TAG and Rainbow sites are shown in Table 12. The filtered seawater samples collected from Niskin bottles were discussed in Chapter 3 while the associated particulate samples (>0.4µm and >0.1µm) will be discussed in Chapter 5.

	Kairei[1]	Edmond[1]	TAG[2]	Rainbow[3]
Temperature (°C)	360	380	360	365
pH	3.5	3.1	3.4	2.8
Alkalinity (meq/kg	-0.46	-0.53	-0.45	-
Chlorinity (mmol/kg)	640	930	640	750
H_2S (mmol/kg)	4.0	4.7	3.0	1.2
Fe (μmol/kg)	5400	13900	5600	24000
Mn (μmol/kg)	840	1430	680	2250
Cu (μmol/kg)	210	160	135	140
Zn (μmol/kg)	80	130	46	160

Table 12. Vent fluid characteristics of the Kairei and Edmond study sites in the Indian Ocean and the TAG and Rainbow sites in the Atlantic Ocean

[1] Data from Gamo et al. (2001) and Gallant & Von Damm (2006)
[2] Data from Edmond et al (1995) and Edmonds et al (1996)
[3] Data from Douville et al. (2002) and Charlou et al. (2002)

4.2 Results

The concentrations of particulate Fe, Al, Mn, Mg, Ca, P, V, As, Cu, Zn, Cd, Pb and Y for the stand alone pump samples (>1.0μm) are shown in Table 13. Particulate rare earth element concentrations for these samples are in Table 14. Na concentrations were also measured and assuming that all Na present is derived from sea salt then for the majority of samples only ~0.5ml of seawater was retained on the filters after rinsing. Two samples had retained ~1ml and one sample ~2.3ml of seawater, however these volumes are still insufficient to cause more than 0.05% difference in concentration between sea salt corrected and non sea salt corrected results for all other elements considered here. The presented results have been corrected for sea salt.

Iron concentrations range from 5 to 55nmol/l and maximum concentrations of 45 to 55nmol/l are observed at the CTD stations in closest proximity (<0.1km) to the vent sites. These concentrations are lower than the maximum of 212nmol/l and 420nmol/l observed in the TAG and Rainbow non-buoyant hydrothermal plumes, respectively, in the Atlantic (German et al., 1991a; Edmonds & German, 2004), also using SAPs. This is despite the fact that the use of real time nephelometry data (as described in Chapter 2) ensured that the SAPs were definitely suspended in the hydrothermal plume. A plot of percentage Fe/(Fe+Mn+Al) against Fe for both the Kairei and Edmond SAPs data are shown in Fig.

24. The ratio of Al to (Fe+Mn+Al) can be used as an indicator of the hydrothermal versus detrital contribution to sediments (Bostrom et al., 1969), where a low value (~less than 10%) indicates very low detrital input. Similarly, a high value for the ratio of Fe to (Fe+Mn+Al) indicates low detrital input and therefore a high hydrothermal input. Here the percentage Fe/(Fe+Mn+Al) are all greater than 80% except for one sample, which suggests that these samples are definitely hydrothermal in origin rather than, for example, re-suspended sediment with a terrigenous origin. The much lower percentage of one sample from the Edmond site is due to an anomalously high manganese concentration, compared to the rest of the samples, of 6.8nmol/l.

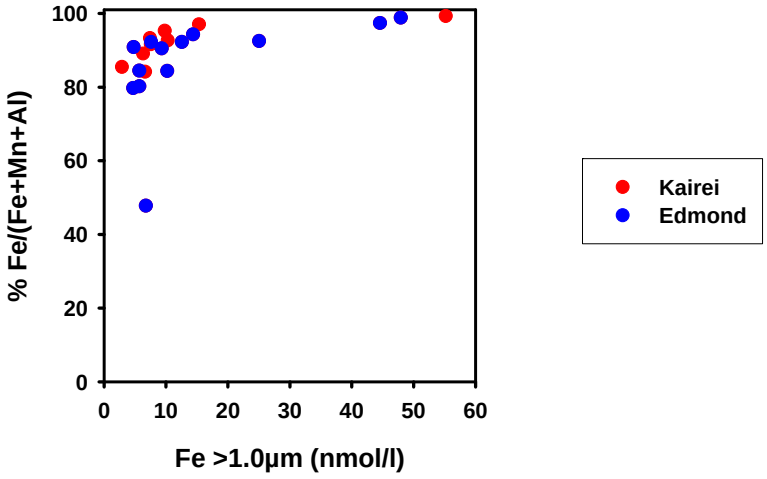

Figure 24 Percentage particulate Fe/(Fe+Al+Mn) versus particulate Fe for Kairei and Edmond hydrothermal plume SAP (>1.0µm) samples

	Fe	Al	Mn	Fe	Mg	Ca	P	V	As	Cu	Zn	Cd	Pb	Y
	nmol/l	nmol/l	nmol/l	(Fe+Mn+Al)	nmol/l	nmol/l	nmol/l	pmol/l	pmol/l	nmol/l	nmol/l	pmol/l	pmol/l	pmol/l
Kairei														
CTD 2 sap003	6.3	0.18	0.58	0.89	24.3	18.1	0.89	15.2	1.1	0.36	0.08	0.11	2.99	0.9
CTD 7 sawp001	15.3	0.28	0.18	0.97	64.5	34.9	2.29	32.1	17.5	1.26	0.28	8.38	5.52	1.4
CTD 7 sap003	10.3	0.20	0.61	0.93	24.5	20.2	1.33	27.8	13.0	0.88	0.17			1.0
CTD 11 sap003	6.6	0.29	0.95	0.84	60.5	31.6	0.97	22.9	10.2	0.12	0.11	0.15		1.2
CTD 17 sap001	2.9	0.27	0.22	0.85	46.8	27.5	0.47		5.3	0.06	0.07	0.06	3.08	0.8
CTD 18 sap003	7.4	0.29	0.25	0.93	46.6	30.6	1.17	24.8	11.4	0.27	0.04	0.15	3.80	1.2
CTD 19 sap001	7.5	0.45	0.24	0.92	35.0	29.0	1.22	16.5	7.5	0.39	0.20			1.1
CTD 20 sap003	9.8	0.26	0.22	0.95	30.8	27.5	1.44	28.6	15.9	0.70	0.18	0.33	2.29	1.1
CTD 21 sap001	55.2	0.23	0.17	0.99	42.4	27.2	6.59	109	60.4	5.84	1.84	107	16.8	2.0
Edmond														
CTD 01 sap003	12.6	0.16	0.90	0.92	13.3	8.4	1.97	39.9	21.0	0.28	0.20	2.93	10.1	0.9
CTD 23 sap002	47.9	0.42	0.15	0.99	32.5	30.9	6.65	130.2	59.0	3.72	2.68			2.3
CTD 23 sap003	44.6	0.56	0.63	0.97	102	42.1	6.05	100	60.0	3.18	2.05	135	47.8	2.4
SAP01 s/n001	4.7	0.20	0.98	0.80	35.9	24.9	0.75	13.8		0.04	0.02	0.11	3.41	1.0
SAP01 s/n002	4.8	0.26	0.22	0.91	14.0	21.1	0.70	17.1	7.9	0.03	0.01			1.0
SAP01 cosap02	5.7	0.51	0.90	0.80	43.4	28.2	0.79	21.6	9.5	0.07	0.02	0.10	5.15	1.1
SAP01 s/n003	6.7	0.54	6.82	0.48	52.1	33.9	1.11	19.4	16.0	0.05	0.05			1.6
SAP01 cosap04	5.7	0.65	0.39	0.84	223	65.6	1.45	21.6	9.4	0.11	0.15			1.0
SAP02 s/n001	10.2	0.41	1.48	0.84	44.6	35.9	1.53	38.9	16.5	0.07	0.03			1.7
SAP02 s/n002	7.6	0.36	0.28	0.92	12.0	26.0	1.13	26.1	12.4	0.04	0.02	0.04	1.63	1.4
SAP02 cosap02	14.4	0.49	0.37	0.94	40.4	33.8	1.99	36.9	28.3	0.93	0.42			1.6
SAP02 s/n003	25.0	0.51	1.52	0.93	67.5	35.9	3.94	80.5	42.2	0.93	0.40	20.6	10.9	2.2
SAP02 cosap04	9.3	0.64	0.34	0.91	27.5	*32.2*	1.28	28.7	6.4	0.09	0.12			1.6

Table 13. Particulate concentrations for Stand Alone Pump (>1.0µm) samples: Molar concentrations (either nmol/l or pmol/l) which have been blank corrected. See Appendix 3 for raw data.

	Fe nmol	La pmol	Ce pmol/	Pr pmol/	Nd pmol/	Sm pmol/	Eu pmol/	Gd pmol/	Tb pmol/	Dy pmol/	Ho pmol/	Er pmol/	Tm pmol/	Yb pmol/	Lu pmol/
Kairei															
CTD 2 sap003	6.3	0.57	1.23	0.137	0.541	0.121	0.039	0.120	0.019	0.113	0.023	0.067	0.009	0.055	0.009
CTD 7 sap001	15.4	1.14	2.11	0.265	1.025	0.215	0.069	0.245	0.039	0.238	0.052	0.139	0.020	0.110	0.018
CTD 11 sap003	6.7	0.82	1.82	0.200	0.769	0.164	0.051	0.159	0.025	0.157	0.031	0.089	0.013	0.077	0.012
CTD 17 sap001	2.9	0.62	1.88	0.145	0.577	0.121	0.037	0.129	0.020	0.119	0.025	0.068	0.010	0.056	0.009
CTD 18 sap003	7.4	0.90	2.11	0.210	0.816	0.173	0.046	0.179	0.028	0.173	0.034	0.097	0.014	0.081	0.014
CTD 20 sap003	9.8	0.74	1.72	0.183	0.718	0.153	0.042	0.156	0.025	0.150	0.030	0.085	0.013	0.072	0.012
CTD 21 sap002	55.2	1.23	1.94	0.265	1.044	0.225	0.078	0.258	0.039	0.254	0.052	0.145	0.022	0.126	0.020
Edmond															
CTD 1 sap003	12.6	0.52	0.43	0.126	0.497	0.112	0.035	0.124	0.020	0.126	0.027	0.074	0.011	0.063	0.010
CTD 23 sap003	44.6	1.51	2.11	0.357	1.404	0.307	0.103	0.341	0.055	0.339	0.086	0.202	0.029	0.165	0.029
SAP01 s/n001	4.7	0.75	1.48	0.187	0.716	0.152	0.041	0.151	0.023	0.146	0.029	0.084	0.012	0.071	0.011
SAP01 cosap02	5.7	0.80	1.58	0.199	0.765	0.163	0.044	0.162	0.025	0.157	0.031	0.089	0.013	0.075	0.012
SAP01 cosap04	5.7	0.88	1.80	0.204	0.788	0.203	0.048	0.172	0.028	0.165	0.043	0.103	0.016	0.081	0.015
SAP02 s/n002	7.6	0.98	1.92	0.242	0.952	0.196	0.054	0.204	0.032	0.196	0.041	0.111	0.016	0.096	0.015
SAP02 s/n003	25.1	1.35	1.93	0.337	1.323	0.269	0.087	0.315	0.049	0.295	0.066	0.179	0.025	0.144	0.024

Table 14. Particulate Rare Earth Element molar concentrations for Stand Alone Pump (>1.0µm) samples Molar concentrations (pmol/l except Fe which is shown for reference in nmol/l) which have been blank corrected (see Appendix 4 for raw data)

Figure 25 shows the same data as Fig. 24 but presented as a ternary plot. This illustrates that the non-hydrothermal component is dominated by a purely Mn-rich phase (most likely Mn oxides) rather than an Al-rich phase (aluminosilicates). This contrasts with the data of Edmonds & German (2004) also shown in Fig. 25, from the Rainbow hydrothermal site in the Atlantic Ocean which were also collected using stand alone pumps. The non-hydrothermal component here is dominated by a mixed Al-rich phase and Mn-rich phase rather than a purely Mn-rich end-member. The presence of high concentrations of Al is usually indicative of re-suspended sediment or detrital aeolian input (e.g. Dymond & Roth, 1988; Sherrell & Boyle, 1992).

Particulate aluminium (pAl) concentrations of 0.2-0.7nmol/l (Table 13) are comparable to those seen in previous particulate samples from hydrothermal plumes in both the Pacific and Atlantic Oceans at similar particulate Fe concentrations (Trocine & Trefry, 1988; German et al., 1991a; Feely et al., 1994a; Edmonds & German, 2004). For comparison, Fig. 26a shows the Edmond and Kairei data plotted together with the TAG hydrothermal plume data of German et al. (1991a) from the Atlantic as these TAG samples were also collected using stand alone pumps and the same pore size filters. The higher pAl concentrations in the TAG samples are most probably a consequence of the higher dust input in the Atlantic from the African continent; similar concentrations of pAl have also been observed at the Rainbow hydrothermal site in the Atlantic (Edmonds & German, 2004). Between 5°N and 30°N in the Atlantic (note the TAG hydrothermal site is at 26°N and the Rainbow hydrothermal site is at 36°N) the dust loadings range between 1 and 700μg/m^3 of air (Chester et al., 1984) whereas in the Southern Indian Ocean where the Kairei and Edmond hydrothermal vents are located, the dust loadings are 2 to 4 orders of magnitude lower (0.01 to 0.25μg/m^3 of air; Chester et al., 1991).

The particulate manganese (pMn) concentrations of 0.2 to 1.5nmol/l are higher than those observed at either TAG (Fig. 26b) or Rainbow (Edmonds & German, 2004) in the Atlantic where the concentrations are all less than 0.4nmol/l, However they are within the range of up to 3nmol/l observed in hydrothermal plumes in the Pacific (Feely et al., 1994a; 1994b)

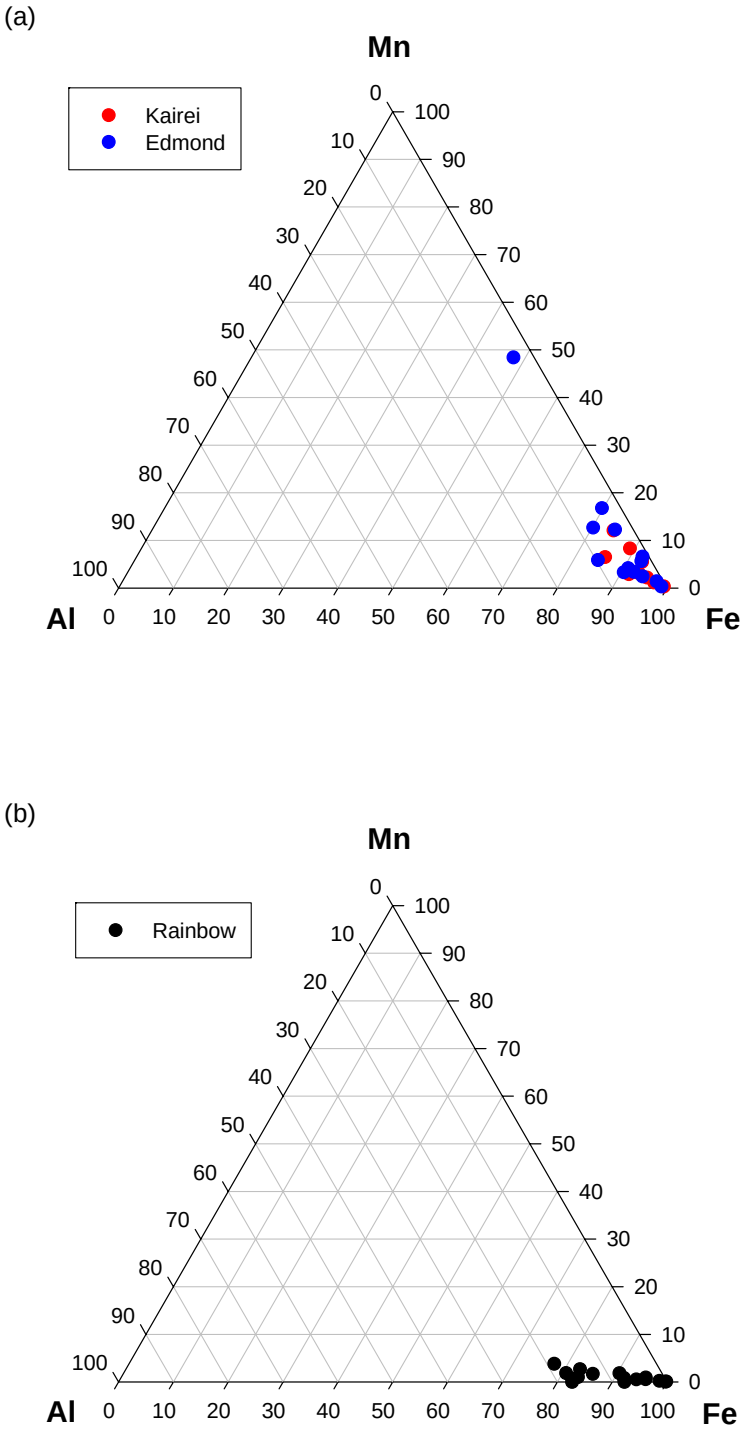

Figure 25 Ternary plots of Fe, Mn, Al composition of hydrothermal particulate SAPs (>1.0µm) samples from (a) Kairei and Edmond (b) Rainbow[1].

[1] Data from Edmonds & German (2004)

Particulate calcium (pCa) and particulate magnesium (pMg) data from Edmond and Kairei and TAG are also shown in Fig. 26 plotted versus pFe. The concentrations from

the Indian Ocean hydrothermal plumes have a much wider range but are comparable to the TAG data except for two samples which have much higher pCa and pMg concentrations. It is also noticeable that pCa and pMg have a good positive correlation with pFe in the TAG hydrothermal plume (German et al., 1991a), although the correlation is much looser for Mg at [pFe] <100nmol/l, but exhibit no apparent correlation in the Kairei and Edmond plumes.

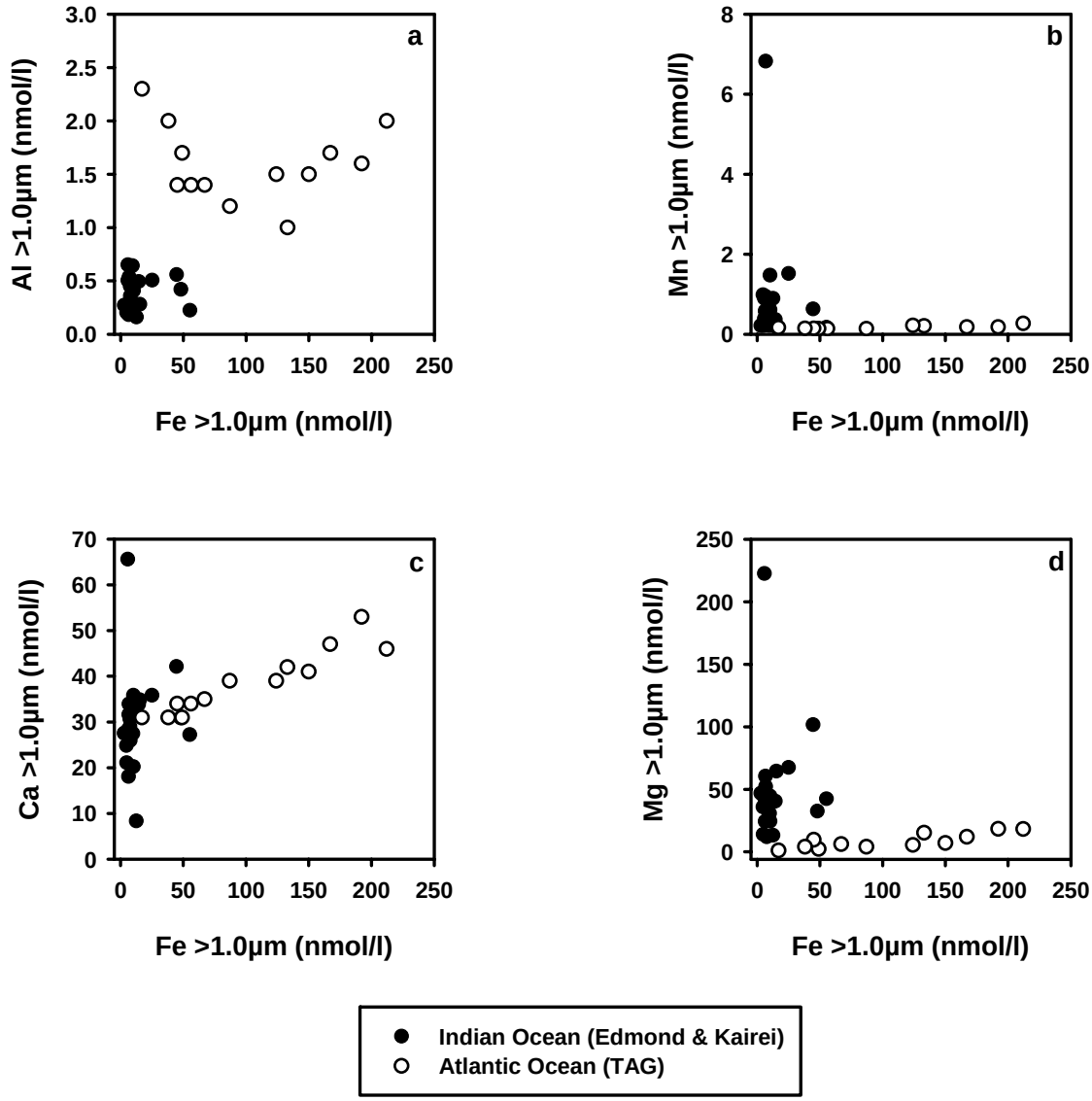

Figure 26 Particulate aluminium, manganese, calcium and magnesium versus particulate iron for SAP (>1.0µm) samples from Indian and Atlantic Ocean hydrothermal plumes. TAG data from German et al., (1991).

4.2.1 Oxyanions

The relationships between particulate phosphorus (pP), particulate vanadium (pV), particulate arsenic (pAs) and particulate iron (pFe) for the SAPs samples are shown in Fig. 27. Particulate P, V and As are all positively correlated to pFe with a linear trend. P concentrations range from 1-7nmol/l, V concentrations range from 20-130pmol/l and As has concentrations up to 70pmol/l, all of which are comparable to previous results in Atlantic and Pacific Ocean hydrothermal plumes when compared to measurements at similar pFe concentrations (German et al., 1991a; Feely et al., 1994a; 1994b; Edmonds & German, 2004).

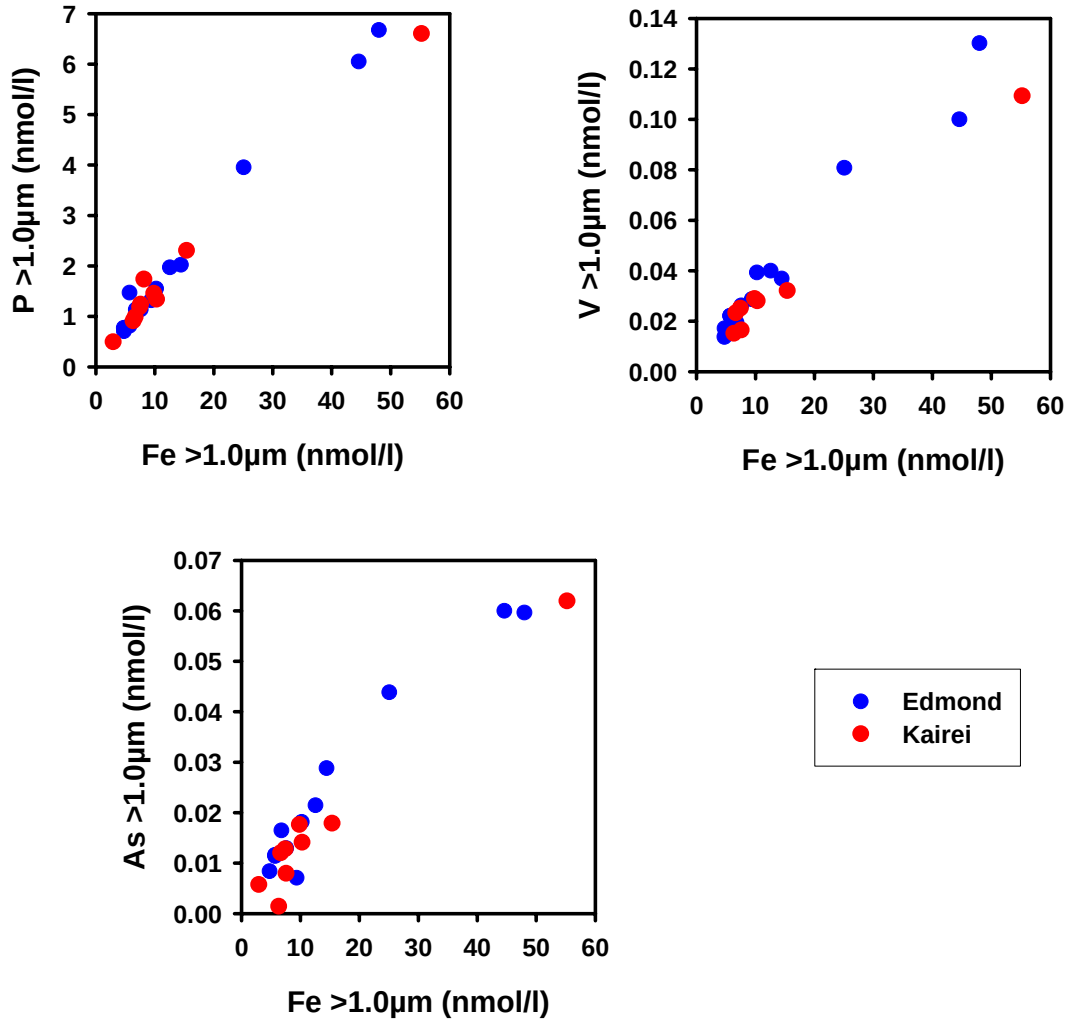

Figure 27 Particulate phosphorus, vanadium and arsenic versus particulate iron for the SAP (>1.0µm) samples from the Kairei and Edmond hydrothermal plumes.

4.2.2 Chalcophile Elements

Figure 28 shows the particulate copper (pCu), particulate zinc (pZn), particulate cadmium (pCd) and particulate lead (pPb) relationships with particulate iron (pFe) for the SAPs samples. In all cases there is a positive correlation with pFe; pCu, pZn, pCd and pPb, concentrations increasing as pFe concentrations increase. The maximum pCu concentrations seen at the Kairei and Edmond sites are 5.8 and 3.7nmol/l respectively which correspond to the maximum pFe concentrations at those sites. These concentrations are comparable to the maximum of 3.3 nmol/l in the Rainbow non-buoyant plume in the Atlantic (Edmonds & German, 2004) and that of 3.0 nmol/l at TAG (German et al., 1991a), also in the Atlantic. Pacific Ocean plume samples at North Cleft on the Juan De Fuca Ridge and the East Pacific Rise (EPR) have lower maximum pCu values of 0.9 and 0.7 nmol/l respectively (Feely et al., 1994a; 1994b). However, overall the Indian Ocean values are in the same range as those from other particulate hydrothermal plume samples.

Zinc concentrations at Kairei and Edmond have a maximum value of 1.8 and 2.7nmol/l respectively but are generally less than 1nmol/l. These values are comparable with particulate plume samples from the Atlantic at both TAG and Rainbow (German et al., 1991a; Edmonds & German, 2004) where Zn concentrations are 1nmol/l or less. Pacific Ocean plume samples are also generally less than 1nmol/l, although there is a maximum [Zn] of 4nmol/l in the North Cleft samples (Feely et al., 1994a; 1994b; 1996).

Particulate Cd concentrations range from less then 1 pmol/l up to 135pmol/l. For similar pFe concentrations, previous results from Atlantic hydrothermal plumes for the >1.0μm size fraction have generally shown pCd concentrations of less than 10pmol/l (German et al., 1991a; Edmonds & German, 2004). The highest [pCd] of 31pmol/l was recorded at the Rainbow hydrothermal site but at a pFe concentration of more than 600nmol/l.

The particulate Pb concentrations reach a maximum of 17pmol/l in the Kairei hydrothermal plume and 47pmol/l in the Edmond plume. These concentrations are comparable to those seen in both the TAG and Rainbow hydrothermal plumes in the Atlantic, where the maximum concentrations are 38 and 29pmol/l respectively. There are no Pb data for Pacific Ocean hydrothermal plumes for comparison.

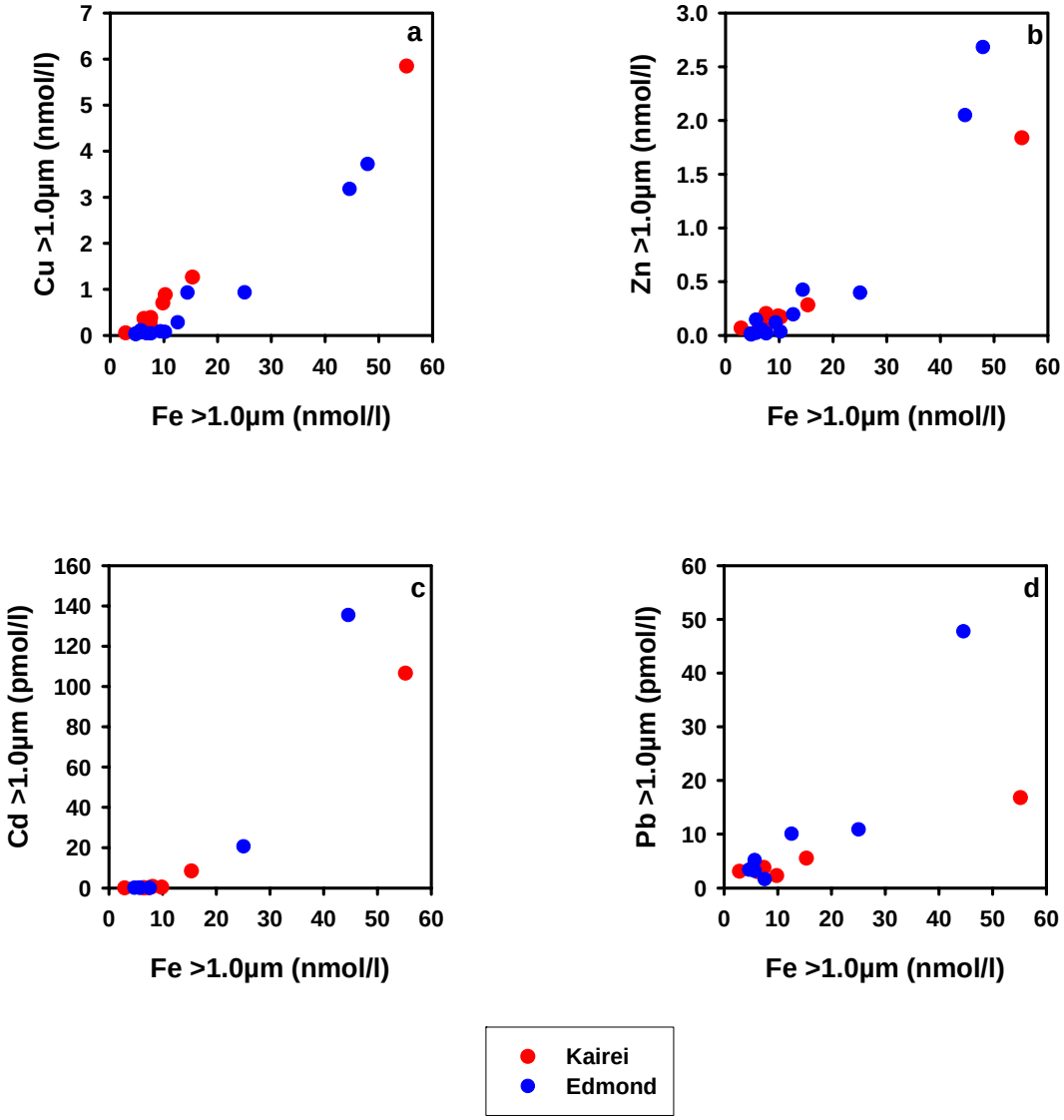

Figure 28 Particulate copper, zinc, cadmium and lead versus particulate iron for the SAP (>1.0µm) samples from the Kairei and Edmond hydrothermal plumes.

4.2.3 Yttrium and Rare Earth Elements

Figure 29 shows the particulate rare earth element (REE) and particulate yttrium (pY) relationships with pFe for the SAP samples. In all cases, there is a positive but non-linear correlation with pFe. The range of concentrations observed for each rare earth element are similar to previous results from the TAG and Rainbow hydrothermal plumes in the Atlantic Ocean (German et al., 1990; Edmonds & German, 2004) and from a hydrothermal plume at 9°45'N on the East Pacific Rise (Sherrell et al., 1999). Particulate Y concentrations vary from 1.1 to 2.4pM and are comparable to values at the Rainbow site in the Atlantic at similar PFe concentrations (Edmonds & German, 2004). Currently there is no Y data available for hydrothermal plumes in the Pacific to enable comparison.

Figure 30 shows the rare earth element patterns for Kairei and Edmond normalised to PAAS (post Archaean Australian Shale, Taylor & McLennan, 1985). Normalisation to PAAS was chosen rather than chondrite or black smoker fluids because our interest is in the impact of hydrothermal activity on oceanic cycles rather than investigating sub-seafloor processes and PAAS normalisation is standard in the literature for deep ocean water column REE data, therefore this enables easier comparison with other datasets. All the samples exhibit a positive europium anomaly and with the exception of one Kairei sample (CTD 17 sap001), a negative cerium anomaly.

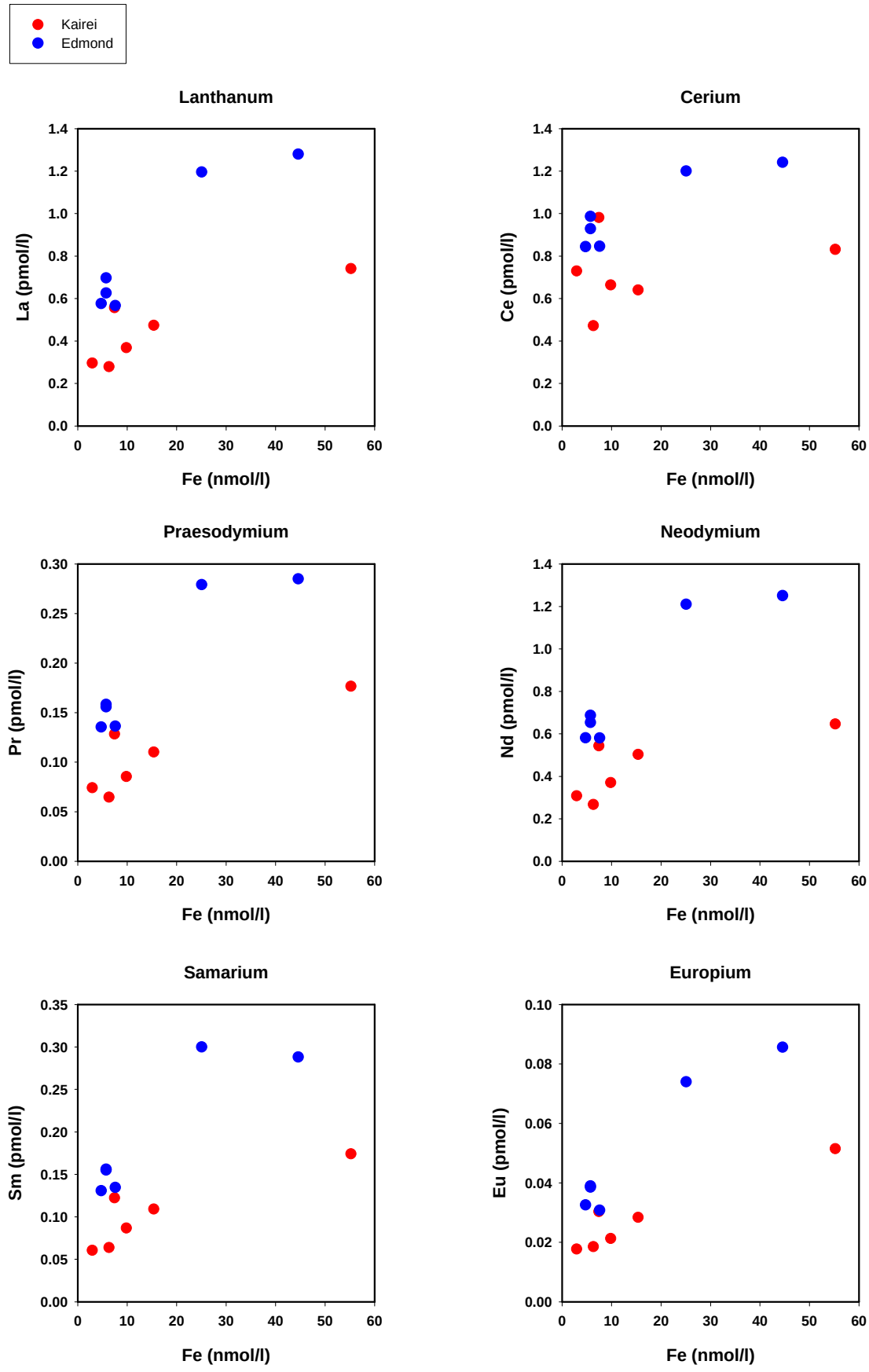

Figure 29 Particulate rare earth elements versus particulate iron for the SAP (>1.0µm) samples from the Kairei and Edmond hydrothermal plumes.

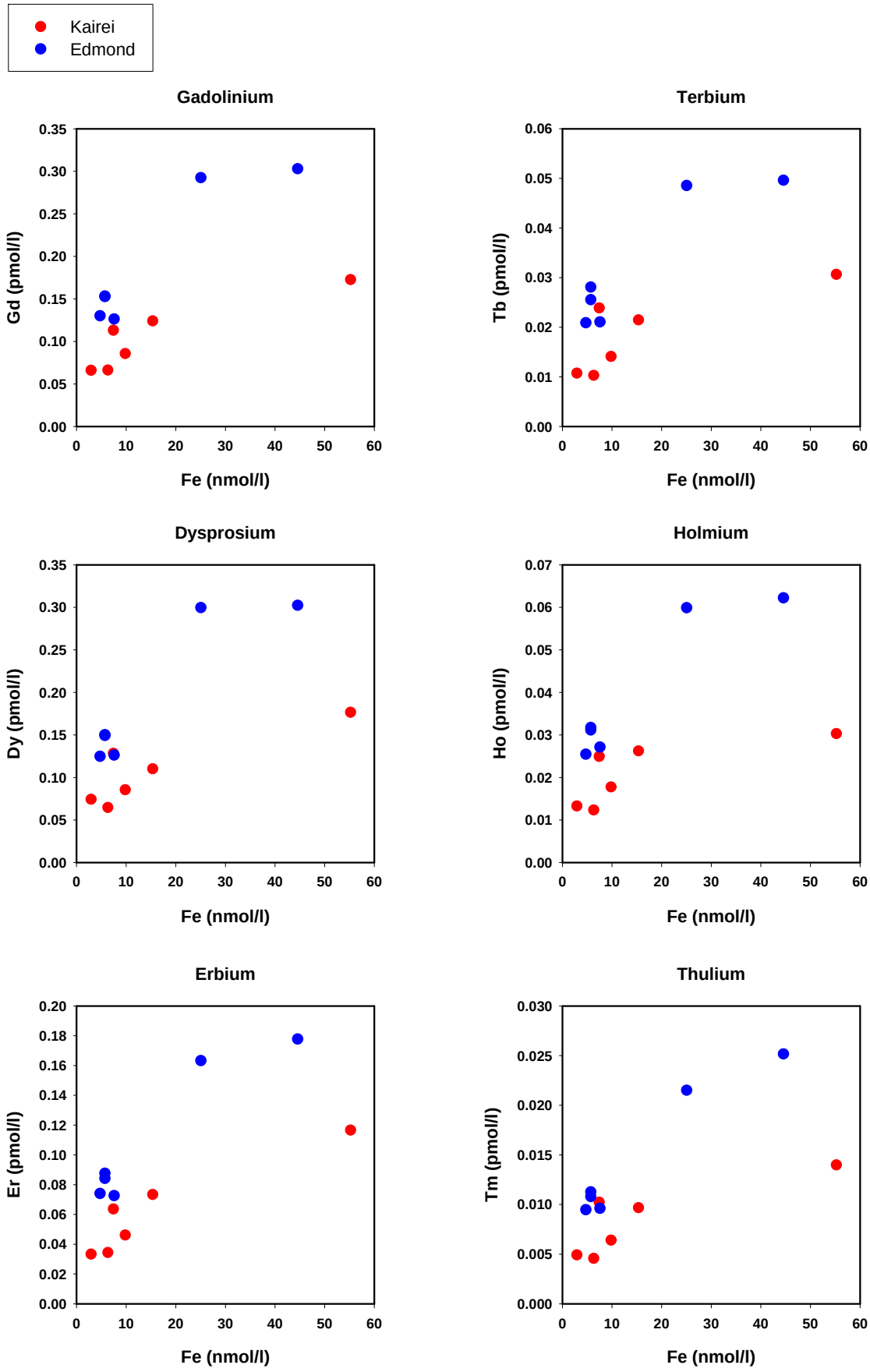

Figure 29 (cont) Particulate rare earth elements versus particulate iron for the SAP (>1.0µm) samples from the Kairei and Edmond hydrothermal plumes.

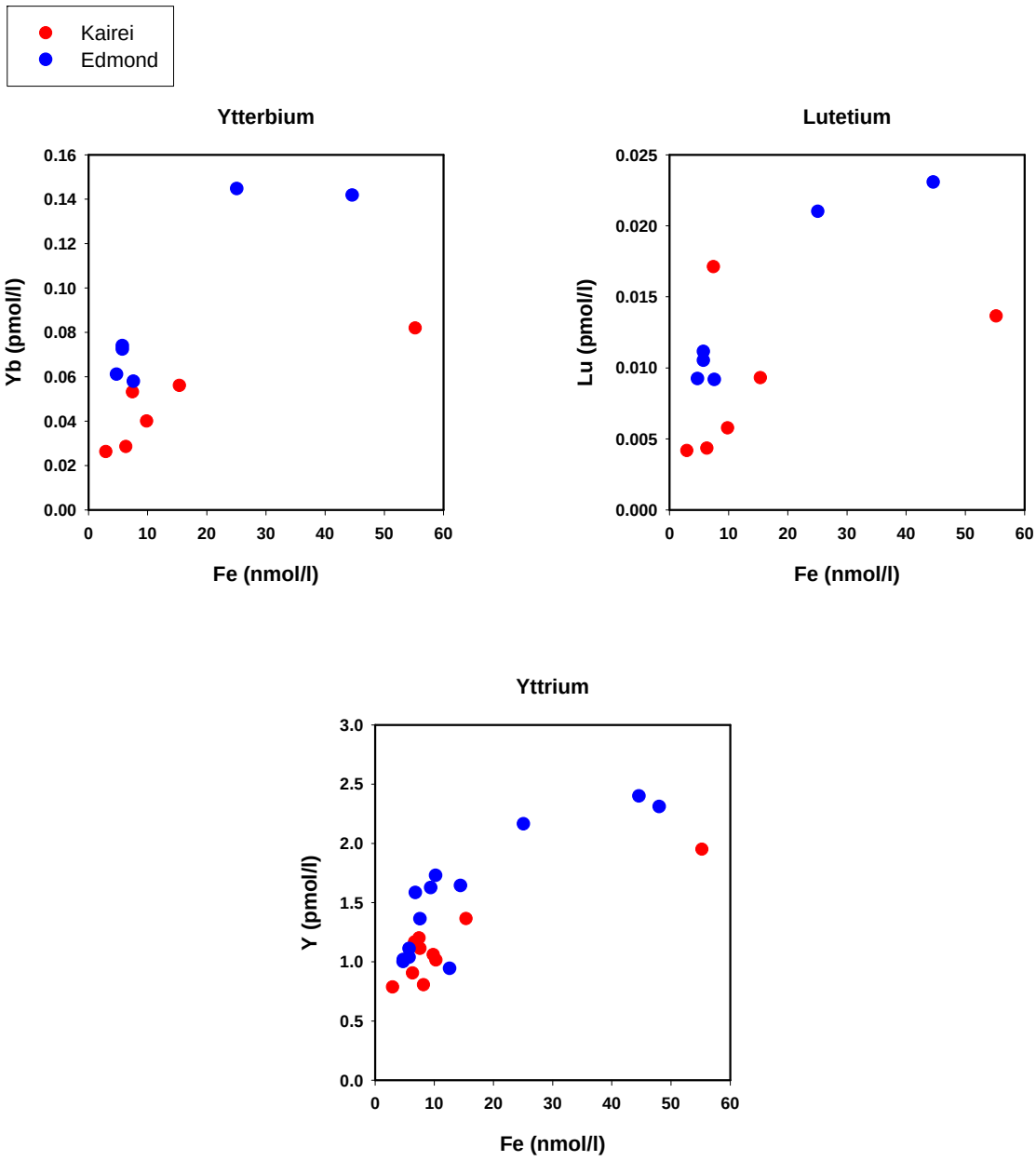

Figure 29 (cont) Particulate rare earth elements and yttrium versus particulate iron for the SAP (>1.0µm) samples from the Kairei and Edmond hydrothermal plumes.

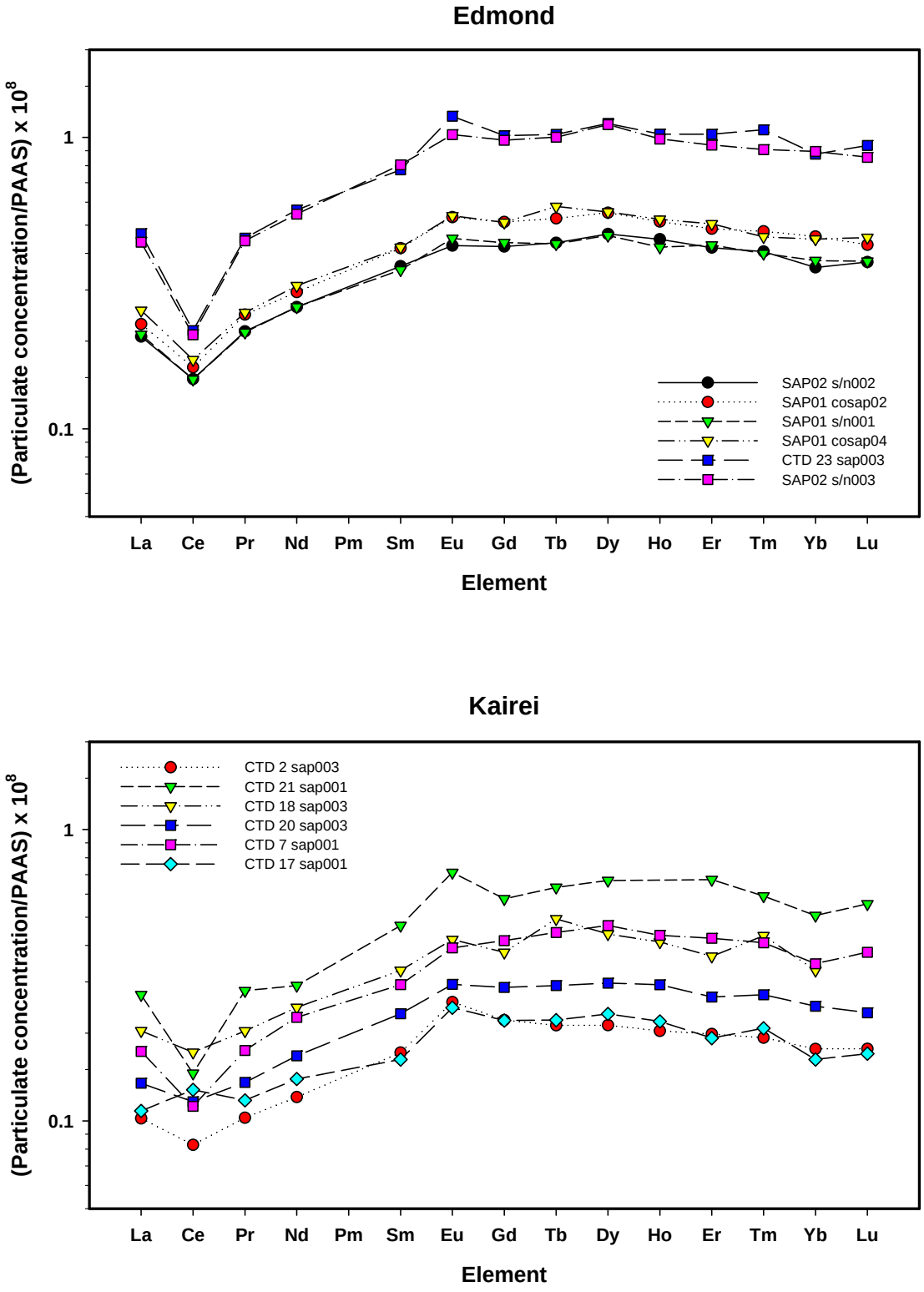

Figure 30 PAAS (post archaean Australian shale) normalised rare earth element patterns for the SAP (>1.0µm) samples from the Kairei and Edmond hydrothermal plumes.

4.3 Discussion

4.3.1 Iron

The concentrations of particulate Fe recorded for these Indian Ocean SAPs samples are much lower than previously recorded at TAG or Rainbow in the Atlantic (see '4.2 Results'). This is not due to poor sampling, the CTD stations were well located, the closest being within 100m of the vent sites and *in situ* light scattering data was used to make sure that the SAPs were within the non-buoyant plume while they were operating. However from the Fe (II) oxidation rates we know that much of the Fe (II) emerging from the vents, if not already precipitated as sulfides, will still be in solution at plume height directly above the vents. This will continue to precipitate over approximately the next 12 hrs (i.e. ~5 half times for Fe (II) oxidation). Therefore, all dissolved Fe (II) will have been quantitatively removed from solution over a distance of ~7-8km (assuming a current speed of 18cm/s as discussed in '3.4.3 Total Fe Calculations'), unlike the Atlantic where the rapid Fe (II) oxidation rate means that all dissolved Fe (II) will have been removed within less than 100m of the vent source.

The precipitation of particulate Fe-oxyhydroxides in the Indian Ocean plumes will occur as the plume is laterally dispersed away from the vent site plume and progressively diluted, hence high concentrations of particulate Fe-oxyhydroxides will not be found directly above the vent site. Consequently, the particulate Fe phases that are collected may be proportionately richer in sulfides than oxides than comparable samples collected from Atlantic hydrothermal plumes.

4.3.2 Oxyanions

A number of elements exist as oxyanions in seawater, e.g. phosphorus, vanadium, chromium, molybdenum and arsenic, and several of these elements have been shown to behave in a linear fashion with Fe in hydrothermal plumes in both Atlantic and Pacific Ocean hydrothermal plumes (Feely et al., 1991; German et al., 1991a; Edmonds & German, 2004).

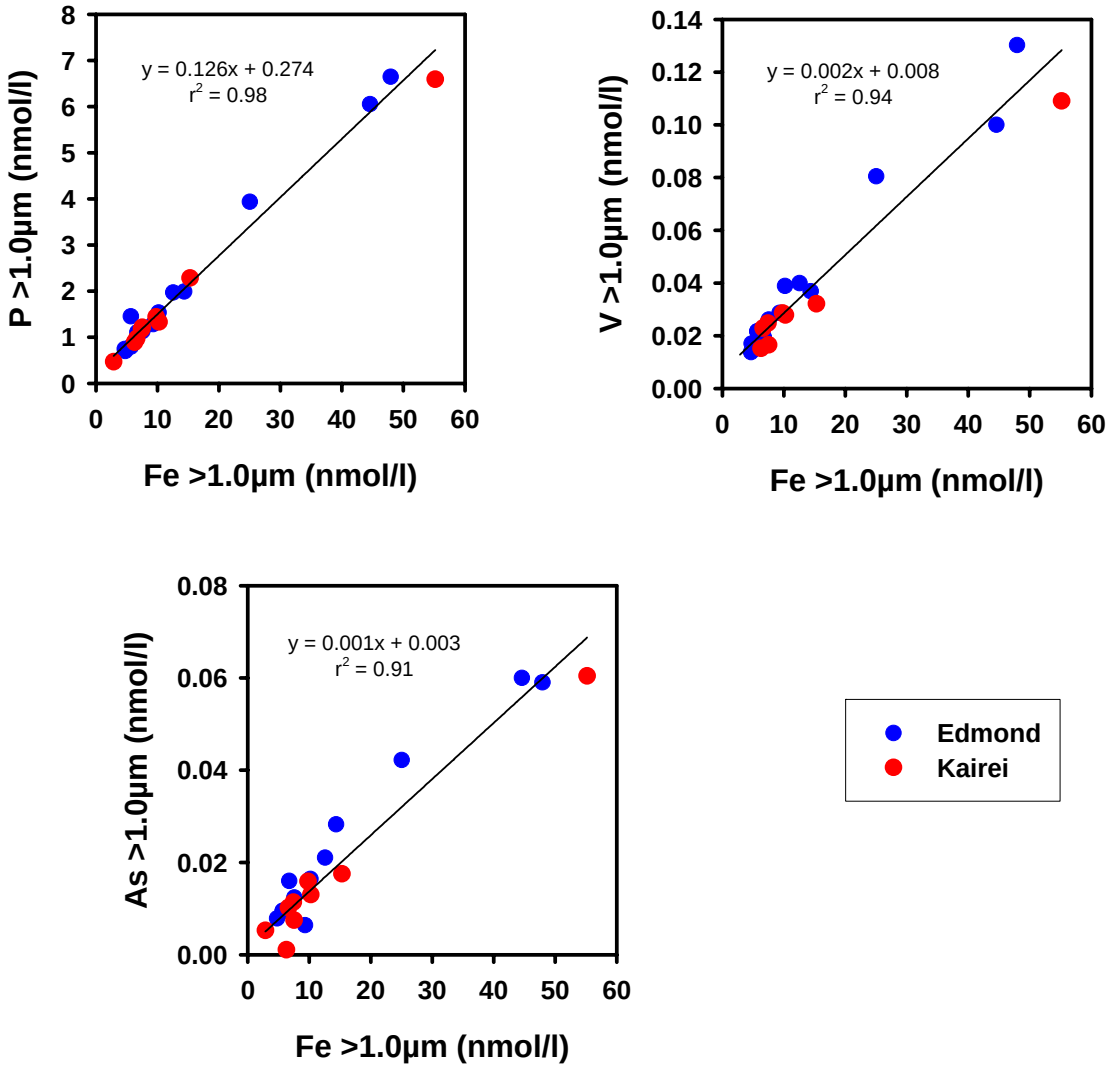

Figure 31 Particulate phosphorus, vanadium and arsenic versus particulate iron for the SAP (>1.0µm) samples from the Kairei and Edmond hydrothermal plumes with linear regressions through all data. Equations of regression line and correlation coefficients are shown on the graphs**.**

Figure 31 shows the same plots as Fig. 27, but with the addition of regression lines through all data. Particulate P exhibits a very good linear correlation ($r^2 = 0.98$) with pFe at the Edmond site, in keeping with the behaviour of particulate P in both Atlantic and Pacific hydrothermal plumes (Feely et al., 1991). Although the Kairei data are biased towards low (<20nmol/l) Fe concentrations with only one other data point at a high [Fe] of 55nmol/l, the data clearly lies along the same trend line as the Edmond data, defining

the same linear trend. Previously this linear behaviour has been attributed to the scavenging and/or co-precipitation of P by/with Fe-oxyhydroxides being restricted to the buoyant plume and ceasing on reaching the non-buoyant plume (German et al., 1991a; Feely et al., 1992). This is possibly due to the change in the surface charge of the FeOOH particles which might be expected to occur as the pH of the plume increases (Ludford et al., 1996). At low pH the surface charge of the FeOOH particles will be positive so the negatively charged oxyanions would be adsorbed but once the pH reaches 7 to 8 the surface charge of the particles becomes negative (Stumm & Morgan, 1996), hence the oxyanions would no longer be attracted to the FeOOH particles The same linear trend observed in all non-buoyant hydrothermal plumes also implies that no P is released from the FeOOH particles as the plume is diluted. It has previously been suggested that the uptake of P onto Fe-oxyhydroxide particles is dependent on the ambient dissolved phosphate concentration (Feely et al., 1998). In that case, it is entirely reasonable that the Kairei and Edmond results co-incide on the same trend line because the deep ocean dissolved phosphate concentrations will not vary significantly over the distance between the two vent sites; at plume height the dissolved phosphate concentrations at Edmond and Kairei will be ~2.2μmol/kg (CLIVAR & Carbon Hydrographic Data Office).

Particulate V and particulate As also exhibit linear relationships with pFe in Atlantic and Pacific hydrothermal plumes (Trefry & Metz, 1989; German et al., 1991a; Feely et al., 1994a). The Edmond and Kairei SAPs data are consistent with these prior observations, pV and pAs having good linear correlations with pFe of $r^2 = 0.94$ and 0.91 respectively (Fig. 31). Again the Kairei and Edmond data co-incide which is consistent with scavenging of V or As from ambient seawater where the concentrations will be very similar at the two locations (Middelburg et al., 1988). As for P, the implication of this linear trend is that no further uptake or release of V or As from the FeOOH particles occurs by the time the non-buoyant plume has been reached. For vanadium, this theory is substantiated by the work of Metz and Trefry (1993) where they found that hydrothermal precipitates maintained a constant V/Fe ratio over seven days despite there being sufficient dissolved V in solution to enable further adsorption by the Fe oxide particles.

4.3.3 Chalcophile Elements

The graph of particulate Cu against pFe (Fig. 28) clearly demonstrates a negative departure from linearity for the Edmond site, a trend which is consistent with observations in Atlantic Ocean hydrothermal plumes (Trocine & Trefry, 1988; German et al., 1991a). Although data are available for hydrothermal plume particles from the East Pacific Rise in the Pacific Ocean (Feely et al., 1994a; 1996), the relationship between Cu and Fe for those plumes does not show a clear trend. The negative departure from linearity in the Edmond plume, by contrast, indicates that Cu is being preferentially removed from the particulate phase in the non-buoyant plume relative to Fe. Cu is believed to be present in the particulate phase as sulfides which precipitate in the early phase of buoyant plume formation (Mottl & McConachy, 1990) and the negative curvature has been attributed to either the preferential settling of denser Cu-rich sulfides relative to fine grained Fe-oxyhydroxide particles or, to the oxidation of the sulfides and their subsequent dissolution (Trocine & Trefry, 1988; German et al., 1991a). The same trend, i.e. negative curvature, should be expected for the Kairei samples based on our existing knowledge. However the absence of data between [pFe] of 20 and 50nmol/l does not allow us to confirm this.

The highest [Fe] samples at Kairei and Edmond have Cu:Fe ratios of 0.094 ± 0.017 and 0.075 ± 0.005 respectively. These values as well as the mean Cu:Fe ratios and ranges for the Kairei and Edmond samples and the vent fluid ratios are shown in Table 15. The ratios of hydrothermal particles from the non-buoyant plumes at the TAG and Rainbow sites in the Atlantic which were also collected using 1.0μm filters in stand alone pumps are also shown for comparison.

The Cu:Fe ratios of the high [Fe] samples (i.e. the 'youngest' samples, closest to the vent) at both Kairei and Edmond are higher than the Cu:Fe ratios in the vent fluids (illustrated in Fig. 32) which is consistent with preferential fractionation of the Cu (relative to Fe) into sulfides in the early phases of plume formation. At TAG, the high [Fe] samples do not have such a high Cu:Fe ratio. Although one of those samples did have a ratio of 0.08, that sample was anomalous compared to the others collected at the time in that it was more sulfidic than the others. This ratio, of 0.08, is also higher than

the vent fluid Cu:Fe ratio, once again consistent with fractionation of the Cu into sulfides.

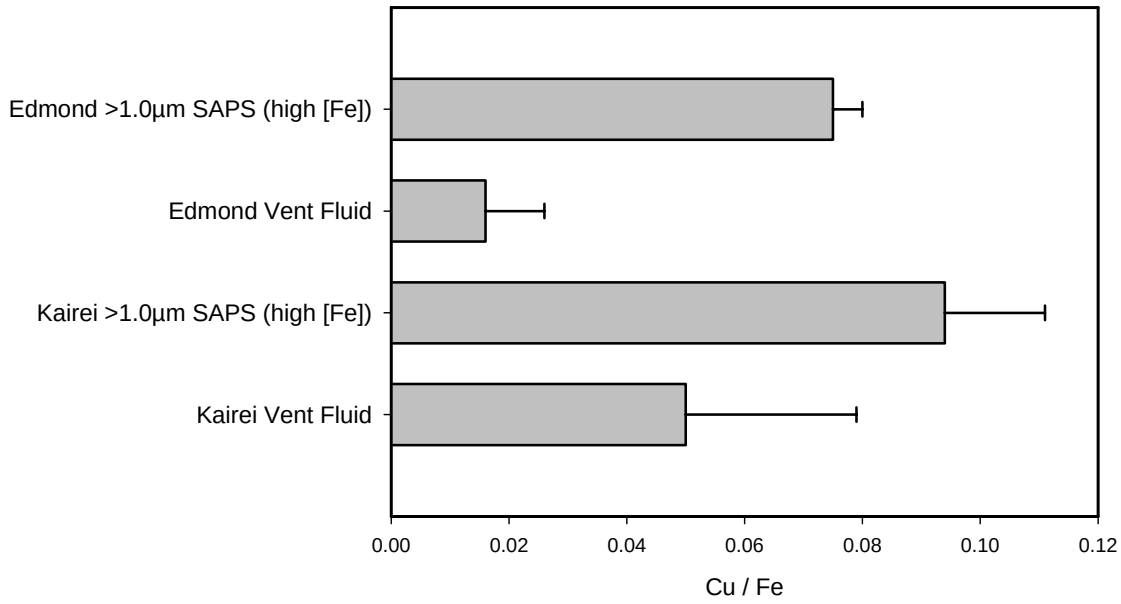

Figure 32 Cu:Fe ratios in vent fluids and non-buoyant plume particles [SAP (>1.0µm) samples] for the two highest [Fe] samples at each site.

At the Rainbow vent site the sample and vent fluid Cu:Fe ratios are the same. This is to be expected because not only is the Fe/H_2S vent fluid ratio of 24 unusually high (Douville et al., 2002), but the Fe:Mn ratio in the plume is almost the same as the vent fluid Fe:Mn ratio suggesting Fe is behaving conservatively (Severmann et al., 2004), i.e. there is little sulfide formation. However there is evidence for some sulfide formation from the three buoyant plume samples collected at Rainbow which have a higher Cu:Fe ratio of 0.016±0.004 compared to the vent fluid ratio of 0.006 (Douville et al., 2002; Edmonds & German, 2004). Again this is consistent with fractionation of Cu into sulfides but obviously the effect is limited at Rainbow by the low H_2S concentration in the vent fluids.

In the Pacific Ocean, although vent fluid data are available for many of the hydrothermal sites (see e.g. Von Damm, 1995) and there are also data for plume particle samples from a number of hydrothermal sites (e.g. Feely et al., 1987; 1990a; Mottl & McConachy, 1990; Feely et al., 1994b), there are few instances where both data are available for the

same location, particularly for non-buoyant plume particle samples. However there are two sites where buoyant plume particle data and the corresponding vent fluid data are available, the OBS vent at 21°N on the East Pacific Rise and the Endeavour site on the Juan de Fuca Ridge. At OBS the vent fluid Cu:Fe ratio is 0.021 (Von Damm, 1995) and the buoyant plume particle Cu:Fe ratio is 0.354±0.065 (Mottl & McConachy, 1990) while at Endeavour, the average vent fluid Cu:Fe ratio for six vents is 0.015±0.007 (Von Damm, 1995) and the buoyant plume particle Cu:Fe ratio is 0.263±0.101 (Feely et al., 1987). These figures are again consistent with fractionation of Cu into sulfides relative to Fe, during early-stage plume formation.

	Kairei[1]	Edmond[1]	TAG[2]	Rainbow[3]
Mean Cu:Fe ratio	0.060±0.029	0.027±0.027	0.016±0.018	0.006±0.003
High [Fe] Cu:Fe ratio	0.094±0.017	0.075±0.005	0.035±0.039	0.008±0.001
Range Cu:Fe ratios	0.019-0.106	0.006–0.078	0.006–0.080	0.003–0.015
Vent fluid Cu:Fe ratio	0.050±0.029	0.016±0.010	0.024	0.006
Mean Zn:Fe ratio	0.030±0.028	0.019±0.017	0.003±0.002	0.019±0.022
High [Fe] Zn:Fe ratio	0.027±0.011	0.051±0.007	0.003±0.001	0.001±0.000
Range Zn:Fe ratios	0.007-0.106	0.003-0.056	0.001-0.008	0.001-0.066
Vent fluid Zn:Fe ratio	0.017±0.003	0.010±0.001	0.008	0.007

Table 15. Cu and Zn to Fe ratios for hydrothermal plume particles and vent fluids

[1] Vent fluid data from Gallant & Von Damm (2006)
[2] Data from German et al. (1991) and Edmond et al. (1995)
[3] Data from Edmonds & German (2004) and Douville et al. (2002)

Zinc has been shown to behave in a similar manner to Cu with respect to particulate Fe in hydrothermal plumes (e.g. German et al., 1991a) and for the Edmond plume, negative curvature is suggested in the Zn versus Fe plot (Fig 28b) similar to that observed for Cu (Fig 28a). For Kairei, unlike the Cu data where it is not possible to determine whether the trend is linear or curved, the Zn versus Fe plot does show a negative departure from linearity and the Kairei and Edmond data are more similar at lower particulate Fe concentrations than the Cu data.

The Zn:Fe ratios for the highest [Fe] samples at Kairei and Edmond as well as mean ratios, range in ratios and vent fluid ratios are shown in Table 15, along with those for the TAG and Rainbow hydrothermal plume particle samples. As for Cu, the Zn:Fe ratios of the highest [Fe] samples at Kairei and Edmond, which represent the 'youngest' samples are higher than the vent fluid Zn:Fe ratios. This is illustrated in Fig. 33 and is consistent with fractionation of the Zn into sulfides.

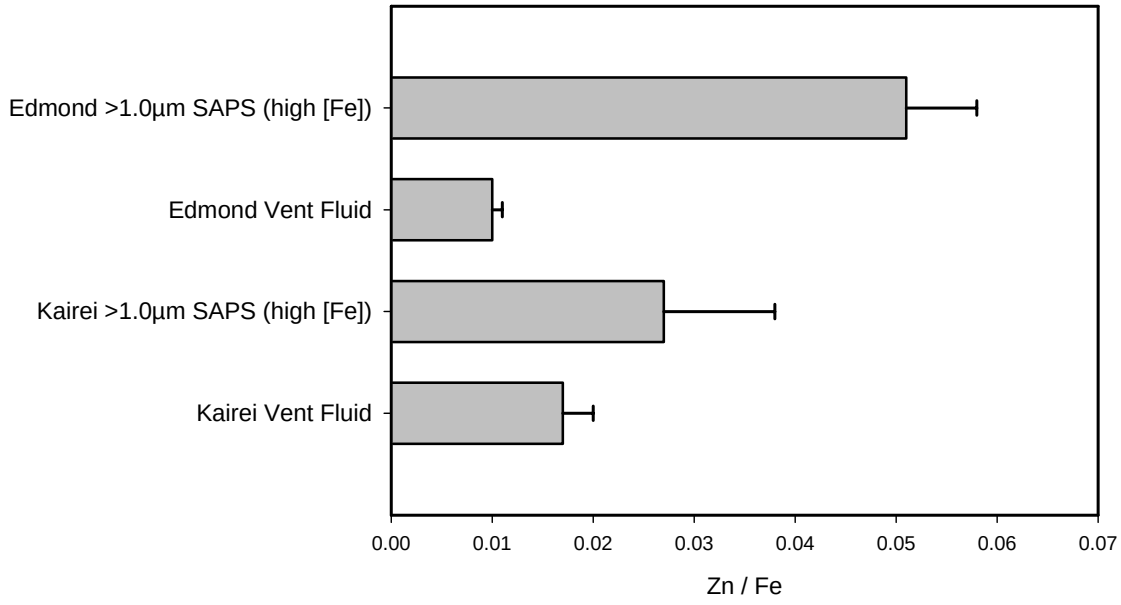

Figure 33 Zn:Fe ratios in vent fluids and non-buoyant plume particles [SAP (>1.0µm) samples] for the two highest [Fe] samples at each site.

At TAG the high [Fe] samples have a lower Zn:Fe ratio than the vent fluid (Table 15), including the anomalous sample mentioned in relation to the Cu:Fe ratios which has a Zn:Fe ratio of 0.005. This is also the case at Rainbow where the Zn:Fe ratio of the high [Fe] samples is 0.001 while the vent fluid has a ratio of 0.007. It is worth noting that the higher overall Zn:Fe ratio at Rainbow is a consequence of very high Zn:Fe ratios in some of the low [Fe] (<10nmol/l) samples. The buoyant plume samples from Rainbow have a ratio of 0.008±0.004 which is very similar to the vent fluid ratio of 0.007 (Douville et al., 2002; Edmonds & German, 2004). This data contrasts with that of Cu where fractionation of Cu into sulfides is clearly illustrated by plume particle Cu:Fe ratios

which are higher than the vent fluid ratios. However, we know that Zn does form sulfides (mainly as sphalerite) in hydrothermal plumes from previous mineralogical studies of hydrothermal plume particles (e.g. Feely et al., 1987; 1990a; Mottl & McConachy, 1990). In addition, samples from the OBS vent and Endeavour site in the Pacific Ocean, like those from Kairei and Edmond also show evidence of fractionation of Zn into sulfides. The vent fluid Zn:Fe ratios for OBS and Endeavour (average for six vents) are 0.064 and 0.034±0.20 respectively (Von Damm, 1995) and the buoyant plume particle ratios are 0.174±0.078 and 0.073±0.033 respectively (Feely et al., 1987; Mottl & McConachy, 1990). Hence it is interesting that the TAG and Rainbow samples do not illustrate this fractionation so clearly for Zn. It could be a consequence of the rapid Fe oxidation ($t_{1/2}$ of ~20mins) at these sites, resulting in a much higher proportion of particulate Fe-oxyhydroxides in even the youngest (including buoyant plume) Atlantic samples, which would lower overall Zn:Fe ratios, when compared to more sulfide dominated plume particles directly above vent sites in the Indian and Pacific Oceans where Fe oxidation rates are slower. However, it should be expected that this same process would affect Cu:Fe ratios in the same manner. At TAG, a previous study by Trocine and Trefry (1988) found that Zn did not persist in the plume as long as Cu, which, could account for the different trend in the Cu:Fe and Zn:Fe ratios. If oxidative dissolution is one of the reasons we observe loss of Cu and Zn from hydrothermal plumes then it is possible that the rates of Zn sulfide dissolution are faster than those for Cu (e.g. although Metz and Trefry (1993) didn't study Zn, they showed faster release rates for Cd than Cu from hydrothermal particles). Further, it may also be possible that, as for Fe oxidation, the rates of oxidative dissolution for the Zn bearing phase are much faster in the Atlantic than the Indian or Pacific Oceans. This could explain why fractionation into sulfides is not so easily illustrated by the Zn:Fe ratios in the Atlantic as it is in Indian and Pacific Ocean samples.

As another of the chalcophile elements, Pb could be expected to behave in a similar way to Cu and Zn in showing a negative departure from linearity in its relationship with Fe. However previous results based on the Pb vs. Fe relationship have been inconclusive. At TAG the Pb vs. Fe relationship could be interpreted as either linear or having negative curvature and at Rainbow the relationship is also unclear. The results from Kairei and Edmond are equally inconclusive (Fig. 28d). However Pb is known to be a particle

reactive element and studies based on Pb isotopes in hydrothermal systems have provided evidence that Pb in the surrounding seawater is scavenged by hydrothermal particles, based upon both stable lead and Pb-210 isotopes (German et al., 1991b; Kadko, 1993; Godfrey et al., 1994). Hence the scatter seen in the Pb:Fe relationships in Fig. 28d could easily be a consequence of two processes; (i) the preferential settling/oxidative dissolution of Pb sulfides and (ii) the scavenging of Pb from ambient seawater by Fe-oxyhydroxide particles.

In contrast to the relationship between particulate Pb and Fe in the Kairei and Edmond hydrothermal plumes, that of pCd and pFe appears to be much clearer (Fig. 28c). There is negative curvature in the Cd vs. Fe plots for both plumes suggesting preferential loss of Cd compared to Fe. This trend is much clearer than the observations of German et al. (1991a) at TAG in the Atlantic where the relationship between pCd and pFe was inferred to show such curvature but could not be confirmed. The Cd:Fe ratios are also higher in the plume particles (0.00033±0.00067 for Kairei, 0.00066±0.00121 for Edmond) than the vent fluids (0.00002 for both Kairei and Edmond, (Gallant & Von Damm, 2006) which is consistent with preferential fractionation of Cd into sulfides relative to Fe. Other results from the TAG and Snakepit hydrothermal sites in the Atlantic however, have suggested that Cd may also be involved in scavenging reactions in a similar manner to Pb (Trocine & Trefry, 1988; James & Elderfield, 1996); measurements of dissolved Cd showed a depletion of Cd compared to ambient seawater for the highest Fe samples.

As already mentioned in the results section the maximum Cd concentration of 135pmol/l in the Kairei and Edmond hydrothermal plume particles is higher than that recorded in any Atlantic hydrothermal plume particles for the >1.0μm size fraction. They are generally less than 10pmol/l except for one very high [Fe] sample (600nmol/l) from Rainbow where [Cd] was 31pmol/l. If, as suggested by the data from TAG and Snakepit, Cd is indeed scavenged by the FeOOH particles then these Cd concentrations may be a consequence of the oceanic variations in ambient dissolved [Cd]. Dissolved Cd concentrations are correlated with those of dissolved phosphate (Boyle et al., 1976), i.e. they increase progressively along the pathway of global thermohaline circulation. Hence higher dissolved Cd concentrations are observed in the deep Indian Ocean (640pmol/l, Morley et al., 1993) compared to the deep Atlantic Ocean (290pmol/l, Bruland & Franks,

1983). Certainly, this trend is consistent with the higher [Cd] of the hydrothermal particles from the Kairei and Edmond plumes. Unfortunately, there are no Cd data available for Pacific Ocean hydrothermal plume particles to enable a full comparison between ocean basins (dissolved [Cd] in the deep Pacific is 940pmol/l; Bruland, 1980).

Once pFe concentrations drop below 10nmol/l in the Kairei and Edmond samples, the pCd concentrations very quickly reach concentrations of less than a picomole/litre which is comparable to background particulate Cd concentrations in the deep Atlantic and Pacific Oceans (Trocine & Trefry, 1988; Sherrell, 1989; German et al., 1991a). This contrasts with the Cu data which does not decrease so rapidly (particularly in the case of Kairei) or to concentrations as low as background. This is consistent with the data of Trocine & Trefry (1988) from the TAG plume in the Atlantic Ocean where they found that particles enriched in Cu persisted in the plume longer than those enriched in Cd, Edmonds & German (2004) reported similar findings in the Rainbow hydrothermal plume. Work by Metz & Trefry (1993) on the uptake and release of metals by hydrothermal precipitates showed that Cd is released more quickly and completely than Cu: over a four day period 99% of Cd was released from hydrothermal precipitates from the TAG hydrothermal plume compared to 44% of Cu over a six day period. Hence it is not unreasonable to expect the Cd to Fe relationship to show a more pronounced negative curvature than that of Cu to Fe if preferential uptake into sulfide precipitates followed by oxidative dissolution is dominating the Cd budget within the Kairei and Edmond hydrothermal plumes.

Trocine & Trefry suggested that Cu may persist in the plume longer than Cd not only due to a possible greater abundance of Cu bearing sulfides which may settle more slowly than the Cd sulfides, but that Cu may also be scavenged by Fe-oxyhydroxide particles. Evidence for scavenging of Cu from seawater in the more dilute plume was also found by Ludford et al. (1996) at the Broken Spur site in the Atlantic where they found positive curvature in the relationship between Cu and Fe at concentrations of Fe <50nmol/l. Scavenging by Fe-oxyhydroxide particles would explain the more linear but scattered trend seen for the Cu data since the plot would be a result of two processes, loss from the plume as sulfides on the one hand, and enrichment in the plume by scavenging of Cu from ambient seawater on the other, as discussed for Pb. However as also discussed,

previous observations have suggested that Cd is scavenged by plume particles and cadmium is known to be adsorbed onto Fe-oxyhydroxide surfaces (e.g. Benjamin & Leckie, 1981) which leads to the question, if Cu is involved in adsorption reactions with Fe-oxyhydroxide particles and hence not showing a clear trend with Fe, why does Cd display very distinct curvature in its relationship with Fe? Either Cd is more preferentially fractionated into sulfides relative to Fe than Cu at these sites or there is more extensive scavenging of Cu rather than Cd onto the Fe-oxyhydroxide particles (or a combination of both). Balistrieri & Murray (1982) showed in experiments with synthetic seawater and goethite that Cu is more effectively adsorbed than Cd, and that the adsorption efficiency of Cd is also reduced in the presence of Cu. In fact, in experiments carried out in a sodium nitrate solutions, Cu actually displaces Cd from the goethite surface (Christophi & Axe, 2000) However this was at micromolar Cu and Cd concentrations. The vent fluid concentration of Cu at Kairei and Edmond is ~200μmol/l and the concentration of Cd is 100-250nmol/l (Gallant & Von Damm, 2006) so in the non-buoyant plume where the mixing ratio with ambient seawater is >1 x 10^4 the [Cu] will soon reach ambient nanomolar concentrations and [Cd] will reach ambient picomolar concentrations, hence competition for adsorption may not be relevant.

4.3.4 Yttrium and rare earths

The relationships between particulate Fe and Y and the rare earth elements at the Edmond and Kairei sites (Fig. 29) show a positive departure from linearity as previously observed in the Atlantic TAG and Rainbow hydrothermal plumes (German et al., 1990; German et al., 1991a; Edmonds & German, 2004). Y is chemically and physically very similar to the rare earth elements and is involved in similar scavenging reactions to the REEs throughout the water column (Zhang et al., 1994). Although Bau & Dulski (1999) found that Y has a lower particle reactivity than the REEs (in fact, at close proximity of <1m to the vent at the Broken Spur site in the Atlantic, Y behaves conservatively whereas the REEs are already being scavenged by FeOOH particles), it can be considered as a proxy for general REE behaviour in this environment. Hence it is entirely reasonable that the same trend with Fe would be observed for both the REEs and Y. Other particle reactive elements known to be involved in scavenging by Fe-

oxyhydroxide particles in hydrothermal plumes include Be and Th (German et al., 1991b, 19901b, 1997, 2001; Kadko et al., 1994).

For yttrium, the Kairei and Edmond data broadly coincide but for the REEs although the two sites have similar trends, the data are offset. REE concentrations in the hydrothermal particles at Kairei are consistently lower than those at Edmond. One possibility is a difference in the REE concentrations of the ambient seawater surrounding each vent site, however, although REE concentrations vary noticeably between different ocean basins (Elderfield & Greaves, 1982; de Baar et al., 1985a; German & Elderfield, 1990; Bertram & Elderfield, 1993), the difference between the two vent sites which are only ~2° apart is unlikely to be significant enough to account for the offset in the Kairei and Edmond datasets. This is illustrated by the Indian Ocean data of Bertram & Elderfield (1993) where data from sites ~9° apart varies by less than 10% at equivalent depths. However, the Kairei and Edmond hydrothermal plumes are located at different depths in the water column (centred around ~2200m and ~2900m respectively). Fig. 34 shows how Nd and Er vary at these depths in this region of the Indian Ocean. Although the concentrations increase with depth, the change is not sufficient to account for the offset in the Edmond and Kairei data, e.g. for an [Fe] of 25-45nmol/l, [Nd]in the Edmond particles is 1.2pmol/l compared to 0.6pmol/l for the Kairei particles at the same [Fe], i.e. the concentration in the Edmond particles is twice that of the Kairei particles compared to a difference in the ambient concentrations of only ~20%.

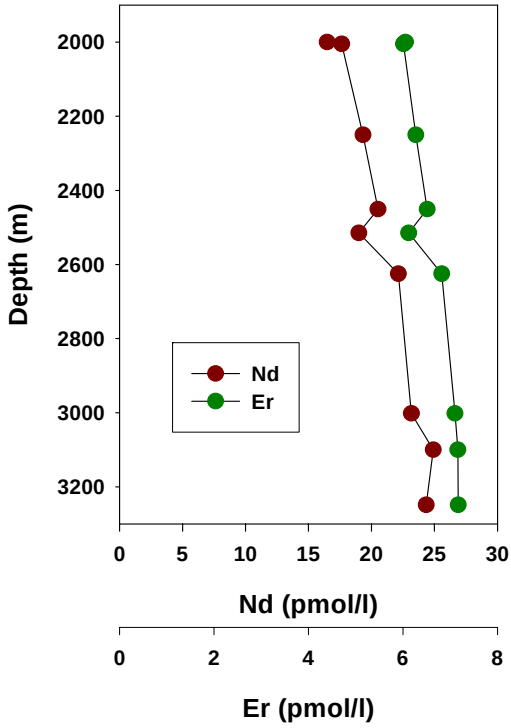

Figure 34 Nd and Er concentrations from 27°00.50'S 56°58.00'E in the Indian Ocean, at the depths of the Kairei and Edmond hydrothermal plumes. Data from Bertram & Elderfield, 1993

The most likely explanation is the extent to which the Kairei and Edmond samples have been diluted. The vent fluid [Fe] at Edmond is more than twice that at Kairei; 12800µmol/kg compared to 5400µmol/kg (Gamo et al., 2001; Gallant & Von Damm, 2006), hence at equivalent [Fe], the Edmond samples are in fact more dilute than the Kairei samples. For example, at an Fe concentration of 50nmol/l the Edmond vent fluid has been diluted by a factor of 2.6×10^5 whereas the Kairei vent fluid has only been diluted by a factor of 1.1×10^5. So the Edmond particles have been exposed to more sea water and have had more opportunity to scavenge the REEs from the ambient sea water.

The positive deviation from linearity observed in the REE and Y versus Fe plots has been interpreted in two ways. Sherrell et al. (1999) suggest that the curvature in the REE

versus Fe plot is caused by a local depletion of dissolved REEs at high Fe concentrations (>100nM) due to scavenging and that this is then followed by re-equilibration of the dissolved and particulate REEs as the plume is diluted and the concentration of Fe decreases. German et al. (1990) and Edmonds & German (2004) suggest that it indicates that the REEs and Y are continuously scavenged by the FeOOH particles as the plume is diluted. This interpretation is supported by results from analysis of hydrothermal flank sediments from the East Pacific Rise and Juan de Fuca Ridge in the Pacific Ocean by both Olivarez & Owen (1989) and German et al. (1997) which had increasing REE/Fe ratios at increasing distances from the ridge axis.

However a further insight into which mechanism may be dominant can be gained by comparing the REE/Fe in particles from different plumes at similar Fe concentrations. Concentrations of the REEs generally increase with depth in each particular ocean (see Table 16 below), hence if equilibration is the dominant mechanism then the REE/Fe ratios should be higher at TAG than at Rainbow and also higher at Edmond than at Kairei for similar Fe concentrations.

	La (pmol/l)	Nd (pmol/l)	Gd (pmol/l)
[1]Kairei @2200m	30	19	5.3
[1]Edmond @3000m	39	23	6.6
[2]Rainbow @2300m	35	-	6.0
[2]TAG @3500m	50	-	7.5

Table 16. Concentrations of selected Rare Earth Elements in the Atlantic and Indian Ocean at the depths of the relevant vent locations.

[1]Data from Bertram & Elderfield (1993)
[2]Data from de Baar et al. (1983; 1985b)

Table 17 shows the REE/Fe ratios for three rare earth elements, La, Nd and Gd. The ratios for Edmond are generally higher than those at Kairei (except for the samples with [Fe] of 12-15nmol/l). This is what would be expected if the equilibration mechanism which Sherrell et al. (1999) suggest is dominant. However for Rainbow and TAG where the ratios at TAG should be higher than those at Rainbow if equilibration is the key process, in fact they are very similar, if slightly lower. Based on the dissolved REE concentrations detailed in Table 14, it might also be expected that ratios at TAG would be higher than Edmond and that the ratios at Rainbow would be higher than at Kairei.

Although there are only limited data with similar [Fe] to compare in this case, the values are all very similar. The lack of consistent trends in the REE/Fe values suggests that it is not equilibration which is the dominant process causing negative curvature in the REE versus Fe plots but the continuous scavenging of the REEs by the FeOOH particles as suggested by German et al. (1990).

	Fe (nmol/l)	La:Fe (x1000)	Nd:Fe (x1000)	Gd:Fe (x1000)
Kairei	6.3	0.091	0.086	0.019
	55.2	0.022	0.019	0.005
	7.4	0.121	0.110	0.024
	9.8	0.076	0.073	0.016
	15.4	0.074	0.067	0.016
	8.2	0.102	0.097	0.021
Edmond	7.6	0.129	0.125	0.027
	5.7	0.140	0.134	0.028
	5.7	0.154	0.138	0.030
	44.6	0.034	0.032	0.008
	25.1	0.054	0.053	0.013
	12.6	0.042	0.040	0.010
Rainbow[1]	9.3	0.126	0.132	0.019
	8.1	0.126	0.152	0.024
	26.4	0.045	0.042	0.008
	35.3	0.059	0.058	0.009
	18	0.086	0.087	0.013
	7.9	0.118	0.132	0.029
TAG[2]	56	0.034	0.033	0.007
	49	0.041	0.041	0.008
	45	0.038	0.038	0.007
	38	0.039	0.043	0.008
	17	0.058	0.060	0.011

Table 17. REE/Fe ratios for hydrothermal plume particle samples from Kairei and Edmond in the Indian Ocean and TAG and Rainbow in the Atlantic Ocean. Only relevant data are shown i.e. for samples with similar Fe concentrations.

[1]Data from Edmonds & German (2004)
[2]Data from German et al. (1990)

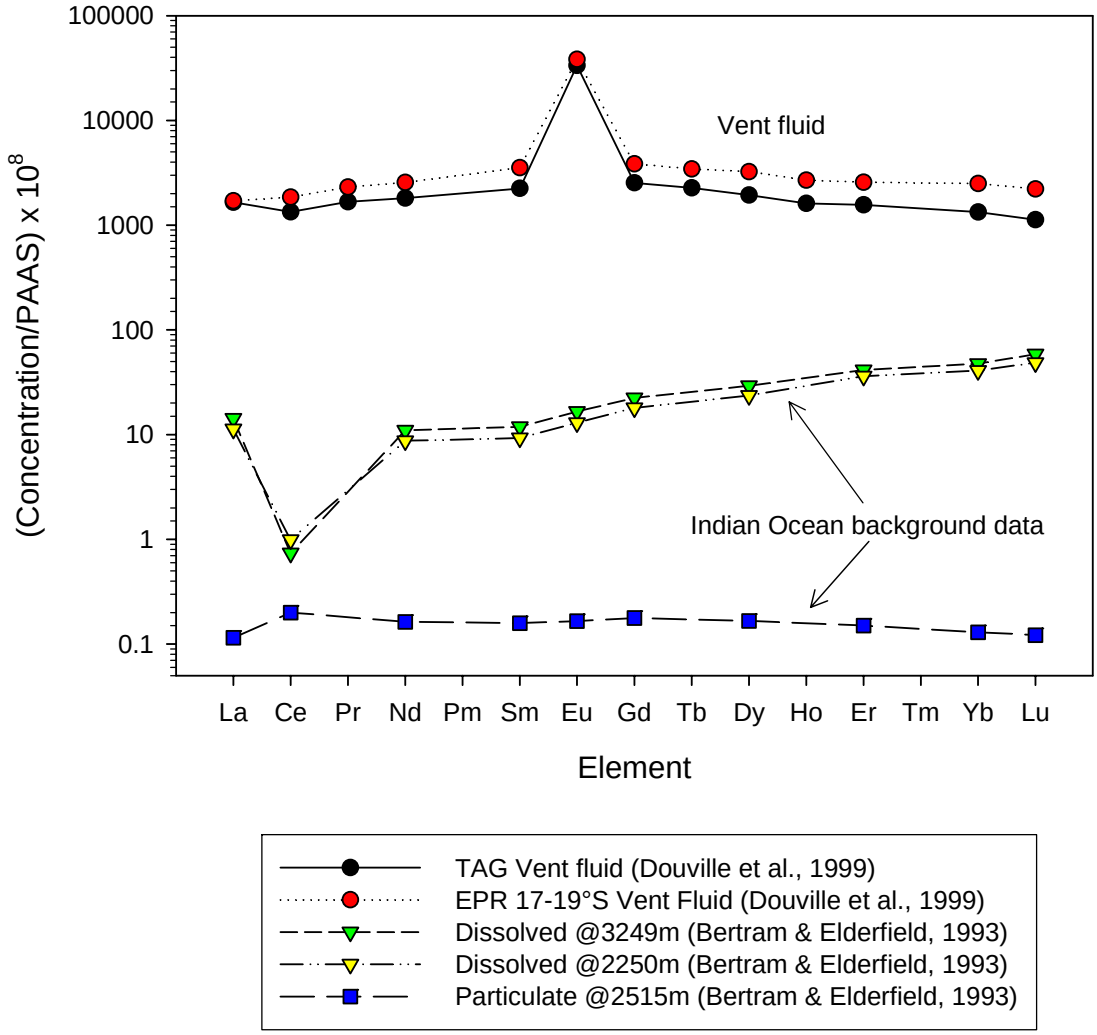

Figure 35 PAAS (post archaean Australian shale) normalised rare earth element patterns for TAG and East Pacific Rise (17-19°S) vent fluids, Indian Ocean background seawater and Indian Ocean background particulate material. TAG and EPR vent fluids chosen for illustration as their properties are closest to the Kairei and Edmond vent fluids respectively (data sources listed in legend).

The REE patterns (Fig. 30) of the hydrothermal particles are influenced by both the REE content of ambient seawater and that of the hydrothermal vent fluids which are highly enriched compared to seawater concentrations (can be greater than a 1000 times that of seawater, e.g. Mitra et al., 1994; Klinkhammer et al., 1994). Figure 35 shows the dissolved REE patterns, normalised to PAAS, for Indian Ocean background seawater samples collected 13° to the west and 2-4° to the south of the Kairei and Edmond sites (Bertram & Elderfield, 1993). The filtered seawater samples shown are from depths of

2250m and 3249m, i.e. comparable to the Kairei and Edmond plume depths respectively. The most striking feature of the seawater REE pattern is the negative cerium anomaly. Also shown is the REE pattern for particulate material collected from the same Indian Ocean location. REE concentrations for the Kairei and Edmond vent fluids are not available, so the REE pattern for vent fluids (again normalised to PAAS) from the TAG hydrothermal site in the Atlantic and from the Akorta hydrothermal vent at 17-19°S EPR in the Pacific are shown (Douville et al., 1999). Vent fluid REE data are available for a number of hydrothermal sites, the TAG data was chosen as the vent fluid temperature, chlorinity, alkalinity, pH and concentrations of Fe and H_2S are similar to those of the Kairei vent fluids (Gamo et al., 2001) and the 17-19°S EPR data was chosen as the properties of the vent fluid are similar to those of the Edmond vent fluids (Gallant & Von Damm, 2006). Although the REE concentrations vary between vent fluids, REE data for all vent fluids are similar in one respect, which is that they all exhibit a positive europium anomaly as illustrated in Fig. 35 and in most cases also exhibit an enrichment of the light REEs (LREE) over the heavy REEs (HREE) when compared to HREE enriched seawater (Douville et al., 1999).

Assuming that the rare earth elements are continuously scavenged by Fe-oxyhydroxide particles, then it might be expected that as vent fluids are diluted in the plume by ambient seawater, the REE pattern associated with aging/dispersing Fe-oxyhydroxide particles would evolve from a vent fluid like pattern to a more seawater like pattern. If this were the case, an increasing Ce anomaly and decreasing Eu anomaly would be seen. This is not necessarily the case and will be discussed further, later in this section. Also, although an increasing HREE enrichment might be expected in the particles as they are dispersed, because seawater is HREE enriched, in fact the LREEs are preferentially scavenged so the particles may become more LREE enriched as the plume is diluted.

The Eu and Ce anomalies are defined as follows and are shown in Table 18, an anomaly of less than one indicates a negative anomaly and greater than one, a positive anomaly.

$$Eu\ anomaly = \frac{2*(Eu/Eu_{shale})}{(Sm/Sm_{shale} + Gd/Gd_{shale})}$$

$$Ce\,anomaly = \frac{2*(Ce/Ce_{shale})}{(La/La_{shale} + Pr/Pr_{shale})}$$

	Particulate [Fe] nmol/l	Ce anomaly	Eu anomaly	Er_{sh}/Nd_{sh}
Kairei				
CTD 2 sap003	6.3	0.81	1.30	1.65
CTD 7 sap001	15.4	0.65	1.11	1.87
CTD 17 sap001	2.9	1.13	1.28	1.38
CTD 18 sap003	7.4	0.84	1.19	1.50
CTD 20 sap003	9.8	0.86	1.13	1.59
CTD 21 sap001	55.2	0.53	1.36	2.31
Edmond				
CTD 23 sap003	44.6	0.47	1.32	1.86
SAP01 s/n001	4.7	0.70	1.14	1.63
SAP01 cosap02	5.7	0.68	1.15	1.65
SAP01 cosap04	5.7	0.68	1.16	1.63
SAP02 s/n002	7.6	0.70	1.08	1.60
SAP02 s/n003	25.1	0.48	1.15	1.73
Indian Ocean Seawater*		Note 1	0.93	4.35

Table 18. Ce and Eu anomalies and Er_{sh}/Nd_{sh} ratios

* Data from Bertram & Elderfield, 1993

Note 1 – no Pr data available to calculate Ce anomaly

Figure 36 shows the Eu anomalies plotted versus Fe concentration for the Kairei and Edmond hydrothermal particle samples. Also shown are the Eu anomalies for samples from hydrothermal plumes from TAG and Rainbow in the Atlantic Ocean and 9°45'N on the East Pacific Rise (EPR) in the Pacific Ocean (see Appendix 5 for values). In the Kairei and Edmond plot, it can be seen that initially, as the Fe concentration decreases so does the Eu anomaly. This is consistent with decreasing influence of the vent fluid rare earth elements. However as the Fe concentration continues to decrease below 10nmol/l, there no longer appears to be a clear relationship with the Eu anomaly. This is most probably due to the influence of background particulate matter as the plume becomes increasingly dilute. The data from the other hydrothermal plumes shown in Fig 36 is in broad agreement with this; in Fig. 36b for TAG where higher Fe concentrations were recorded there is a general overall trend of decreasing Eu anomaly with decreasing [Fe] while at the EPR in Fig. 36d where the Fe concentrations were all very low it is difficult to detect a clear trend. The Rainbow plot (Fig. 36c) which has data with much higher

[Fe] also has much higher Eu anomalies while the lower [Fe] data points have anomalies in a similar range to equivalent [Fe] at the other sites, so again this is consistent with the greater influence of the vent fluid REEs at higher Fe concentrations.

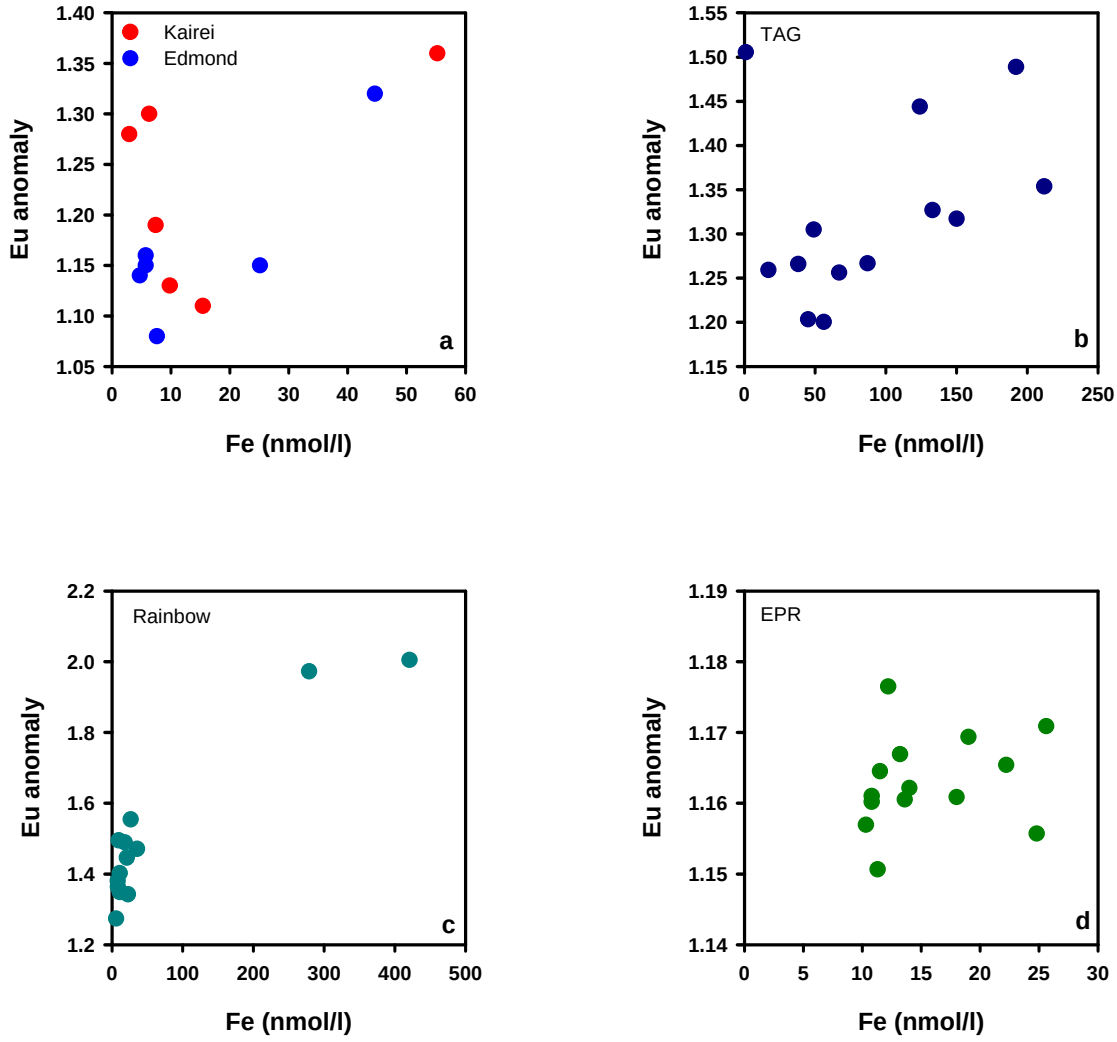

Figure 36 Eu anomalies for particulate hydrothermal plume samples from the Kairei and Edmond sites, TAG[1] and Rainbow[2] in the Atlantic and 9°45'N East Pacific Rise[3] in the Pacific (note that scales vary).

[1] German et al., 1990 [2] Edmonds & German, 2004 [3] Sherrell et al., 1999

In Figure 37 Ce anomalies for the Kairei and Edmond samples and the TAG, Rainbow and EPR samples from the Atlantic and Pacific Oceans are shown plotted versus the Fe

concentration. In all cases there is a correlation between the Ce anomaly and the Fe concentration, the Ce anomaly becoming less pronounced (i.e. less negative) as the Fe concentration decreases. This may seem counter-intuitive; as the plume is diluted and the FeOOH particles are exposed to an increasing concentration of REEs with a seawater pattern (i.e. with a negative Ce anomaly) then it might be expected that the Ce anomaly will become more negative, rather than more positive. However, positive Ce anomalies have been observed in Mn-oxide rich oceanic particulate material (e.g. Masuzawa, 1989; Sholkovitz et al., 1994; Tachikawa et al., 1997)] suggesting that Ce may be preferentially scavenged compared to the other REEs. This is also suggested by the fact that the fraction of REEs residing in the particulate phase rather than the dissolved phase for all the REEs except Ce is up to 5%, but for Ce, more than 33% is associated with the particulate phase (Nozaki, 2001). This suggests two possibilities which may be contributing to the Ce anomaly becoming less negative as the Fe concentration decreases, not only may preferential scavenging of the Ce be taking place in association with proportionally higher Mn-oxide concentrations, but as the plume becomes increasingly dilute, the incorporation of background material with a positive Ce anomaly may occur e.g. at TAG, the average Ce anomaly for three background samples collected was 1.06.

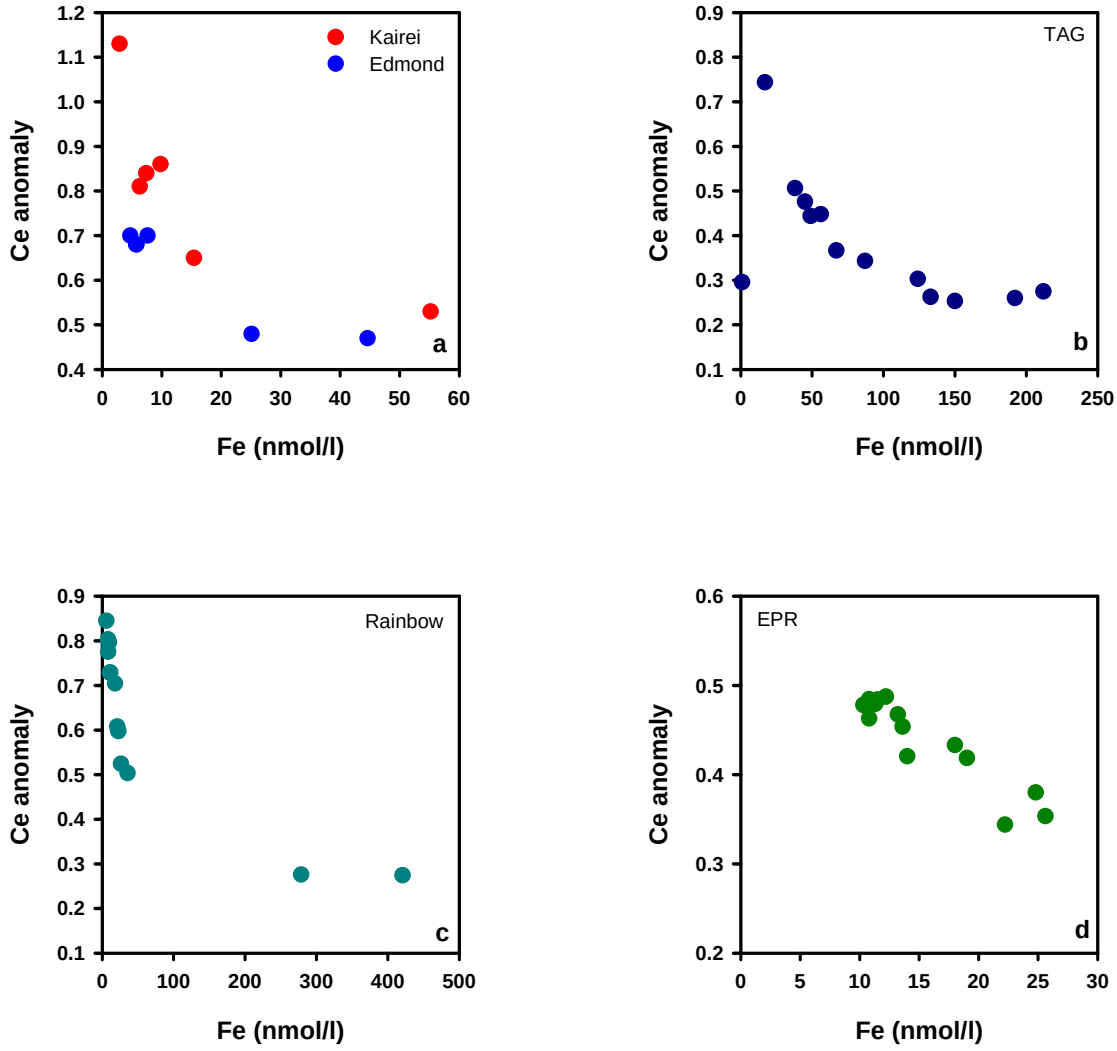

Figure 37 Ce anomalies for particulate hydrothermal particle samples from the Kairei and Edmond sites, TAG and Rainbow in the Atlantic and 9°45'N on the East Pacific Rise in the Pacific (note that scales vary, sources of data are as for Figure 36).

An indication of the extent of HREE enrichment over that of the LREEs can be gained from the PAAS normalised Er/Nd ratio (Er_{sh}/Nd_{sh}); the higher the value, the greater the HREE enrichment. Hence the mean Indian Ocean seawater Er_{sh}/Nd_{sh} value is 4.35 (Bertram & Elderfield, 1993) whereas for the TAG vent fluid and 17-19°S EPR vent fluid data used here the Er_{sh}/Nd_{sh} values are 0.80 and 1.00 respectively (see Appendix 5). Figure 38 shows the Er_{sh}/Nd_{sh} values plotted versus the Fe concentration for the particulate samples from Kairei and Edmond, as well as those of samples from TAG, Rainbow and EPR hydrothermal plumes in the Atlantic and Pacific Oceans (Er_{sh}/Nd_{sh} values for Kairei and Edmond are also shown in Table 16, values for the other sites are shown in Appendix 5). In Fig. 38a both the Kairei and Edmond samples show a

decreasing Er_{sh}/Nd_{sh} with decreasing [Fe], i.e. as the plume is diluted, the FeOOH particles are becoming enriched in the lighter rare earth elements. This is due to two reasons. Firstly the LREEs are being preferentially scavenged compared to the HREEs; this behaviour had previously been observed for the REEs in association with particulate matter (Elderfield, 1988; Sholkovitz et al., 1994). Secondly, the HREEs are better stabilised by carbonate complexation in solution (Byrne & Kim, 1990) which means they are 'less available' for scavenging. The trend is also seen for the samples from other hydrothermal plumes in the Atlantic and Pacific Oceans.

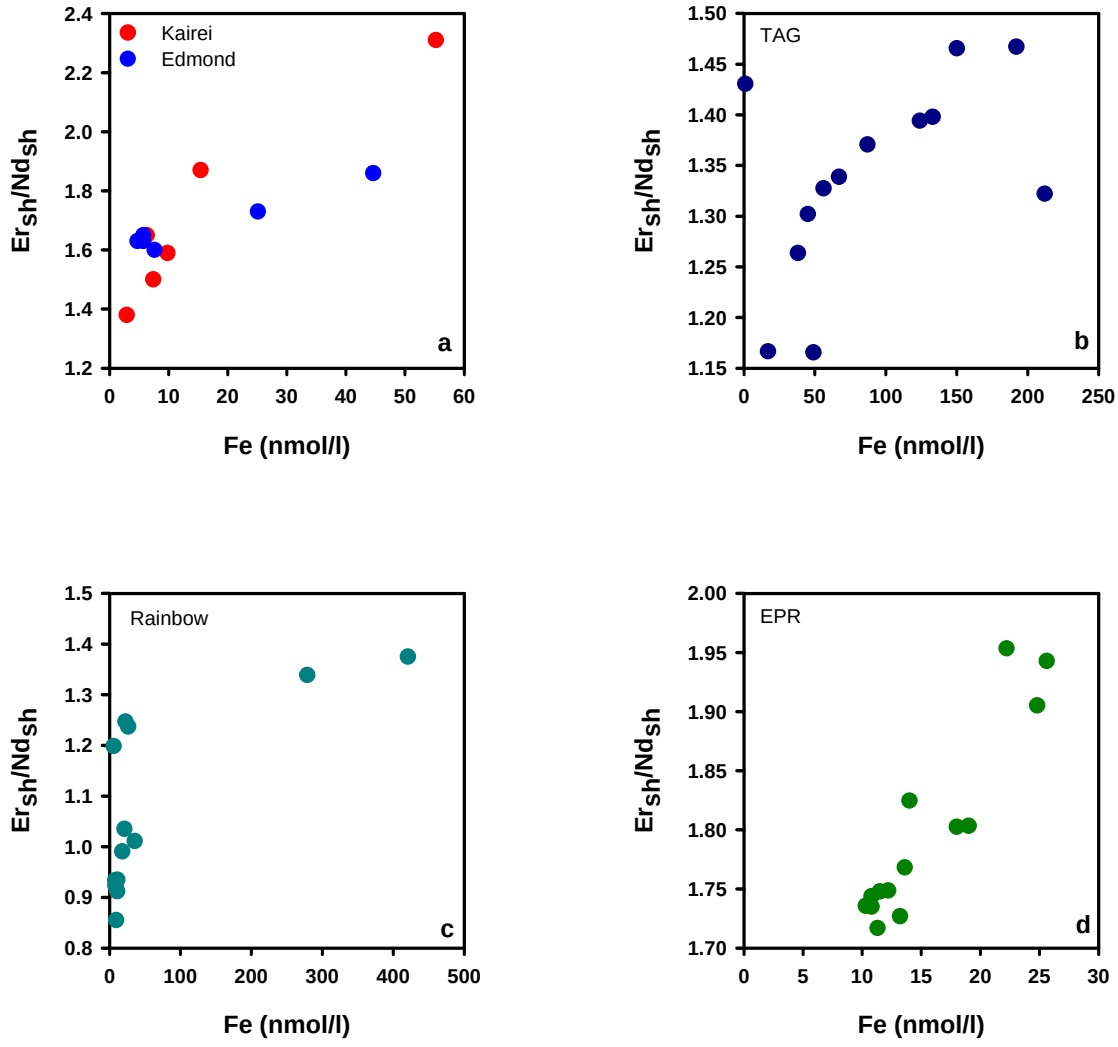

Figure 38 PAAS normalised Er/Nd values for particulate hydrothermal plume samples from the Kairei and Edmond sites, TAG and Rainbow in the Atlantic and 9°45'N East Pacific Rise in the Pacific relative to particulate Fe (note that scales vary, sources of data are as for Figure 36)**.**

4.3.5 Summary

The rate of iron (II) oxidation varies considerably between the three major oceans and changes systematically along the path of thermohaline circulation such that the rate in the Indian Ocean is intermediate to that in the Atlantic and Pacific Oceans (Field & Sherrell, 2000; Statham et al., 2005). Because of this, the absolute concentrations of particulate Fe available to be collected by filtration, *in situ*, in Indian Ocean plumes are lower than the comparable particulate [Fe] reported from similarly occupied sampling stations within 100m of active vent sites on the mid-Atlantic ridge at TAG and Rainbow. Despite this, the patterns of behaviour observed for elements within the Kairei & Edmond hydrothermal plumes in the Indian Ocean are broadly similar to those already observed in Atlantic and Pacific Ocean hydrothermal plumes.

Hence, the oxyanions such as P, V and As exhibit a linear relationship with Fe suggesting initial co-precipitation and/or scavenging by the Fe-oxyhydroxide particles but no further uptake once the non-buoyant hydrothermal plume is reached. Of the chalcophile elements, Zn and Cd exhibit negative curvature in their relationship with Fe, as does Cu in the Edmond hydrothermal plume. This is consistent with initial precipitation of chalcophile sulfides followed by loss of the sulfides, either by preferential settling out or their oxidative dissolution. However, Cu in the Kairei plume and Pb at both sites do not exhibit clear negative curvature in their relationships with Fe suggesting that other processes may be involved such as adsorption onto the Fe-oxyhydroxide particles. The rare earth elements and yttrium show positive curvature in their relationship with Fe, consistent with the theories that either, there is depletion of the REEs at [Fe]>100nmol/l followed by re-equilibration or, based on evidence from sediments, that they are continuously scavenged as the plume is diluted.

These results suggests that while the differing rates of iron (II) oxidation may impact the dispersal distance of the dissolved iron (II), the fundamental processes occurring within plumes do not change significantly between hydrothermal plumes in different ocean basins.

5 Chapter 5 Comparison of particulate, colloidal and dissolved phases

5.1 Introduction

Previous studies of hydrothermal plumes, with the exception of James & Elderfield (1996), James et al. (1995) and Massoth et al. (1994) have focussed on either the dissolved or particulate phases, and where the particulate phase has been studied, only one size fraction had been considered. In Chapters 3 and 4, results were presented from the dissolved phase and coarse particulate (>1.0µm) fraction as collected from SAPs. In this chapter, complementary results from the >0.4µm and >0.1µm phases are presented.

The aim of studying the dissolved and various particulate fractions was to establish if there are any additional processes taking place in the smaller size fractions (e.g. in the colloidal Fe-oxide phase) other than those already observed and/or to provide evidence for previously proposed processes such as oxidative dissolution of sulfides formed in the buoyant plume. It is also possible that the >1.0µm SAP samples are biased towards coarse grained particles and may contain a higher proportion of sulfides (Feely et al., 1987) than the >0.4µm Niskin samples.

Seawater was collected in 10l Niskin bottles deployed on a CTD rosette as detailed in Chapter 2. Approximately 1 litre of seawater was filtered through a 47mm Whatman Cyclopore 0.4µm or 0.1µm filter to provide the particulate samples. This is in contrast to the >1.0µm SAP samples which were collected via in situ filtration. The differences in the two sampling methods and the consequences that this may have for the results are briefly discussed.

5.2 Results

Table 19 shows the major element concentrations (Mg, Al, P, Ca, Mn, Fe, Cu and Zn) for the >0.4µm and >0.1µm particulate samples which were collected using Niskin bottles.

Na concentrations were also measured and assuming that all Na present in the samples is due to sea salt then less than 100µl of seawater was retained on each filter. As discussed in reference to the SAPs samples, any contribution from sea salt to the concentrations of the particulate elements in these results is insignificant from such a small volume of seawater for the elements considered here. Discussion of the 0.1µm samples will be confined to the section on size fractionation in the Edmond plume later in this chapter (5.3.3). In the preceding sections the discussion relates to the 0.4µm samples only.

The maximum concentrations observed for these samples are an order of magnitude higher than those seen for the SAPs samples. Particulate Fe reaches 440nmol/l in the Edmond samples and 350nmol/l at Kairei, compared to the SAPs samples which have a maximum pFe concentration of 55nmol/l. Although slightly higher values may be expected due to the different filter pore sizes, it is mainly a function of the differing sampling methods and the Fe (II) oxidation rate. The SAPs are suspended in the hydrothermal plume for ~2 hours while 100's of litres of the surrounding plume are pumped through them whereas, the 0.4µm samples are taken from Niskin bottles which collect instantaneous plume samples. Although the SAPs are likely to move in and out of the plume, thus filtering both particle rich plume waters and ambient seawater (and hence diluting the actual plume particle concentrations in the samples), Fig. 39 which is a plot of the Seatech LSS signal for CTD 21 over the time period that the SAPs were operating, shows that the SAPs were suspended in the densest part of the plume for ~75% of the operational period. Despite this well positioned sampling, the slower Fe (II) oxidation rate in the Indian Ocean (compared to the Atlantic) means that, as discussed in Chapter 3 ('3.4.4. *In situ* particulate Fe calculations') there will have been very little particulate Fe present in the non-buoyant plume for the SAPs filters to collect anyway.

In contrast, for the Niskin bottle samples, there is the elapsed time between the Niskin bottle being fired and the sample being filtered back on board ship to take into consideration, unlike the SAP samples where the filtration occurs in situ. While the Niskin sample is being returned to the ship and waiting to be processed (the elapsed time for this was between 2 and 5 hours), further Fe oxidation is taking place within the Niskin bottle. As the half time for Fe (II) oxidation in the Indian Ocean is 2.3 hours (Statham et al., 2005) there will still be >50% of Fe (II) in solution >1hr after reaching

	Fe nmol/l	Mn nmol/l	Al nmol/l	Fe (Fe+Mn+Al)	Mg nmol/l	Ca nmol/l	P nmol/l	Cu nmol/l
Kairei								
CTD5 2076m 0.4µm	8.2	0.23	1.12	0.87	357	46.0	2.0	0.12
CTD5 2150m 0.4µm	51.6	0.23	1.04	0.98	461	120	9.3	11.7
CTD5 2175m 0.4µm	183	0.16	1.63	0.99	1605	338	29.3	14.8
CTD5 2199m 0.4µm	280	0.22	1.19	1.00	87.0	48.7	46.3	13.6
CTD5 2224m 0.4µm	254	0.12	0.83	1.00	1260	216	43.2	12.1
CTD5 2273m 0.4µm	344	0.23	1.27	1.00	214	95.3	58.2	14.4
CTD5 2295m 0.4µm	31.9	0.15	0.79	0.97	532	108	5.4	3.27
CTD5 2350m 0.4µm	18.4	0.34	1.08	0.93	114	42.4	3.2	0.43
CTD5 2373m 0.4µm	7.8	0.13	0.71	0.91	663	141	1.9	0.21
CTD5 2435m 0.4µm	9.9	0.19	0.77	0.93	66.3	18.0	2.5	0.25
CTD7 2176m 0.1µm	224	0.10	2.00	0.99	223	65.6	38.5	6.90
CTD7 2232m 0.1µm	19.2	0.16	2.16	0.93	839	159	4.24	0.77
CTD7 2268m 0.1µm	39.9	0.21	1.96	0.96	260	75.3	7.49	4.05
CTD7 2273m 0.1µm	39.9	0.22	4.92	0.90	5354	1015	7.63	1.80
CTD7 2320m 0.1µm	25.2	0.26	4.40	0.86	467	119	3.64	0.99
CTD7 2322m 0.1µm	27.1	0.11	2.34	0.94	5043	405	4.78	9.91
CTD7 2347m 0.1µm	19.5	0.26	3.28	0.87	515	118	5.18	0.82
CTD7 2371m 0.1µm	121	0.16	1.53	0.99	1639	303	22.3	2.95
CTD7 2176m 0.4µm	1034	0.43	4.45	1.00	1346	330	169	35.6
CTD7 2232m 0.4µm	41.5	0.67	3.32	0.92	941	252	8.72	1.33
CTD7 2268m 0.4µm	34.6	0.27	2.06	0.95	726	159	6.33	4.01
CTD7 2273m 0.4µm	21.8	0.29	2.46	0.90	419	103	4.50	1.15
CTD7 2320m 0.4µm	13.8	0.22	2.11	0.88	722	85.6	2.62	0.67
CTD7 2347m 0.4µm	10.5	0.19	1.82	0.87	848	73.7	2.69	0.41
CTD7 2371m 0.4µm	170	0.58	3.51	0.98	641	190	26.7	6.40

Table 19. Particulate concentrations for Niskin bottle (>0.4µm) samples: Molar concentrations (nmol/l) which have been blank corrected. See Appendix 6 for raw data

	Fe nmol/l	Mn nmol/l	Al nmol/l	Fe (Fe+Mn+Al)	Mg nmol/l	Ca nmol/l	P nmol/l	Cu nmol/l
Kairei (cont)								
CTD21 2026m 0.4µm	17.5	0.65	3.43	0.82	370	86.8	5.08	0.68
CTD21 2120m 0.4µm	220	0.15	1.89	0.99	305	101	33.8	15.0
CTD21 2199m 0.4µm	98.1	0.06	1.54	0.99	1180	231	13.7	8.12
CTD21 2220m 0.4µm	96.3	0.06	1.40	0.99	368	105	16.3	5.15
CTD21 2273m 0.4µm	118	0.14	1.79	0.99	1353	293	18.5	9.38
CTD21 2298m 0.4µm	288	0.17	3.66	0.99	702	174	45.8	16.3
CTD21 2320m 0.4µm	54.6	0.22	2.20	0.97	578	153	9.77	3.48
CTD21 2372m 0.4µm	21.5	0.21	2.15	0.92	748	179	5.33	1.51
Edmond								
CTD23 2469m 0.1µm	14.2	0.30	2.50	0.87	1203	245	4.09	0.40
CTD23 2781m 0.1µm	559	0.24	3.62	0.99	1795	425	103.5	6.61
CTD23 2819m 0.1µm	252	0.19	2.98	0.99	1137	264	46.1	4.35
CTD23 2960m 0.1µm	13.4	0.26	1.87	0.90	1211	247	3.92	0.79
CTD23 3008m 0.1µm	329	0.24	2.58	0.99	1757	393	60.4	4.05
CTD23 3019m 0.1µm	312	0.18	1.90	1.00	288	86.9	55.8	2.61
CTD23 3057m 0.1µm	184	0.30	3.58	0.98	2225	470	34.4	2.39
CTD23 3107m 0.1µm	256	0.28	5.12	0.98	376	105	45.4	2.50
CTD23 3156m 0.1µm	28.3	0.36	5.45	0.84	1604	348	7.92	1.23
CTD23 2469m 0.4µm	12.9	0.33	1.99	0.87	416	60.9	4.19	0.13
CTD23 2781m 0.4µm	440	0.19	1.33	1.00	1742	352	79.3	5.91
CTD23 2819m 0.4µm	103	0.21	2.78	0.98	831	185	17.6	4.03
CTD23 2960m 0.4µm	10.3	0.29	2.10	0.83	808	103	3.43	0.12
CTD23 3008m 0.4µm	177	0.16	2.22	0.99	302	86.5	31.7	1.85
CTD23 3019m 0.4µm	264	0.32	2.76	0.99	399	135	44.4	3.72
CTD23 3057m 0.4µm	57.4	0.31	2.90	0.95	381	114	11.6	1.34
CTD23 3107m 0.4µm	117	0.28	2.68	0.98	443	125	21.7	1.58

Table 19 (cont.). Particulate concentrations for Niskin bottle (>0.4µm) samples

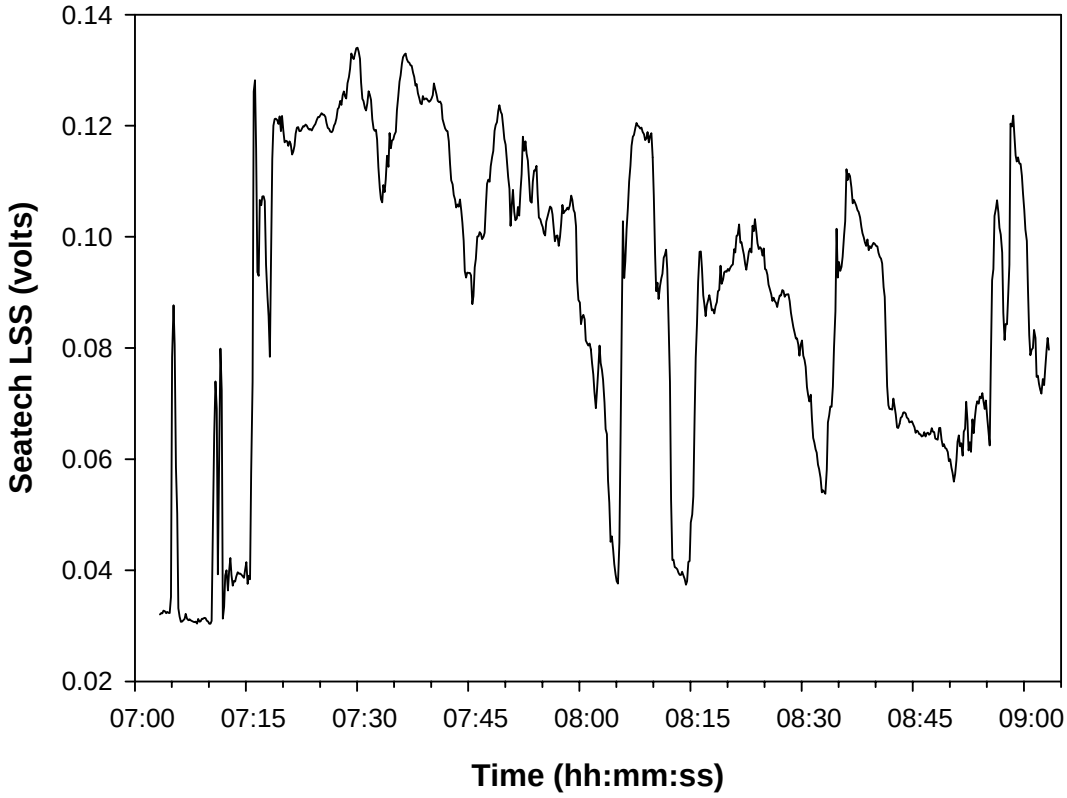

Figure 39 Seatech light scattering sensor profile for CTD 21 at Kairiei, during the time period that the stand alone pumps were operating.

the non-buoyant plume which will be available for oxidation. This will result in higher particulate Fe in the Niskin samples than the SAP samples. This is in contrast to the Atlantic Ocean where more rapid Fe (II) oxidation rates [half time of 20-30mins (Field & Sherrell, 2000)] mean that by the time the non-buoyant plume is reached at TAG, all the Fe (II) has precipitated, hence samples collected by SAPs (German et al., 1991a) or Niskin (Trocine & Trefry, 1988) have similar maximum Fe concentrations (212nmol/l and 276nmol/l respectively).

As already discussed in Chapter 3, the elapsed time between the Niskin bottle being fired and the sample being filtered back on board ship will have allowed time for further Fe (II) oxidation. However this does not mean that the resulting analyses are unrepresentative of the hydrothermal plume particles. The average time between firing the Niskin bottle and filtering the samples was 2.5hrs; assuming as in previous calculations, a mean current speed of 2cm/s, then, in 2.5hrs, the plume will have been

advected ~200m. We can estimate the dilution that will have occurred if we utilise the maximum dissolved Mn concentrations in samples from CTD 5 and CTD 21 which were ~240m apart. These give dilutions of 6800 and 8100 respectively (Table 6), i.e. the plume will have been diluted by only a further ~20%. It is also possible that the Fe (II) oxidation rate of the sample in the Niskin bottle may be affected by a change in temperature. The change in temperature is difficult to estimate, a large heat input would be required to change the temperature of the seawater in the bottle significantly. The ambient plume temperature was ~2.0°C while the clean room temperature was ~20°C. If we assume a worst case scenario that the temperature of the sample increased to 10°C, then the Fe (II) oxidation half time would be decreased from 2.3 to 1.6 hrs. This would mean in 2.5hrs ~13% more Fe (II) would be oxidised (but note that the sample would not be at 10°C for the whole of that time anyway). These calculations illustrate that there is probably very little difference between particles which would precipitate in a further 2.5 hrs while dispersing in the plume compared to those precipitating in the Niskin bottle.

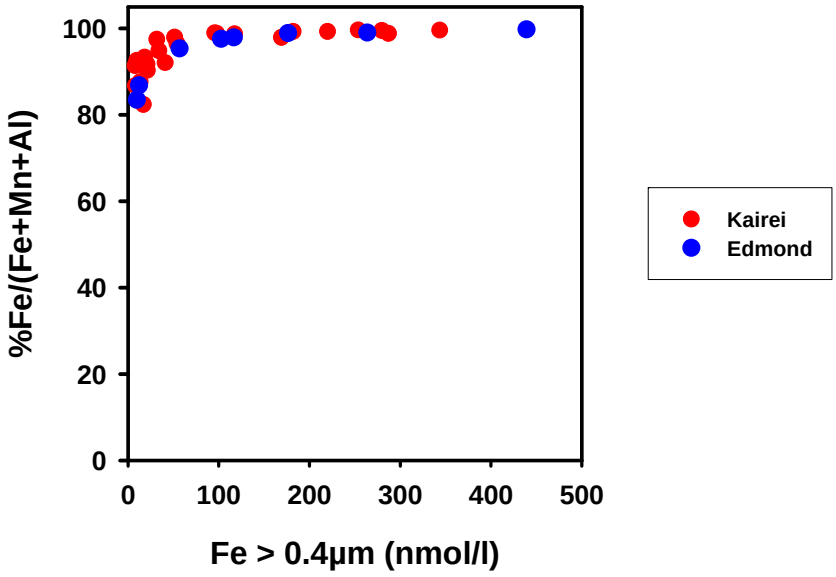

Figure 40 Percentage particulate Fe/(Fe+Mn+Al) versus particulate Fe for Kairei and Edmond hydrothermal plume Niskin (>0.4µm) samples

Figure 40 shows a plot of percentage Fe/(Fe+Mn+Al) versus [Fe] for the 0.4µm samples. As detailed in Chapter 4 this ratio can be used as an indication of detrital versus hydrothermal input, a high value (as is the case here, all percentages are >80%) indicating that the samples are predominantly hydrothermal in origin.

The data are shown again in Fig. 41 but as a ternary plot which contrasts with the ternary plot for the SAP samples in Chapter 4 (Fig. 25) where it shows the non-hydrothermal component is dominated by a Mn-rich phase. Here the plot suggests that the non-hydrothermal component is dominated by an Al-rich phase and that there is linear mixing between an Fe rich endmember (i.e. the hydrothermal component) and the Al-rich phase (which is most likely to be suspended sediment). This is like the 2-endmember mixing plot presented by Sherrell et al. (1999) for hydrothermal plume particles at 9°45'N on the East Pacific Rise.

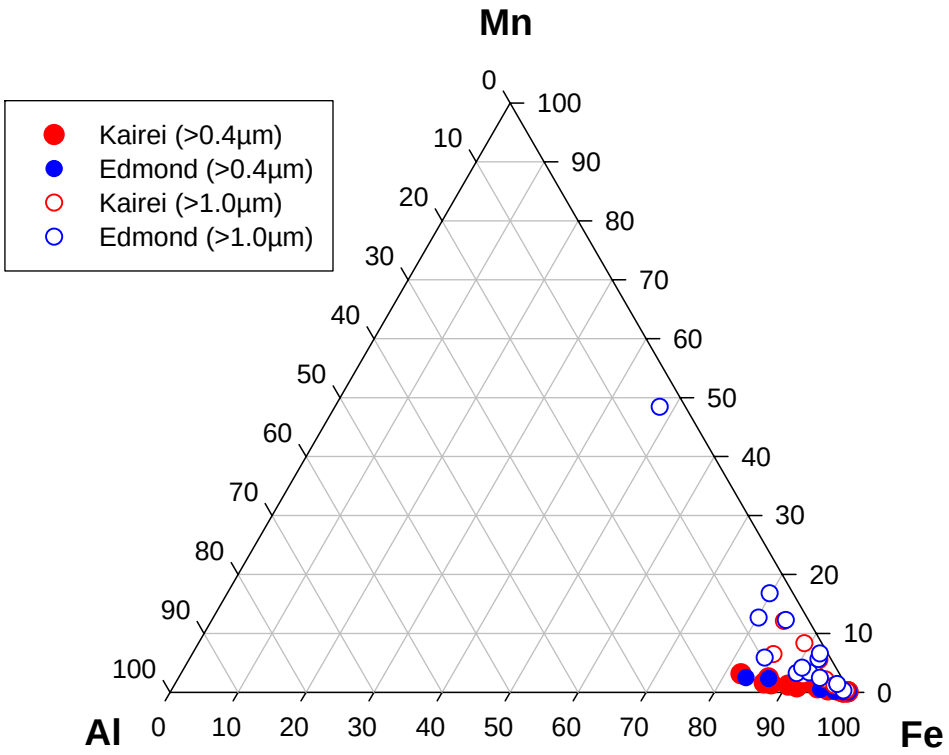

Figure 41 Ternary plot of Fe, Mn, Al composition of hydrothermal particle Niskin (>0.4µm) samples (closed circles) from the Kairei and Edmond plumes. Data for the SAPs (>1.0µm) samples (previously shown in Fig. 25) are also included (open circles) for comparison.

The most notable feature of the 0.4µm data shown in Table 17 are the high particulate Ca and Mg concentrations; pCa reaches a maximum concentration of 340-350nmol/l in both plumes and pMg has a maximum concentration of 1600-1700nmol/l. Figures 42a and 42b show the pCa and pMg data plotted against pFe together with the >1.0µm particulate data already presented in the previous chapter for comparison. The pCa concentrations are ~ 4 fold higher for the >0.4µm samples than for the >1.0µm samples while pMg concentrations are almost an order of magnitude higher. The pCa concentrations are also an order of magnitude higher than observed in either the TAG hydrothermal plume in the Atlantic Ocean (Trocine & Trefry, 1988; German et al., 1991a) or hydrothermal plumes on the East Pacific Rise and Juan de Fuca Ridge in the Pacific Ocean (Feely et al., 1994a; Feely et al., 1994b) while the pMg concentrations are two orders of magnitude higher

than those recorded at TAG in the Atlantic (pMg data for hydrothermal plumes in the Pacific are not available).

Also in Fig. 42, particulate Al and Mn are shown plotted against pFe for both the >0.4µm and >1.0µm data. Although the pAl data for the >0.4µm samples also show a similar increase to pCa over that of the >1.0µm samples (~ 4-fold), the pAl concentrations are in the same range as those measured in the TAG hydrothermal plume >0.4µm particulate samples of Trocine & Trefry (1988). The >0.4µm particulate Mn concentrations are slightly lower than those of the >1.0µm samples but again are in the same range as those measured by Trocine & Trefry (1988) for similar samples from the TAG hydrothermal plume.

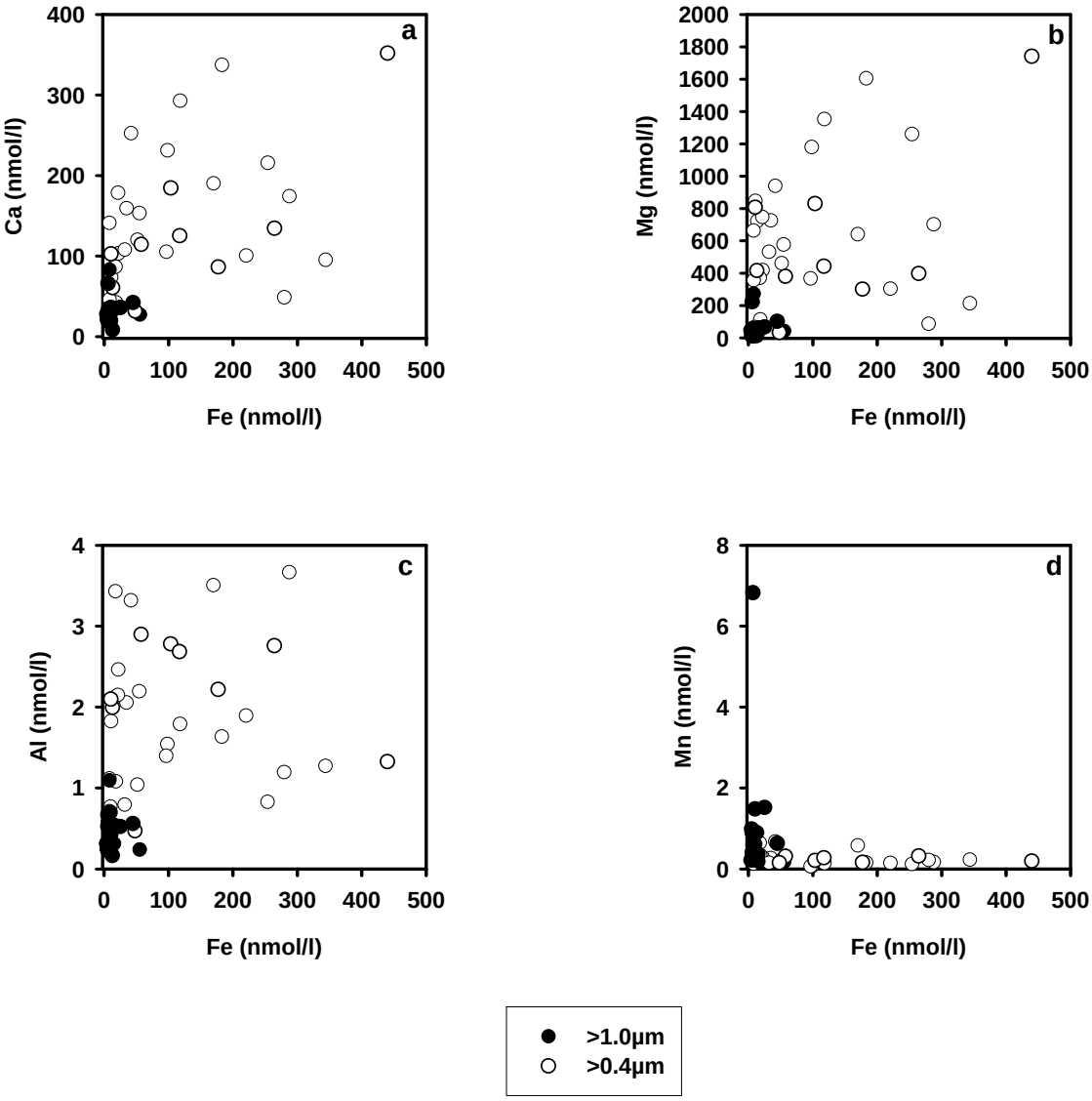

Figure 42 Particulate calcium, magnesium, aluminium and manganese versus particulate iron for the Edmond and Kairei >1.0µm SAPS and >0.4µm Niskin samples.

5.2.1 Oxyanions

The relationship between particulate phosphorus and iron for the >0.4µm fraction is shown in Fig. 43. They are positively correlated with a linear relationship. Phosphorus concentrations range from 2-60nmol/l for Kairei and 4-80nmol/l for Edmond. The highest concentrations are an order of magnitude greater than for the >1.0µm samples

(Table 13 and 19) but are associated with Fe concentrations which, as previously mentioned are also an order of magnitude greater.

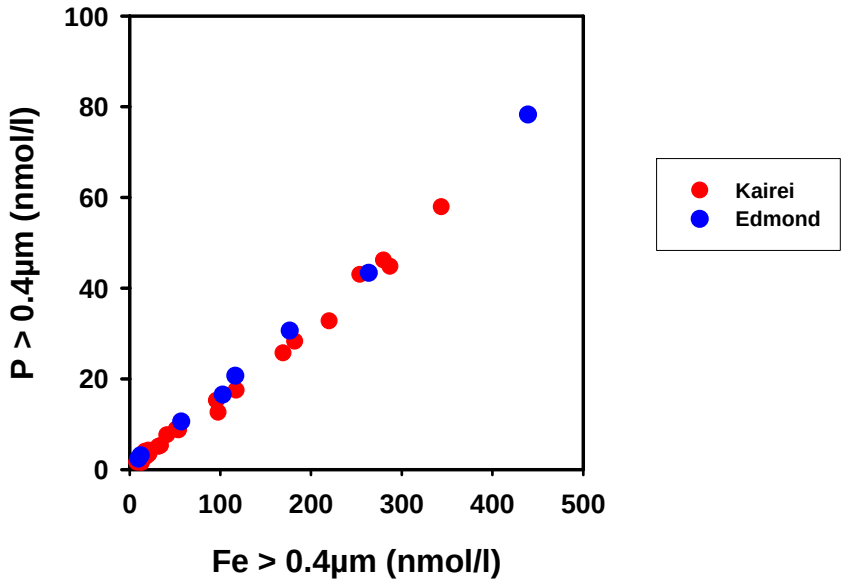

Figure 43 Phosphorus versus iron relationship for the >0.4µm particulate fractions in the Edmond and Kairei hydrothermal plumes.

5.2.2 Chalcophile Elements

A graph of particulate Cu versus particulate Fe is shown in Fig. 44. As for the 1.0µm SAPs samples, pCu and pFe are positively correlated (Fig. 28), the pCu concentrations decreasing as the pFe concentrations decrease. Although there is some possibility of negative curvature in the Edmond data, it is not as obvious as for the SAPs and in fact, linear or quadratic regressions give the same correlation coefficient of 0.78. The Kairei data are more scattered than for the SAPs samples and again, just as for the SAPs data, there is no clear specific Cu vs. Fe trend in the data.

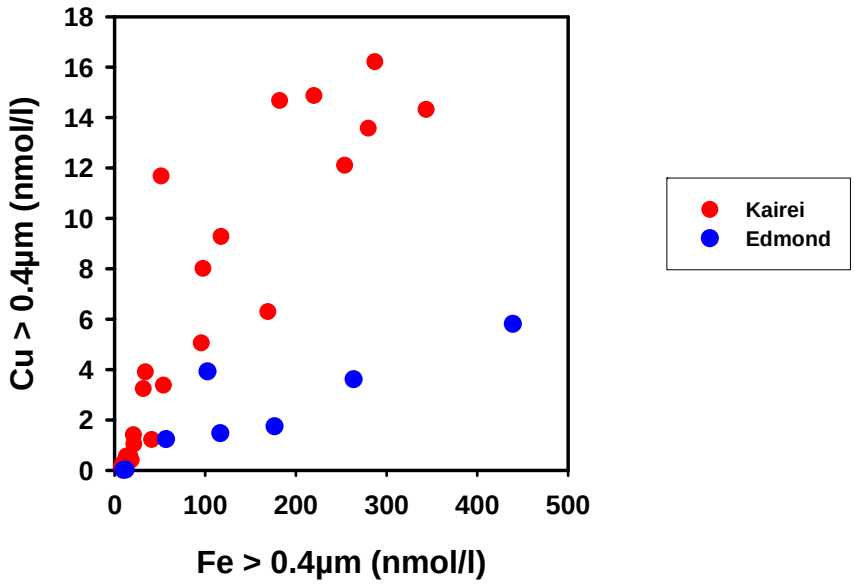

Figure 44 Copper versus iron relationship for the >0.4µm particulate fractions in the Edmond and Kairei hydrothermal plumes.

The maximum pCu concentration at Edmond is 5.9nmol/l which is comparable to the maximum concentrations of ~3.0nmol/l seen at TAG and Rainbow in the Atlantic (German et al., 1991a; Edmonds & German, 2004). At Kairei however, the maximum pCu concentration is 16nmol/l. This is higher than any previous measurements of hydrothermal plume particles in either the Atlantic or Pacific Oceans (Trocine & Trefry, 1988; Feely et al., 1990a, 1992, 1994a; German et al., 1991a).

Although Zn data are presented in Appendix 6, it is not presented in Table 19 or used in the discussion of particulate element behaviour due to the high and variable blank concentrations recorded for these samples (this problem was not encountered for the SAP samples).

5.3 Discussion

5.3.1 Calcium and Magnesium

Possible reasons for the presence of high concentrations of particulate Ca and Mg in the Kairei and Edmond samples could include biogenic input of Ca (i.e. as $CaCO_3$ which would also have some associated Mg), aeolian dust input, incorporation of basaltic seafloor material into the hydrothermal plume or inclusion of black smoker chimney material into the plume. Another possibility for the high [pMg] is adsorption of Mg onto Fe-oxyhydroxide particles (Trocine & Trefry, 1988). Figure 45 shows a plot of pCa versus pMg for the >0.4μm samples, the correlation between pCa and pMg (a linear fit gives an r^2 value of 0.80) suggests that it is most probably one source that is responsible for both the pCa and pMg concentrations rather than two distinct sources. This implies that the high [pMg] is probably not a result of adsorption onto FeOOH particles and the lack of clear correlation between pMg and pFe (Fig. 42b) in these samples unlike those of Trocine & Trefry (Fig. 46) also suggests this. This source of the pCa and pMg must also be richer in pMg than pCa. The data of Trocine & Trefry (1988) from the TAG hydrothermal plume in the Atlantic also shows a correlation between pCa and pMg, with a correlation coefficient of 0.82 (Fig. 46). Correlations between Ca and Mg for the Rainbow site in the Atlantic are not as tight (r^2 of 0.53) but in both cases the concentration of particulate calcium exceeds that of particulate magnesium. There are no magnesium data from any of the Pacific hydrothermal sites to allow comparison in that ocean.

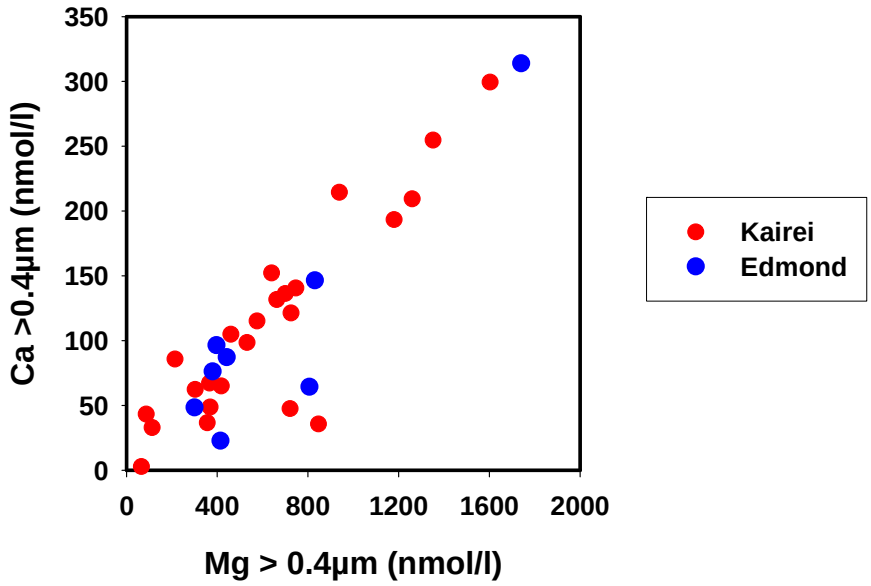

Figure 45 Relationship between particulate Ca and Mg in the Kairei and Edmond hydrothermal plumes for >0.4µm fraction.

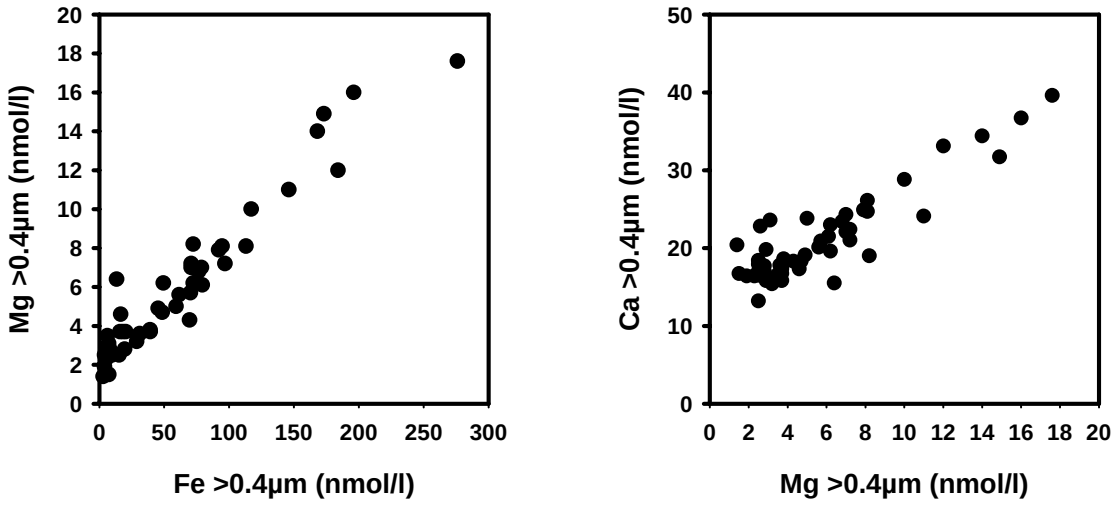

Figure 46 Data from Trocine & Trefry (1988) for the TAG hydrothermal plume showing relationship between particulate Mg and Fe and between particulate Ca and Mg.

The ternary plot presented earlier in Fig. 41 suggests that, unlike the SAP samples where the non-hydrothermal component is dominated by an Mn-rich phase, there is an aluminosilicate phase mixing with the hydrothermal particles. As the Ca and Mg concentrations are much higher in these Niskin samples than the >1.0µm SAP samples then this suggests that it could possibly be this aluminosilicate phase, not evident in the >1.0µm SAP samples which is responsible for the Ca and Mg present in the Niskin samples. The most likely Ca and Mg rich aluminosilicate which could be a possible source in the vicinity would be basalt.

A suite of eleven whole rock samples collected from the Rodriguez Triple Junction had an average composition of 16.0% by weight of aluminium oxide, 11.0% by weight of calcium oxide and 8.4% by weight of magnesium oxide (Price et al., 1986). Although the composition of basalts varies by a few percent, these values are sufficient for the purposes of illustrating whether incorporation of this material into the particulate samples could account for the concentrations of pCa and pMg. The maximum [Al] in the >0.4µm samples is 3.7nmol/l; if the basalt contains 16.0% Al_20_3 by weight then ~1.3µg/l of basalt would be required to account for all the Al in the samples. Although total suspended matter (TSM) concentrations are not available for these samples, an estimate can be made from the available data and literature data in order to assess whether 1.3µg/l of basaltic material is a feasible quantity. The estimate of TSM for these samples is shown in Table 20 below; compared to available literature data for TSM in hydrothermal particle samples, e.g. Feely et al. (1994b) recorded a maximum TSM of 90µg/l in non-buoyant plume samples from the Juan de Fuca Ridge in the Pacific, some of these values are high but they still serve to illustrate that inclusion of 1.3µg/l of basalt would be reasonable. However this quantity of basalt would only result in 2.5nmol/l of Ca and 2.7nmol/l of Mg which is 2-3 orders of magnitude lower than the concentrations recorded in the samples and still leaves the majority of Ca and Mg unaccounted for.

	[Fe+Mn+Al+Ca+P+Cu] (µg/l)	Calculated Total Suspended Matter (µg/l)	Measured [Mg] nmol/l	Measured [Ca] nmol/l
CTD5 2076m 0.4µm	2.0	14	357	46.0
CTD5 2150m 0.4µm	8.1	58	461	120
CTD5 2175m 0.4µm	24.0	172	1600	338
CTD5 2199m 0.4µm	19.7	141	87.0	48.7
CTD5 2224m 0.4µm	24.7	176	1260	216
CTD5 2273m 0.4µm	25.4	181	214	95.3
CTD5 2295m 0.4µm	6.1	44	532	108
CTD5 2350m 0.4µm	2.5	18	114	42.4
CTD5 2373m 0.4µm	5.8	41	663	141
CTD5 2435m 0.4µm	0.8	5	66.3	18.0
CTD7 2232m 0.4µm	11.3	81	941	252
CTD7 2268m 0.4µm	4.0	29	726	159
CTD7 2273m 0.4µm	7.2	52	419	103
CTD7 2320m 0.4µm	2.8	20	722	85.6
CTD7 2347m 0.4µm	2.1	15	848	73.7
CTD7 2371m 0.4µm	16.8	120	641	190
CTD21 2026m 0.4µm	3.2	23	370	86.8
CTD21 2120m 0.4µm	16.8	120	305	101
CTD21 2199m 0.4µm	14.1	101	1180	231
CTD21 2220m 0.4µm	8.9	63	368	105
CTD21 2273m 0.4µm	17.9	128	1350	293
CTD21 2298m 0.4µm	24.0	171	702	174
CTD21 2320m 0.4µm	8.2	58	578	153
CTD21 2372m 0.4µm	7.1	51	748	179
CTD23 2469m 0.4µm	1.8	13	416	60.9
CTD23 2781m 0.4µm	39.9	285	1740	352
CTD23 2819m 0.4µm	12.4	89	831	185
CTD23 2960m 0.4µm	3.3	23	808	103
CTD23 3008m 0.4µm	12.9	92	302	86.5
CTD23 3019m 0.4µm	20.2	145	399	135
CTD23 3057m 0.4µm	6.7	48	381	114
CTD23 3107m 0.4µm	10.8	77	443	125

Table 20. Calculated total suspended matter for Niskin (>0.4µm) samples.
Calculation based on composition of hydrothermal plume particles from Feely et al. (1994): comparison of the total suspended matter and total [Fe+Mn+Al+Ca+P+Cu] of their samples shows that [Fe+Mn+Al+Ca+P+Cu] varies from 3 to 30% of the overall TSM with an average of 14%. This average is used to calculate the likely TSM of these samples from the measured [Fe+Mn+Al+Ca+P+Cu] (individual values are in Appendix 6). The molar Mg and Ca concentrations are shown for reference.

Open ocean particulate measurements of Ca are not available for the Indian Ocean in the region of the Rodriguez Triple Junction. Instead data are only available for much more biologically productive areas such as the Arabian Sea and Bay of Bengal which would not be an appropriate comparison. Therefore the next best comparison is data from low productivity areas in either the Pacific or Atlantic Oceans. Particulate pCa concentrations in the North East Pacific are less than 10nmol/l (Sherrell, 1989),and background data from the TAG area in the Atlantic are less than 30nmol/l which

suggests that biogenic input could not account for the pCa concentrations recorded in these hydrothermal plume particles. Also, although Mg is found within biogenic calcite, it is only a small percentage (up to 4% by molar ratio, Hardy & Tucker, 1988) therefore input of biogenic calcite could certainly not account for the Mg concentrations recorded in these samples where pMg and pCa are so closely correlated but with pMg > pCa..

Aeolian dust inputs to the northern Indian Ocean, particularly in the region of the Arabian Sea are known to contain a significant proportion of dolomite which is a calcium magnesium carbonate, aerosol samples from the region can contain up to 25% of dolomite (Sirocko et al., 1991). This originates in the Persian Gulf region where it precipitates from the shallow Mg rich brines which occur (Reichart et al., 1997). Although it is unlikely the aeolian input as far south as the Kairei and Edmond hydrothermal sites would still contain 25% dolomite, lets assume this is the case for the purposes of an estimate. Estimates of total aeolian flux in the Southern/Equatorial Indian Ocean are 0.27µg/m^3 of air (Savoie et al., 1987) and 0.16µg/$m^3$of air (Chester et al., 1991). If we take 0.2µg/m^3 of air as an estimate, this gives 0.05µg dolomite /m^3 of air which equals 0.05 x 10^{-6}µg/cm^3.

Assuming dry deposition only (this is the dominant deposition mechanism in this area, accounting for 75-85% of total deposition (Ginoux et al., 2004)) which is given by:

$$F_p = (C_p)_{air} V_d \qquad \text{(where } C_p \text{ = concentration and } V_d \text{ = depositional velocity)}$$

and a settling velocity of 1cm/s based on dolomite being 'crustal' material in the size range of 1-3µm (e.g. Chester et al., 1991), this gives a flux to the surface ocean of:

$$(0.05 \times 10^{-6}\mu g/cm^3)(1cm/s) = 0.05 \times 10^{-6}\mu g/cm^2$$

If we then assume a settling velocity in the ocean of 0.04m/d[1] which is the approximate settling velocity of a 1µm particle and equals 4.6 x 10^{-7} cm/s then, assuming concentration = flux/settling velocity:

[1] Settling velocity is given by Stokes Law: $V_o = 2gr^2(d1-d2)/9\mu$ where
g = gravitational constant (9.8m/s^2)
r = radius of particle (assume an average for 1-3µm diameter crustal material of 1µm)
d1 = density of particle (assume dolomite for the purposes of this illustration = 2840kg/m^3)
d2 = density of medium (1025kg/m^3)
µ = viscosity of fluid (0.00905kg/ms)

Concentration of dolomite = $(0.05 \times 10^{-6} \mu g/cm^2) / (4.6 \times 10^{-7}$ cm/s)

which = $0.01 \mu g/cm^3 = 10 \mu g/l$ of dolomite

Assuming the most extreme case, that this is all transported to the deep ocean then 10µg/l of dolomite would give 41nmol/l of Mg (and also Ca) which is still not sufficient to account for the concentrations measured in the Kairei and Edmond samples.

Hydrothermal black smoker chimneys consist primarily of sulfides (e.g. Von Damm, 1990), however the initial formation of the chimney begins with the precipitation of anhydrite (Haymon, 1983). Anhydrite (calcium sulphate) has previously been observed in plume particles in samples from the TAG hydrothermal plume in the Atlantic (Godfrey et al., 1994) and also in samples from the Endeavour hydrothermal plume on the Juan de Fuca Ridge in the Pacific Ocean (Feely et al., 1987). In order to produce a [pCa] of 350nmol/l, ~50µg/l of anhydrite would need to be incorporated within the particulate material. Based on the TSM calculations above, this means approximately a fifth of the particulate sample would need to be anhydrite. Quantitative data regarding the mineralogy of hydrothermal plume particle samples is not available, although Feely et al. (1990a) detailed the anhydrite component of plume particle samples and sediment trap samples from the ASHES hydrothermal vent field as being 'very abundant'. However these samples were from the buoyant plume and sediment traps <18m from the vent and their data indicated that the larger grained sulphate minerals (i.e. including anhydrite) settled out of the plume very quickly. Dissolution studies of hydrothermal minerals also showed that anyhydrite undergoes rapid dissolution such that large quantities are unlikely to persist into the non-buoyant plume (e.g. Feely et al., 1987). Hence, it is unlikely that incorporation of black smoker chimney debris into the hydrothermal plume could account for the presence of higher concentrations of pCa. Also the presence of anhydrite certainly would not explain the high pMg concentrations observed.

Other minerals have also been found in black smoker chimney structures, e.g. caminite (Haymon & Kastner, 1981; Haymon & Kastner, 1986) which is a magnesium hydroxysulphate hydrate and starkeyite (Brett et al., 1987) which is a magnesium sulphate hydrate. Also, chimney structures in the Lost City hydrothermal field, which is

hosted on older oceanic crust away from the mid-ocean ridge in the Atlantic are composed of brucite ($Mg(OH)_2$) and calcium carbonate minerals (Kelley et al., 2001). Caminite with a formula of $Mg_7(SO_4)_5(OH)_{10}.H_20$ was found in the exterior of active black smoker chimneys on the East Pacific Rise at 21°N in association with anhydrite. To produce a [pMg] of 1700nmol/l would require ~200µg/l of caminite. There are no data on the percentage of caminite which is incorporated within the anhydrite, partly because caminite readily undergoes hydration and/or dissolution, however the anhydrite is more abundant (Haymon & Kastner, 1986) so it is unlikely that 50µg/l of anhydrite (the quantity required to give 300nmol/l of pCa) would have 200µg/l of caminite (the quantity required to give 1700nmol/l of pMg) associated with it.

Another possible source for the Mg and Ca is seawater itself, however a pMg concentration of 1700nmol/l would require the retention and evaporation on the filters of ~30ml of seawater. As mentioned at the start of '5.2 Results', the Na concentrations indicate that <100µl was retained on the filters meaning that seawater cannot be the source of the Mg and Ca.

In order to determine the origin of the high concentrations of particulate Ca and Mg observed in the Kairei and Edmond samples, it would be necessary to investigate the mineralogy of the samples. Identifying the Ca and Mg bearing phases within the samples should allow a more accurate assessment of their origin.

5.3.2 Chalcophile Elements

The most noticeable feature of the Cu versus Fe plot for the >0.4µm particulate fraction (Fig. 42) is that the Edmond and Kairei 0.4µm datasets do not co-incide, the Kairei data having a steeper gradient than the Edmond data. In fact this is also the case for the >1.0µm SAPs data although it is not so immediately obvious (Fig. 28) but is apparent from the Cu:Fe ratios of the samples (Table 15). The difference between the two data sets is probably a reflection of the differing vent fluid Cu:Fe ratios (see Table 21 below). The mean Cu:Fe ratios for the >0.4µm samples (shown in Table 21, together with the ratios for hydrothermal plume particles from the TAG site in the Atlantic which were also collected using Niskin bottles and 0.4µm filters) are the same as that of the >1.0µm

SAP samples for Kairei whereas for the Edmond samples the mean Cu:Fe ratio is slightly lower than for the >1.0μm samples (0.014 compared to 0.027).

	Kairei[1]	Edmond[1]	TAG[2]
Mean Cu:Fe ratio	0.060±0.044	0.014±0.012	0.009±0.007
[Fe] >100nmol/l Cu:Fe ratio	0.057±0.017	0.018±0.012	0.015±0.009
Range Cu:Fe ratios	0.015-0.227	0.010–0.038	0.002–0.029
Vent fluid Cu:Fe ratio	0.050±0.029	0.016±0.010	0.024

Table 21. Cu to Fe ratios for hydrothermal plume particles and vent fluids

[1] Vent fluid data from Gallant & Von Damm (2006)
[2] Data from Trocine & Trefry (1988) and Edmond et al. (1995)

Also shown in Table 21 are the mean Cu:Fe ratios for the highest [Fe] samples (where [Fe] exceeds 100nmol/l). In Chapter 4 the high [Fe] >1.0μm SAP samples showed evidence for the fractionation of Cu into sulfides in the early stages of plume formation, the Cu:Fe ratios being higher than the overall mean Cu:Fe ratio and higher than the vent fluid ratios. This is not the case for the >0.4μm samples where the ratios are for the high [Fe] samples are similar to the vent fluid ratio and the overall mean Cu:Fe ratio (see also Fig. 47 below). However this is entirely reasonable when the differing sampling methods are considered. As discussed earlier in this chapter, the >1.0μm SAP samples are collected in situ and therefore represent the true particulate [Fe] in the plume. However for the >0.4μm Niskin samples, there is time between sample collection and processing for further Fe (II) oxidation to take place so the actual Cu:Fe ratio at the time of collection will be reduced due to the increasing particulate Fe-oxyhydroxide concentration that will not be as Cu-rich as the initially precipitated sulphide phases..

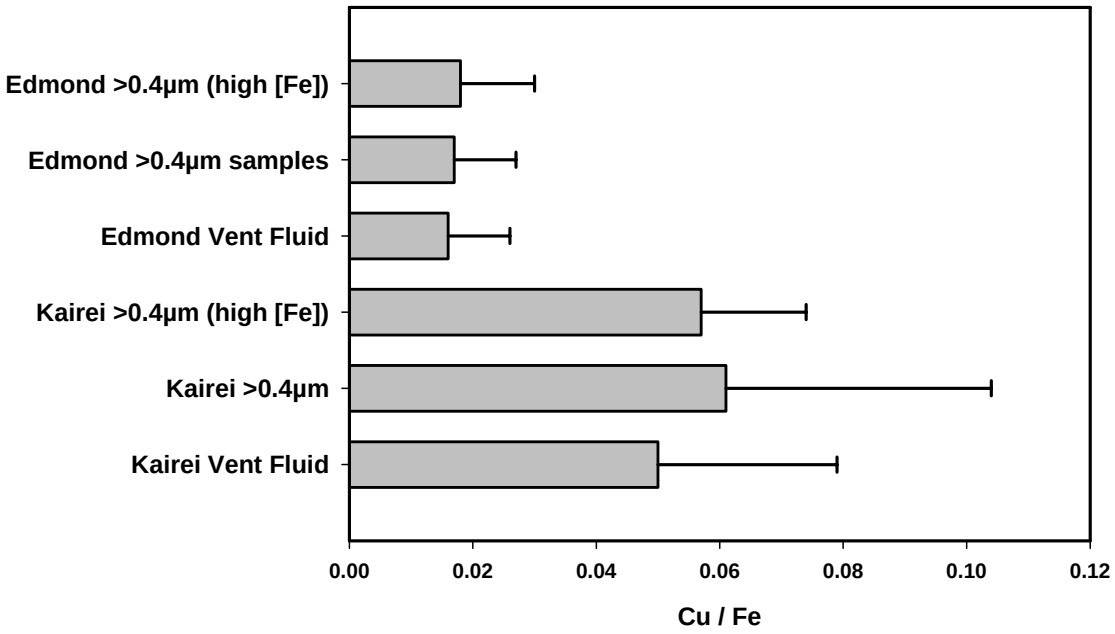

Figure 47 Copper to iron ratios for >0.4µm hydrothermal plume samples and vent fluids at Kairei and Edmond. High Fe ratios are the average ratios for samples where [Fe] is greater then 100nmol/l. See Table 19 for figures**.**

The high particulate Cu concentrations seen in the Kairei samples (maximum of 16nmol/l) could be a consequence of the vent fluid Cu concentrations which at ~210µmol/kg for Kairei (Gallant & Von Damm, 2006) are higher than any other published data for vent fluids [see for example, compilations in Butterfield (2003) and Von Damm (1995)]. The Edmond vent fluids also have a similar Cu concentration of ~220µmol/kg but the highest [pCu] measured is 6nmol/l. However we also know from the dissolved Mn measurements that the Edmond samples have a higher dilution factor than the Kairei samples (Table 5) so it would be expected that the Edmond [pCu] would be lower than at Kairei; if there were no removal of Cu from the plume, i.e. just straightforward dilution (as calculated from dissolved Mn) then the maximum [Cu] in the Edmond samples would be 20nmol/l whereas for the Kairei samples it would be 30nmol/l.

5.3.3 Size fractionation of metals in the Edmond hydrothermal plume

Previous studies of hydrothermal plume processes have typically focused on either the particulate or dissolved fraction of the hydrothermal plume material and, in the case of the particulate fraction, on just one size fraction (generally either >1.0µm or >0.4µm). It is already known that in the open ocean, dissolved Fe (II) initially forms fine colloids (<0.4µm) when it is oxidised. These colloids then aggregate to form particulate (i.e. >0.4µm) Fe (III) (Honeyman & Santschi, 1989; Wu & Luther III, 1994). If this same process is occurring in hydrothermal plumes, then analysis of just one size fraction may be insufficient to determine the processes which are taking place. Consequently, for this study, particulate samples, both >1.0µm (SAPs) and >0.4µm, as well as colloidal (defined for this study as between 0.1µm and 0.4µm) and dissolved (<0.1µm) samples were collected from the Edmond hydrothermal plume. This enables an investigation of the distribution of trace metals between the dissolved, colloidal and particulate phases within the hydrothermal plume. Data are presented in Table 22 below. Detailed discussion of the >1.0µm SAPs samples was presented in Chapter 4 and the 0.4µm samples have been discussed in this chapter, while the dissolved sample data were presented in Chapter 3. As described in Chapter 2, the >0.1µm fraction was collected by filtering approximately 1 litre of seawater from the Niskin bottle samples through a 0.1µm filter, i.e. the samples were not pre-filtered through a 0.4µm filter. Therefore the >0.1µm particulate sample will contain particles in the >0.4µm size fraction in addition to any 'particles' in the 0.1µm to 0.4µm colloidal phase. The colloidal fraction can therefore be calculated by either subtracting the >0.4µm [pFe] (or other element) from the >0.1µm [pFe] or subtracting the <0.1µm [dFe] from the <0.4µm [dFe]. Here it has been calculated from the particulate data for consistency throughout the elemental comparisons as there is only particulate data available for phosphorus.

Four elements were chosen for this more detailed analysis; iron, due to its abundance in vent fluids and the significant influence it has on chemical processes taking place within hydrothermal plumes, manganese as it is one of the most abundant elements in vent fluids and persists in the plume even at very high dilution, copper, as being representative of chalcophile element behaviour and phosphorus, as being representative of oxyanion behaviour. In the previous chapter it was shown that in the Indian Ocean, for coarse

particles (>1.0µm fraction), these elements show broadly similar behaviour with respect to iron to that observed previously in the Atlantic Ocean. This is despite the systematic decrease in the rate of dissolved Fe (II) oxidation from the Atlantic to the Indian and Pacific Oceans (Statham et al., 2005)

	Edmond CTD 23								
Depth	**2469m**	**2781m**	**2819m**	**2960m**	**3008m**	**3019m**	**3057m**	**3107m**	**3156m**
Iron									
Total	22.5	705	458	19.9	336	367	237	285	40.2
>0.4µm	12.9	440	103	10.3	177	264	57.4	117	
>0.1µm	14.2	559	252	13.4	329	312	184	256	28.3
<0.1µm	9.5	91.4	210	8.9	35.7	28.1	58.5	35.6	52.1
Colloidal	1.3	119	149	3.1	152	48	126	139	
Manganese									
Total	3.4	108	55	3.4	52	58	37	51	14
>0.4µm	0.3	0.2	0.2	0.3	0.2	0.3	0.3	4.9	
>0.1µm	0.3	0.2	0.2	0.3	0.2	0.2	0.3	6.5	5.3
<0.1µm	3.2	83.7	54.3	3.4	46.9	51.8	35.6	39.9	11.6
Colloidal	0	0	0	0	0	-	0	1.6	0
Copper									
Total	4.1	9.4	7.2	4.2	10.7	3.1	5.3	5.5	4.4
>0.4µm	0.1	5.9	4.0	0.1	1.9	3.7	1.3	1.6	
>0.1µm	0.4	6.6	4.4	0.8	4.1	2.6	2.4	2.5	1.2
<0.1µm	3.8	3.1	3	3.8	7.4	2.9	3.4	3	3.4
Colloidal	0.3	0.7	0.4	0.7	2.2	-	1.1	0.9	
Phosphorus									
>0.4µm	4.2	79.3	17.6	3.4	31.7	44.4	11.6	21.7	
>0.1µm	4.1	104	46.1	3.9	60.4	55.8	34.4	45.4	7.9
Colloidal	-	24.2	28.5	0.5	28.7	11.4	22.8	23.7	

Table 22. Size fractions for Fe, Mn, Cu and P in the Edmond hydrothermal plume (all concentrations are nmol/l)

'Total' fraction is the dissolved plus the particulate fraction. This can be calculated from either the particulate >0.4µm fraction plus the dissolved <0.4µm fraction (presented in Chapter 4) or the particulate >0.1µm fraction plus the dissolved <0.1µm fraction; figures presented are an average of those two calculations (difference between the two figures varies from 3 to 20%).

Manganese

Figure 48 shows plots of dissolved Mn, dissolved plus colloidal Mn and particulate Mn (>0.4µm) versus total Fe (i.e. dissolved plus particulate Fe). Dissolved Mn (<0.1µm) shows a good positive correlation with total Fe. The dissolved plus colloidal Mn

(i.e.<0.4µm) is also positively correlated with Fe. The dashed line represents the regression line from the dissolved Mn (<0.1µm) plot and this shows that there is some evidence for the presence of Mn in the colloidal phase; up to 20%. The highest [Fe] sample suggests up to a third of the Mn may be in the colloidal phase; however it is likely that this data point is anomalous. The plot is based on the dissolved data, whereas the colloidal data in Table 22 (which is based on the particulate data) suggests little evidence of Mn in the colloidal phase. There are no analytical reasons to doubt the validity of the dissolved Mn data, however data from three depths at CTD 7 where both 0.1µm and 0.4µm samples were collected also show little or no Mn in the colloidal phase whether calculating the value from particulate or dissolved data (see Table 23 below).

Kairei CTD 7			
Depth	**2268m**	**2273m**	**2320m**
Manganese			
Particulate > 0.4µm	0.3	0.3	0.2
Particulate > 0.1µm	0.2	0.2	0.2
Dissolved < 0.4µm	24.1	11.5	6.7
Dissolved < 0.1µm	20.8	11.4	6.8
Colloidal calculated from particulate data	0	0	0
Colloidal calculated from dissolved data	3.3	0.1	0.1

Table 23. Size fractions for Mn in the Kairei hydrothermal plume (all concentrations are nmol/l)

(CTD 7 data are not presented in detail in this chapter due to large inconsistencies in the two values for total Fe data calculated from either the 0.1µm or 0.4µm data and also because in some cases the >0.1µm particulate [Fe] which should be higher than the >0.4µm particulate [Fe] was much lower, suggesting a possible filtration problem. The three samples used here had valid Fe data)

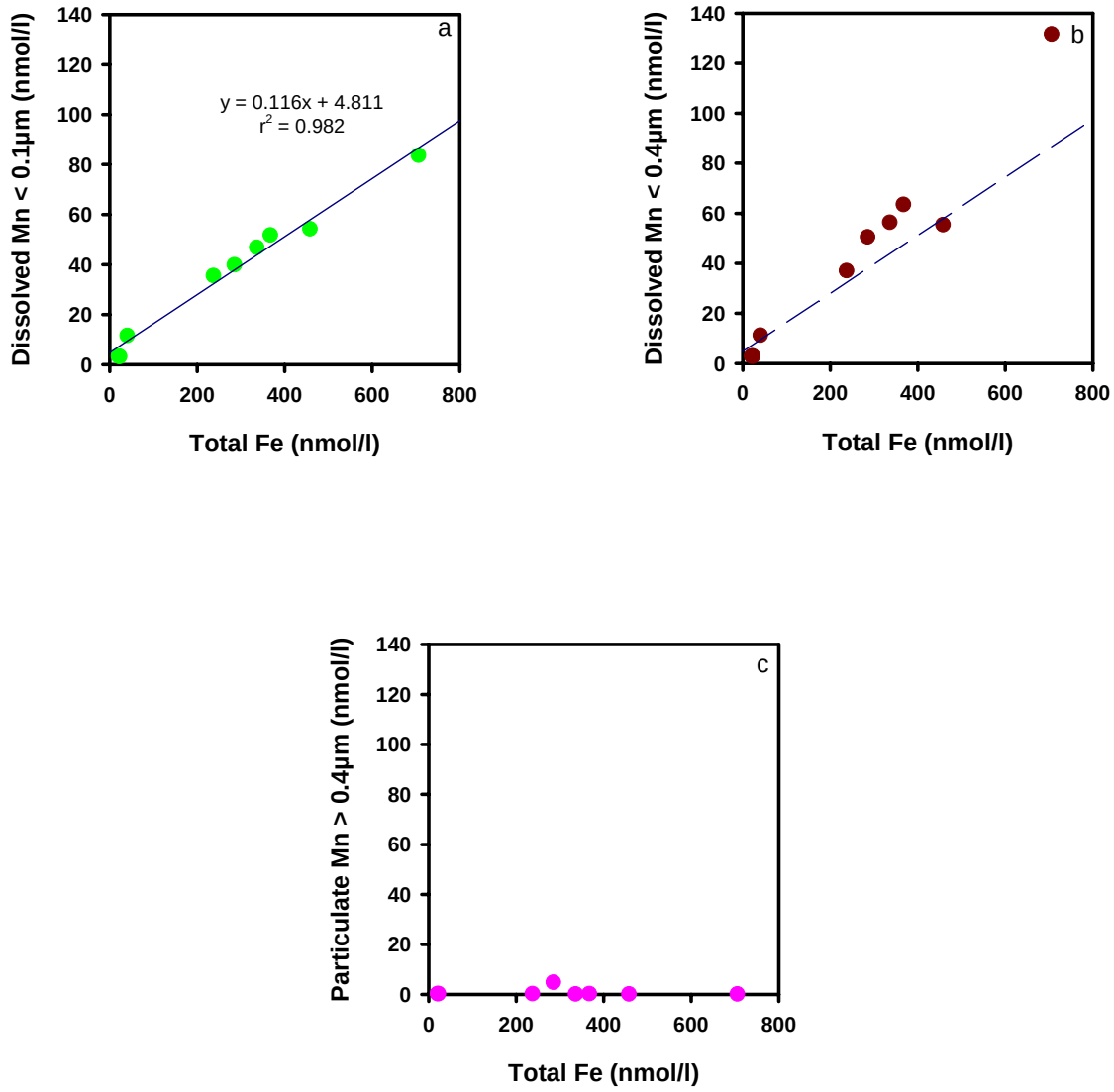

Figure 48 Size fractions of Mn versus total Fe. (a) shows the dissolved (<0.1µm) Mn fraction versus total Fe (i.e. dissolved plus particulate) with regression through all data, (b) shows the dissolved (<0.4µm) Mn fraction versus total Fe. The dashed line is the regression line from (a) for comparison and (c) shows the particulate (>0.4µm) Mn fraction versus total Fe.

The particulate Mn versus total Fe plot is consistent with existing knowledge of the behaviour of Mn within hydrothermal plumes in that there is very little Mn in this phase, Mn is present almost entirely in the dissolved and/or colloidal phase. Dissolved Mn (II) has been shown to behave conservatively within hydrothermal plumes close to the vent source, persisting for at least two weeks in, for example, the Endeavour Ridge

hydrothermal plume (Kadko et al., 1990). The oxidation and/or scavenging of dissolved Mn (II) is microbially mediated (Cowen et al., 1986) and has been observed as far as 20km from the vent source (Cowen et al., 1990).

Copper

Figure 49 shows particulate Cu, both the >1.0µm and >0.4µm fraction, colloidal Cu (<0.4µm, > 0.1µm) and dissolved Cu (<0.1µm) plotted against their corresponding Fe fractions. The strong positive correlation already seen for the >1.0µm SAP Edmond samples (shown again in Fig. 49a) is also evident in the 0.4µm particulate fraction (Fig. 49b). In the colloidal phase (Fig. 49c) there is very little Cu (generally less than 2nmol/l) despite the colloidal Fe concentration reaching >100nmol/l and there is no apparent correlation.

Also shown in the plots in Fig. 49 is the Edmond Cu:Fe vent fluid ratio (Gallant & Von Damm, 2006). The coarse >1.0µm particles have Cu:Fe ratios higher than the vent fluid, the >0.4µm particles have Cu:Fe ratios similar to the vent fluids, while the colloidal fraction has Cu:Fe ratios which are lower than the vent fluids. This is consistent with fractionation of the Cu into coarser grained sulfides, and little or no association of the Cu with the fine colloidal fraction. This helps to explain why the >1.0µm samples show some evidence of loss of Cu relative to Fe (i.e. negative curvature in the Cu vs. Fe relationship) while the >0.4µm samples appear more linear, it is because the sulfides are concentrated in the coarser fraction. These observations are also consistent with those of James & Elderfield (1996), one of the few other studies to look at dissolved and particulate samples. They found that the Cu:Fe ratios in samples from the Snakepit site in the Atlantic were greater than the vent fluid Cu:Fe ratio for the >0.4µm fraction but slightly lower than the vent fluid for the <0.4µm fraction. However they could not determine from their data whether the Cu in the <0.4µm fraction was truly dissolved or associated with the colloidal phase, this data confirms that Cu resides in the truly dissolved phase.

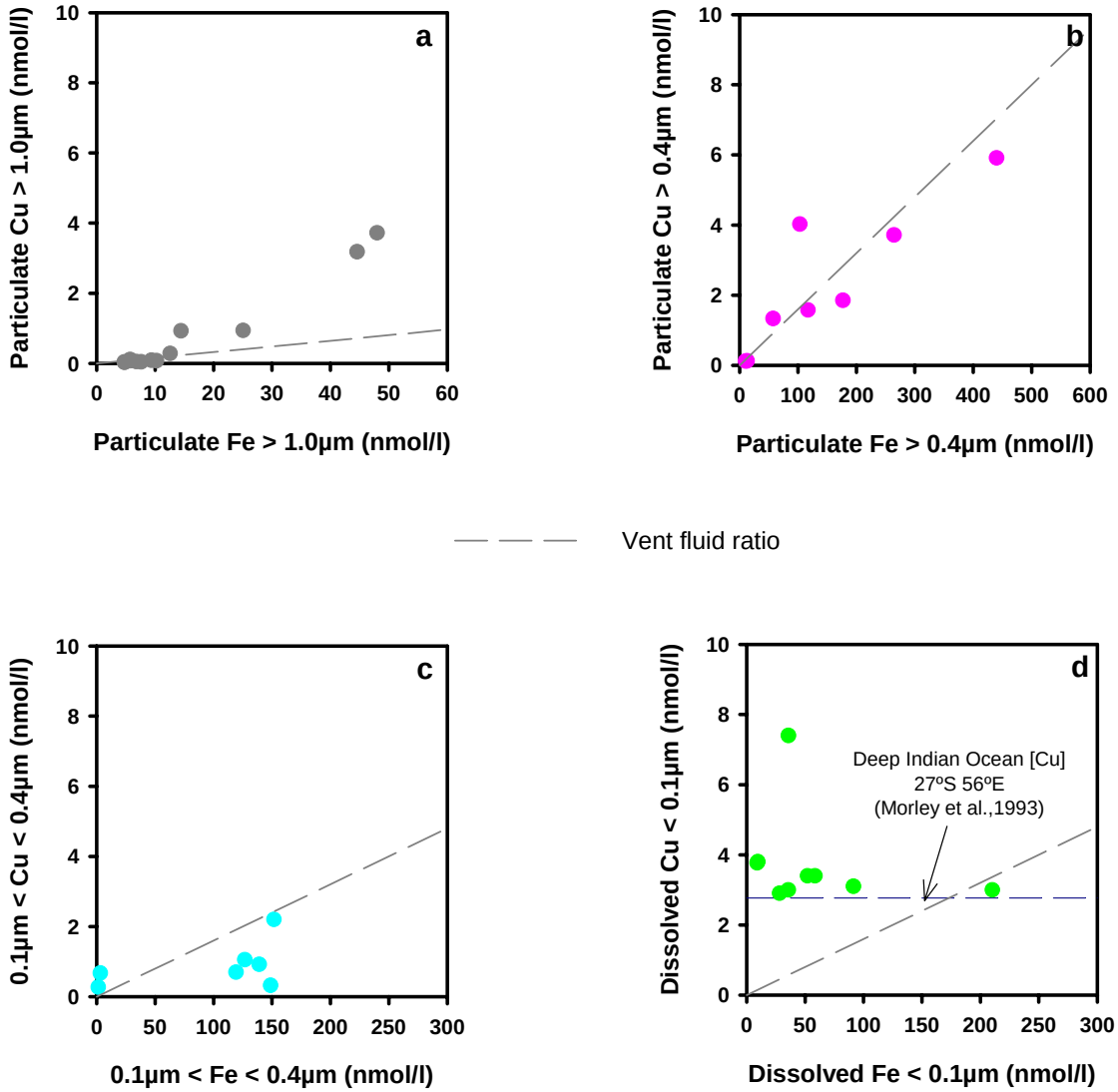

Figure 49 Size fractions of Cu versus Fe. (a) shows the particulate (>1.0µm) fractions (i.e. the SAP samples), (b) shows the particulate (>0.4µm) fractions, (c) shows the colloidal (between 0.1 and 0.4µm) fractions and (d) shows the dissolved (<0.1µm) fraction. The dashed line in all plots represents the Edmond vent fluid Cu:Fe ratio (Gallant & Von Damm, 2006).

The dissolved phase (Fig. 49d) shows no correlation between Cu and Fe, in fact the dissolved Cu concentrations measured in the Edmond hydrothermal plume are very similar to those measured previously for the open Indian Ocean (Morley et al., 1993) except for one value which looks to be abnormally high. One of the suggested mechanisms for loss of Cu from hydrothermal plumes relative to Fe is that the Cu sulfides formed early in the buoyant plume phase are oxidised and return to solution, if

this were the case then it could be argued that there should be some evidence of increased [Cu] in the dissolved phase. This is not apparent in the dissolved Cu data (Fig. 49d). However if we look at the >1.0μm plot where negative curvature is apparent, the maximum loss from the particulate phase which results in the curvature is ~1nmol/l. This loss will be partly accounted for by the settling of sulfides, hence the Cu enrichment which might be observed in the dissolved phase could be considerably less than 1nmol/l. This may be difficult to detect against the background dissolved Cu concentration of 2.8nmol/l (Morley et al., 1993).

The coarser (>1.0μm) fraction has an average Cu:Fe ratio of 0.027±0.027 which exceeds the vent fluid ratio (as illustrated in Fig. 49a). It is also higher than the average Cu:Fe ratio of the >0.4μm fraction which is 0.014±0.012. This suggests that the particulate Cu resides predominantly in the coarser (>1.0μm) fraction, i.e. that Cu is dominated by coarse sulfide phases rather than finer grained and/or colloidal Fe-oxyhydroxides.

Phosphorus

For particulate phosphorus (>0.4μm) there is a strong positive correlation with total Fe (Fig. 50a). However colloidal P is not correlated with total Fe although there is a significant component of P (between 10 and 30 nmol/l) associated with the colloidal phase (Fig. 50b). Comparison of P fractions to the corresponding Fe fractions rather than total Fe reveals much tighter correlations as illustrated in Fig. 50c and 50d. This is similar to the correlations observed in Atlantic and Pacific Ocean hydrothermal plumes for particulate fractions (Feely et al., 1998) as well as for the SAPs (>1.0μm) samples from this study (Fig. 27)

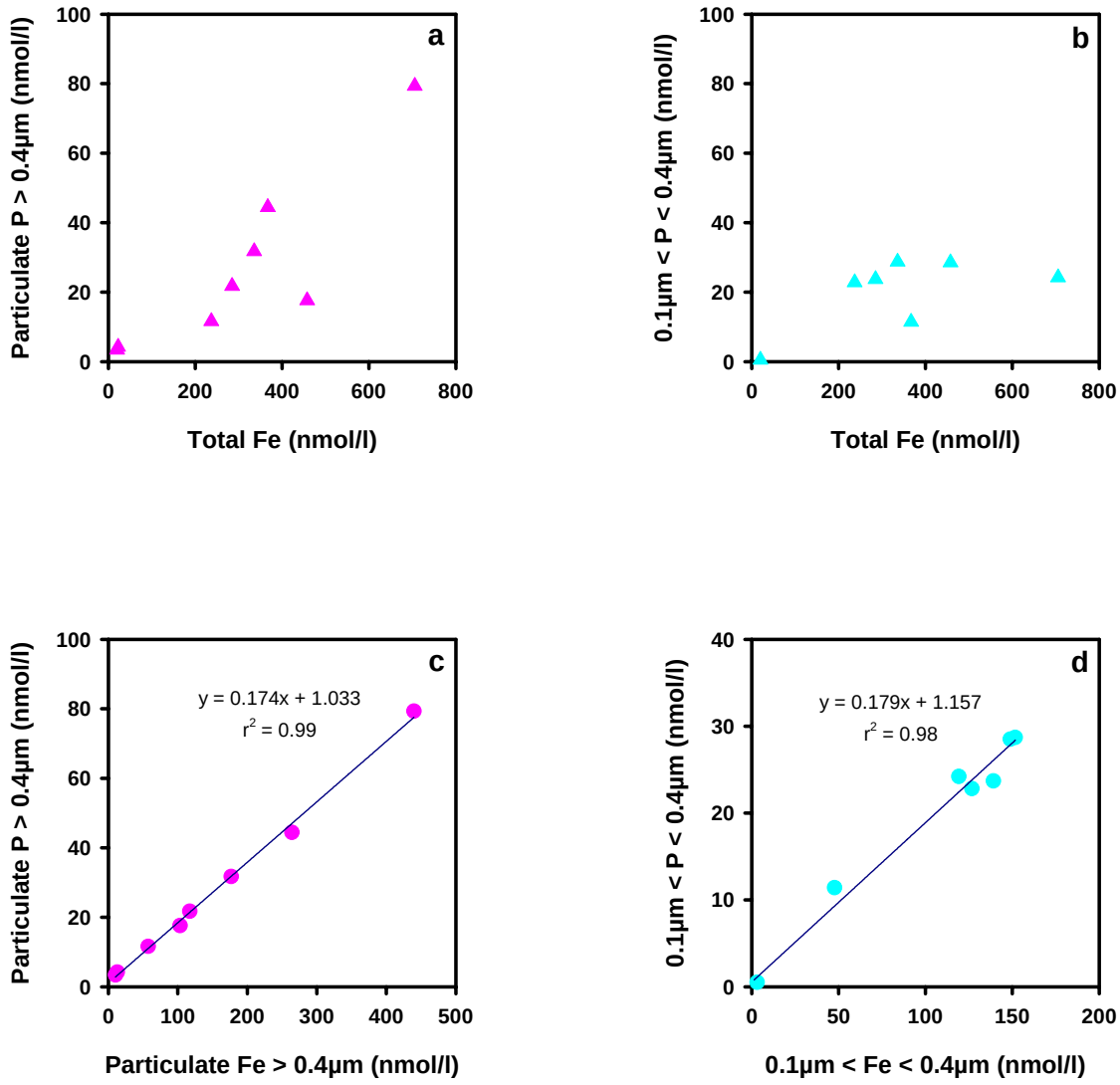

Figure 50 Size fractions of P versus total Fe and Fe size fractions. (a) shows the particulate (>0.4µm) P fraction versus total Fe and (b) shows the colloidal (between 0.1 and 0.4µm) P fraction versus total Fe while (c) shows P versus Fe for the particulate (>0.4µm) fraction and (d) shows P versus Fe for the colloidal (between 0.1 and 0.4µm) fraction.

Note that the correlations for the >0.4µm and colloidal fractions in Figs. 50c and d are almost identical. Fig. 51 shows the P and Fe data from these fractions plus the >1.0µm data plotted together along with the regression through all data. The tight correlation between all the fractions for phosphorus indicates that all three size fractions of the Fe-oxyhydroxide material have a common origin, i.e. initial precipitation of the dissolved Fe

(II) as colloids with associated co-precipitation or scavenging of the P, followed by aggregation into larger particles. This is consistent with scanning electron microscopy analysis of P-enriched particles by Feely et al. (1990b) which found the particles ranged in size from 0.1µm to aggregates of 2.0µm. The similarity between the fractions suggests that there is little further scavenging taking place as the particles aggregate and increase in size, otherwise we would expect to see some divergence of the correlations for each fraction. This is in direct contrast to the copper to iron relationships shown in Fig. 49 which are not the same for all the size fractions.

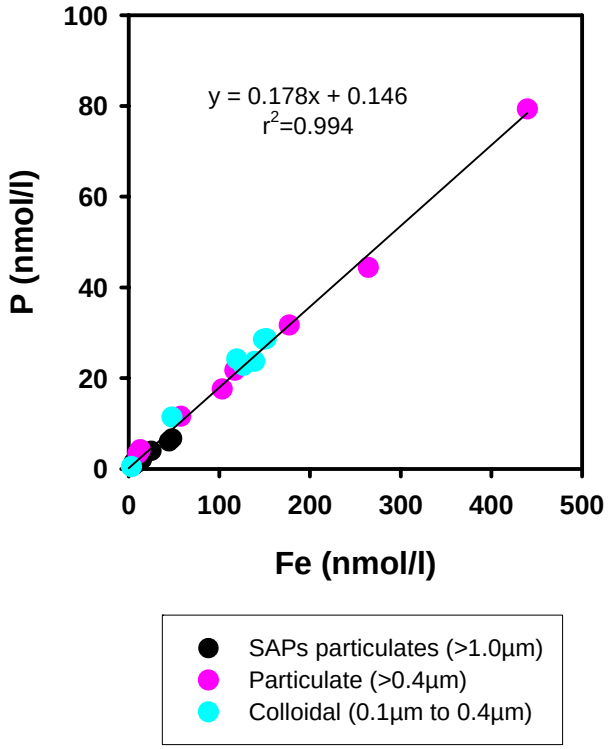

Figure 51 Phosphorus versus iron relationship for particulate (>1.0µm and >0.4µm) and colloidal size fractions with regression through all data.

5.3.4 P/Fe and V/Fe Ratios

From observations of Pacific and Atlantic Ocean hydrothermal plumes Feely et al. (1991) found a direct correlation between the P/Fe ratios in hydrothermal plume particles and the ambient dissolved P concentration. Hence in the Pacific Ocean where the

dissolved P concentration is higher than in the Atlantic (Table 24), the P/Fe ratio is also higher. However V, which has less variable dissolved concentrations than P throughout the deep oceans (Middelburg et al., 1988) has a higher V/Fe ratio in the Atlantic than in the Pacific (Metz & Trefry, 1993; Feely et al., 1994a). Feely et al. (1998) further investigated the V/Fe ratios at several sites in the Pacific and Atlantic and demonstrated that there is an inverse correlation between the V/Fe ratio in hydrothermal plumes and ambient dissolved phosphate concentrations. A suggested reason for this relationship is that P competes more effectively for the sites on the Fe-oxyhydroxide particles, hence where dissolved P concentrations are high, V/Fe ratios will be low and vice versa (Metz & Trefry, 1993; Feely et al., 1994a). Like V, As has similar concentrations throughout the deep oceans (Table 24), however in contrast to V, it exhibits a more constant ratio with Fe. At TAG in the Atlantic the molar As:Fe ratio of hydrothermal plume particles is 0.0017 while at North Cleft on the Juan de Fuca Ridge in the Pacific it is 0.0018 (Feely et al., 1991). For the Kairei and Edmond >1.0μm SAP samples it is 0.0016.

	Phosphorus[1] (nmol/l)	**Vanadium[2] (nmol/l)**	**Arsenic[2] (nmol/l)**
Pacific Ocean	2840	36.4	24.0
Indian Ocean	2380	35.6	22.5
Atlantic Ocean	1490	32.6	19.0

Table 24. Dissolved concentrations of P, V and As in the deep oceans.
[1]WOCE data (CLIVAR & Carbon Hydrographic Data Office))
[2]Middleburg (1988)

Dissolved P concentrations in the Indian Ocean are intermediate to that of the Atlantic and Pacific Oceans (Fig. 52 and Table 24). Therefore, based on the above observations, both the V/Fe and P/Fe ratios should also be intermediate to those measured in the Atlantic and Pacific

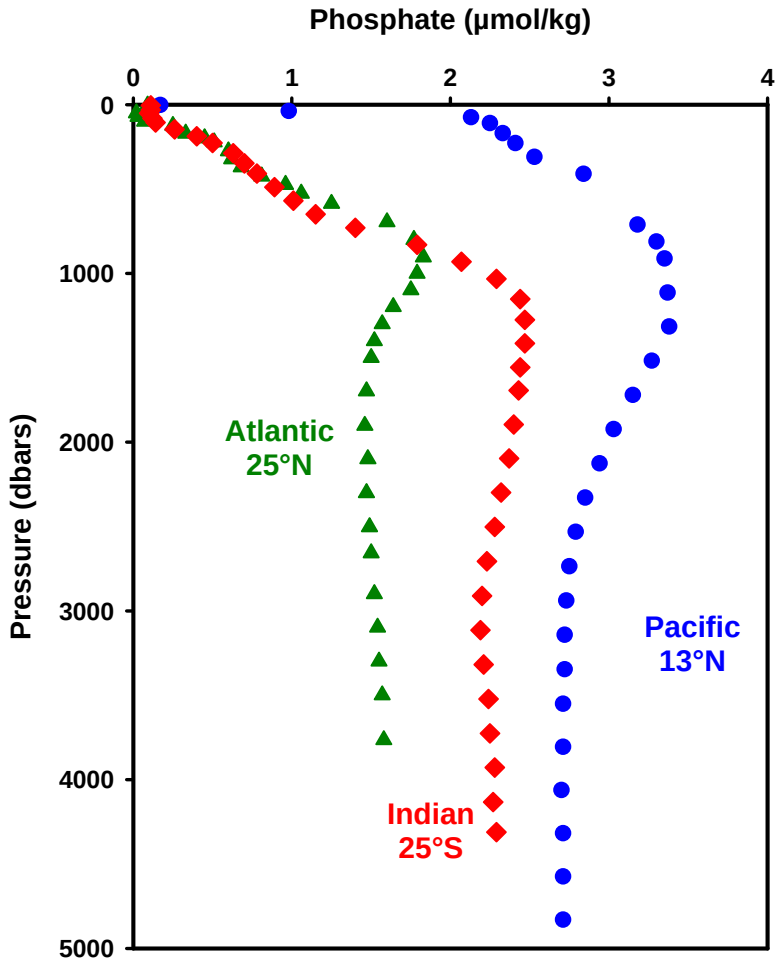

Figure 52 Phosphate depth profiles in the world oceans, data from World Ocean Circulation Experiment (CLIVAR & Carbon Hydrographic Data Office)

Figure 53 shows the average molar P/Fe and V/Fe ratios for the Kairei and Edmond 1.0µm SAPs samples plotted alongside the data from Feely et al. (1998). Dissolved phosphate data from the nearest GEOSECS station at the appropriate depth range has been used in place of actual data from cruise CD128 which is unavailable. The graphs show that data from both Edmond and Kairei are indeed intermediate to that of the Pacific and the Atlantic, consistent with the arguments of Feely et al. (1998).

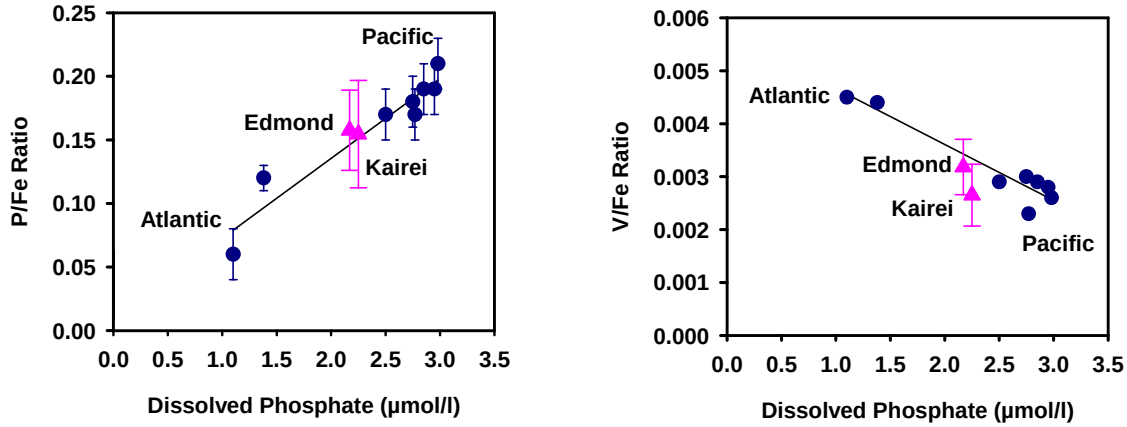

Figure 53 Molar P/Fe and V/Fe ratios for the SAP (>1.0µm) samples versus ambient dissolved phosphate. Atlantic and Pacific data (circles) from Feely et al. (1998), linear regression through all data.

If data from the >0.4µm Niskin samples are added to the plot for P/Fe ratios in Fig. 53 the result is higher ratios for Kairei and Edmond (~0.18 compared to ~0.16) with larger errors as illustrated in Fig. 54. This is unexpected as it has already been established from the size fractionation study that all the P fractions come from a single source and show extremely good co-variation between P and Fe in all size fractions (see Fig. 51)

.

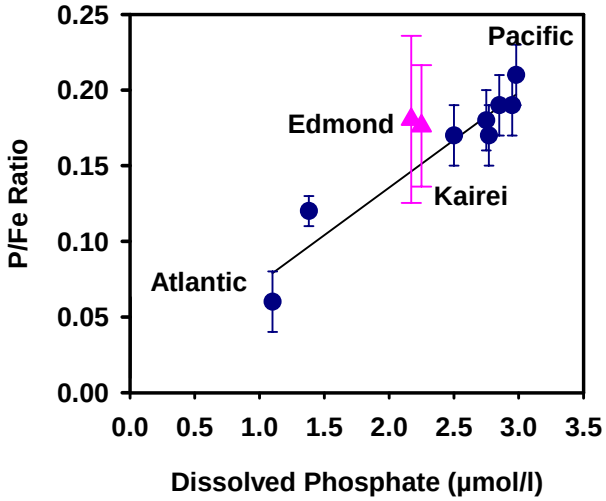

Figure 54 Molar P/Fe ratios for the SAP (>1.0µm) and Niskin (>0.4µm) samples versus ambient dissolved phosphate. Atlantic & Pacific data as for Fig. 53, linear regression through all data.

Plotting the P/Fe ratios versus dissolved manganese (as a tracer of plume dilution) for the >0.4µm Niskin samples as shown in Fig.55 gives an indication of why this may be the case. The plot shows that P/Fe ratios remain constant until dissolved [Mn] reaches <15nmol/l where they then rise exponentially. The most likely explanation is that, at these dilutions (a dissolved [Mn] of <15nmol/l represents a vent fluid dilution of >60,000 fold based on the vent fluid [Mn] (Gamo et al., 2001; Gallant & Von Damm, 2006)), input of non-hydrothermal particles is becoming influential. This is similar to the rare earth elements in the SAP samples in Chapter 4 where the relationship between the Ce and Eu anomalies and particulate Fe start to break down at low pFe concentrations as incorporation of background material becomes influential. If we look at the Fe/(Fe+Mn+Al) ratios of the particles, where dissolved [Mn] is greater than 15nmol/l the ratio is 0.98±0.02 but below dissolved [Mn] of 15nmol/l the ratio is 0.88±0.03 which is consistent with the influence of background material. Although background open ocean particulate P and particulate Fe values are not available, Feely et al. (1990a; 1996; 1998) collected background samples along with their hydrothermal plume particle samples from various sites in the Pacific Ocean. The background P/Fe ratios vary between 0.23±0.06 at the ASHES site on the Juan de Fuca Ridge, 0.74±0.82 on the Southern East Pacific Rise (SEPR) from 13°30'S to 18°40'S and 0.092±0.008 on the Gorda Ridge.

These values exhibit a variation both above and below the P/Fe ratio of the hydrothermal plume particles. However, it does illustrate the point that if background P/Fe ratios in the vicinity of the Kairei and Edmond hydrothermal sites are high like those on the SEPR, then incorporation of 10-20% of background material (see plot of percentage Fe/(Fe+Mn+Al) versus Fe in Fig. 40 earlier in this chapter) with a P/Fe ratio of 0.74 in combination with 80-90% of hydrothermal material with a P/Fe ratio of 0.16 would result in a P/Fe ratio of 0.22 to 0.28 which is not dissimilar to the ratios observed in Fig. 55 as higher plume dilutions are reached.

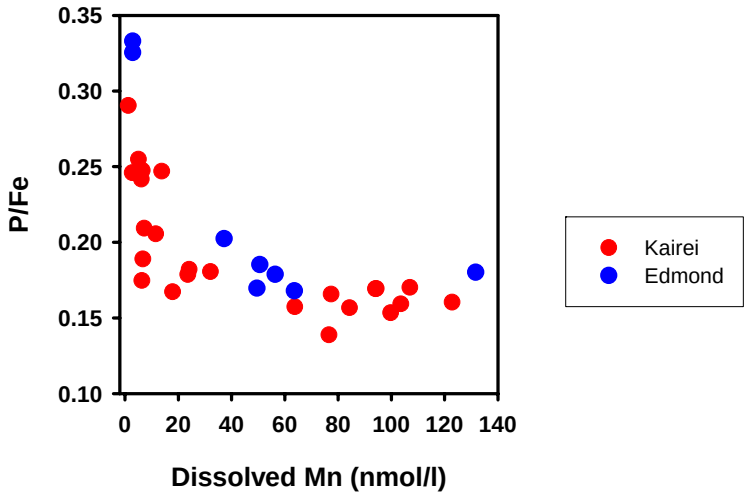

Figure 55 Molar P/Fe ratio versus dissolved Mn for the Niskin (>0.4µm) samples.

If we assume that the P/Fe ratios at low dissolved Mn concentrations are being affected by other inputs of non-hydrothermal particles and calculate the average P/Fe ratio based on just the 0.4µm samples where [Mn] >15nmol/l and the 1.0µm samples, (dissolved Mn measurements are not available for the SAPs samples so are all included), i.e. only the hydrothermal particles, then the average P/Fe for Kairei and Edmond is ~0.16 with a smaller associated error (see Fig. 56 below).

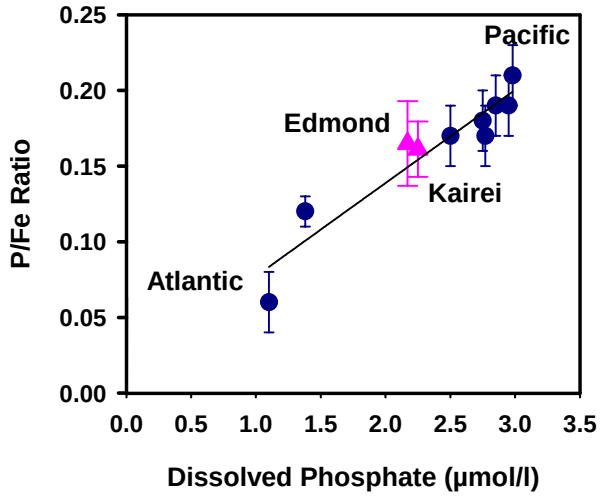

Figure 56 Molar P/Fe ratios for SAPs (>1.0µm) and Niskin (>0.4µm) samples versus ambient dissolved phosphate where dissolved [Mn] > 15nmol/l. Atlantic & Pacific data as for Fig. 53, linear regression through all data.

Feely et al. (1998) suggested that the correlation between the P/Fe ratios and dissolved phosphate and also between V/Fe ratios and dissolved phosphate was linear in nature. The addition of data from the Indian Ocean gives linear regression correlation coefficients of 0.90 and 0.93 respectively for P/Fe and V/Fe versus dissolved phosphate. However a quadratic fit gives slightly better correlation coefficients of 0.92 and 0.89 and as can be seen in Fig. 57 produces an improved fit to the data. For the relationship to be truly linear, the dissolved phosphate concentration at these locations would need to be in the range of 2.5-2.8µmol/l. Although dissolved phosphate concentrations are not reported from this study, comparison with available dissolved phosphate data for all oceans available from both the Geochemical Ocean Section Study (GEOSECS) and the World Ocean Circulation Experiment (WOCE) shows that concentrations in this range are only recorded at comparable depths considerably further north in the Indian Ocean, both at the most northern end of the Ninety East Ridge in the Bay of Bengal[2] and in the Arabian Sea in the proximity of the most north western end of the Carlsberg Ridge[3] (CLIVAR). Elsewhere these phosphate concentrations are not observed any closer than

[2] WOCE, Line I09, Station 234, 10°00'N 90°44E
[3] WOCE, Line I01E, Stations 893, 10°48'N 53°22'E and 889, 14°30'N 50°50'E

the Southern Pacific Ocean at 9-11°S 125-103°W[4] (CLIVAR, ; Broecker et al., 1982). This additional Indian Ocean data shows that as Feely et al. (1998) predicted, there is indeed a progressive change in P/Fe and V/Fe ratios along the global thermohaline circulation. However, in order to confirm the exact nature of the P/Fe and V/Fe relationship with ambient dissolved phosphate, additional data are required from hydrothermal plumes at locations intermediate to the Indian Ocean sites studied here and the Atlantic Ocean sites cited by Feely et al. (1998) at dissolved phosphate concentrations of ~1.8-1.9µmol/l. The most promising locations to conduct such future study, based on GEOSECS and WOCE dissolved phosphate data would be along the Mid Atlantic Ridge at 34-42°S[5] (CLIVAR, ; Broecker et al., 1982) an area as yet unexplored with respect to hydrothermal activity.

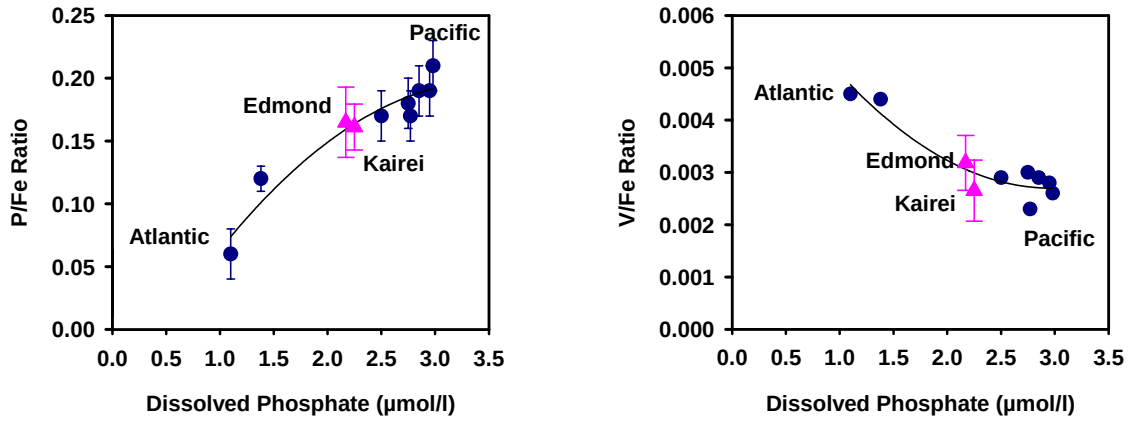

Figure 57 Molar P/Fe and V/Fe ratios versus dissolved ambient phosphate with quadratic fit. (P/Fe values are those from Fig. 56, V/Fe values from Fig. 54)

It has been suggested that if P/Fe and V/Fe ratios are preserved in the sediments, then they could be used as indicators of past seawater phosphate concentrations (Feely et al., 1998). The ratios are only like to be maintained if the sediments remain oxic, otherwise P and V may be remobilised and although they may still ultimately remain in, or return to the sediments (e.g. Fillippelli & Delaney, 1996), they will no longer be in association

[4] e.g. GEOSECS, Station 328, 9°16'S 125°32'W or WOCE, Line P18, Station 115, 11°60'S 103°00'W
[5] e.g. GEOSECS, Station 93, 41°46'S 18°27'E or WOCE, Line A14, Stations 84, 34°00'S 9°00'W and 95, 39°30'S 9°00'W

with the hydrothermal component. The hydrothermal P/Fe ratio in sediments may be difficult to determine due to other variable inputs of P to the sediments (e.g. in association with organic matter), in fact as mentioned earlier the hydrothermal P/Fe ratio in mature plume particles may already be affected by other processes before they even reach the sediments. Despite this, at the Rainbow hydrothermal site in the Atlantic, Edmonds & German (2004) found the P/Fe ratio in the plume particles (0.100 ± 0.002) matched the ratio in Rainbow surface sediments (0.08-0.10, Cave et al.,2002). However, on the Southern East Pacific Rise (EPR) at 14°S, even under oxic conditions, Dunk & Mills (2004) found that the P/Fe ratio in the sediments was both variable and lower than the corresponding plume particles.

Preservation of the V/Fe ratios is also an unresolved issue. In the same samples from the Southern EPR, Dunk & Mills (2004) found that the V/Fe ratios were directly comparable to plume particles. The average V/Fe ratio (0.0027 ± 0.0003) in a core from the Cleft Segment on the Juan de Fuca Ridge analysed by German et al. (1997) also compares very well with the average V/Fe ratio (0.0026 ± 0.0001) found by Feely et al. (1998) in plume particles from the same location. However, Schaller et al. (2000) who studied a core from the Southern EPR at 11°S found lower V/Fe ratios in the sediments (0.0024) than in corresponding plume particles (0.0030) and this is also the case for V/Fe ratios in sediments at the TAG hydrothermal mound (0.0010 to 0.0018 in the hydrothermal portion of the sediment (Metz et al., 1988)) compared to TAG plume particles (0.0045 ± 0.0003 (German et al., 1991a)). To add further complication, V/Fe ratios in the Rainbow hydrothermal surface sediments from the Atlantic where the P/Fe ratios correspond well to the plume particle ratios are actually higher than the V/Fe ratios in the plume particles; 0.007-0.008 compared to 0.0043 ± 0.0002 (Cave et al., 2002; Edmonds & German, 2004).

The conflicting results for P/Fe and V/Fe ratios in the sediments and in plume particles at different locations means that their use as paleo-proxies for phosphate concentrations in seawater is still an unresolved issue. However, all paleo-proxies have their weaknesses and results from even the most robust proxies often need to be treated with care. If the use of these ratios as a proxy is to be further explored then firstly, it is important to establish whether the P/Fe and V/Fe versus dissolved phosphate relationships are linear

or follow some more complex trend, as well as determining how well the ratios are preserved in the sediments through investigation of further sites. Careful consideration should be given to the selection of sediment core sites to ensure that they have been predominantly hydrothermally influenced over time and that the sediments are, and have been oxic.

5.3.5 Flux Calculations

As discussed in Chapter 1, hydrothermal activity, either by circulation of seawater through the hydrothermal systems or by reactions in hydrothermal plumes may act as a source or a sink for some elements. The global cycle of phosphorus is affected by the scavenging of this element onto the FeOOH particles which are then deposited in the sediments. Vanadium is also affected in the same manner. Previous estimates of this sink for both P and V along with estimates from this study are show in Table 25 below. For the estimates from this study a global Fe flux has been calculated by using the best estimate of global high temperature hydrothermal water flux from Schultz & Elderfield (1997) of 3.0×10^{13}kg/yr and a median value of 12400µmol/kg for the vent fluid Fe concentration from the global range of 750-24000µmol/kg (Von Damm, 1995). Assuming that 20-30% of this Fe is lost as sulphides (see Chapter 3), this means there is 9300µmol/kg available for Fe-oxide formation and scavenging giving a global Fe flux of 2.8×10^{11}mol/yr. For the P/Fe and V/Fe ratios, median values from the observed global ranges of 0.06-0.21 and 0.023-0.045 respectively have been used (this study having confirmed that values for these ratios are dependent on ambient dissolved phosphate concentrations and therefore should all be within these ranges).

The values from this study are consistent with estimates from previous authors, however in effect the values are little better constrained than the previous estimates. To improve the estimates further, initially a better constrained Fe flux is required. Although this study has provided a much better estimate of the Fe loss due to sulphides and therefore the Fe that is available for Fe-oxide formation, the main uncertainty lies in determining an average value across all vent fluids (aside from the associated uncertainties in estimating a global high temperature hydrothermal water flux).

	Global P removal flux (10^{10} mol/yr)	Notes
This study	3.9	Based on P/Fe ratio of 0.14 (see text for further details)
Wheat et al. (1996)	0.8	Based on Fe flux estimated from Fe/heat ratios and ^{3}He flux data from the Juan de Fuca Ridge and using a P/Fe ratio of 0.18
Kadko et al. (1994)	0.2	Based on Juan de Fuca Ridge data – used similar method to Feely et al. (1990b) i.e. determining uptake rate per km of ridge segment but using ^{234}Th and P/^{234}Th ratios.
Rudnicki & Elderfield (1993)	1.1	Same principle as this study but using TAG data only for available Fe estimate and P/Fe ratio.
Feely et al. (1990b)	0.4	Based on Juan de Fuca Ridge data – used flux of hydrothermal suspended matter from ridge crest with its P and Fe content to determine an uptake rate per km of ridge segment – then multiplied by estimated length of active venting sites.
	Global V removal flux (10^{8} mol/yr)	**Notes**
This study	9.5	Based on V/Fe ratio of 0.0034 (see text for further details)
Rudnicki & Elderfield (1993)	4.3	As for P, i.e. same method as this study but using TAG data as basis.
Trefry & Metz (1989)	1.4	Same method as this study but with different values as best estimated of Fe flux and V/Fe ratios

Table 25. Global P and V hydrothermal removal flux estimates.
Compare to riverine flux of these elements which are 3-10 x 10^{10}mol/yr for P (Delaney, 1998) and 5.0 x 10^{8}mol/yr for V (Trefry & Metz, 1989), hence the hydrothermal removal fluxes represent a significant fraction of the riverine input.

The rare earth elements are also subject to removal to the sediments via scavenging by the FeOOH particles, however unlike P and V the REE/Fe ratios are highly variable within each plume. Hence although a maximum removal rate could be estimated using the highest REE/Fe ratios this would not be a significant improvement on the estimate of Rudnicki & Elderfield (1993) where they constructed a scavenging model from TAG data and estimated scavenging constants for the REEs.

For the other elements discussed in this study, Cu, Zn and Mn, there is limited information which can be extracted from the new data in this study to enable better

estimates than those in existing literature. This is because the main dependencies for estimates of the hydrothermal fluxes are the vent fluid concentrations and the global water flux.

5.3.6 Summary

While much of the data obtained for the particulate (>0.4µm) Niskin samples relates predominantly to particles that will have formed in the Niskin bottle during the elapsed time from bottle firing to sample filtration, the samples are comparable to those that would have formed during the same time period (~2.5hrs) during gentle dispersion in the non-turbulent non-buoyant plumes at Kairei and Edmond. Direct evidence for this is seen in the P/Fe ratios which are consistent with the ratios in the SAP (>1.0µm) samples. Hence the Niskin samples can be confidently interpreted as being representative of processes active within these non-buoyant hydrothermal plumes.

The patterns of behaviour observed for P and Cu with respect to Fe for the >0.4µm particulate fraction in the Kairei and Edmond hydrothermal plumes are consistent with those observed for the >1.0µm SAPs samples described in Chapter 4. The samples have unusually high concentrations of particulate Ca and Mg but this does not appear to impact the behaviour of the other elements which are in agreement with previous studies of hydrothermal plume particle behaviour.

The distribution of the trace elements, Mn, Cu and P between the different size fractions in the Edmond hydrothermal plume generally follows what would be predicted from the observations of the particulate phases providing supporting evidence for the proposed models of behaviour of these elements, i.e. the persistence of Mn in the dissolved/colloidal phase even at high plume dilution, the loss of buoyant plume formed Cu sulfides as the plume is diluted and the adsorption/co-precipitation of P in association with the early forming Fe-oxyhydroxides.

The consistency of the P/Fe relationship between the size fractions and the fact that the P/Fe and V/Fe ratios are, as predicted, intermediate to those in the Pacific and Atlantic

Oceans are positive results in light of their suggested use as paleo-proxies for dissolved phosphate concentrations, assuming that these ratios are preserved in the sediments. However more detailed investigation is required of both the exact nature of the inter-relationship and inter-dependency between dissolved phosphate, P/Fe and V/Fe ratios (which can be best achieved through investigation of further hydrothermal plumes situated in ocean waters with dissolved phosphate intermediate between Central Indian Ocean and North Atlantic water, e.g. the southern mid-Atlantic Ridge) and the preservation of these ratios once the hydrothermal plume particles have been deposited in the sediments is required (which is best achieved through the analysis of cores from sites that have remained oxic and have been predominantly hydrothermally influenced).

6 Chapter 6 Conclusions and Future Work

6.1 Conclusions

The main questions that this first study of hydrothermal plumes in the Indian Ocean set out to address were:

1. Does the Fe (II) oxidation rate in the Indian Ocean affect the fundamental processes taking place within the plume or do we see the same patterns of behaviour previously observed in Atlantic and Pacific hydrothermal plumes?
2. Can we elucidate the processes occurring in the plume from the complementary particulate, colloidal and dissolved fraction data?
3. Does the linear relationship for P/Fe and V/Fe versus ambient dissolved phosphate hold true in the Indian Ocean so that they still have potential as paleo-proxies for past seawater phosphate concentrations?

The Fe (II) oxidation rate in the Indian Ocean, with a half-life of 2.3hrs is intermediate to that of the Atlantic and Pacific Oceans. This does have an effect on the concentration of particulate Fe present in the collected samples; the SAP (>1.0μm) samples which were collected *in situ* have much lower concentrations of particulate Fe than observed in Atlantic Ocean hydrothermal plume samples also collected using SAPs and >1.0μm filters. Although the measured particulate Fe concentrations in the Niskin (>0.4μm) samples are higher, the *in situ* concentrations calculated using the Fe (II) oxidation rate suggest there is very little particulate Fe in the early non-buoyant plume (as inferred from the dissolved Mn measurements) consistent with a slower Fe (II) oxidation rate than for the Atlantic Ocean. Conversely the dissolved Fe concentrations measured are higher than those in similar samples from Atlantic hydrothermal plumes.

The measurement of complementary dissolved and particulate Fe and Mn in the samples has allowed a more accurate estimate of the loss of Fe (II) from the plume than was previously possible in studies where just one phase was measured. Loss of Fe (II) initially occurs due to the formation and subsequent settling of Fe sulfides. At both the Kairei and Edmond sites the estimated loss due to sulfide formation is ~20-30%, lower

than previous estimates of ~50% based on the particulate phase alone. Further loss of Fe (II) then occurs via oxidation and formation of Fe-oxyhydroxide particles. Knowing the Fe (II) oxidation rate has made it possible to ascertain that there was most likely very little or no *in situ* particulate Fe in samples collected in close proximity to the vent sources. However we are still able to estimate that ~2.5hrs beyond the time the samples were collected, that the loss of dissolved Fe (II) due to oxidation equates to a further 20-40% of the total Fe (II) which emerged from the vent.

Although the Fe (II) oxidation rate in the Indian Ocean does affect the concentrations of particulate and dissolved Fe found within samples of similar age compared to those from different oceans, apparently it does not fundamentally affect the particle formation processes which have previously been observed in hydrothermal plumes in other oceans. The chalcophile elements are known to precipitate as poly-metallic sulfides in the early stages of the buoyant plume, and these sulfides subsequently settle out of the plume, or may return to solution via oxidative dissolution. Consequently a positive correlation between particulate Fe and the particulate chalcophile elements in hydrothermal plume samples, but with negative curvature due to the loss of the chalcophile elements relative to particulate Fe, has been observed in Atlantic hydrothermal plumes. At Kairei and Edmond the relationships of particulate Zn and Cd with that of particulate Fe in the hydrothermal plumes also show negative curvature, consistent with these previous observations. Particulate copper at the Edmond site also exhibits this trend and additional measurements of Cu and Fe in the dissolved, colloidal, fine particulate and coarse particulate fractions have allowed us to confirm that Cu resides predominantly in the coarse particulate phase. Measurements of these fractions also suggest that if oxidative dissolution of the sulfides is taking place, then it does not have a significant impact on the Cu chemistry within the plume. In contrast to Zn and Cd, particulate Pb exhibits a positive correlation with particulate Fe but with no clear trend at either Kairei or Edmond. This is not surprising as Pb is known to be a particle reactive element, and hence it is likely to be involved in scavenging reactions with the Fe-oxyhydroxide particles. Once again these Indian Ocean results are consistent with previous observations in the Atlantic Ocean and, as the chalcophile element behaviour is dominated by poly-metallic sulfide precipitation which is independent of Fe (II)

oxidation kinetics, the behaviour therefore appears to be unaffected by the differing Fe (II) oxidation rates.

Particle reactive elements such as the rare earth elements and yttrium are known to be involved in scavenging reactions with the Fe-oxyhydroxide particles. They exhibit a positive correlation with particulate Fe, which has positive curvature, indicating the uptake of the REEs and Y relative to particulate Fe. This behaviour has previously been observed in Atlantic and Pacific hydrothermal plumes and is also seen here in the Indian Ocean at both the Kairei and Edmond sites. Hence the differing Fe (II) oxidation rates do not have an influence on the scavenging reactions which occur.

The particulate oxyanion species such as P, V and As have been shown to exhibit linear correlations with particulate Fe in both Atlantic and Pacific hydrothermal plumes. A strong linear relationship is also apparent in both the Kairei and Edmond hydrothermal plume samples which suggests that the interaction of the oxyanion species with the Fe-oxyhydroxide particles is also unaffected by the Fe (II) oxidation rate. The measurement of phosphorus and iron in the colloidal, fine particulate and coarse particulate fractions gives a further insight into this relationship; the same tight linear relationship is observed in all the fractions. This implies that the P/Fe ratio in the particles is set on formation of the colloidal Fe (III) and that no further uptake of phosphorus occurs as the colloids aggregate to form larger particles.

Comparison of the P/Fe ratios of the hydrothermal plume particles with ambient dissolved phosphate in the Indian Ocean, in conjunction with similar data from the Atlantic and Pacific suggests that it is the ambient dissolved phosphate concentration which controls the P/Fe ratio in the colloids; where the ambient dissolved phosphate is higher, the P/Fe ratio is higher. Likewise the V/Fe ratios also have a dependency on the ambient dissolved phosphate, however this is an inverse correlation; higher dissolved phosphate results in a lower V/Fe ratio. The Indian Ocean has ambient dissolved deep water phosphate concentrations which are intermediate to that of the Atlantic and Pacific Oceans and the P/Fe and V/Fe ratios are also intermediate to those found in Atlantic and Pacific hydrothermal plumes. This is positive news in light of their potential use a paleo-proxies for past seawater phosphate concentrations. However it is not clear from the new

data obtained in this study whether the relationship between the ratios and dissolved phosphate is strictly linear or more complex relationship applies. The validity of using P/Fe ratios in hydrothermal sediments as paleo-proxies will also critically depend on possible diagenetic changes in the sediment core.

6.2 Future work

The collection of samples using Niskin bottles mounted on a CTD rosette, which are then later processed back on board ship and analysed in the laboratory, as well as the use of stand alone pumps (SAPs) to carry out *in situ* filtration to provide particulate samples for subsequent processing, has provided significant advances in our understanding of processes in hydrothermal plumes. However, if we are to further advance our understanding of these processes, it would be advantageous to focus on gathering further *in situ* measurements. Take, for example, the calculation of *in situ* particulate Fe. There are uncertainties in back-calculating the *in situ* concentrations; e.g. making sure the elapsed time from the firing of the Niskin bottle to the processing of the samples is recorded accurately, as well as determining an accurate Fe (II) oxidation half-life. The differences in calculated and experimental values for the Fe (II) oxidation rates, both in this study and others, show that ideally this would need to be done experimentally for each individual plume, at least until the reasons for the discrepancy between the two values are fully understood. Even then, it is apparent that there are other factors affecting the Fe (II) oxidation kinetics (not strictly first order) which mean determining the Fe (II) oxidation half time experimentally is not straightforward.

Although direct *in situ* particulate concentration measurements (i.e. rather than, for example, correlations with nephelometry data) may not be feasible in the immediate future, combining *in situ* dissolved measurements with the types of measurements made in this study would still provide further insights into the plume processes. *In situ* analysers for dissolved Fe and Mn are available and have been proven for use in hydrothermal plume research. Detection limits of these systems are continuously improving, thus enabling the mapping of plumes to greater distances from their source.

This does not mean that the collection of samples for subsequent processing either on board ship or later in the laboratory is redundant, in fact there is information that can only be gained in this way, such as the mineralogy of the hydrothermal plume particles. This is crucial to fully understanding, for example, the processes of Fe removal and equilibration within hydrothermal plumes which is fundamental to predicting the potential of hydrothermal Fe as a source of Fe to the oceans. A study of the mineralogy of the samples using for example, Scanning Electron Microscopy (SEM) or thin film x-ray diffraction (XRD), in conjunction with the elemental analyses such as those made in this study would allow us an even greater understanding of the particle processes in the plume. We already know that poly-metallic sulfides are formed early in the buoyant plume and subsequently settle out of the plume or undergo oxidative dissolution. However we assume that some of these sulfides reach the non-buoyant plume as we find elevated (compared to background) concentrations of, for example, Cu and Zn in hydrothermal plume particles. Mineralogy studies would give us an indication of how far these sulfides (including the Fe-sulfides) persist in the non-buoyant plume. This may be important as the oxidation of Fe-sulfides could be an '*in situ*' source of dissolved Fe (II) and we currently know nothing about the rates of sulfide oxidation within plumes. There is also the possibility that some of the chalcophile elements are involved in scavenging reactions with the Fe-oxyhydroxide particles, and examination of the mineralogy would confirm if, for example, Cd is found in association with the Fe-oxyhydroxide particles. Studying the mineralogy of the samples would also provide information on the particle size spectrum in hydrothermal plumes. This is important to help us understand the formation of larger particles which eventually settle out, leading to the loss of elements from the plume and deposition into underlying sediments.

In addition to improved sampling and measurements that could be employed in the future, there are also new locations for future hydrothermal research to be considered. Determining the exact relationship between P/Fe and V/Fe ratios in hydrothermal plumes and ambient dissolved phosphate (linear or more complex) requires data from sites which have dissolved ambient phosphate concentrations intermediate to that of the Indian Ocean and the North Atlantic, the most suitable being the southern Mid-Atlantic ridge around 34-42°S, an area as yet unexplored in terms of hydrothermal activity.

Appendix 1 Analytical data for ICP/AES and ICP/MS measurements

For ICP/AES and ICP/MS measurements the limits of detection are calculated from 3 x standard deviation of the blank measurements. External precision is calculated from the relative standard deviation of repeated measurements of a standard. For the ICP/MS measurements, internal precision is calculated from the 4 replicate measurements of each sample. Accuracy is calculated from comparison with a reference standard.

	External Precision (%)	Limit of detection (µg/l)
Mg	0.7	1.3
Al	1.0	0.8
P	1.0	14.3
Ca	0.8	13.3
V	1.9	1.1
Mn	0.9	0.9
Fe	1.0	2.7
Cu	0.6	2.1
Zn	1.1	8.6
As	9.7	8.9
Y	1.9	0.0

Analytical performance of ICP/AES method for measurement of trace metals in stand alone pump (>1.0µm) hydrothermal plume particle samples

	External Precision (%)	Limit of detection (µg/l)
Mg	0.8	0.2
Al	4.0	0.3
P	0.8	1.8
Ca	0.6	0.5
Mn	0.8	0.1
Fe	0.6	0.1
Cu	0.8	0.1
Zn	0.8	0.3

Analytical performance of ICP/AES method for measurement of trace metals in Niskin bottle (>0.4µm) hydrothermal plume particle samples

	Limit of detection (ng/l except Pb, µg/l)	Internal precision (%)	External precision (%)	Accuracy (%)
La	5.5	2.2	8.3	7.2
Ce	9.0	3.4	8.5	4.8
Pr	2.2	2.5	3.8	4.8
Nd	5.0	2.6	5.0	5.1
Sm	1.7	2.8	3.6	2.3
Eu	0.7	3.1	4.3	6.5
Gd	1.3	2.3	4.8	4.4
Tb	0.2	3.7	4.1	4.0
Dy	1.3	3.1	3.9	5.7
Ho	0.2	3.1	5.7	5.0
Er	0.4	3.7	3.2	7.8
Tm	0.2	4.1	6.5	6.3
Yb	1.1	3.4	6.1	6.7
Lu	0.3	3.9	4.9	6.9
Cd	9.8	12.1		3.1
Pb	0.5	3.1	2.9	1.4

Analytical performance of ICP/MS method for measurement of trace metals in stand alone pump (>1.0µm) hydrothermal plume particle samples

Appendix 2 Dissolved (<0.1µm and <0.4µm) Fe and Mn concentrations

CTD #	Depth (m)	Dissolved (<0.4µm) Fe (nmol/l)	Standard Deviation	Dissolved (<0.4µm) Mn (nmol/l)	Standard Deviation	Dissolved (<0.1µm) Fe (nmol/l)	Standard Deviation	Dissolved (<0.1µm) Mn (nmol/l)	Standard Deviation
			Kairei						
CTD 4	2076	**18.4**	0.9	**1.4**	0.0				
	2175	**31.2**	3.0	**10.0**	1.3				
	2224	**27.8**	2.8	**9.3**	0.1				
	2273	**36.3**	5.4	**9.3**	0.5				
	2322	**26.1**	2.2	**8.0**	0.7				
	2383	**28.4**	1.7	**8.4**	0.5				
CTD 5	2076	**7.5**	0.2	**2.7**	0.2				
	2150	**110**	16.9	**32.1**	3.6				
	2175	**332**	31.2	**123**	4.5				
	2199	**290**	15.1	**77.5**	1.5				
	2224	**368**	12.2	**107**	6.5				
	2248	**302**	2.9	**94.6**	10.4				
	2273	**254**	13.6	**94.3**	4.8				
	2295	**58.8**	2.1	**17.9**	1.2				
	2322	**54.6**	5.1	**18.0**	2.6				
	2347	**19.5**	3.0	**6.3**	0.8				
	2373	**21.3**	5.3	**6.1**	0.3				
	2435	**16.1**	2.3	**6.5**	0.3				

Dissolved Fe and Mn concentrations for Niskin bottle (>0.4µm and >0.1µm) samples. Results are mean of two or three analyses except where no standard deviation is shown, where the result is from one analysis. >0.4µM results are also summarized in Chapter 3 Table 3. >0.1µm results are used in Chapter 5 in discussion of size fractionation in the Edmond hydrothermal plume.

CTD #	Depth (m)	Dissolved (<0.4µm) Fe (nmol/l)	Standard Deviation	Dissolved (<0.4µm) Mn (nmol/l)	Standard Deviation	Dissolved (<0.1µm) Fe (nmol/l)	Standard Deviation	Dissolved (<0.1µm) Mn (nmol/l)	Standard Deviation
			Kairei						
CTD 6	2076	**3.9**	0.1	**1.4**	0.0				
	2174	**7.1**	0.4	**2.5**	0.6				
	2224	**15.1**	1.4	**4.1**	0.4				
	2273	**18.6**	6.4	**4.6**	0.0				
	2321	**41.9**	0.5	**11.7**	0.2				
	2357	**37.5**	3.7	**8.1**	0.0				
CTD 7	2175	**41.8**	0.2	**80.7**	7.4	**199**	8.8	**85.4**	4.1
	2232	**21.5**	0.2	**7.2**	1.2	**32.0**	2.1	**8.9**	0.5
	2268	**75.4**	8.7	**24.1**	0.4	**71.6**	3.8	**20.8**	0.9
	2273	**43.0**	0.2	**11.5**	1.7	**26.6**	0.1	**11.7**	0.4
	2320	**26.2**	6.0	**6.7**	1.1	**20.9**	1.6	**6.8**	1.2
	2322	**50.9**	0.6	**15.2**	0.4	**54.7**	6.5	**17.9**	0.7
	2346	**11.9**	0.6	**5.0**	0.2	**13.5**	3.3	**5.6**	0.9
	2371	**191**	7.4	**63.7**	6.1	**76.9**	12.1	**70.7**	0.6
CTD 10	1978	**8.9**	0.3	**0.7**	0.2				
	2175	**23.1**	2.1	**9.5**	0.6				
	2224	**19.8**	2.3	**2.2**	0.1				
	2273	**28.9**	6.0	**7.0**	1.0				
	2297	**29.9**	0.6	**8.3**	0.5				
	2322	**26.3**	2.1	**7.8**	0.6				
	2347	**26.2**		**7.2**					
	2371	**13.1**	2.8	**4.1**	0.0				

Dissolved Fe and Mn concentrations for Niskin bottle (>0.4µm and >0.1µm) samples (cont.)

CTD #	Depth (m)	Dissolved (<0.4µm) Fe (nmol/l)	Standard Deviation	Dissolved (<0.4µm) Mn (nmol/l)	Standard Deviation	Dissolved (<0.1µm) Fe (nmol/l)	Standard Deviation	Dissolved (<0.1µm) Mn (nmol/l)	Standard Deviation
			Kairei						
CTD 11	2076	**5.0**	0.4	**1.9**	0.3				
	2175	**4.0**	1.2	**1.9**	0.3				
	2224	**3.6**	0.1	**1.6**	0.1				
	2273	**27.2**	24.2	**3.6**	0.8				
	2371	**21.1**	0.8	**6.3**	0.8				
CTD 18	2076	**6.3**	1.0	**1.2**	0.1				
	2272	**15.4**	1.7	**3.5**	0.0				
	2322	**18.4**	4.4	**5.2**	1.4				
	2345	**20.4**	1.1	**6.9**	1.3				
	2371	**9.6**	4.7	**2.6**	0.1				
	2420	**7.2**	0.3	**2.2**	0.0				
CTD 20	1980	**31.3**	1.7	**1.0**	0.2				
	2273	**12.2**	3.7	**2.2**	0.0				
	2298	**77.4**	6.4	**21.9**	1.6				
	2307	**51.3**	9.0	**12.9**	0.3				
	2322	**33.1**	1.5	**8.1**	1.0				
	2347	**20.6**	1.0	**7.9**	0.0				
	2371	**14.9**	7.4	**5.3**	1.7				
	2298	**300**	5.4	**104**	13.7				
	2320	**89.7**	4.1	**23.6**	4.3				
	2372	**52.8**	4.4	**13.8**	0.9				

Dissolved Fe and Mn concentrations for Niskin bottle (>0.4µm and >0.1µm) samples (cont.)

CTD #	Depth (m)	Dissolved (<0.4µm) Fe (nmol/l)	Standard Deviation	Dissolved (<0.4µm) Mn (nmol/l)	Standard Deviation	Dissolved (<0.1µm) Fe (nmol/l)	Standard Deviation	Dissolved (<0.1µm) Mn (nmol/l)	Standard Deviation
			Kairei						
CTD 21	2026	**26.4**	1.2	**1.2**	0.0				
	2120	**310**	9.1	**99.7**	4.0				
	2199	**316**	3.0	**76.6**	3.7				
	2220	**275**	1.3	**94.0**	1.4				
	2273	**291**	5.7	**84.3**	2.4				
	2298	**300**	5.4	**104**	13.7				
	2320	**89.7**	4.1	**23.6**	4.3				
	2372	**52.8**	4.4	**13.8**	0.9				
			Edmond						
CTD 23	2469	**8.5**	2.3	**2.9**	0.1	**9.5**	0.1	**3.2**	0.3
	2781	**321**	7.2	**132**	10.4	**91.4**	17.6	**83.7**	11.6
	2819	**350**	29.0	**55.4**	11.1	**210**	17.9	**54.3**	5.0
	2960	**7.3**	1.6	**2.9**	0.4	**8.9**	0.1	**3.4**	0.2
	3008	**131**	8.4	**56.4**	5.6	**35.7**	5.0	**46.9**	3.6
	3009							**74.6**	8.4
	3019	**130**	2.2	**63.5**	4.5	**28.1**	15.8	**51.8**	0.4
	3057	**174**	20.9	**37.1**	3.0	**58.5**	12.7	**35.6**	1.6
	3107	**161**	1.2	**50.6**	3.1	**35.6**	6.2	**39.9**	2.3
	3156	**50.6**	10.6	**11.3**	0.1	**52.1**	7.0	**11.6**	0.6

Dissolved Fe and Mn concentrations for Niskin bottle (>0.4µm and >0.1µm) samples (cont.)

CTD #	Depth (m)	Dissolved (<0.4µm) Fe (nmol/l)	Standard Deviation	Dissolved (<0.4µm) Mn (nmol/l)	Standard Deviation	Dissolved (<0.1µm) Fe (nmol/l)	Standard Deviation	Dissolved (<0.1µm) Mn (nmol/l)	Standard Deviation
			Background						
CTD 16	1978	**15.1**	0.6	**0.6**	0.2				
	2076	**16.0**		**2.7**	0.4				
	2174	**2.7**	0.5	**1.4**	0.2				
	2273	**14.5**	1.5	**1.7**	0.2				
	2371	**7.4**	0.1	**2.6**	0.7				
	2469	**3.5**	0.8	**2.6**	0.0				
CTD 22	1978	**18.0**	5.6	**1.4**	0.4				
	2076	**5.0**	0.3	**1.4**	0.4				
	2175	**13.9**		**1.7**					
	2273	**7.3**	4.4	**2.2**	0.4				
	2371			**2.5**	0.9				
	2469	**4.7**		**1.7**					

Dissolved Fe and Mn concentrations for Niskin bottle (>0.4µm and >0.1µm) samples (cont.)

Appendix 3 Stand alone pump (>1.0µm) particulate data

	Volume of seawater filtered (litres)	**Fe** mg/l	**Al** mg/l	**Mn** mg/l	**Mg** mg/l	**Ca** mg/l	**P** mg/l	**V** µg/l	**As** µg/l	**Cu** mg/l	**Zn** mg/l	**Y** µg/l
Batch 1												
Kairei												
CTD 2 sap003	1006.2	17.8	0.29	1.62	29.8	37.3	1.42	38.9	5.48	1.17	0.31	4.05
CTD 7 sap001	988.9	42.4	0.42	0.50	77.6	69.9	3.53	80.9	66.3	3.97	0.96	6.00
CTD 17 sap001	741.7	6.07	0.31	0.45	42.3	41.8	0.57	-2.5	16.0	0.13	0.21	2.59
CTD 19 sap001	768.5	16.3	0.51	0.50	32.8	45.6	1.48	32.4	23.0	0.95	0.56	3.80
Edmond												
CTD 23 sap002	600.4	80.5	0.38	0.25	23.8	38.0	6.21	199	134	7.10	5.32	6.17
SAP01 s/n001	728	9.61	0.24	1.97	31.8	37.2	0.87	25.6	-18.4	0.09	0.09	3.24
SAP01 s/n003	740.3	14.0	0.58	13.9	47.0	51.2	1.30	36.7	45.7	0.11	0.18	5.22
SAP02 cosap02	641.1	25.8	0.47	0.65	31.6	44.3	2.00	60.2	69.2	1.90	0.94	4.69
SAP02 cosap04	530.1	13.9	0.50	0.49	17.8	35.1	1.08	38.8	14.1	0.15	0.26	3.83
Blanks												
Dip blank		0.52	0.07	0.41	2.62	0.98	7.47	-0.45	0.18	0.03	0.01	0.02
Blank γ counted		0.20	0.04	0.00	0.01	0.12	4.87	-0.53	0.52	0.00	0.08	0.00
Procedural blank		0.01	0.03	0.00	0.00	0.05	0.88	-0.50	2.21	0.01	0.02	0.00

Particulate concentrations for Stand Alone Pump (>1.0µm) samples: Results of analyses of samples are shown in mg/l or µg/l for comparison with blank measurements. Final results in nmol/l or pmol/l after taking the volume of seawater filtered into account are shown in Chapter 4, Table 11. Samples were processed in two separate batches, each with a set of blanks. Blank correction was done using the filter blanks and procedural blanks, dip blanks were ignored as it is possible to filter a significant quantity of water if the SAPs are pulled through the water too quickly and the high concentrations for the dip blanks suggest this may have been the case

	Volume of seawater filtered (litres)	**Fe** mg/l	**Al** mg/l	**Mn** mg/l	**Mg** mg/l	**Ca** mg/l	**P** mg/l	**V** µg/l	**As** µg/l	**Cu** mg/l	**Zn** mg/l	**Y** µg/l
Batch 2												
Kairei												
CTD 7 sap003	981.5	28.2	0.28	1.64	29.3	40.0	2.04	70.1	52.0	2.76	0.58	4.43
CTD 11 sap003	619.4	11.5	0.26	1.62	45.6	39.5	0.95	36.7	28.0	0.24	0.26	3.21
CTD 18 sap003	802.3	16.7	0.33	0.54	45.5	49.5	1.47	51.3	38.5	0.70	0.14	4.28
CTD 20 sap003	634.3	17.4	0.24	0.39	23.8	35.2	1.43	46.8	42.0	1.42	0.41	2.99
CTD 21 sap001	753.1	116	0.24	0.36	38.9	41.3	7.70	210	174	14.0	4.57	6.53
Edmond												
CTD 01 sap003	2447.0	86.0	0.54	6.03	39.6	41.3	7.47	249	196	2.21	1.60	10.3
CTD 23 sap003	605.8	75.4	0.46	1.06	74.9	51.2	5.68	156	130	6.12	4.07	6.39
SAP01 s/n002	2077.2	27.7	0.75	1.24	35.3	88.1	2.27	90.9	65.3	0.19	0.10	9.39
SAP01 cosap02	537.3	8.58	0.38	1.32	28.4	30.6	0.68	30.2	23.4	0.12	0.08	2.66
SAP01 cosap04	554.6	8.86	0.50	0.60	150	73.1	1.26	31.2	23.7	0.19	0.31	2.56
SAP02 s/n001	654.2	18.7	0.37	2.66	35.5	47.2	1.57	65.4	44.5	0.15	0.12	5.03
SAP02 s/n002	2050.2	43.5	1.01	1.56	30.0	107	3.60	137	99.7	0.29	0.17	12.4
SAP02 s/n003	671.5	47.0	0.47	2.80	55.1	48.5	4.11	138	110	2.00	0.91	6.46
Blanks												
Dip blank		0.65	0.06	1.06	37.5	12.9	0.06	3.52	6.84	0.06	0.12	0.22
Filter out of box		0.09	0.02	0.00	0.06	0.36	0.02	0.99	6.95	0.01	0.06	0.00
Procedural blank		0.01	0.00	0.00	0.01	0.09	0.01	0.25	1.44	0.00	0.02	-0.02

Particulate concentrations for Stand Alone Pump samples (cont.)

Appendix 4 Stand alone pump (>1.0µm) REE particulate data

	Cd ng/g	Pb ng/g	La ng/g	Ce ng/g	Pr ng/g	Nd ng/g	Sm ng/g	Eu ng/g	Gd ng/g	Tb ng/g	Dy ng/g	Ho ng/g	Er ng/g	Tm ng/g	Yb ng/g	Lu ng/g
Kairei																
CTD 2 sap003	0.31	15.6	0.97	1.66	0.23	0.97	0.24	0.07	0.26	0.04	0.24	0.05	0.14	0.02	0.12	0.02
CTD 7 sap001	23.3	28.3	1.63	2.22	0.38	1.79	0.41	0.11	0.48	0.08	0.51	0.11	0.30	0.04	0.24	0.04
CTD 11 sap003	0.17															
CTD 17 sap001	0.12	11.9	0.76	1.90	0.19	0.83	0.17	0.05	0.19	0.03	0.19	0.04	0.10	0.02	0.08	0.01
CTD 18 sap003	0.34	15.8	1.55	2.76	0.36	1.57	0.37	0.09	0.36	0.08	0.39	0.08	0.21	0.03	0.18	0.06
CTD 20 sap003	0.58	7.51	0.81	1.48	0.19	0.85	0.21	0.05	0.21	0.04	0.21	0.05	0.12	0.02	0.11	0.02
CTD 21 sap002	226	65.6	1.94	2.19	0.47	1.75	0.49	0.15	0.51	0.09	0.55	0.09	0.37	0.04	0.27	0.04
Edmond																
CTD 1 sap003	20.1	128	2.64	1.57	0.62	2.71	0.69	0.21	0.78	0.13	0.82	0.16	0.46	0.06	0.37	0.06
CTD 23 sap003	154	99.9	1.79	1.76	0.41	1.82	0.44	0.13	0.48	0.08	0.50	0.10	0.30	0.04	0.25	0.04
SAP01 s/n001	0.15	8.57	0.97	1.44	0.23	1.02	0.24	0.06	0.25	0.04	0.25	0.05	0.15	0.02	0.13	0.02
SAP01 cosap02	0.10	9.56	0.78	1.17	0.20	0.84	0.21	0.05	0.22	0.04	0.22	0.05	0.13	0.02	0.11	0.02
SAP01 cosap04	0.24	6.07	0.90	1.28	0.21	0.92	0.22	0.05	0.22	0.04	0.23	0.05	0.14	0.02	0.12	0.02
SAP02 s/n002	0.22	17.3	4.03	6.07	0.99	4.29	1.04	0.24	1.02	0.17	1.05	0.23	0.62	0.08	0.51	0.08
SAP02 s/n003	25.9	25.2	1.86	1.88	0.44	1.95	0.50	0.13	0.51	0.09	0.55	0.11	0.31	0.04	0.28	0.04
Blanks																
Dip blank	0.07	1.38	0.03	0.033	0.004	0.026	0.009	0.005	0.012	0.002	0.011	0.002	0.007	0.001	0.005	0.001
Filter blank	0.01	1.34	0.01	0.032	0.004	0.012	0.002	0.001	0.001	0.000	0.002	0.000	0.002	0.000	0.001	0.000
Procedural blank	0.00	0.05	0.00	0.001	0.000	0.001	0.002	0.000	0.000	0.000	0.000	0.000	0.000	0.000	0.000	0.000

Cd, Pb and Rare Earth Element particulate concentrations as measured for Stand Alone Pump Samples (i.e. prior to processing to take account of volumes of seawater filtered) so that blank concentrations can be compared. Final results are shown in Chapter 4, Table 12.

Appendix 5 Ce and Eu anomalies in hydrothermal plume particles

	Particulate [Fe] nmol/l	Ce anomaly	Eu anomaly	Er_{sh}/Nd_{sh}
TAG, Atlantic[1]				
TAG:14	56	0.45	1.20	1.33
TAG:18	87	0.34	1.27	1.37
TAG:19	67	0.37	1.26	1.34
TAG:22	192	0.26	1.49	1.47
TAG:32T	212	0.28	1.35	1.32
TAG:32B	49	0.44	1.30	1.17
TAG:35T	133	0.26	1.33	1.40
TAG:35B	45	0.48	1.20	1.30
TAG:39T	150	0.25	1.32	1.47
TAG:39B	38	0.51	1.27	1.26
TAG:43T	124	0.30	1.44	1.39
TAG:43B	17	0.74	1.26	1.17
TAG:53B	167	0.30	1.51	1.43
Rainbow, Atlantic[2]				
SAP01_1	11.0	0.73	1.35	0.93
SAP01_3	10.7	0.73	1.40	0.91
SAP03_1	9.3	0.80	1.49	0.86
SAP03_3	8.1	0.80	1.38	0.93
SAP05_1	279	0.28	1.97	1.34
SAP05_3	421	0.27	2.01	1.37
SAP06_1	26.4	0.52	1.55	1.24
SAP06_3	35.3	0.50	1.47	1.01
SAP07_1	18.0	0.70	1.49	0.99
SAP07_3	8.3	0.78	1.36	0.92
SAP08_1	22.4	0.60	1.34	1.25
SAP08_3	20.9	0.61	1.45	1.04
SAP10_3	7.9	0.84	1.27	1.20
9°45'N EPR Pacific[3]				
2B	24.8	0.38	1.16	1.91
2T	14.0	0.42	1.16	1.82
4B	22.2	0.34	1.17	1.95
4T	25.6	0.35	1.17	1.94
5B	11.3	0.48	1.15	1.72
5T	10.3	0.48	1.16	1.74
6B	13.2	0.47	1.17	1.73
6T	10.8	0.48	1.16	1.74
7B	10.8	0.46	1.16	1.73
7T	12.2	0.49	1.18	1.75
10B	13.6	0.45	1.16	1.77
10T	11.5	0.48	1.16	1.75
11B	19.0	0.42	1.17	1.80
11T	18.0	0.43	1.16	1.80

Ce and Eu anomalies and HREE/LREE enrichment ratios

[1] Data from German et al. 1990

[2] Data from Edmonds and German, 2004

[3] Data from Sherrell et al. 1999

Appendix 6 Niskin bottle (>0.4µm) particulate data

	Fe mg/l	Al µg/l	Mn µg/l	Mg mg/l	Ca mg/l	P µg/l	Cu µg/l	Zn µg/l
15 June batch								
CTD7 2175m 0.1µm	0.71	3.05	0.30	0.31	0.15	67.4	24.8	36.6
CTD7 2232m 0.1µm	0.06	3.19	0.47	1.12	0.35	7.19	2.67	15.5
CTD7 2268m 0.1µm	0.23	5.56	1.19	0.66	0.32	24.4	27.0	34.0
CTD7 2273m 0.1µm	0.11	6.57	0.60	6.45	2.02	11.7	5.66	31.4
CTD7 2320m 0.1µm	0.08	6.95	0.83	0.67	0.28	6.62	3.67	94.5
CTD7 2322m 0.1µm	0.10	4.00	0.39	7.76	1.03	9.38	39.9	26.2
CTD7 2346m 0.1µm	0.06	5.08	0.83	0.72	0.27	9.22	2.98	17.3
CTD7 2371m 0.1µm	0.47	2.89	0.63	2.79	0.85	48.4	13.1	28.0
CTD7 2175m 0.4µm	5.78	12.0	2.36	3.27	1.32	523	226	72.8
CTD7 2232m 0.4µm	0.23	8.95	3.71	2.29	1.01	27.0	8.42	36.8
CTD7 2273m 0.4µm	0.12	6.64	1.58	1.02	0.41	13.9	7.29	22.6
CTD21 2120m 0.4µm	1.23	5.11	0.82	0.74	0.40	105	95.2	49.9
CTD21 2273m 0.4µm	0.66	4.83	0.78	3.29	1.17	57.4	59.6	52.7
CTD21 2298m 0.4µm	1.61	9.89	0.92	1.71	0.70	142	104	46.0
CTD21 2320m 0.4µm	0.30	5.92	1.18	1.41	0.61	30.3	22.1	34.8
CTD21 2372m 0.4µm	0.12	5.80	1.14	1.82	0.72	16.5	9.62	37.7
Filter out of box blank	0.01	4.71	0.11	0.04	0.24	4.24	0.74	32.9
Filter out of box blank	0.01	3.43	0.08	0.04	0.21	0.20	0.65	14.7
Procedural blank	0.00	1.51	0.02	0.00	0.01	2.19	-0.09	4.07
Procedural blank	0.00	0.94	0.01	0.00	0.01	2.75	2.92	6.12
16 July batch								
CTD7 2268m 0.4µm	0.19	5.55	1.46	1.77	0.64	19.6	25.5	26.1
CTD7 2320m 0.4µm	0.08	5.70	1.21	1.76	0.34	8.11	4.26	34.2
CTD7 2346m 0.4µm	0.06	4.92	1.03	2.06	0.30	8.34	2.61	13.8

Particulate concentrations for Niskin bottle (>0.4µm) samples: Results of analyses of samples are shown in mg/l or µg/l for comparison with blanks measurements. Final results in nmol/l or pmol/l are in Chapter 5, Table 16. Samples were processed in three batches. Blank corrections were done using the procedural and acid washed filter blanks.

	Fe mg/l	Al µg/l	Mn µg/l	Mg mg/l	Ca mg/l	P µg/l	Cu µg/l	Zn µg/l
16 July batch (cont)								
CTD7 2471m 0.4µm	0.95	9.46	3.19	1.56	0.76	82.8	40.6	60.2
CTD21 2026m 0.4µm	0.10	9.25	3.54	0.90	0.35	15.7	4.30	79.9
CTD21 2199m 0.4µm	0.55	4.16	0.33	2.87	0.93	42.3	51.6	42.5
CTD21 2220m 0.4µm	0.54	3.77	0.35	0.89	0.42	50.5	32.8	50.2
CTD23 2469m 0.1µm	0.04	3.57	0.86	1.55	0.52	6.69	1.33	15.6
CTD23 2781m 0.1µm	1.65	5.18	0.71	2.31	0.90	170	22.3	64.8
CTD23 2819m 0.1µm	0.85	4.85	0.63	1.67	0.64	86.0	16.7	30.7
CTD23 2960m 0.1µm	0.05	3.04	0.86	1.78	0.60	7.32	3.04	12.6
CTD23 3008m 0.1µm	1.05	3.99	0.75	2.45	0.90	107	14.8	25.2
CTD23 3019m 0.1µm	0.98	2.88	0.56	0.39	0.20	97.0	9.29	23.4
CTD23 3057m 0.1µm	0.49	4.58	0.77	2.56	0.89	50.4	7.19	17.4
CTD23 3107m 0.1µm	0.73	7.00	0.77	0.46	0.21	71.3	8.04	21.5
CTD23 3156m 0.1µm	0.10	8.92	1.19	2.37	0.85	14.9	4.74	20.9
CTD23 2469m 0.4µm	0.07	5.38	1.80	1.01	0.24	13.0	0.80	23.1
CTD23 2781m 0.4µm	2.46	3.58	1.05	4.23	1.41	246	37.6	40.1
CTD23 2819m 0.4µm	0.58	7.50	1.14	2.02	0.74	54.4	25.6	58.4
CTD23 2960m 0.4µm	0.06	5.66	1.61	1.96	0.41	10.6	0.77	43.6
CTD23 3008m 0.4µm	0.99	5.98	0.87	0.73	0.35	98.0	11.8	19.0
CTD23 3019m 0.4µm	1.48	7.44	1.76	0.97	0.54	138	23.6	44.9
CTD23 3057m 0.4µm	0.32	7.82	1.71	0.93	0.46	36.0	8.49	29.7
CTD23 3107m 0.4µm	0.65	7.24	1.51	1.08	0.50	67.3	10.0	32.0
Acid washed filter blank	0.01	3.17	0.08	0.00	0.13	4.02	0.27	98.2
Acid washed filter blank	0.01	1.60	0.07	0.00	0.04	0.52	0.22	32.7
Procedural blank	0.00	1.08	0.03	0.02	0.88	12.1	1.20	12.2

Particulate concentrations for Niskin bottle (>0.4µm) samples (cont.)

	Fe mg/l	**Al** µg/l	**Mn** µg/l	**Mg** mg/l	**Ca** mg/l	**P** µg/l	**Cu** µg/l	**Zn** µg/l
5th Aug Batch								
CTD5 2150m 0.4µm	0.72	7.03	3.12	2.81	1.20	72.3	186	63.8
CTD5 2347m 0.4µm	0.41	11.9	7.47	1.11	0.68	39.8	10.9	44.7
CTD5 2295m 0.4µm	0.71	8.56	3.33	5.18	1.73	66.3	83.0	30.3
CTD5 2224m 0.4µm	8.51	13.4	3.97	18.4	5.19	803	462	189
CTD5 2175m 0.4µm	1.02	4.41	0.87	3.91	1.35	90.9	93.9	44.9
CTD5 2076m 0.4µm	0.18	12.1	5.00	3.47	0.74	25.0	3.11	41.4
CTD5 2435m 0.4µm	0.14	5.19	2.64	0.40	0.18	19.1	4.01	10.6
CTD5 2373m 0.4µm	0.17	7.69	2.82	6.46	2.27	23.8	5.46	25.0
CTD5 2199m 0.4µm	10.9	22.6	8.52	1.48	1.37	1004	605	228
CTD5 2273m 0.4µm	7.68	13.8	5.06	2.08	1.53	721	365	135
Procedural blank	0.00	0.17	0.01	0.00	0.00	0.69	-0.07	2.35
Procedural blank	0.00	0.29	0.00	0.00	0.00	0.09	0.04	4.49

Particulate concentrations for Niskin bottle (>0.4µm) samples (cont.)

References

Aballea, M., Radford-Knoery, J., Appriou, P., Bougault, H., Charlou, J. L., Donval, J. P., Etoubleau, J., Fouquet, Y., German, C. R. & Miranda, M. (1998) Manganese distribution in the water column near the Azores Triple Junction along the Mid-Atlantic Ridge and in the Azores domain. *Deep Sea Res. I* **45**: 1319-1338.

Bach, W., Banerjee, N. R., Dick, H. J. B. & Baker, E. T. (2002) Discovery of ancient and active hydrothermal systems along the ultra-slow spreading Southwest Indian Ridge 10°-16°E. *Geochem. Geophys. Geosystems.* **3**(7): 2001GC000279.

Baker, E. T. & Hammond, S. R. (1992) Hydrothermal venting and the apparent magmatic budget of the Juan de Fuca Ridge. *J. Geophys. Res.* **97**(B3): 3443-3456.

Baker, E. T., German, C. R. & Elderfield, H. (1995). Hydrothermal plumes over spreading center axes: global distributions and geological inferences. In *Seafloor hydrothermal systems: physical, chemical, biological and geological interactions*, Eds., S. E. Humphris, R. A. Zierenberg, L. S. Mullineaux & R. E. Thomson. Am. Geophys. Union, AGU Monograph, **91:** pp47-71.

Baker, E. T., John Chen, Y. & Phipps Morgan, J. (1996) The relationship between near-axis hydrothermal cooling and the spreading rate of mid-ocean ridges. *Earth Planet. Sci. Lett.* **142**: 137-145.

Baker, E. T., Tennant, D. A., Feely, R. A., Lebon, G. T. & Walker, S. L. (2001) Field and laboratory studies on the effect of particle size and composition on optical backscattering measurements in hydrothermal plumes. *Deep Sea Res. I* **48**: 593-604.

Baker, E. T. & German, C. R. (2004). On the global distribution of hydrothermal vent fields. In *Mid Ocean Ridges: Hydrothermal interactions between the lithosphere and oceans*, Eds., C. R. German, J. Lin & L. M. Parson. Am. Geophys. Union, AGU Monograph, **148:** pp245-266.

Balistrieri, L. S. & Murray, J. W. (1982) The adsorption of Cu, Pb, Zn and Cd on goethite from major ion seawater. *Geochim. Cosmochim. Acta* **46**: 1253-1265.

Bau, M. & Dulski, P. (1999) Comparing yttrium and rare earths in hydrothermal fluids from the Mid-Atlantic Ridge: implications for Y and REE behaviour during near-vent mixing and for the Y/Ho ratio of Proterozoic seawater. *Chem. Geol.* **155**: 77-90.

Bender, M., Broecker, W., Gornitz, V., Middel, U., Kay, R., Sun, S. S. & Biscaye, P. (1971) Geochemistry of three cores from the East Pacific Rise. *Earth Planet. Sci. Lett.* **12**: 425-433.

Benjamin, M. M. & Leckie, J. O. (1981) Competitive adsorption of Cd, Cu, Zn, and Pb on amorphous iron oxyhydroxide. *Journal of Colloid and Interface Science* **83**(2): 410-419.

Bertram, C. J. & Elderfield, H. (1993) The geochemical balance of rare earth elements and neodymium isotopes in the oceans. *Geochim. Cosmochim. Acta* **57**: 1957-1986.

Bogdanov, Y. A., Sagatevich, A. M., Chernyayev, Y. S., Ashadze, A. M., Gurvich, Y. G., Lukashin, V. N. & Ivanov, G. V. (1996) Hydrothermal field on the Mid-Atlantic Ridge at latitude 14°45'N. *Transactions (Doklady) of the Russian Academy of Science, Earth Sciences Section* **345**: 167-172.

Bonatti, E. (1975) Metallogenesis at oceanic spreading centers. *Ann. Rev. Earth Planet. Sci.* **3**: 401-431.

Bostrom, K. & Peterson, M. N. A. (1969) The origin of aluminium-poor ferromanganoan sediments in areas of high heat flux on the East Pacific Rise. *Mar. Geol.* **7**: 427-447.

Bostrom, K., Peterson, M. N. A., Joensuu, O. & Fisher, D. E. (1969) Aluminium-poor ferromanganoan sediments on active oceanic ridges. *J. Geophys. Res.* **74**(12): 3261-3270.

Boyle, E. A., Sclater, F. & Edmond, J. M. (1976) On the marine geochemistry of cadmium. *Nature* **263**: 42-44.

Brett, R., Evans, H. T., Gibson, E. K., Hedenquist, J. W., Wandless, M. V. & Sommer, M. A. (1987) Mineralogical studies of sulfide samples and volatile concentrations of basalt glasses from the Southern Juan de Fuca Ridge. *J. Geophys. Res.* **91**(B11): 11373-11379.

Broecker, W. S. & Peng, H. S. (1982). *Tracers in the sea*, Eldigio Press. 690pp

Broecker, W. S., Spencer, D. & Craig, H. (1982). *GEOSECS Pacific Ocean Expedition, Hydrographic Data 1973– 1974*. Washington, D. C., Natl. Sci. Found. 137pp

Bruland, K. W., Franks, R. P., Knauer, G. A. & Martin, J. H. (1979) Sampling and analytical methods for the determination of copper, cadmium, zinc and nickel at the nanogram per liter level in sea water. *Anal. Chim. Acta* **105**: 233-245.

Bruland, K. W. (1980) Oceanographic distributions of cadmium, zinc, nickel, and copper in the North Pacific. *Earth Planet. Sci. Lett.* **47**: 176-198.

Bruland, K. W. (1983). Trace elements in seawater. In *Chemical Oceanography*, Eds., J. P. Riley & R. Chester. Academic Press, London, **8:** pp157-220.

Butterfield, D. A., Seyfried, W. E. & Lilley, M. D. (2003). Composition and evolution of hydrothermal fluids. In *Energy and Mass Transfer in Marine Hydrothermal Systems*, Eds., P. E. Halbach, V. Tunnicliffe & J. R. Hein. Dahlem University Press, Dahlem Workshop Report, **89:** pp123-161.

Byrne, R. H. & Kim, K. H. (1990) Rare earth element scavenging in seawater. *Geochim. Cosmochim. Acta* **54**: 2645-2656.

Cave, R. R., German, C. R., Thomson, J. & Nesbitt, R. W. (2002) Fluxes to sediments underlying the Rainbow hydrothermal plume at 36°14'N on the Mid-Atlantic Ridge. *Geochim. Cosmochim. Acta* **66**(11): 1905-1923.

Charlou, J. L., Fouquet, Y., Donval, J. P., Auzende, J. M., Jean-Baptiste, P., Stievenard, M. & Michel, S. (1996) Mineral and gas chemistry of hydrothermal fluids on an ultrafast spreading ridge: East Pacific Rise, 17° to 19°S (Naudur Cruise, 1993) phase separation processes controlled by volcanic and tectonic activity. *J. Geophys. Res.* **101**(B7): 15899-15919.

Charlou, J. L., Donval, J. P., Fouquet, Y., Jean-Baptiste, P. & Holm, N. (2002) Geochemistry of high H_2 and CH_4 vent fluids issuing from ultramafic rocks at the Rainbow hydrothermal field (36°14'N, MAR). *Chem. Geol.* **191**: 345-359.

Chester, R., Sharples, E. J. & Murphy, K. J. T. (1984) The distribution of particulate Mo in the Atlantic aerosol. *Oceanol. Acta* **7**: 441-50.

Chester, R., Berry, A. S. & Murphy, K. J. T. (1991) The distributions of particulate atmospheric trace metals and mineral aerosols over the Indian Ocean. *Mar. Chem.* **34**: 261-290.

Chin, C. S., Coale, K. H., Elrod, V. A., Johnson, K. S., Massoth, G. J. & Baker, E. T. (1994) In situ observations of dissolved iron and manganese in hydrothermal vent plumes, Juan de Fuca Ridge. *J. Geophys. Res.* **99**: 4969-4984.

Chin, C. S., Klinkhammer, G. P. & Wilson, C. (1998) Detection of hydrothermal plumes on the northern Mid-Atlantic Ridge: results from optical measurements. *Earth Planet. Sci. Lett.* **162**: 1-13.

Christophi, C. A. & Axe, L. (2000) Competition of Cd, Cu, and Pb adsorption on goethite. *Journal of Environmental Engineering-Asce* **126**(1): 66-74.

Clarke, W. B., Beg, M. A. & Craig, H. (1969) Excess ^{3}He in the sea: Evidence for terrestrial primordial helium. *Earth Planet. Sci. Lett.* **6**: 213-217.

CLIVAR & Carbon Hydrographic Data Office, viewed January 2005. http://whpo.ucsd.edu.

Connelly, D. P., Prien, R. D., German, C. R. & Statham, P. J. (2005). Development of a multi-platform in situ analyser for dissolved iron and manganese. *EGU General Assembly, Vienna, 24-29 April 2005. Abstracts.*, EGU05-A-01655.

Corliss, J. B. (1971) The origin of metal-bearing submarine hydrothermal solutions. *J. Geophys. Res.* **76**(33): 8128-8138.

Corliss, J. B., Dymond, J., Gordon, L. I., Edmond, J. M., von Herzen, R. P., Ballard, R. D., Green, K., Williams, D., Bainbridge, A., Crane, K. & van Andel, T. H. (1979) Submarine thermal springs on the Galapagos Rift. *Science* **203**: 1073-1082.

Cowen, J. P., Massoth, G. J. & Baker, E. T. (1986) Bacterial scavenging of Mn and Fe in a mid- to far-field hydrothermal particle plume. *Nature* **322**: 169-171.

Cowen, J. P., Massoth, G. J. & Feely, R. A. (1990) Scavenging rates of dissolved manganese in a hydrothermal plume. *Deep Sea Res.* **37**(10): 1619-1637.

Cowen, J. P. & German, C. R. (2001). Biogeochemical cycling in hydrothermal plumes. In *Energy and mass transfer in marine hydrothermal systems*.

Craig, H., Clarke, W. B. & Beg, M. A. (1975) Excess ^{3}He in deep water on the East Pacific Rise. *Earth Planet. Sci. Lett.* **26**: 125-132.

Danielsson, L. G., Magnusson, B. & Westerlund, S. (1978) An improved metal extraction procedure for the determination of trace metals in sea water by atomic absorption spectrometry with electrothermal atomization. *Anal. Chim. Acta* **98**: 47-57.

de Baar, H. J. W., Bacon, M. P. & Brewer, P. G. (1983) Rare-earth distributions with a positive Ce anomaly in the Western North Atlantic Ocean. *Nature* **301**: 324-327.

de Baar, H. J. W., Bacon, M. P., Brewer, P. G. & Bruland, K. W. (1985a) Rare earth elements in the Pacific and Atlantic Oceans. *Geochim. Cosmochim. Acta* **49**: 1943-1959.

de Baar, H. J. W., Brewer, P. G. & Bacon, M. P. (1985b) Anomalies in rare earth distributions in seawater: Gd and Tb. *Geochim. Cosmochim. Acta* **49**: 1961-1963.

Degens, E. T. & Ross, D. A. (1969). *Hot Brines and Recent Heavy Metal Deposits in the Red Sea*. New York, Springer. 600pp

Delaney, M. L. (1998) Phosphorus accumulation in marine sediments and the oceanic phosphorus cycle. *Global Biogeochem. Cycles* **12**(4): 563-572.

DeMets, C., Gordon, R. G., Argus, D. F. & Stein, S. (1990) Current plate motions. *Geophys. J. Int.* **101**: 425-478.

Douville, E., Bienvenu, P., Charlou, J. L., Donval, J. P., Fouquet, Y., Appriou, P. & Gamo, T. (1999) Yttrium and rare earth elements in fluids from various deep-sea hydrothermal systems. *Geochim. Cosmochim. Acta* **63**(5): 627-643.

Douville, E., Charlou, J. L., Oelkers, E. H., Bienvenu, P., Jove Colon, C. F., Donval, J. P., Fouquet, Y., Prieur, D. & Appriou, P. (2002) The Rainbow vent fluids (36°14'N, MAR): the influence of ultramafic rocks and phase separation on trace metal content in Mid-Atlantic Ridge hydrothermal fluids. *Chem. Geol.* **184**: 37-48.

Drever, J. I. (1974). The magnesium problem. In *The Sea*, Ed., E. D. Goldberg. Wiley-Interscience, **5:** pp337-357.

Dunk, R. M. & Mills, R. A. (2004) Diagenetic alteration of hydrothermal plume precipitates: transition metal and oxyanion associations. *EOS: Trans AGU* **85**(47): F1082.

Dymond, J., Corliss, J. B., Heath, G. R., Field, C. W., Dasch, E. J. & Veeh, H. H. (1973) Origin of metalliferous sediments from the Pacific Ocean. *Geol. Soc. Am. Bull.* **84**: 3355-3372.

Dymond, J. & Roth, S. (1988) Plume dispersed hydrothermal particles: A time-series record of settling flux from the Endeavour Ridge using moored sensors. *Geochim. Cosmochim. Acta* **52**: 2525-2536.

Edmond, J. M., Measures, C., McDuff, R. E., Chan, L. H., Collier, R. & Grant, B. (1979) Ridge crest hydrothermal activity and the balances of the major and minor elements in the ocean: the Galapagos data. *Earth Planet. Sci. Lett.* **46**: 1-18.

Edmond, J. M., Von Damm, K. L., McDuff, R. E. & Measures, C. I. (1982) Chemistry of hot springs on the East Pacific Rise and their effluent dispersal. *Nature* **297**: 187-191.

Edmond, J. M., Campbell, A. C., Palmer, M. R., Klinkhammer, G. P., German, C. R., Edmonds, H. N., Elderfield, H., Thompson, G. & Rona, P. A. (1995). Time series studies of vent fluids from the TAG and MARK sites (1986, 1990) Mid-Atlantic Ridge: a new solution chemistry model and a mechanism for Cu/Zn zonation in massive sulphide orebodies. In *Hydrothermal Vents and Processes*, Eds., L. M. Parson, C. L. Walker & D. R. Dixon. Geological Society, London, Special Publication, **87:** pp77-86.

Edmonds, H. N., German, C. R., Green, D. R. H., Huh, Y., Gamo, T. & Edmond, J. M. (1996) Continuation of the hydrothermal fluid chemistry time series at TAG, and the effects of ODP drilling. *Geophys. Res. Lett.* **23**(23): 3487-3489.

Edmonds, H. N. & German, C. R. (2004) Particle geochemistry in the Rainbow hydrothermal plume, Mid-Atlantic Ridge. *Geochim. Cosmochim. Acta* **68**(4): 759-772.

Elderfield, H. & Greaves, M. J. (1982) The rare earth elements in seawater. *Nature* **296**: 214-219.

Elderfield, H. (1988) The oceanic chemistry of the rare-earth elements. *Phil. Trans. R. Soc. Lond. A* **325**: 105-126.

Elderfield, H. & Schultz, A. (1996) Mid-ocean ridge hydrothermal fluxes and the chemical composition of the ocean. *Ann. Rev. Earth Planet. Sci.* **24**: 191-224.

Feely, R. A., Lewison, M., Massoth, G. J., Robert-Baldo, G., Lavelle, J. W., Byrne, R. H., Von Damm, K. L. & Curl, H. C. (1987) Composition and dissolution of black smoker particulates from active vents on the Juan de Fuca Ridge. *J. Geophys. Res.* **92**(B11): 11347-11363.

Feely, R. A., Geiselman, T. L., Baker, E., Massoth, G. J. & Hammond, S. R. (1990a) Distribution and composition of hydrothermal plume particles from the ASHES vent field at Axial Volcano, Juan de Fuca Ridge. *J. Geophys. Res.* **95**(B8): 12855-12873.

Feely, R. A., Massoth, G. J., Baker, E. T., Cowen, J. P., Lamb, M. F. & Krogslund, K. A. (1990b) The effect of hydrothermal processes on midwater phosphorus distributions in the northeast Pacific. *Earth Planet. Sci. Lett.* **96**: 305-318.

Feely, R. A., Trefry, J. H., Massoth, G. J. & Metz, S. (1991) A comparison of the scavenging of phosphorus and arsenic from seawater by hydrothermal iron oxyhydroxides in the Atlantic and Pacific Oceans. *Deep Sea Res.* **38**(6): 617-623.

Feely, R. A., Massoth, G. J., Baker, E. T., Lebon, G. T. & Geiselman, T. L. (1992) Tracking the dispersal of hydrothermal plumes from the Juan de Fuca Ridge using suspended matter compositions. *J. Geophys. Res.* **97**: 3457-3468.

Feely, R. A., Gendron, J. F., Baker, E. T. & Lebon, G. T. (1994a) Hydrothermal plumes along the East Pacific Rise, 8°40' to 11°50'N: particle distribution and composition. *Earth Planet. Sci. Lett.* **128**: 19-36.

Feely, R. A., Massoth, G. J., Trefry, J. H., Baker, E. T., Paulson, A. J. & Lebon, G. T. (1994b) Composition and sedimentation of hydrothermal plume particles from North Cleft segment, Juan de Fuca Ridge. *J. Geophys. Res.* **99**: 4985-5006.

Feely, R. A., Baker, E. T., Marumo, K., Urabe, T., Ishibashi, J., Gendron, J. F., Lebon, G. T. & Okamura, K. (1996) Hydrothermal plume particles and dissolved phosphate over the superfast-spreading southern East Pacific Rise. *Geochim. Cosmochim. Acta* **60**(13): 2297-2323.

Feely, R. A., Trefry, J. H., Lebon, G. T. & German, C. R. (1998) The relationship between P/Fe and V/Fe ratios in hydrothermal precipitates and dissolved phosphate in seawater. *Geophys. Res. Lett.* **25**(13): 2253-2256.

Field, M. P. & Sherrell, R. M. (2000) Dissolved and particulate Fe in a hydrothermal plume at 9°45'N, East Pacific Rise: slow Fe (II) oxidation kinetics in Pacific plumes. *Geochim. Cosmochim. Acta* **64**(4): 619-628.

Fillippelli, G. M. & Delaney, M. L. (1996) Phosphorus geochemistry of equatorial Pacific sediments. *Geochim. Cosmochim. Acta* **60**(9): 1479-1495.

Froelich, P. N., Bender, M. L. & Heath, G. R. (1977) Phosphorus accumulation rates in metalliferous sediments on the East Pacific Rise. *Earth Planet. Sci. Lett.* **34**: 351-359.

Gallant, R. M. & Von Damm, K. L. (2006) Geochemical controls on hydrothermal fluids from the Kairei and Edmond Vent Fields, 23-25°S, Central Indian Ridge. *Geochem. Geophys. Geosystems.* **7**(6): 2005GC001067.

Gamo, T., Nakayama, E., Shitashima, K., Isshiki, K., Obata, H., Okamura, K., Kanayama, S., Oomori, T., Koizumi, T., Matsumoto, S. & Hasumoto, H. (1996) Hydrothermal plumes at the Rodriguez triple junction, Indian ridge. *Earth Planet. Sci. Lett.* **142**: 261-270.

Gamo, T., Chiba, H., Yamanaka, T., Okudaira, T., Hashimoto, J., Tsuchida, S., Ishibashi, J., Kataoka, S., Tsunogai, U., Okamura, K., Sano, Y. & Shinjo, R. (2001) Chemical characteristics of newly discovered black-smoker fluids and associated hydrothermal plumes at the Rodriguez Triple Junction, Central Indian Ridge. *Earth Planet. Sci. Lett.* **193**: 371-379.

Gendron, J. F., Todd, J. F., Feely, R. A., Baker, E. T. & Kadko, D. C. (1994) Excess ^{222}Rn above Cleft segment of the Juan de Fuca Ridge. *J. Geophys. Res.* **99**(B3): 5007-5015.

German, C. R. & Elderfield, H. (1990) Rare earth elements in the NW Indian Ocean. *Geochim. Cosmochim. Acta* **54**: 1929-1940.

German, C. R., Klinkhammer, G. P., Edmond, J. M., Mitra, A. & Elderfield, H. (1990) Hydrothermal scavenging of rare-earth elements in the ocean. *Nature* **345**: 516-518.

German, C. R., Campbell, A. C. & Edmond, J. M. (1991a) Hydrothermal scavenging at the Mid-Atlantic Ridge: modification of trace element dissolved fluxes. *Earth Planet. Sci. Lett.* **107**: 101-114.

German, C. R., Fleer, A. P., Bacon, M. P. & Edmond, J. M. (1991b) Hydrothermal scavenging at the Mid-Atlantic Ridge: radionuclide distributions. *Earth Planet. Sci. Lett.* **105**: 170-181.

German, C. R. & Sparks, R. S. J. (1993) Particle recycling in the TAG hydrothermal plume. *Earth Planet. Sci. Lett.* **116**: 129-134.

German, C. R., Bourles, D. L., Brown, E. T., Hergt, J., Colley, S., Higgs, N. C., Ludford, E. M., Nelson, T. A., Feely, R. A., Raisbeck, G. & Yiou, F. (1997) Hydrothermal scavenging on the Juan de Fuca Ridge: $^{230}Th_{xs}$, ^{10}Be, and REEs in ridge-flank sediments. *Geochim. Cosmochim. Acta* **61**(19): 4067-4078.

German, C. R., Mevel, C. & Tamaki, K. (1998a) Hydrothermal activity along the southwest Indian ridge. *Nature* **395**: 490-493.

German, C. R. & Parson, L. M. (1998) Distributions of hydrothermal activity along the Mid-Atlantic Ridge: interplay of magmatic and tectonic controls. *Earth Planet. Sci. Lett.* **160**: 327-341.

German, C. R., Richards, K. J., Rudnicki, M. D., Lam, M. M. & Charlou, J. L. (1998b) Topographic control of a dispersing hydrothermal plume. *Earth Planet. Sci. Lett.* **156**: 267-273.

German, C. R., Connelly, D. P., Evans, A. J., Murton, B. J., Curewitz, D., Okino, K., Statham, P. J. & Parson, L. M. (2001) Hydrothermal activity along the Central Indian Ridge: Ridges, hotspots and philately. *EOS: Trans AGU (abstr)* **82**(47).

German, C. R., Colley, S., Palmer, M. R., Khripounoff, A. & Klinkhammer, G. P. (2002) Hydrothermal plume-particle fluxes at 13°N on the East Pacific Rise. *Deep Sea Res. I* **49**: 1921-1940.

German, C. R. & Von Damm, K. L. (2004). Hydrothermal Processes. In *Treatise on Geochemistry*, Eds., H. D. Holland & K. K. Turekian. Elsevier, **6**.

German, C. R., Parson, L. M., Murton, B. J., Bennet, S. A., Connelly, D. P., Evans, A. J., Prien, R. D., Ramirez-Llodra, E. Z., Shank, T. M., Yoerger, D. R., Jakuba, M., Bradley, A. M., Baker, E. T. & Nakamura, K. (2005) Hydrothermal activity on the Southern Mid-Atlantic Ridge: Tectonically and volcanically hosted high temperature venting at 2-7°S. *EOS: Trans AGU* **86**(52): Fall Meet. Suppl., Abstract OS21C-04.

Ginoux, P., Prospero, J. M., Torres, O. & Chin, M. (2004) Long-term simulation of global dust distribution with the GOCART model: correlation with North Atlantic Oscillation. *Environmental Modelling & Software* **19**: 113-128.

Godfrey, L. V., Mills, R., Elderfield, H. & Gurvich, E. (1994) Lead behaviour at the TAG hydrothermal vent field 26°N, Mid-Atlantic Ridge. *Mar. Chem.* **46**: 237-254.

Govindaraju, K. (1994) 1994 Compilation of working values and sample description for 383 geostandards. *Geostandards Newsletter* **18**: 1-158.

Green, D. R. H., Cooper, M. J., German, C. R. & Wilson, P. A. (2003) Optimization of an inductively coupled plasma-optical emission spectrometry method for the rapid determination of high-precision Mg/Ca and Sr/Ca in foraminiferal calcite. *Geochem. Geophys. Geosystems.* **4**(6): 2002GC000488.

Hardy, R. G. & Tucker, M. E. (1988). X-ray powder diffraction of sediments. In *Techniques in Sedimentology*, Ed., M. E. Tucker. Blackwell**:** pp394.

Haymon, R. (1983) Growth history of hydrothermal black smoker chimneys. *Nature* **301**: 695-698.

Haymon, R. M. & Kastner, M. (1981) Hot spring deposits on the East Pacific Rise at 21ºN: preliminary description of mineralogy and genesis. *Earth Planet. Sci. Lett.* **53**: 363-381.

Haymon, R. M. & Kastner, M. (1986) Caminite: A new magnesium-hydroxide-sulfate-hydrate mineral found in a submarine hydrothermal deposit, East Pacific Rise 21°N. *Am. Mineral.* **71**: 819-825.

Honeyman, B. D. & Santschi, P. H. (1989) A Brownian-pumping model for trace metal scavenging: evidence from Th isotopes. *J. Mar. Res.* **47**: 951-992.

James, R. H., Elderfield, H., Rudnicki, M. D., German, C. R., Palmer, M. R., Chin, C., Greaves, M. J., Gurvich, E., Klinkhammer, G. P., Ludford, E., Mills, R. A., Thomson, J. & Williams, A. C. (1995). Hydrothermal plumes at Broken Spur, 29°N Mid-Atlantic Ridge: chemical and physical characteristics. In *Hydrothermal Vents and Processes*, Eds., L. M. Parson, C. L. Walker & D. R. Dixon. Geological Society, London, Special Publication, **87:** pp97-110.

James, R. H. & Elderfield, H. (1996) Dissolved and particulate trace metals in hydrothermal plumes at the Mid-Atlantic Ridge. *Geophys. Res. Lett.* **23**(23): 3499-3502.

Jean-Baptiste, P., Mantisi, F., Pauwells, H., Grimaud, D. & Patriat, P. (1992) Hydrothermal ^{3}He and manganese plumes at 19°29'S on the Central Indian Ridge. *Geophys. Res. Lett.* **19**(17): 1787-1790.

Jenkins, W. J., Beg, M. A., Clarke, W. B., Wangersky, P. J. & Craig, H. (1972) Excess ^{3}He in the Atlantic Ocean. *Earth Planet. Sci. Lett.* **16**: 122-126.

Jenkins, W. J. & Clarke, W. B. (1976) Distribution of ^{3}He in the western Atlantic Ocean. *Deep Sea Res. I* **23**: 481-494.

Jenkins, W. J., Edmond, J. M. & Corliss, J. B. (1978) Excess ^{3}He and ^{4}He in Galapagos submarine hydrothermal waters. *Nature* **272**: 156-158.

Johnson, K. S., Gordon, R. M. & Coale, K. H. (1997) What controls dissolved iron concentrations in the world ocean? *Mar. Chem.* **57**: 137-161.

Kadko, D. C., Rosenberg, N. D., Lupton, J. E., Collier, R. W. & Lilley, M. D. (1990) Chemical reaction rates and entrainment within Endeavour Ridge hydrothermal plume. *Earth Planet. Sci. Lett.* **99**: 315-335.

Kadko, D. C. (1993) An assessment of the effect of chemical scavenging within submarine hydrothermal plumes upon ocean geochemistry. *Earth Planet. Sci. Lett.* **120**: 361-374.

Kadko, D. C., Feely, R. A. & Massoth, G. J. (1994) Scavenging of ^{234}Th and phosphorus removal from the hydrothermal effluent plume over the North Cleft segment of the Juan de Fuca Ridge. *J. Geophys. Res.* **99**: 5017-5024.

Kelley, D. S., Karson, J. A., Blackman, D. K., Fruh-Green, G. L., Butterfield, D. A., Lilley, M. D., Olson, E. J., Schrenk, M. O., Roe, K. K., Lebon, G. T. & Rivizzigno, P. (2001) An off-axis hydrothermal vent field near the Mid-Atlantic Ridge at 30°N. *Nature* **412**: 145-149.

Khripounoff, A., Vangriesheim, A., Crassous, P., Segonzac, M., Colaco, A., Desbruyeres, D. & Barthelemy, R. (2001) Particle flux in the Rainbow hydrothermal vent field (Mid Atlantic Ridge): dynamics, mineral and biological composition. *J. Mar. Res.* **59**: 633-656.

King, D. W., Lounsbury, H. A. & Millero, F. J. (1995) Rates and mechanism of Fe (II) oxidation at nanomolar total iron concentrations. *Environ. Sci. Tech.* **29**: 818-824.

Kingston, H. M., Barnes, I. L., Brady, T. J., Rains, T. C. & Champ, M. A. (1978) Separation of eight transition elements from alkali and alkaline earth elements in estuarine and seawater with chelating resin and their determination by graphite furnace atomic absorption spectrometry. *Anal. Chem.* **50**(14): 2064-2070.

Kinrade, J. D. & Van Loon, J. C. (1974) Solvent extraction for use with Flame Atomic Absorption Spectrometry. *Anal. Chem.* **46**(13): 1894-1898.

Klinkhammer, G. P., Rona, P. A., Greaves, M. J. & Elderfield, H. (1985) Hydrothermal manganese plumes in the Mid-Atlantic Ridge rift valley. *Nature* **314**: 727-731.

Klinkhammer, G. P., Elderfield, H., Edmond, J. M. & Mitra, A. (1994) Geochemical implications of rare earth element patterns in hydrothermal fluids from mid-ocean ridges. *Geochim. Cosmochim. Acta* **58**(23): 5105-5113.

Kremling, K., Andreae, M. O., Brugmann, L., Van den Berg, C. M. G., Prange, A., Schirmacher, M., Koroleff, F. & Kuss, J. (1999). Determination of trace elements. In *Methods of seawater analysis*, Eds., K. Grasshoff, K. Kremling & E. M. Wiley-VCH.

Lavelle, J. W., Cowen, J. P. & Massoth, G. J. (1992) A model for the deposition of hydrothermal manganese near ridge crests. *J. Geophys. Res.* **97**: 7413-7427.

Lewis, E. & Wallace, D. W. R. (1998). Program developed for CO_2 system calculations. ORNL/CDIAC-105. Carbon Dioxide Information Analysis Center, Oak Ridge National Laboratory, U.S. Department of Energy, Oak Ridge, Tennessee.

Lilley, M. D., Feely, R. A. & Trefry, J. H. (1995). Chemical and biochemical transformations in hydrothermal plumes. In *Seafloor hydrothermal systems: physical, chemical, biological and geological interactions*, Eds., S. E. Humphris, R. A. Zierenberg, L. S. Mullineaux & R. E. Thomson. Am. Geophys. Union, AGU Monograph, **91:** pp369-391.

Ludford, E. M., Palmer, M. R., German, C. R. & Klinkhammer, G. P. (1996) The geochemistry of Atlantic hydrothermal particles. *Geophys. Res. Lett.* **23**(23): 3503-3506.

Lupton, J. E. & Craig, H. (1975) Excess ^{3}He in oceanic basalts: Evidence for terrestrial primordial helium. *Earth Planet. Sci. Lett.* **26**: 133-139.

Lupton, J. E., Weiss, R. F. & Craig, H. (1977) Mantle helium in Red Sea brines. *Nature* **266**: 244-246.

Lupton, J. E. & Craig, H. (1981) A major helium-3 source at 15°S on the East Pacific Rise. *Science* **214**: 13-18.

Lupton, J. E., Baker, E. T., Mottl, M. J., Sansone, F. J., Wheat, C. G., Resing, J. A., Massoth, G. J., Measures, C. J. & Feely, R. A. (1993) Chemical and physical diversity of hydrothermal plumes along the East Pacific Rise 8°45' to 11°50'N. *Geophys. Res. Lett.* **20**: 2913-2916.

Lupton, J. E. (1995). Hydrothermal plumes: near and far field. In *Seafloor hydrothermal systems: physical, chemical, biological and geological interactions*, Eds., S. E. Humphris, R. A. Zierenberg, L. S. Mullineaux & R. E. Thomson. Am. Geophys. Union, AGU Monograph, **91:** pp317-346.

Lupton, J. E. (2001). Volcanic helium. In *Encyclopedia of Ocean Sciences*, Eds., J. H. Steele, S. A. Thorpe & K. K. Turekian. Academic Press, London**:** pp3166-3173.

Massoth, G. J., Baker, E. T., Lupton, J. E., Feely, R. A., Butterfield, D. A., Von Damm, K. L., Roe, K. K. & Lebon, G. T. (1994) Temporal and spatial variability of hydrothermal manganese and iron at Cleft segment, Juan de Fuca Ridge. *J. Geophys. Res.* **99**: 4905-4923.

Massoth, G. J., Baker, E. T., Feely, R. A., Lupton, J. E., Collier, R. W., Gendron, J. F., Roe, K. K., Maenner, S. M. & Resing, J. A. (1998) Manganese and iron in hydrothermal plumes resulting from the 1996 Gorda Ridge event. *Deep Sea Res. II* **45**: 2683-2712.

Masuzawa, T. (1989) Settling particles with positive Ce anomalies from the Japan Sea. *Geophys. Res. Lett.* **16**(6): 503-506.

McDuff, R. E. (1995). Physical dynamics of deep-sea hydrothermal plumes. In *Seafloor hydrothermal systems: physical, chemical, biological and geological interactions*, Eds., S. E. Humphris, R. A. Zierenberg, L. S. Mullineaux & R. E. Thomson. Am. Geophys. Union, AGU Monograph, **91:** pp357-368.

McLaughlin-West, E. A., Olson, E. J., Lilley, M. D., Resing, J. A., Lupton, J. E., Baker, E. T. & Cowen, J. P. (1999) Variations in hydrothermal methane and hydrogen concentrations following the 1998 eruption at Axial Volcano. *Geophys. Res. Lett.* **26**(23): 3453-3456.

Metz, S., Trefry, J. H. & Nelsen, T. A. (1988) History and geochemistry of a metalliferous sediment core from the Mid-Atlantic Ridge at 26°N. *Geochim. Cosmochim. Acta* **52**: 2369-2378.

Metz, S. & Trefry, J. H. (1993) Field and laboratory studies of metal uptake and release by hydrothermal precipitates. *J. Geophys. Res.* **98**: 9661-9666.

Middelburg, J. J., Hoede, D., Vandersloot, H. A., Vanderweijden, C. H. & Wijkstra, J. (1988) Arsenic, Antimony and Vanadium in the North-Atlantic Ocean. *Geochim. Cosmochim. Acta* **52**(12): 2871-2878.

Millero, F. J., Sotolongo, S. & Izaguirre, M. (1987) The oxidation kinetics of Fe (II) in seawater. *Geochim. Cosmochim. Acta* **51**: 793-801.

Mitra, A., Elderfield, H. & Greaves, M. J. (1994) Rare earth elements in submarine hydrothermal fluids and plumes from the Mid-Atlantic Ridge. *Mar. Chem.* **46**: 217-235.

Moody, J. R. & Lindstrom, R. M. (1977) Selection and cleaning of plastic containers for storage of trace element clean samples. *Anal. Chem.* **49**(14): 2264-2267.

Morley, N. H., Statham, P. J. & Burton, J. D. (1993) Dissolved trace metals in the southwestern Indian Ocean. *Deep Sea Res. I* **40**(5): 1043-1062.

Mortlock, R. A., Froelich, P. N., Feely, R. A., Massoth, G. J., Butterfield, D. A. & Lupton, J. E. (1993) Silica and germanium in Pacific Ocean hydrothermal vents and plumes. *Earth Planet. Sci. Lett.* **119**: 365-378.

Mottl, M. J. (1983) Metabasalts, axial hot springs, and the structure of hydrothermal systems at mid-ocean ridges. *Geol. Soc. Am. Bull.* **94**: 161-180.

Mottl, M. J. & McConachy, T. F. (1990) Chemical processes in buoyant hydrothermal plumes on the East Pacific Rise near 21°N. *Geochim. Cosmochim. Acta* **54**: 1911-1927.

Muller, F. L. L., Burton, J. D. & Statham, P. J. (1991) Long-term changes in the adsorptive properties of FEP separating funnels used in a mixed dithiocarbamate-Freon-TF extraction system. *Anal. Chim. Acta* **245**: 21-25.

Munschy, M. & Schlich, R. (1989) The Rodriguez Triple Junction (Indian Ocean): structure and evolution for the past one million years. *Mar. Geophys. Res.* **11**: 1-14.

Nelsen, T. A., Klinkhammer, G. P., Trefry, J. H. & Trocine, R. P. (1986) Real-time observation of dispersed hydrothermal plumes using nephelometry: examples from the Mid-Atlantic Ridge. *Earth Planet. Sci. Lett.* **81**: 245-252.

Nozaki, Y. (2001). Rare Earth Elements and their isotopes in the ocean. In *Encyclopedia of Ocean Sciences*, Eds., J. H. Steele, S. A. Thorpe & K. K. Turekian. Academic Press, London**:** pp2354-2366.

Obata, H., Karatani, H. & Nakayama, E. (1993) Automated determination of iron in seawater by chelating resin concentration and chemiluminescence detection. *Anal. Chem.* **65**: 1524-1528.

Olivarez, A. M. & Owen, R. M. (1989) REE/Fe variations in hydrothermal sediments: Implications for the REE content of seawater. *Geochim. Cosmochim. Acta* **53**(3): 757-762.

Owen, R. M. & Olivarez, A. M. (1988) Geochemistry of rare earth elements in Pacific hydrothermal sediments. *Mar. Chem.* **25**: 183-196.

Palmer, M. R. & Edmond, J. M. (1989) The strontium isotope budget of the modern ocean. *Earth Planet. Sci. Lett.* **92**: 11-26.

Piper, D. Z. (1973) Origin of metalliferous sediments from the East Pacific Rise. *Earth Planet. Sci. Lett.* **19**: 75-82.

Pluger, W. L., Herzig, P. M., Becker, K. P., Deissmann, G., Schops, D., Lange, J., Jenisch, A., Ladage, S., Richnow, H. H., Schulze, T. & Michaelis, W. (1990) Discovery of hydrothermal fields at the Central Indian Ridge. *Mar. Mining* **9**: 73-86.

Pollard, R. T. & Read, J. F. (2001) Circulation pathways and transports of the Southern Ocean in the vicinity of the Southwest Indian Ridge. *J. Geophys. Res.* **106**(C2): 2881-2898.

Polzin, K. L., Toole, J. M., Ledwell, J. R. & Schmitt, R. W. (1997) Spatial variability of turbulent mixing in the abyssal ocean. *Science* **276**: 93-96.

Price, R. C., Kennedy, A. K., Riggs-Sneeringer, M. & Frey, F. A. (1986) Geochemistry of basalts from the Indian Ocean triple junction: implications for the generation and evolution of Indian Ocean ridge basalts. *Earth Planet. Sci. Lett.* **78**: 379-396.

Prien, R. D., Connelly, D. P. & German, C. R. (2006) A compact in situ Iron (II) and Manganese (II) analyser: Development and first results. *In prep.*

Radford-Knoery, J., German, C. R., Charlou, J. L., Donval, J. P. & Fouquet, Y. (2001) Distribution and behaviour of dissolved hydrogen sulfide in hydrothermal plumes. *Limnol. Oceanogr.* **46**(2): 461-464.

Ramondenc, P., Germanovich, L. N., Von Damm, K. L. & Lowell, R. P. (2006) The first measurements of hydrothermal heat output at 9°50'N, East Pacific Rise. *Earth Planet. Sci. Lett.* **245**: 487-497.

Reichart, G. J., den Dulk, M., Visser, H. J., van der Weijden, C. H. & Zachariasse, W. J. (1997) A 225 kyr record of dust supply, paleoproductivity and the oxygen minimum zone from the Murray Ridge (northern Arabian Sea). *Palaeogeogr. Palaeoclimatol. Palaeoecol.* **134**: 149-169.

Rimstidt, J. D. & Vaughan, D. J. (2003) Pyrite oxidation: A state of the art assessment of the reaction mechanism. *Geochim. Cosmochim. Acta* **67**(5): 873-880.

Rona, P. A. & Trivett, D. A. (1992) Discrete and diffuse heat transfer at ASHES vent field, Axial Volcano, Juan de Fuca Ridge. *Earth Planet. Sci. Lett.* **109**: 57-71.

Rudnicki, M. D. & Elderfield, H. (1992) Helium, radon and manganese at the TAG and Snakepit hydrothermal vent fields, 26° and 23°N, Mid-Atlantic Ridge. *Earth Planet. Sci. Lett.* **113**: 307-321.

Rudnicki, M. D. & Elderfield, H. (1993) A chemical model of the buoyant and neutrally buoyant plumes above the TAG vent field, 26 degrees N, Mid-Atlantic Ridge. *Geochim. Cosmochim. Acta* **57**: 2939-2957.

Rudnicki, M. D., James, R. H. & Elderfield, H. (1994) Near-field variability of the TAG non-buoyant plume, 26°N, Mid-Atlantic Ridge. *Earth Planet. Sci. Lett.* **127**: 1-10.

Rudnicki, M. D. & German, C. R. (2002) Temporal variability of the hydrothermal plume above the Kairei vent field, 25°S, Central Indian Ridge. *Geochem. Geophys. Geosystems.* **3**(2): 2001GC000240.

Saager, P. M., de Baar, H. J. W. & Burkhill, P. H. (1989) Manganese and iron in Indian Ocean waters. *Geochim. Cosmochim. Acta* **53**: 2259-2267.

Santana-Casiano, J. M., Gonzalez-Davila, M., Rodriguez, M. J. & Millero, F. J. (2000) The effect of organic compounds in the oxidation kinetics of Fe(II). *Mar. Chem.* **70**: 211-222.

Savoie, D. L., Prospero, J. M. & Nees, R. T. (1987) Nitrate, non sea-salt sulphate and mineral aerosol over the North Western Indian Ocean. *J. Geophys. Res.* **91**: 933-942.

Schaller, T., Morford, J., Emerson, S. R. & Feely, R. A. (2000) Oxyanions in metalliferous sediments: tracers for paleoseawater metal concentrations. *Geochim. Cosmochim. Acta* **63**(13): 2243-2254.

Scheirer, D. S., Baker, E. T. & Johnson, K. T. M. (1998) Detection of hydrothermal plumes along the Southeast Indian Ridge near the Amsterdam-St Paul Plateau. *Geophys. Res. Lett.* **25**(1): 97-100.

Schultz, A., Delaney, J. R. & McDuff, R. E. (1992) On the partitioning of heat flux between diffuse and point source seafloor venting. *J. Geophys. Res.* **97**(B9): 12299-12314.

Schultz, A. & Elderfield, H. (1997) Controls on the physics and chemistry of seafloor hydrothermal circulation. *Phil. Trans. R. Soc. Lond. A* **355**: 387-425.

Scott, R. B., Rona, P. A. & McGregor, B. A. (1974) The TAG hydrothermal field. *Nature* **251**: 301-302.

Sempere, J. C. & Klein, M. (1995) New insights in crustal accretion expected from Indian Ocean spreading centers. *EOS: Trans AGU* **76**: 113-116.

Severmann, S., Johnson, C. M., Beard, B. L., German, C. R., Edmonds, H. N., Chiba, H. & Green, D. R. H. (2004) The effect of plume processes on the Fe isotope composition of hydrothermally derived Fe in the deep ocean as inferred from the Rainbow vent site, Mid-Atlantic Ridge, 36°14'N. *Earth Planet. Sci. Lett.* **225**: 63-76.

Sherrell, R. M. (1989). The trace metal geochemistry of suspended oceanic particulate matter. Ph.D. thesis, Woods Hole Oceanographic Institute/Massachusetts Institute of Technology, 211pp.

Sherrell, R. M. & Boyle, E. A. (1992) The trace metal composition of suspended particles in the oceanic water column near Bermuda. *Earth Planet. Sci. Lett.* **111**: 155-174.

Sherrell, R. M., Field, M. P. & Ravizza, G. (1999) Uptake and fractionation of rare earth elements on hydrothermal plume particles at 9°45'N, East Pacific Rise. *Geochim. Cosmochim. Acta* **63**(11/12): 1709-1722.

Sholkovitz, E. R., Landing, W. M. & Lewis, B. L. (1994) Ocean particle chemistry: The fractionation of rare earth elements between suspended particles and seawater. *Geochim. Cosmochim. Acta* **58**(6): 1567-1579.

Sirocko, F., Sarnthein, M., Lange, H. & Erlenkreuser, H. (1991) Atmospheric summer circulation and coastal upwelling in the Arabian Sea during the Holocene and the Last Glaciation. *Quat. Res.* **36**: 72-93.

Speer, K. G. & Rona, P. A. (1989) A model of an Atlantic and Pacific hydrothermal plume. *J. Geophys. Res.* **94**: 6213-6220.

Speer, K. G. & Helfrich, K. R. (1995). Hydrothermal plumes: a review of flow and fluxes. In *Hydrothermal Vents and Processes*, Eds., L. M. Parson, C. L. Walker & D. R. Dixon. Geological Society, London, Special Publication, **87:** pp373-385.

Speer, K. G., Maltrud, M. & Thurnherr, A. (2002). A global view of dispersion on the Mid-Ocean Ridge. In *Energy and mass transfer in hydrothermal systems*, Eds., P. E. Halbach, V. Tunnicliffe & J. R. Hein. Dahlem University Press, Dahlem Workshop Report.

Spiess, F. N., Macdonald, K. C., Atwater, T., Ballard, R., Carranza, A., Cordoba, D., Cox, C., Diaz Garcia, V. M., Francheteau, J., Guerrero, J., Hawkins, J., Haymon, R., Hessler, R., Juteau, T., Kastner, M., Larson, R., Luyendyk, B., Macdougall, J.

D., Miller, S., Normark, W. R., Orcutt, J. & Rangin, C. (1980) East Pacific Rise: Hot springs and geophysical experiments. *Science* **206**: 1421-1433.

Statham, P. J. (1985) The determination of dissolved manganese and cadmium in sea water at low nmol l^{-1} concentrations by chelation and extraction followed by electrothermal atomic absorption spectrometry. *Anal. Chim. Acta* **169**: 149-159.

Statham, P. J., German, C. R. & Connelly, D. P. (2005) Iron (II) distribution and oxidation kinetics in hydrothermal plumes at the Kairei and Edmond vent sites, Indian Ocean. *Earth Planet. Sci. Lett.* **236**: 588-596.

Stumm, W. & Morgan, J. J. (1996). *Aquatic Chemistry: Chemical Equilibria and Rates in Natural Waters*, John Wiley & Sons. 1022pp

Tachikawa, K., Jeandel, C. & Dupre, B. (1997) Distribution of rare earth elements and neodymium isotopes in settling particulate material of the tropical Atlantic Ocean (EUMELI site). *Deep Sea Res. I* **44**(11): 1769-1792.

Tapscott, C. R., Patriat, P., Fisher, R. L., Sclater, J. G., Hoskins, H. & Parsons, B. (1980) The Indian Ocean Triple Junction. *J. Geophys. Res.* **85**(B9): 4723-4739.

Taylor, S. R. & McLennan, S. M. (1985). *The continental crust: its composition and evolution*. Oxford, UK, Blackwell Scientific

Tivey, M. K., Craddock, P., Seewald, J., Ferrini, V., S., K., Mottl, M. J., Sterling, N. A., Reysenbach, A. L. & Wheat, C. G. (2005) Characterization of six vent fluids within the Lau Basin. *EOS: Trans AGU* **86**(52): Fall Meet. Suppl., Abstract T31A-0477.

Toole, J. M. & Warren, B. A. (1993) A hydrographic section across the subtropical South Indian Ocean. *Deep Sea Res. I* **40**(10): 1973-2019.

Trefry, J. H. & Metz, S. (1989) Role of hydrothermal precipitates in the geochemical cycling of vanadium. *Nature* **342**: 531-533.

Treguer, P., Nelson, D. M., Van Bennekom, A. J., DeMaster, D. J., Leynaert, A. & Queguiner, B. (1995) The silica balance in the world ocean: a reestimate. *Science* **268**: 375-379.

Trocine, R. P. & Trefry, J. H. (1988) Distribution and chemistry of suspended particles from an active hydrothermal vent site on the Mid-Atlantic Ridge at 26°N. *Earth Planet. Sci. Lett.* **88**: 1-15.

Turekian, K. K. & Imbrie, J. (1966) The distribution of trace elements in deep sea sediments of the Atlantic Ocean. *Earth Planet. Sci. Lett.* **1**: 161-168.

Turner, J. S. (1973). *Buoyancy effects in fluids*. New York, Cambridge University Press. 367pp

Tyler, P. A. & CD128 Science Party (2001) RRS Charles Darwin CD128 Cruise Report.

Tyler, P. A., German, C. R., Ramirez-Llodra, E. Z. & Van Dover, C. L. (2002) Understanding the biogeography of chemosynthetic ecosystems. *Oceanol. Acta* **25**(5): 227-241.

van Aken, H. M., Ridderinkhof, H. & de Ruijter, W. P. M. (2004) North Atlantic deep water in the south-western Indian Ocean. *Deep Sea Res. I* **51**: 755-776.

Van Dover, C. L., Humphris, S. E., Fornari, D., Cavanaugh, C. M., Collier, R., Goffredi, S. K., Hashimoto, J., Lilley, M. D., Reysenbach, A. L., Shank, T. M., Von Damm, K. L., Banta, A., Gallant, R. M., Gotz, D., Green, D., Hall, J., Harmer, T. L., Hurtado, L. A., Johnson, P., McKiness, Z. P., Meredith, C., Olson, E., Pan, I. L., Turnipseed, M., Won, Y., Young III, C. R. & Vrijenhoek, R. C. (2001) Biogeography and ecological setting of Indian Ocean hydrothermal vents. *Science* **294**: 818-823.

Van Dover, C. L., German, C. R., Speer, K. G., Parson, L. M. & Vrijenhoek, R. C. (2002) Evolution and Biogeography of Deep-Sea Vent and Seep Invertebrates. *Science* **295**: 1253-1257.

Veirs, S. R., McDuff, R. E. & Stahr, F. R. (2006) Magnitude and variance of near-bottom horizontal heat flux at the Main Endeavour hydrothermal vent field. *Geochem. Geophys. Geosystems.* **7**(2): 2005GC000952.

Von Damm, K. L. (1990) Seafloor hydrothermal activity: black smoker chemistry and chimneys. *Ann. Rev. Earth Planet. Sci.* **18**: 173-204.

Von Damm, K. L. (1995). Controls on the chemistry and temporal variability of seafloor hydrothermal fluids. In *Seafloor hydrothermal systems: physical, chemical, biological and geological interactions*, Eds., S. E. Humphris, R. A. Zierenberg, L. S. Mullineaux & R. E. Thomson. Am. Geophys. Union, AGU Monograph, **91:** pp223-247.

Welhan, J. A. & Craig, H. (1983). Methane, hydrogen and helium in hydrothermal fluids at 21°N on the East Pacific Rise. In *Hydrothermal processes at seafloor spreading centres*, Eds., P. A. Rona, K. Bostrom, L. Laubier & K. L. Smith. Plenum Press**:** pp391-409.

Welhan, J. A. (1988) Origins of methane in hydrothermal systems. *Chem. Geol.* **71**: 183-198.

Wheat, C. G., Feely, R. A. & Mottl, M. J. (1996) Phosphate removal by oceanic hydrothermal processes: an update of the phosphorus budget in the oceans. *Geochim. Cosmochim. Acta* **60**(19): 3593-3608.

Wu, J. & Luther III, G. W. (1994) Size fractionated iron concentrations in the water column of the western North Atlantic Ocean. *Limnol. Oceanogr.* **39**(5): 1119-1129.

Zhang, J., Amakawa, H. & Nozaki, Y. (1994) The comparative behaviours of Yttrium and Lanthanides in the seawater of the North Pacific. *Geophys. Res. Lett.* **21**(24): 2677-2680.